CORA Cork Open Research Archive
Cartlann Taighde Oscailte Chorcaí

Title	Atomic layer deposition of copper – study through density functional theory
Authors	Dey, Gangotri
Publication date	2014
Original Citation	Dey, G. 2014. Atomic layer deposition of copper – study through density functional theory. PhD Thesis, University College Cork.
Type of publication	Doctoral thesis
Rights	© 2014, Gangotri Dey. - http://creativecommons.org/licenses/by-nc-nd/3.0/
Download date	2026-11-06 23:01:50
Item downloaded from	https://hdl.handle.net/10468/1757

UCC
University College Cork, Ireland
Coláiste na hOllscoile Corcaigh



Atomic Layer Deposition of Copper – Study through Density Functional Theory

A thesis presented to the National University of Ireland for the degree of Doctor Of Philosophy in chemistry

By

Gangotri Dey

Under the supervision of Dr. Simon D. Elliott

October 2014

Tyndall National Institute (Cork, Ireland)

Funded by SFI - Grant 09.IN1.I2628



……*When you want something, all the universe conspires in helping you to achieve it – Paulo Coelho (The Alchemist)*

…… *Nuair atá ní ar bith uait, beidh rath ort le cúnamh na cruinne - Paulo Coelho (The Alchemist)*

…..To my Parents and Grandparents

Declaration:

Hereby I Gangotri Dey declare that all the work reported in this thesis is my own.

Signature: ----------

Date: ----------

Acknowledgement

My sincere thanks to Dr. Simon D. Elliott for his supervision during my PhD studies. It has been a great experience working with a perfectionist like him. I have developed better understanding for research activity and learnt proper scientific approach under him.

I would also like to thank Prof. Jim Greer, Dr. Michael Nolan, Dr. Damien Thompson (now in UL) for their support. Many thanks to Dr. James Rohan from Tyndall National Institute and Dr. Orla Ni Dhubhghaill from UCC Chemistry Department for being a part of my advisory committee. Dr. Mahdi Shirazi is a great friend and colleague. His motivational speech during those tough times had given me a boost. (Would be Dr.) Yasheng Maimaiti and Merid Legesse has been a good company. Cheers! To all the MMD group members (former ETG), you guys rock.

My sincere acknowledgement to Dr. Dirk Hagen, Dr. Lynette Keeney, Dr. Jacqueline Wrench and Prof. Martyn Pemble from AMSG group here in Tyndall National Institute for their contribution in my research project and Roger Nagle, Scott B. Clendenning and Harsono Simka from Intel for their useful discussion during the initial part of my Ph.D.

Go raibh maith agat to Science Foundation Ireland (SFI) for funding.

Thanks to Ma, Baba and Buchum (my brother). Without you guys I am incomplete. I would like to thank Dr. Biswajit Santra for being a great motivation. Throughout my PhD journey your support was of great help. I am lucky to have you as my partner.

Thanks to Dr. Megha Aggarwal, my high school friend. Finally Megha we both can call ourselves Dr.'s in our own way. Cheers to both of us!

My sincere gratitude to my teachers from school and college days. They are Dr. Anupa Saha, Dr. Anup Pathak and Dr. Rana Sen from Scottish Church College, Miss Santa Mukherjee from Our Lady Queen Of the Missions and Dr. Krishna Mukherjee from Auxilium Convent School, Kolkata, India. You all trusted me more than I did myself. Thank

you to Prof. Anjali Athawale and Prof. S.R. Gadre from Pune University for their inspiration during my Master's studies.

Finally big thanks to my adopted family in Cork. I will restrict the names to few as otherwise the list will make my PhD thesis look thicker. Anushka Gangnaik, Anjana Kulkarni, Santosh Kulkarni, Tuhin Subhra Maity, Dhiman Mallick, Ricky Anthony, Pranay Podder, Preeti Balaji, Nitin Deepak, Sibu, KK, Prasanna, Lehre, Satish, UK, Tayabba and the rest. A special shout out to you Sumreen. I will always love and cherish the moments I had with you guys. You have given me an unforgettable experience here in Cork.

Abstract

The wonder of the last century has been the rapid development in technology. One of the sectors that it has touched immensely is the electronic industry. There has been exponential development in the field and scientists are pushing new horizons. There is an increased dependence in technology for every individual from different strata in the society.

Atomic Layer Deposition (ALD) is a unique technique for growing thin films. It is widely used in the semiconductor industry. Films as thin as few nanometers can be deposited using this technique. Although this process has been explored for a variety of oxides, sulphides and nitrides, a proper method for deposition of many metals is missing. Metals are often used in the semiconductor industry and hence are of significant importance. A deficiency in understanding the basic chemistry at the nanoscale for possible reactions has delayed the improvement in metal ALD.

In this thesis, we study the intrinsic chemistry involved for Cu ALD. This work reports computational study using Density Functional Theory as implemented in TURBOMOLE program. Both the gas phase and surface reactions are studied in most of the cases. The merits and demerits of a promising transmetallation reaction have been evaluated at the beginning of the study. Further improvements in the structure of precursors and co-reagent have been proposed. This has led to the proposal of metallocenes as co-reagents and Cu(I) carbene compounds as new set of precursors. A three step process for Cu ALD that generates ligand free Cu layer after every ALD pulse has also been studied.

Although the chemistry has been studied under the umbrella of Cu ALD the basic principles hold true for ALD of other metals (e.g. Co, Ni, Fe) and also for other branches of science like thin film deposition other than ALD, electrochemical reactions, etc.

Table of Contents

List of Figures: 10
List of Tables: 15
Conversions: 18
Abbreviations 18
1 Introduction 21
1.1 What are the latest targets for semiconductor industry? 22
1.2 Atomic Layer Deposition (ALD): 28
1.3 ALD of metals/pure elements: 33
1.4 ALD of Cu metal. 39
1.5 Objective of the thesis: 46
2. Computational Techniques used 48
2.1 The Schrödinger Equation: 49
2.2 First Principle methods - Density Functional Theory: 51
2.3 Basis Sets: 54
2.4 Molecular Dynamics 55
2.5 Population Analysis: 56
2.6 DFT methods in ALD: 57
Chapter 3: Mechanism for the atomic layer deposition of copper using diethylzinc as the reducing agent – a Density Functional Theory study using gas phase molecules as a model 62
3.1. Introduction 63
3.2. Methods 66
3.3. Results 68
3.3.1.a Structure of Cu(II) and Zn(II) compounds 68
3.3.1.b Structure of Cu(I) and Zn(I) compounds 68
3.3.1.c Entropy 72
3.3.2 Reaction Mechanism 72
3.4. Discussion 80
3.4.1 Geometry of the compounds: 80
3.4.2 Reactions 82
3.5. Conclusion 87
Chapter 4: Quantum chemical study of effect of precursor stereochemistry on dissociative chemisorption and surface redox reactions during the atomic layer deposition of the transition metal copper 89

4.1. Introduction....90
4.2. Methods....95
4.3. Results....98
4.3.a. Adsorption of copper precursors onto bare copper surface:....100
4.3.b. Adsorbed Intermediates....107
4.3.c. Population Analysis of $PyrIm^{iPr}$, dmap and AbaCus precursors:....111
4.3.d. Interaction of $ZnEt_2$ with a bare copper surface:....112
4.4 Discussion:....114
4.4.a. Adsorption of CuL_2 onto the surface:....115
4.4.c. Interaction of co-reagent $ZnEt_2$ with the surface:....121
4.5. Conclusion:....121
Chapter 5: Transmetallation reaction mechanism for Atomic Layer Deposition of Copper Using Diethylzinc as the Reducing Agent –A study through Density Functional Theory....126
5.1. Introduction....127
5.2. Methods:....129
5.3. Results and Discussion:....130
(i) Stable Cu/Zn intermediate onto the copper surface in absence of the alternative metal in the adsorbate:....131
(ii) Is ligand exchange possible between the two adsorbate metals?....133
(iii) Electron flow during ligand exchange reaction....137
(iv). Auxiliary side reactions:....139
(v). Desorbed half ligand exchanged product (LMEt)....140
(vi). Complete story of the transmetallation reaction....152
5.5. Conclusion:....154
Chapter 6: Metallocene as the reducing agent for atomic layer deposition of copper....157
6.1. Introduction:....158
6.2. Proposal for new Cu(0) pathway:....160
6.3. Methods used:....163
6.4. Results and Discussion (Computational study):....164
6.4.i. Reduction by abstraction of ligands from the precursor:....165
6.4.ii. Reduction by abstraction of oxygen:....168
6.4..iii. Reduction by abstraction of sulfur:....169
6.4.iv. Desorption of the by-products:....170
6.5. Solution phase reactions....172

6.6. Deposition onto Ru and Si surfaces from vapor 178
6.7. Conclusion: 179
Chapter 7: Copper(I) carbene hydride complexes acting both as a reducing agent and precursor for Cu ALD - A study through Density Functional Theory 185
7.1. Introduction 186
7.2. Methods 189
7.3. Results and discussion: evaluation of the copper carbene as a new precursor and reducing agent 189
7.3.1. Weakly bound hydride source 189
7.3.2. Exothermic reaction energy 192
7.3.3. Precursors should adsorb and by-products should desorb readily 194
7.3.4. Free of foreign metals 197
7.3.5. Synthesizable and commercially available 197
7.3.6. Volatile and stable during delivery 197
7.4. Conclusion 198
Chapter 8: Deposition of Copper by Plasma-Enhanced Atomic Layer Deposition Using a Novel N-Heterocyclic Carbene Precursor 200
8.1. Introduction: 201
8.2. Results and Discussion 203
8.3 Conclusion 208
Chapter 9: Copper reduction and atomic layer deposition by oxidative decomposition of formate by hydrazine. 211
9.1 Introduction: 212
9.2. Method: 212
9.3. Results and Discussion 213
9.4. Conclusions 220
Chapter 10: Computing Phase Change in Organometallic Compounds 224
10.2.a. Background 226
10.2.b. Research Approach 227
10.2.c. Benefit from the project 229
Chapter 11: Conclusion 230
Workshop, Conferences and Schools Attended 237
List of Courses attended in PhD both in UCC and outside. UCC module codes are listed 238
List of Publications: 239

List of Figures:

Figure 1: Graph showing Moor's Law. (Source of the picture - Intel) 21
Figure 2: Cross-section of an MPU (Semiconductor Industry Association. The International Technology Roadmap for Semiconductors, 2009 Edition. International SEMATECH:Austin, TX, 2009) 23
Figure 3: Shows the difference between conformal and non-conformal layers[6] coating a 3D feature such as a pore or trench. (a) shows substrate only (b) Conformal layer and (c) non-conformal layer. 24
Figure 4: Voids during ^{i}PVD growth. 25
Figure 5: Island formation of copper (picture courtesy James Connolly from Applied Materials at Tyndall National Institute). The copper was deposited using AbaCus as the Cu source and H_2 as the reducing agent. Here the substrate is Si. 25
Figure 6: The various steps involved in CVD reactions. Here the two reactants are transported to the system simultaneously. This may lead to the deposition of non-conformal layers..... 29
Figure 7: Steps involved in one cycle of Atomic Layer Deposition of a binary compound. Here the two reacting compounds (precursors) are transported to the chamber in two different pulses. It leads to the formation of conformal layers. 'I' shows the precursor pulse. 'II' shows the adsorbed precursor saturating the surface. 'III' shows the incoming co-reagents and 'IV' the deposition of the binary material. 29
Figure 8: ALD saturation curve (left) vs CVD growth curve (right). 30
Figure 9: Periodic table, not including hydrogen, halogens and noble gases, highlighting metals that have been deposited by thermal ALD or pulsed-CVD. Metals that have been deposited by ALD are enclosed by solid black boxes. Metals (or alloys) that have been deposited only by pulsed-CVD are enclosed by dashed black boxes. Atomic numbers are shown above the atom symbols and Pauling electronegativities are shown below (for values with two decimal places, the oxidation state is: 'I' for groups 1 and 11, 'II' for groups 2, 4–10 and 12, 'III' for groups 3 and 13, and 'IV' for group 14). Non-metals (including semi-metals) and elements without significant natural abundance are shown in white. The remaining elements are shaded. (Reproduced from Price *et al.* review article[32].) 33
Figure 10: Summary of the most important characteristics for an ideal CVD (red) and ALD (red + blue) precursor. Reproduced from Anjana Devi review article[55] 39
Figure 11: Common Cu ALD precursors. 1: $Cu(hfac)_2$ hfac = 1,1,1,5,5,5-hexafluoro-2,4-pentadionate. 2: $[Cu(sBu\text{-}Me\text{-}amd)]_2$ copper(I) N,N′-di-sec-butylacetamidinate . 3: bis(tri-butylphosphane)copper(I)acetylacetonate. 4: $Cu(tmhd)_2$ tmhd = = 2,2,6,6-tetramethyl-3,5-heptanedionat 5: Cu(I)-diketiminate diethylsilane. 6: $Cu(dmap)_2$, dmap = 3-dimethylamino-2-butoxide 7: Cu(II) pyrrolylaldiminate. 8: $Cu(acac)_2$ copper(II)acetylacetonate 43
Figure 12: Schematic of reactions of $[Cu(sBu\text{-}amd)]_2$ (a,b) and H_2 (c,d) on the OH-terminated SiO_2 surface. (Reprinted with permission from American Chemical Society. Adapted from Dai *et al.*[78]).. 46
Figure 13: This scheme gives an overview of the computational techniques. 60
Figure 14: Stick representation of computed structures of precursors and intermediates. (a) $Cu(acac)_2$, (b) $Cu(hfac)_2$, (c) $Cu(dmap)_2$, (d) $Cu(PyrIm^{iPr})_2$, (e) $Cu(PyrIm^{Et})_2$ are the precursors used to understand the mechanism. (f) Cu(dmap)Et is a sample intermediate during the course of the reaction. The Zn by-products are similar to these structures, where the Cu atom is replaced with Zn. Quantitative differences in structure between the copper precursor and the zinc by-product are given in Table 6. 70
Figure 15: Stick representation of computed structures of intermediates of the type Cu_2L_2. (a) $Cu_2(dmap)_2$ (b) $Cu_2(PyrIm^{iPr})_2$ and (c) $Zn_2(PyrIm^{iPr})_2$ are nonplanar structures and (d) $Cu_2(acac)_2$ (e) $Zn_2(acac)_2$ are planar. 71
Figure 16: Cu_2LEt compounds where (a) L=dmap and (b) $L=PyrIm^{iPr}$ 71
Figure 17: Zn_2LEt compounds with (a) L=dmap and (b) $L=PyrIm^{iPr}$. 72

Figure 18 : Zn_2LEt compounds with (a) L=dmap and (b) L=$PyrIm^{iPr}$. 73
Figure 19: (a) and (b) shows the flow chart to depict the possible ALD mechanism for both the precursor pulse and the reducing agent pulse respectively. Rectangular shapes denote the starting reagents and the end products and slanted boxes denote the intermediates. The upward arrow designates desorption of volatile species. 82
Figure 20: This figure shows various ALD cycle for proposed transmetallation reaction between copper precursor CuL_2 and reducing agent $ZnEt_2$. Each ALD pulse has been divided conceptually into two halves (a, b). The Cu precursor pulse on the right side with light pink shade is denoted as 1 and the reducing agent pulse on the left side with light blue shade is denoted as 2. Section 1a describes the reaction in a mixed surface between the incoming copper precursor and previously adsorbed Et ligands. Section 1b describes the reaction when the Et ligand has been exhausted and fresh copper precursor adsorbs onto a bare copper surface. Section 2a involves the same reactions as 1a but this is during the reducing agent pulse when incoming $ZnEt_2$ interacts with previously adsorbed ligands from the Cu precursor. Section 2b shows the reaction when an excess of reducing agent adsorbs onto a bare copper surface. 95
Figure 21: Side view and top view of the 3-layer deep Cu_{55} cluster, which is used as a model for the Cu(111) surface to investigate the adsorption of the copper precursors, intermediates and by-products. 98
Figure 22: Lowest energy isomer computed in gas phase for potential Cu ALD precursors. (i) $Cu(PyrAld)_2$ (ii) $AbaCus^{(TM)}$. Structural parameters are quoted in Table 11. Color code: Red = oxygen, Blue = nitrogen, Grey = carbon, White = hydrogen, Light brown = copper. 99
Figure 23: Optimized structures of precursors adsorbed onto the bare copper (111) surface. (i) $Cu(acac)_2$, (ii) $Cu(PyrAld)_2$, (iii) $Cu(PyrIm^{iPr})_2$, (iv) $Cu(dmap)_2$, (v) $AbaCus^{(TM)}$. The energetic of the adsorption energy is in Table 12 and the structural changes in the precursor before and after adsorption in Table 11. Color code: Red = oxygen, Grey = carbon, White = hydrogen, Light brown = copper, Blue = nitrogen..... 99
Figure 24: Lowest energy isomer of $PyrIm^{iPr}$ precursor, which does not chemisorb in any orientation onto the copper surface due to steric hindrance (Figure 23 (iii)). Color code: Red = oxygen, Blue = nitrogen, Grey = carbon, White = hydrogen, Light brown = copper. 103
Figure 25: (i) The Cu_2L_2 (L=dmap) intermediate where there are two ligands, each attached to two adsorbed copper atoms. The corresponding gas phase structure is shown to the right. In the gas phase the distance between the two Cu atoms is $|Cu^{(I)}\text{-}Cu^{(I)}|_{(g)}$ 2.48 Å and after adsorption onto the surface the distance is $|Cu\text{-}Cu|_{surf}$ 3.55 Å. (ii) Cu_2L + L where the first ligand is attached to two adsorbed copper atoms. The corresponding gas phase structure is also shown. In this case $|Cu\text{-}Cu|_{(g)}$ = 2.51 Å and $|Cu\text{-}Cu|_{surf}$ = 2.67 Å. 104
Figure 26: Energetics of surface intermediates during transmetallation when L = dmap is the ligand. The lower the energy in the graph, the more stable the system. (i) Red lines: The energy ΔE needed to transform the intermediate species into another on a bare copper surface. (ii) Green triangles: The desorption energy (ΔE_{des}) of the respective species into the gas phase relative to the red line. In the first structure the desorbed molecule is CuL_2, second Cu_2L_2, third CuL, and the last Cu_2L. (iii) Horizontal Blue lines: The free energy (ΔG^{393}) including the entropy factor at 393 K needed for the species in order to desorb into the gas phase relative to the red line. Any particular intermediate has the probability of either desorption from the surface (red → blue) or else can form another surface intermediate (red → red). The data are presented in the supplementary information. No barriers have been computed. 109
Figure 27: The graph shows similar results to that of Figure 26 but using L = $PyrIm^{iPr}$ as the ligand. 110

Figure 28: Optimized structure of $Cu(dmap)_2$ adsorbed on the (111) face of the copper coin. The differences in NPA charges on the Cu, O and N atoms between the gas phase precursor and the adsorbed precursor have been shown. The charges are more delocalized in the adsorbed structure compared to the gas phase and so the change is always positive. There are also changes in the surface with a total change of charge ~0.40. Color code: Red = Oxygen, Blue = Nitrogen, Grey = Carbon, White = Hydrogen, Light brown = Copper. 110
Figure 29: *Ab initio* Molecular Dynamics study for $ZnEt_2$ on Cu(111) surface. (i) Time *t*=0 shows $ZnEt_2$ attached to the surface. (ii) At time *t*=1.17 ps breaking of the C-Zn bond is apparent. Distance between C-Zn is 2.38 Å (C from the ethyl group). (iii) At time *t*=2.17ps, ZnEt and Et are separately attached to the copper surface. The above structures are not optimized geometries. Color code: brown=copper, blue-grey=zinc, grey=carbon and white=hydrogen. 113
Figure 30: The graph shows similar results to that of Figure 26 but using L = Et as the ligand. The most important reaction shown in the graph is the interaction between two CuEt and formation of butane with deposition of $Cu^{(0)}$. The same reaction can also be formed when Cu_2Et_2 dimer dissociates. The last intermediate has two new Cu atom adsorbed to the surface and butane in gaseous form.... 114
Figure 31: This picture shows the probable places where substitution favors the adsorption of the copper precursors. It has been assumed the precursor is a hexagonal complex. In (i) the substitution is in two opposite direction of the plane. There is no adsorption site as the Cu_{pre} cannot access the surface. In (ii) the substitution is in one direction of the plane, which makes the other plane available for adsorption site. In (iii) the substuation is in the same plane as the copper complex. This does not hinder adsorption. 119
Figure 32: The picture shows the division of parts for this chapter. Here, we are studying the chemistry of a mixed surface that is seen in an ALD chamber after the precursor and $ZnEt_2$ pulse. The most stable structure of Cu and Zn atoms attached to precursor ligand L or Et is explored in part I. The desorption energies of the Cu and Zn by-products are seen in part II. The complete story of transmetallation reaction is seen at the end. 130
Figure 33: The graph shows the ligand exchange between the copper in the precursor and copper from the surface for two ligands L = dmap and $PyrIm^{iPr}$. The pathway might follow two different intermediates for each L. It might either form an intermediate redox compound of LCuEt or else there might be formation of gaseous LEt with the desposition of Cu. The two ligand exchanged intermediates have similar energy when L = dmap. But for L = $PyrIm^{iPr}$ the intermediate with the ligand attached to the copper surface is more stable due to downhill in energy. 132
Figure 34: The graph shows the ligand exchange between the Zn in the reducing agent and copper from the surface for two ligands L = dmap and $PyrIm^{iPr}$. The pathway might follow two different intermediates. Zn(dmap) is more stable than ZnEt and ZnEt is more stable than $Zn(PyrIm^{iPr})$ in terms of ligand exchange with the copper surface. 133
Figure 35: Graph shows the energetics of ligand (L = $PyrIm^{iPr}$) exchange between the two metals Cu and Zn following three possible intermediate pathways. All the intermediates are higher in energy compared to the reactants and products. It shows that ligand exchange is unfavourable for $PyrIm^{iPr}$ ligand. The energy values are presented in the supplementary data. 135
Figure 36: Graph showing the energetics of ligand (L = dmap) exchange between the two metals Cu and Zn following three possible intermediate pathways. It shows that ligand exchange is favourable for dmap ligand as the reaction is downhill. The energy values are presented in the supplementary data present at the end of the chapter. 137
Figure 37: Lowest energy isomer computed in gas phase for potential LCuEt compounds. (i) L = $PyrIm^{iPr}$ (ii) L = dmap (iii) L = acac (iv) L = $AbaCus^{(TM)}$. The corresponding Zn compounds can be obtained by a change in the central copper atom to zinc. Structural parameters are quoted in Table 17

for copper and Table 18 for zinc compounds. Color code: Red = oxygen, Blue = nitrogen, Grey = carbon, White = hydrogen, Light brown = copper. 144
Figure 38: Optimized structures of LCuEt precursors adsorbed onto the bare copper (111) surface. (i) L = $PyrIm^{iPr}$ (ii) L = dmap (iii) L = acac (iv) L = $AbaCus^{(TM)}$. Structural changes between the gas phase structure and the adsorbed structure are shown in Table 17. Color code: Red = oxygen, Grey = carbon, White = hydrogen, Light brown = copper, Blue = nitrogen. 147
Figure 39: Potential Zn by-products adsorbed on the copper (111) surface. (i) $Zn(acac)_2$, (ii) $Zn(PyrIm^{iPr})_2$, (iii) $Zn(dmap)_2$, (iv) AbaZns. Color code: Red = oxygen, Grey = carbon, White = hydrogen, shaded grey = zinc, Blue = nitrogen. 150
Figure 40: The flowchart shows the possible transmetallation reaction process for any copper precursor and $ZnEt_2$ as the co-reagent. The reactions progresses following the steps shown in the diagram. In case the energy computed for any step is endothermic, the reaction stops at that step indicating a dead end. The top left side indicates the reaction that happens in copper precursor pulse as in Step 1a and Step 1b in Figure 20, Chapter 4. The top right side indicates reaction after $ZnEt_2$ pulse as in Step 2a and 2b in the same diagram. The different processes are indicated in the boxes. 152
Figure 41: The picture shows the proposed deposition of copper from copper precursor with the intermediate formation of copper sulfide or copper oxide. 'A' shows the precursor pulse. 'B' shows the saturation of the precursors onto the surface. 'C' shows the H_2O or else H_2S pulse. 'D' shows the formation of oxide or else sulfide. 'E' shows the incoming metallocene and 'F' the deposition of copper with the formation of substituted metallocene products. Steps C and D can be omitted and there can be direct deposition of copper from the precursor as described in equations 1 and 2. 161
Figure 42: Stick model of (i) Vanadocene. Colour code: Grey – Carbon, White – Hydrogen, Light Grey – Vanadium, Dark Blue – Nitrogen. 162
Figure 43: Schematic diagram showing the precursor pulsing sequence for $[Cu(acac)_2]$ (a), Vanadocene (b) and the three different places for methanol (c) introduction. 177
Figure 44: (i) Shows stick model of $Cu(acaca)_2(MeOH)$. Here the O from MeOH is coordinatively bonded to the copper in the copper precursor. (ii) shows two MeOH bonded to $Cu(acac)_2$. (iii) shows the side view of (ii). Here, one MeOH is coordinatively bonded to Cu and the other has H-bonding between the H from MeOH and O from the precursor. (iv) shows $Cu(acac)_2$ coordinatively bonded to THF. (v) shows $Cu(acac)_2$ co-ordinately bonded to two THF molecules. 177
Figure 45: SEM images of experiments grown at 250 °C using ratios of $Cu(acac)_2$:vanadocene of a) 1:1 and b) 1:2 on Si(100) substrate. 178
Figure 46: The N-heterocyclic-Cu hydride 1,3-diphenyl-imidazolin-2-ylidene (NHC) copper hydride. Color code: brown copper, white hydrogen, blue nitrogen, gray carbon. 189
Figure 47: (S-NHC)CuH showing S substituted for H at 4 and 5 positions. 192
Figure 48: Flowchart showing the three-step ALD cycle for the deposition of Cu with the intermediate formation of CuS layer. *L* ligand and *S* sulfide 193
Figure 49: (a) NHC carbene chemisorbed onto the bare copper surface via C. (b) dmapH protonated ligand physisorbed onto the surface. (c) (S-NHC)CuH adsorbed onto the surface via Cu and S. (d) is the same as c from a different viewpoint.
C*olor* code: *brown* copper, *white* hydrogen, *blue* nitrogen, *gray* carbon, *yellow* sufhur. 196
Figure 50: N-heterocyclic - Cu hydridedimer. Color code: brown copper, white hydrogen, blue nitrogen, gray carbon. The computed dihedral angle between C–Cu–Cu–C where the C is from the ligated carbene molecule is 16° 198
Figure 51: The structures of 1,3-diisopropyl-imidazolin-2-ylidene copper hexamethyldisilazide (1) and 4,5-dimethyl-1,3-diisopropyl-imidazol-2-ylidene copper hexamethyldisilazide (2). 203
Figure 52: Scanning electron micrographs of deposited copper films. a) Plan view of copper nanoparticles deposited using a 1 s pulse length. b) Plan view of crystalline copper deposited using a 4

s pulse length. c) Plan view of crystalline copper deposited using a 6 s pulse length. d) a profile of crystalline copper deposited using a 6 s pulse length. This is from the paper by Coyle *et al.*[1] 206
Figure 53: Optimized geometries of (a) 2 molecularly physisorbed on a smooth Cu (111) surface; (b) $CuN(SiMe_3)_2$ chemisorbed on the smooth surface; (c) NHC from 2 chemisorbed onto a rough surface; (d) NHC from 2 physisorbed on the smooth surface. 207
Figure 54: Optimized structure of (i) dmap ligand adsorbed on the smooth model copper surface, (ii) physisorbed formic acid (iii) adsorbed NH_2 radical, (iv) adsorbed formate anion. (Figure 57 for formate adsorption onto a rough surface). Colour code: brown=Cu, blue=N, red=O, grey=C, white=H. 214
Figure 55: Some snapshots of MD simulation of dmap anion interacting with formic acid in order to form copper formate and dmap-H. The above structures are not optimized. Colour code: brown=Cu, blue=N, red=O, grey=C, white=H. 215
Figure 56: Hess cycle showing the formation of surface adsorbed NH_2 from surface adsorbed N_2H_4. All the energies are in kJ/mol of hydrazine. 217
Figure 57: When the NH_2 radical attacks the H of Cu(HCOO), it forms CO_2 and NH_3 as by-products, leaving an atom of copper metal on the surface. Colour code: brown=Cu, blue=N, red=O, grey=C, white=H. 218
Figure 58: Redox reaction of equation 1 221
Figure 59: Comparison between the current procedure for precursor synthesis and evaluation and a proposal for the future. 226
Figure 60: Plots of pressure vs temperature using the Clausius-Clapeyron equation. 226
Figure 61: The figure shows the Clausius - Clapeyron equation plot for various alkanes as studied by Martin *et al.*[222] The solid lines depict the experimental data (upper curve, n-octane; lower curve, n-dodecane). Open circles, filled circles, and stars show the simulation results of the TraPPE, SKS, and OPLS force fields for n-octane, respectively. Open and filled diamonds represent the TraPPE and SKS results for n-dodecane. 228
Figure 62: Metric for selecting suitable precursor and co-reagent for successful ALD reaction. 234

List of Tables:

Table 1: Reduction potential of selected metal cations. 36
Table 2: The practical use of transition metals and noble metals. The uses reported here are the applications after a thin film deposition of the elements. 37
Table 3: Metal precursors, co-reagents and typical temperature for elemental deposition of the metals by ALD. The most promising technique has been reported here. Cu is not included in the list as it is discussed in the section 1.4. 38
Table 4: The table shows different Cu(I) compounds with the structure, corresponding name and the reference 41
Table 5: Different combinations of reducing agent and precursor for the purpose of Cu ALD, divided according to the co-reagents used in the deposition 42
Table 6: Optimized structural parameters of the copper precursors CuL_2 and their corresponding zinc compounds ZnL_2. The dihedral angle is between the four coordinating atoms of the ligand, for example in $Cu(acac)_2$ the angle is between the four oxygen atoms ∟O-O-O-O. 74
Table 7: Computed structural parameters for intermediate species Cu_2X_2 and Zn_2X_2. The dihedral angle is between the two coordinating atoms of one ligand and the copper atoms, for example in $Cu_2(acac)_2$ the angle is between two oxygen atoms of one acac and the copper atoms ∟Cu-O-O-Cu. 75
Table 8: Computed entropy (kJ/mol/K) of the precursors and the corresponding by-products calculated at 120°C. 76
Table 9: Mechanism for the copper ALD is divided into three classes of reaction: ligand exchange, reductive elimination and disproportionation. The various reaction energies computed for different precursors are presented here. 77
Table 10: Mechanism for the copper ALD is divided into three parts: ligand exchange, reductive elimination and disproportionation. The various reaction energies are presented here for Zn compounds 78
Table 11: Comparison of the structural properties of copper precursors when in the gas phase and after molecular adsorption onto the surface. Comparison has also been made with possible $copper^{(I)}$ intermediate. The dihedral angle is between the four coordinating atoms to the copper in the precursor, for example in $Cu(acac)_2$ the angle is between four oxygen atoms ∟O-O-O-O. The distance from the copper in the precursor to the nearest copper atom on the surface has also been noted and is represented as Cu-Cu. Here L = ligand in the precursor. 105
Table 12: Computed molecular adsorption energy (ΔE_{ad}) of copper precursors onto the copper surface along with the computed entropy contribution ($T\Delta S_{ad}$) of the molecules at T = 393 K. ΔG_{ad}^{393} denotes the free energy. All the values are in kJ/mol. Table 13 shows the gas phase structure of precursor compounds and Figure 23 the adsorbed counterparts. 106
Table 13: Computed adsorption energy (ΔE_{ad}), entropy contribution at 393 K ($T\Delta S_{ad}$) and free energy (ΔG^{393}_{ad}) of possible intermediates ($Cu_2^{(I)}L_2$) on the Cu surface during transmetallation reaction. All the values are in kJ/mol. 107
Table 14: Population analysis with NPA of the net charge in units of electronic charge on groups of atoms in the CuL_2 precursor, both in the gas phases (Figure 22) and then adsorbed onto the surface (Figure 23). Negative sign indicates negative charge. The same study has been done for the corresponding $Cu^{(I)}{}_2L_2$ surface intermediate. Cluster surface refers to the (111) copper surface atoms of the whole coin. 111

Table 15: Population analysis for L = $PyrIm^{iPr}$ and dmap precursor using four different models. Model I denotes ZnEt and CuL adsorbed onto a bare copper surface. Model II denotes LCuEt and metallic zinc over the surface. Model III denotes LZnEt and metallic copper onto the surface. Model IV shows adsorbed CuEt and ZnL 139
Table 16: Computed energetics of auxiliary side reactions during the transmetallation reaction process. The energies are quoted in kJ/mol. 140
Table 17: Comparison of the computed bond distances of copper precursors when in the gas phase and after molecular adsorption onto the surface. The structures of half ligand exchanged LCuEt are also given. The distance from the copper in the precursor to the nearest copper atom on the surface has also been noted and is represented as Cu-Cu. Here L = ligand in the precursor. 144
Table 18: The computed bond distances and the dihedral angle of the zinc compounds when in the gas phase and after adsorption onto the surface. The dihedral angle is between the four coordinating atoms to the zinc atom in the precursor, for example in $Zn(acac)_2$ the angle is between four oxygen atoms ∟O-O-O-O. The distance from the zinc atom in the precursor to the nearest copper atom in the surface has also been measured and is denoted by Zn-Cu. 145
Table 19: Computed molecular desorption energy (ΔE_{des}), entropy contribution at 393 K ($T\Delta S_{des}$) and free energy (ΔG^{393}_{des}) of possible half ligand exchanged (LMEt) on the Cu surface during transmetallation reaction. Here L = dmap, acac, AbaCus and $PyrIm^{iPr}$ and M = Cu/Zn. The structure of the compounds has been shown in Figure 33. All the values are in kJ/mol. 146
Table 20: Computed molecular desorption energy (ΔE_{des}) of zinc compounds onto the copper surface along with the entropy contribution ($T\Delta S_{des}$) of the molecules at T = 393 K. $\Delta G_{des}{}^{393}$ denotes the free energy. All the values are in kJ/mol. 149
Table 21: Computed molecular desorption energy (ΔE_{des}), entropy at 393 K ($T\Delta S_{des}$) and free energy (ΔG^{393}_{des}) of possible organic gaseous by-products on the Cu surface during transmetallation reaction. Here L = dmap and $PyrIm^{iPr}$. All the values are in kJ/mol. 151
Table 22: Literature values for reduction potential of some of the metallocenes that are studied here and aqueous copper. 162
Table 23: This table shows the energetics of five different copper precursors interacting with different metallocene compounds to form metallic Cu following equation 1 and 2. The energies are computed using DFT as the level of calculation and def-SV(P) as the basis set. In cases like vanadocene where the computed ground state has spin contamination, the energies are corrected using the spin projection formula described by Swart[169]. The energies are quoted in kJ/mol. The energy values in italics indicate endothermic reactions. 167
Table 24: Energies (ΔE_{des}) and Gibbs free energies of desorption (ΔG_{des}) including entropy contribution ($T\Delta S$) at T = 393 K of the vanadocene by-products as discussed in section 6.4.i, 6.4.ii and 6.4.iii. In all the cases the vanadium atom is in +4 oxidation state. Data are computed at PBE/SV(P) level and compared to PBE/TZVPP in selected cases (in parentheses). 171
Table 25 : Energies (ΔE_{des}) and Gibbs free energies of desorption (ΔG_{des}) including entropy contribution ($T\Delta S$) at T = 393 K of the vanadocene by-products where the vanadium atom is in III oxidation state. 172
Table 26: The table shows reaction and reaction energies for different solvents MeOH and THF coordination energies for $Cu(acac)_2$ and vanadocene. All the energies are in kJ/mol. '*' indicates that there is no optimized structure of the product. 175
Table 27: Elemental Analysis of complexes with methanol adducts 176
Table 28: Homolytic bond dissociation energy for copper ligand complexes XCuH according to Eqs. 3 and 4 with the copper-ligating atom bond length shown as Cu–X 190

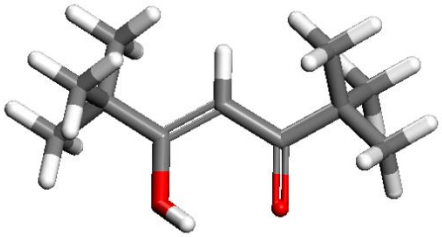
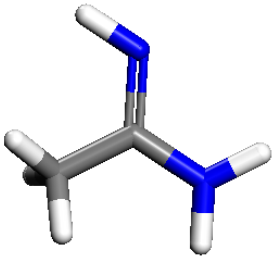
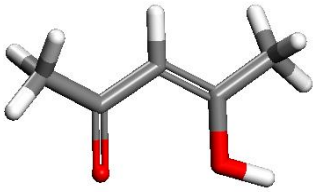
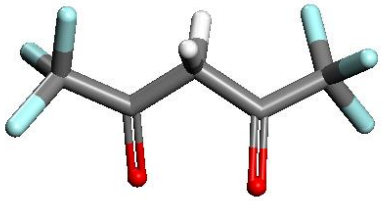
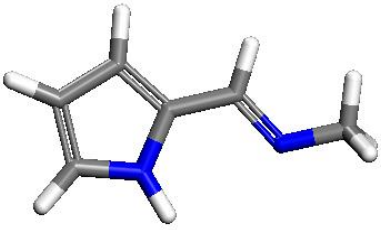
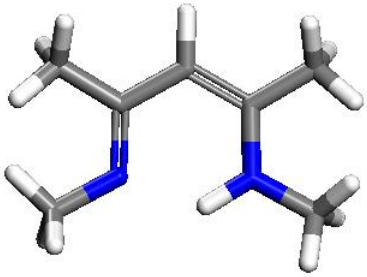
Table 29: Energy of adsorption of the molecules onto a Cu(111) model surface computed by SV(P)/PBE. Negative energy shows that adsorption of the molecule is favorable. The entropy contribution of the molecules has been calculated at T = 120 °C. The energies are in kJ/mol 195
Table 30: Selected bond lengths and bond angles for the structures of 1 and 2 205
Table 31: Computed adsorption energy ΔEad (kJ/mol) of the precursors and their probable by-products on the models for a smooth Cu(111) surface and for a rough surface with one extra Cu+. 207
Table 32: The adsorption energies ($\Delta E_{ad)}$ of the following adsorbate from their respective gas phase geometries adsorbed onto the copper surface. The energies are in kJ/mol. 215
Table 33: Reaction energies showing the gas phase dissociation of NH2-NH¬2 and $(CH_3)_2N$-NH_2 molecule. All the energies are in kJ/mol. 216
Table 34: Gas phase reaction energies showing the interaction of hydrazine with higher acids and dmap precursor 220
Table 35: Summary of the key reaction energies of the 3-step process 222

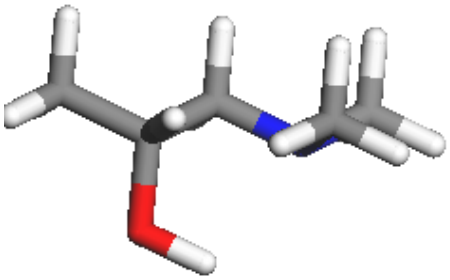
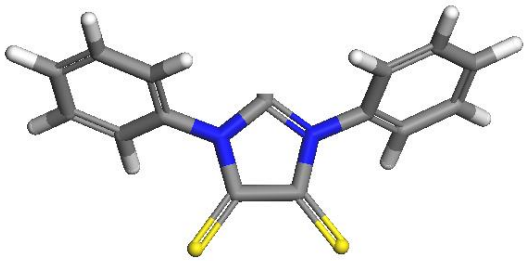
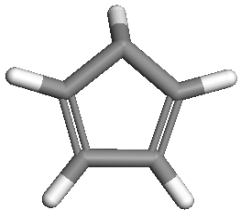
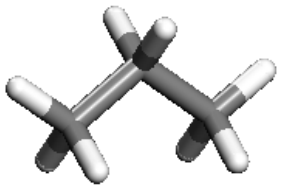
Conversions:

2600 kJ/mol =	360 kcal/mol=	1 Hartree =	27 eV
1/1000 km =	1 m =	10^9 nm =	10^{10} Å

Abbreviations

Acronym	**Full Form**
ALD	Atomic Layer Deposition
CC	Coupled Cluster
CI	Configuration Interaction
CVD	Chemical Vapor Deposition
FEOL	Front end of the Line
GGA	Generalized Gradient Approximation
GEMC	Gibbs Ensemble Monte Carlo
^{i}PVD	Ionized physical vapor deposition
ITRS	International Technology Roadmap for semiconductors
SAM	Self-Assembled Mono Layer
TGA	Thermogravimetric analysis

Acronym	Full form	Structure
tmhd-H	2,2,6,6-tetramethyl-3,5-heptanedionate	
amd-H	acetamidinate	
acac-H	acetylacetone	
hfac-H	hexafluoroacetylacetonate	
PyrIm-H	pyrrolylaldiminate	
nacnac-H	N,N-dimethyl-β-diketiminate	

dmap-H	dimethylamino-2-propoxide	
NSC	Sulfur substituted N-heterocyclic carbene	
Cp	cyclopentadiene	
^{i}Pr-H	isopropyl ($CH_2(CH_3)_2$)	

Colour code: Red = oxygen, Grey = carbon, White = hydrogen, Blue = Nitrogen, Sky blue = Fluorine, yellow = sulfur.

1 Introduction

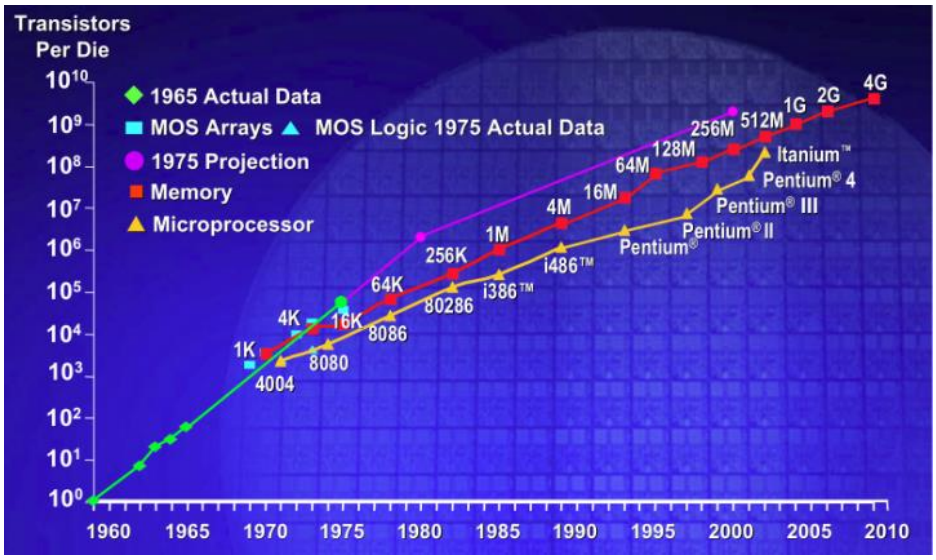


Figure 1: Graph showing Moore's Law for various electronic technologies. (Source of the picture - Intel)

If Sir Isaac Newton were to come alive today, even he would be baffled by the spectacular advancement in technology. Multi-functional mobile phones, tablets, laptops are the new basic essentials for the present human generation. Life has gained a different momentum due to these gadgets. Communication is faster, smoother and more reliable than ever before. However, there is an increasing demand to decrease the cost of production and reduce the size of these gadgets.

In this thesis, we will learn about a unique modern day technique known as Atomic Layer Deposition (ALD) for depositing materials using the bottom up approach. It is a revolutionary technique used today in the semiconductor industry. This work mainly focuses on the use of copper and its deposition by ALD. Chapter 1 gives a brief overview of the thesis.

1.1 What are the latest targets for semiconductor industry?

Gordon E. Moore, in a landmark 1965 paper, reported that the density of transistors on an integrated circuit (IC) doubles approximately every two years and that with this comes increased performance and lower cost. Since the size of a fully operational IC is reduced, this proposal is known as "Moore's Law"[1]. Scientists have created amazing tools that are still emerging to solve the ever exponentially increasing problems. There is a constant demand for new materials to be formed, which can be deposited at nanometer scale. These materials should be deposited in 3D to keep up with the aforesaid law.

One such need is in interconnects. Figure 2 shows a schematic of a typical microprocessor unit (MPU) in cross-section.

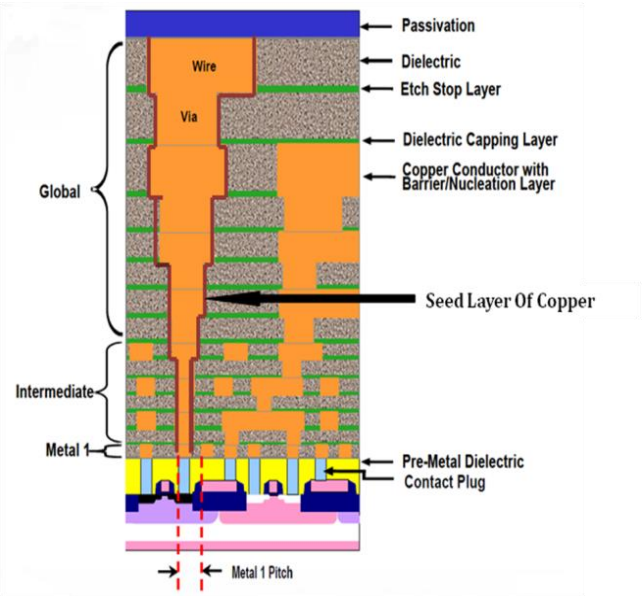


Figure 2: Cross-section of an MPU (Semiconductor Industry Association. The International Technology Roadmap for Semiconductors, 2009 Edition. International SEMATECH: Austin, TX, 2009)

The lowest layer in the MPU contains the transistor. The fabrication inside the transistor is called front end of the line (FEOL). The layers above the transistors are hierarchically ordered metallization levels fabricated in the back end of line (BEOL). The International Technology Roadmap for semiconductors, ITRS[2] has targeted a downscaling of this region. But there are various challenges in achieving this target. The narrow "contacts" in the CMOS transistors should be filled with metals. For the previous generation of devices, the choice of the metal to fill the gap in interconnects was Al. However, since Cu has low resistivity and is able to reliably carry high current densities, it is considered as an alternative choice. Since Cu has a melting point and atomic weight both higher than those of Al, it is expected to have better resistance to electromigration of metal into the dielectric and it has been found that Cu exhibits a roughly 10×improvement in electromigration characteristics relative to Al alloys[2]. The alternative to Cu might be Ag as it has lower resistivity. However, due to the higher cost of Ag, Cu is the proposed choice. The complete replacement of Al by Cu has presented a challenge.

Cu cannot be etched in a similar way to Al and thus a new etching technique has been introduced called the Dual Damascene Process[3]. This process requires a uniform, thin layer of copper called the seed layer. Currently, the seed layer is deposited using ionized physical vapor deposition (^{i}PVD)[4]. However, ^{i}PVD cannot meet the requirements of scaling down of the device size, as this will result in increase of the aspect ratio of interconnect. At film thickness of 3 nm and less ^{i}PVD produces defective nonconformal layers on 3D geometries with high aspect ratios (Figure 3), which might result in overhanging of the copper films at certain places. The voids (Figure 4) within the copper deposit can only be filled during electrodeposition. This lowers the reliability of interconnect due to fast electromigration pathways on the void surfaces. The ITRS has set the target of forming a 2 nm thin, conformal and uniform copper seed layer as one of its main goals[2].

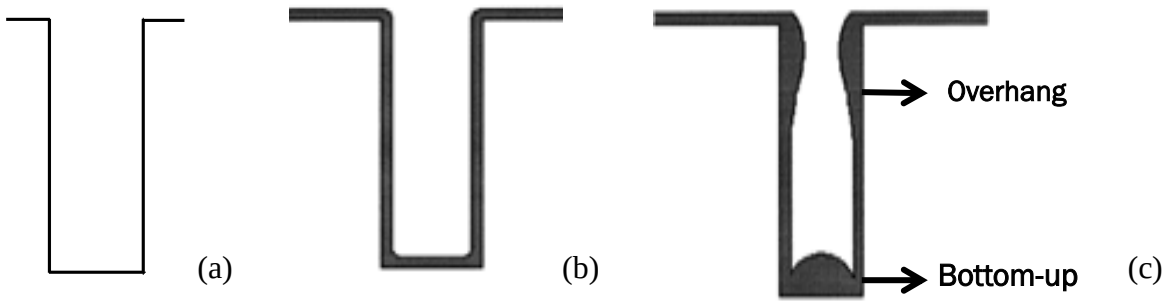


Figure 3: Shows the difference between conformal and non-conformal layers[5] coating a 3D feature such as a pore or trench. (a) shows substrate only (b) Conformal layer and (c) non-conformal layer.

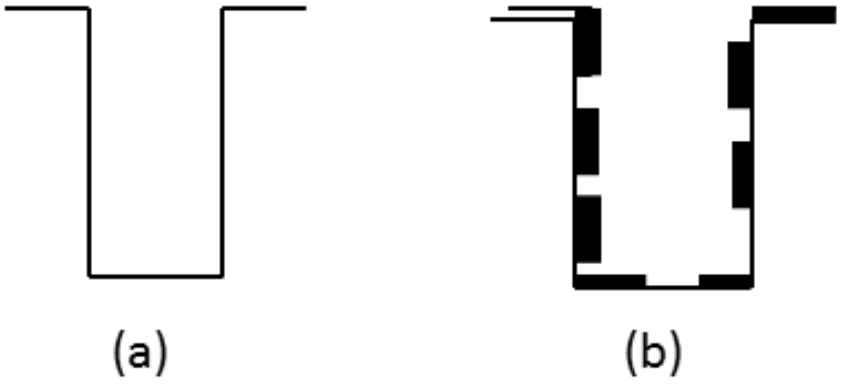


Figure 4: Voids during iPVD growth[6]. (a) shows substrate only (b) Voids during iPVD

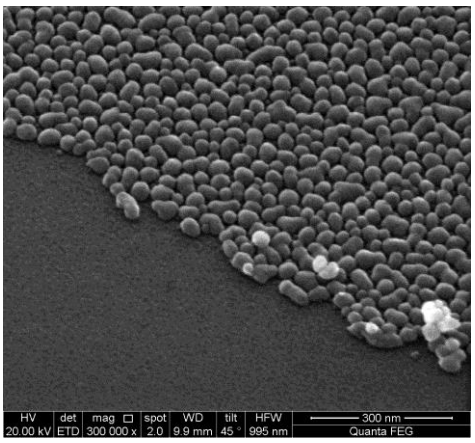


Figure 5: Island formation of copper (picture courtesy James Connolly from Applied Materials at Tyndall National Institute). The copper was deposited using AbaCus as the Cu source and H_2 as the reducing agent. Here the substrate is Si.

Some of the difficulties faced for copper are nucleation of copper in the form of islands (Figure 5) and the need for a barrier layer to prevent the copper leaking into the silica dielectric layer. In addition the choice of reducing co-reagents also limits the use. The limitations extend to the range of temperatures that can be used as will be discussed in sections 1.3 and 1.4. Some reagents are not active at lower temperatures and at higher temperatures the copper forms small islands.

Various thin film deposition techniques are known today[7]. Since, the concern here is with thin-film deposition methods for forming layers in the thickness range of a few nanometers to about ten micrometers, the task of classifying the techniques is made simpler by limiting the

number of techniques to be considered. The known thin film deposition techniques can be grouped under few headings as listed below.

A] Evaporative Methods

- Vacuum Evaporation
- Conventional vacuum evaporation
- Molecular-beam epitaxy (MBE)
- Electron-beam evaporation
- Reactive evaporation

B] Glow-Discharge Processes

Sputtering	*Plasma Processes*
• Diode sputtering	• Plasma-enhanced CVD
• Reactive sputtering	• Plasma oxidation
• Bias sputtering (ion plating)	• Plasma anodization
• Magnetron sputtering	• Plasma polymerization
• Ion beam deposition	• Plasma nitridation
• Ion beam sputter deposition	• Plasma reduction
• Reactive ion plating	• Microwave Electron cyclotron resonance (ECR) plasma CVD
• Cluster beam deposition (CBD)	• Cathodic arc deposition

C] Liquid-Phase Chemical Techniques

Electro Processes	*Mechanical Techniques*
• Electroplating	• Spray pyrolysis
• Electroless plating	• Spray-on techniques
• Electrolytic anodization	• Spin-on techniques
• Chemical reduction plating	• Chemical displacement plating
• Electrophoretic deposition	• Liquid phase epitaxy

D] Gas-Phase Chemical Processes

Chemical Vapor Deposition (CVD)	*Thermal Forming Processes*
• CVD epitaxy	• Thermal oxidation
• Atmospheric-pressure CVD (APCVD)	• Thermal nitridation
• Low-pressure CVD (LPCVD)	• Thermal polymerization
• Metal-organic CVD (MOCVD)	
• Laser-induced CVD (PCVD)	
• Ion implantation	
• Electron-enhanced CVD	
• Photo-enhanced CVD (PHCVD)	
•Atomic Layer Deposition (ALD)	

Among above techniques Atomic Layer Deposition (ALD) is one of the leading process solution in the electronic industry today[8] and so we limit our studies to this technique. Continued device miniaturization in the semiconductor industry has led to a need for thin, conformal films with excellent thickness control at the nanoscale regime. In complex 3D wiring of interconnect, ALD would be very helpful because it deposits materials layer by layer. Intense research in this field over the past decade has brought ALD for commercial use. It is used to deposit high-permittivity (high-k) materials like Al_2O_3 onto semiconductors as part of the gate stack in CMOS transistors. However, to date no perfectly useful ALD process has been found for depositing a seed layer of Cu. The current PhD work is dedicated to investigating the chemical properties of different copper precursors, co-reagents, mechanism and other aspects of chemistry that can be used for successful ALD. As a tool for the study, simulation using Density Functional Theory (DFT) has been chosen. This is equivalent to running experiments in cyber space.

1.2 Atomic Layer Deposition (ALD):

The principle of ALD was first published under the name "Molecular Layering" (ML) in the early 1960s by Prof. S.I. Koltsov from the Leningrad (Lensovet) Technological Institute (LTI). Following this was the work of Tuomo Suntola and co-workers in 1970's for the production of electroluminescent flat panel displays[9]. ALD is able to coat high-aspect-ratio features with perfect conformity and excellent thickness control. Today, a google scholar search on "Atomic Layer Deposition" generates 1,970,000 results (journal papers + patents + books chapters + articles + different almetrics feed).

ALD is regarded as a branch of chemical vapor deposition (CVD)[10]. The process of CVD is often used in the semiconductor industry to produce thin films. In typical CVD, the substrate is exposed to one or more volatile precursors, which react and/or decompose in the gas phase and/or on the substrate surface to produce the desired depositing material. Frequently, volatile by-products are also produced, which are removed by gas flow through the reaction chamber (Figure 6).

In contrast to CVD, the surface is exposed to the gas phase precursors alternately in ALD. The reactor is purged with inert gas to expel out the by-products and excess precursors that did not chemisorb during the pulse. The separation of the two pulses does not let the precursor complexes react in the gas phase. It is basically a pulse-purge technique where one cycle is composed of two pulses and two purges sequentially. This process is repeated until a layer of desired thickness is formed. The steps are explained in Figure 7. In ALD, a precursor adsorbs onto the active surface sites on the target substrate. Once all of the active sites are occupied, excess precursor molecules are purged out of the reaction chamber[11]. If the precursor is thermally stable at the deposition temperature, no further film growth reactions occur (Figure 8). The ALD reactions are self-limiting when it is operating ideally.

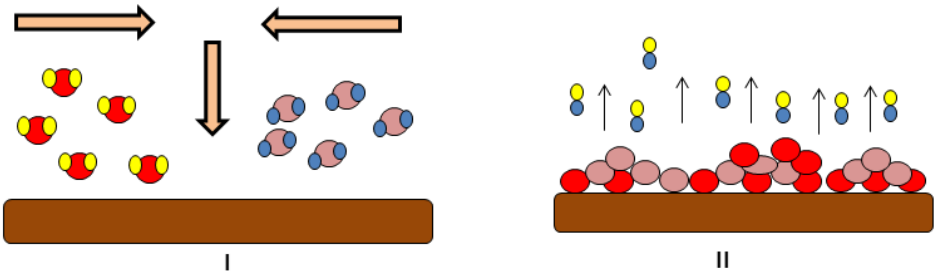


Figure 6: The various steps involved in CVD reactions. Here the two reactants are transported to the system simultaneously. This may lead to the deposition of non-conformal layers.

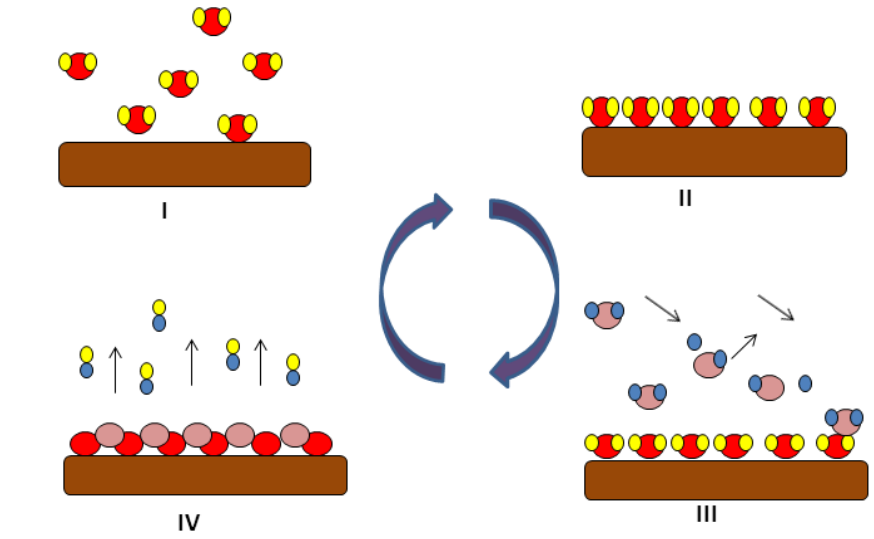


Figure 7: Steps involved in one cycle of Atomic Layer Deposition of a binary compound. Here the two reacting compounds (precursors) are transported to the chamber in two different pulses. It leads to the formation of conformal layers. 'I' shows the precursor pulse. 'II' shows the adsorbed precursor saturating the surface. 'III' shows the incoming co-reagents and 'IV' the deposition of the binary material.

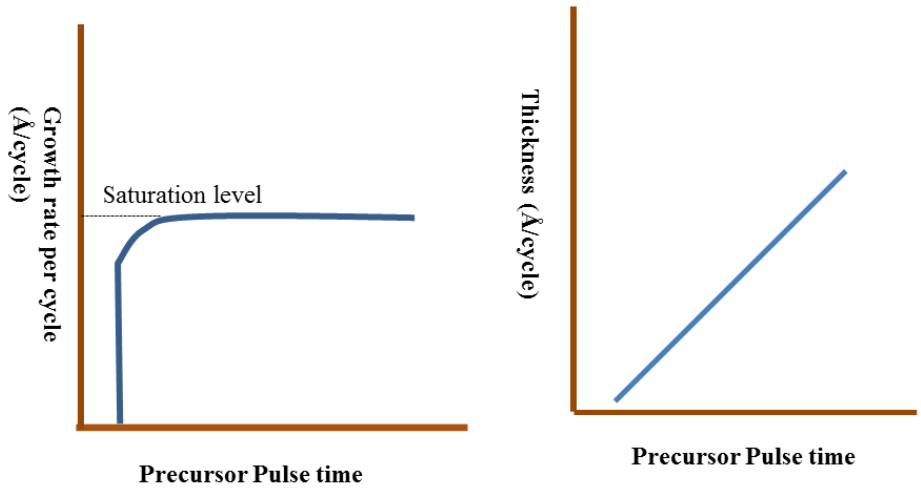


Figure 8: ALD saturation curve (left) vs CVD growth curve (right).

Many of the unique advantages of the ALD are due to control of layer thickness at the Ångstrom level. The self-limiting nature of the surface reactions also produces nonstatistical deposition because the randomness of the precursor flux is removed as an important factor. In principle, the discrete cycles of ALD can be used to deposit different layers. There have been some reports of this, especially in ZAZ dielectrics[12,13].

The precursors used in an ALD process should have certain qualities so as to achieve self-limiting growth. These are :

- Volatile - For efficient transportation, a limit of 0.1 Torr at the applicable maximum source temperature. The source should be preferably in liquid or gaseous state[14].
- Stable against Self-Decomposition – The self-limiting film growth via the surface exchange reactions is achievable only under conditions where the precursors do not decompose on their own[14].
- Undergo Aggressive and Complete Growth Reactions with surface species – Thermodynamically the ALD reactions should be feasible.
- No Side-Reactions – There should not be any alternative reactions as this might lead to impurities.

- No Dissolution to the film or the substrate – The dissolution of the film onto the surface might be harmful. This can be seen in the case of Cu onto the Si surface. The copper brings down the band gap of Si[15].
- Un-reactive byproducts – Reactive byproducts may cause corrosion problems in the reactor or in the exhaust[16].
- Practical Requirements like the ease of synthesis, level of impurities, safe handling and commercial availability also matters.

However, all these requirements cannot be completely fulfilled simultaneously and often the last ones can be sacrificed while developing a new ALD precursor[14].

Broadly there are two types of ALD (i) Thermal ALD[17] and (ii) Plasma ALD[18] also known as Plasma enhanced ALD (PEALD). In the former case of thermal ALD, the thermodynamics of the reaction drives the process. Favorable reactions are enthalpically downhill (exothermic, $\Delta H < 0$). This is the most common technique for deposition. Therefore, a good balance is required when choosing the ALD precursor. It should be thermally stable during delivery but also react with the surface. The thermal energy helps the precursor and the co-reagent to react onto the surface. The co-reagents might be a secondary compound that can be deposited (as H_2O in the deposition of Al_2O_3) or else a reducing agent (like H_2 for the deposition of metals). The thermal energy also helps to activate the surface for the complexes to react[19]. Insufficient reaction energy or too much thermal energy might lead to impurities in some cases[20]. Thermal ALD can be extended to include techniques where additional chemical energy is supplied in the form of reactive species as in Plasma ALD or else the co-reagent is heated before being pulsed to the system.

Plasma assisted ALD is an alternative to thermal ALD. The PEALD can also be termed as radical-enhanced ALD. This involves the reaction of the material at the surface with active ions and/or radicals from gaseous products like $O_2/H_2/NH_3/H_2O$. Some radicals

act like a reducing agent for the materials and are therefore favorable for depositing elemental materials like metals. For metal ALD, plasma of H_2 is normally used. However, there are limitations of this process as there are strong chances for recombination of the radicals in high aspect ratio structures. For further information of the different techniques used in plasma ALD, the reader is directed to the review by Kessels *et al*.[19]

Atomic Layer Deposition has been used with great success for the deposition of oxides and nitrides in the past decade, including Al_2O_3[21], Nb_2O_5[22], TiO_2[23], and ZrO_2[24]. In a similar way, ALD of nitrides of Ti and Ta have also gained importance[25]. The main commercial applications are in the electronics industry for these materials. ZrO_2 and HfO_2 are used as sensors, mirrors and as dielectric layers in transistors and thin film electroluminescent (TFEL) devices[26]. Al_2O_3 films are used in dynamic random access memory (DRAM) trenches, read-write heads or in the interpoly stack of flash memories[27]. Being able to deposit a thin conformal layer of these materials decreases the size of the electronic devices.

Despite the wide scale importance of ALD, we believe that labelling a process as ALD is often an illusion as there is no confirmation of what exactly happens on the surface barring very few *in-situ* experimental studies. Conclusions can also be drawn by examining the nature of the products. Only in few cases, by-products have been conclusively identified at the end of the reaction[28]. Without evidence of by-products, proper reaction stoichiometry cannot be deduced. For example, equation (1) has been proposed by Lee *et al*.[29], but equation (2) can also be proposed.

$$CuL_2 + ZnEt_2 \rightarrow Cu^{(0)} + ZnL_2 + Butane\uparrow \quad \ldots(1)$$

$$CuL_2 + ZnEt_2 \rightarrow Cu^{(0)} + LZnEt + LEt\uparrow \quad \ldots(2)$$

Theoretical studies, mainly based on Density Functional Theory (DFT) can help to understand the reaction mechanism for the process. Further insight into how DFT has helped in the development of the ALD chemistry can be found in section 2.6.

1.3 ALD of metals/pure elements:

Unlike the deposition of binary compounds, metal ALD is still in its infancy[30]. ALD processes of few metals are known in the literature. However, there are reports of metals being deposited by CVD[31].

In the case of metal ALD a complete reduction of the metal cation present in the precursor is needed. Hence, the electrons need to be drained towards the metal. This is the main difference between the metal ALD and ALD of binary compounds.

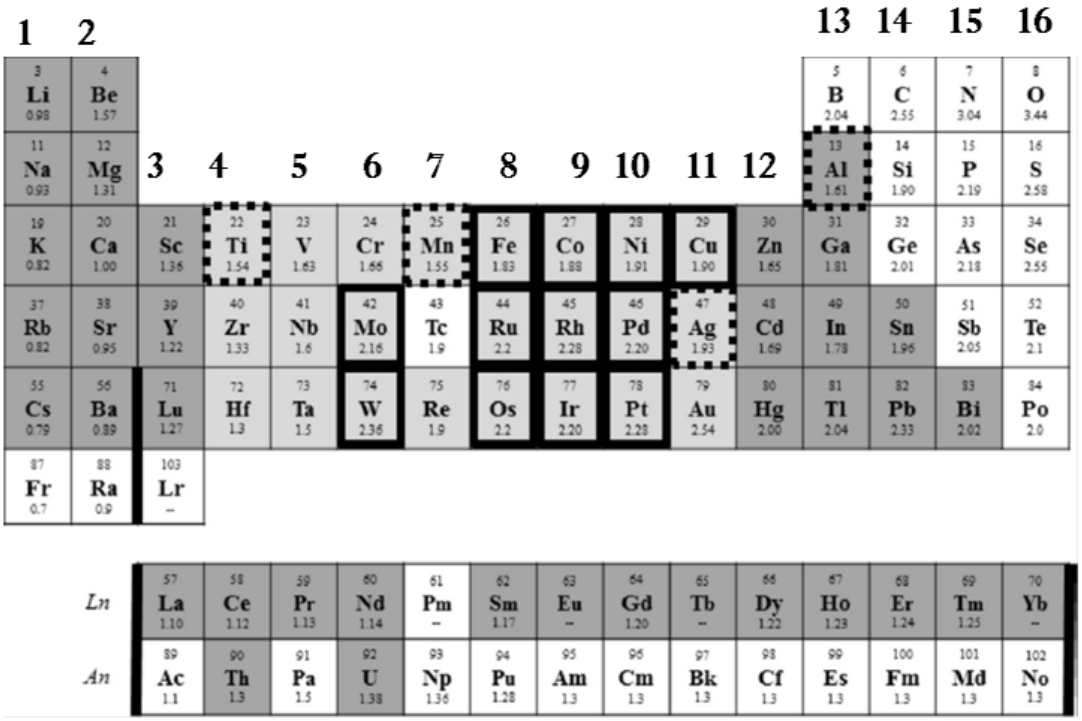


Figure 9: Periodic table, not including hydrogen, halogens and noble gases, highlighting metals that have been deposited by thermal ALD or pulsed-CVD. Metals that have been deposited by ALD are enclosed by solid black boxes. Metals (or alloys) that have been deposited only by pulsed-CVD are enclosed by dashed black boxes. Atomic numbers are shown above the atom symbols and Pauling electronegativities are shown below (for values with two decimal places, the oxidation state is: ‘I’ for groups 1 and 11, ‘II’ for groups 2, 4–10 and 12, ‘III’ for groups 3 and 13, and ‘IV’ for group 14). Non-metals (including semi-metals)

and elements without significant natural abundance are shown in white. The remaining elements are shaded. (Reproduced from Price *et al*. review article[32].)

The other barriers towards achieving metal ALD may include:

- Unavailability of the proper precursor molecules.
- Unavailability of a good reducing agent that can lead to the complete reduction of the metal.
- The reactions usually take place at high temperatures.
- No proper knowledge of the mechanism[33].
- Often the reaction follows a CVD pathway rather than an ALD[34,35].
- Small island formation of the metals rather than a uniform thin layer. The islands are of a thickness more than that of the target film.
- Impurities are deposited along with the target materials.
- Expensive process to synthesize new prospective precursor compound.
- Long incubation time before film growth on a certain substrate.
- Poor adhesion to the substrate.
- Low vapor pressure of the precursor complex.
- Following the laws of electrochemistry, only metals that have higher reduction potential can be reduced by common reducing agents like H_2. However, the metals, specially the first row transition metals have lower reduction potential. Hence, it is difficult for them to be deposited.

The use of some elements at nm level is already known in the literature. The prospective applications of the metals in terms of ALD have been summarized in the following paragraphs. They are grouped according to the columns in the periodic table. The alkali and alkaline earth metals (columns 1-2), transition metals (including noble metals) (3-12) and soft

metals/non-metals (13-18). We exclude the lanthanides and actinides from our study as they are too costly to be tested in a laboratory scale. Halides are always found in combination with other elements. Noble metals are very inert for any prospective reaction.

Alkali and Alkaline Earth Metals: The alkali and alkaline earth metals are very reactive. Lithium is an important constituent of functional materials in lithium ion batteries and in integrated optics. A nm level deposition of Li has been studied[36,37]. Also ALD of LiF (a binary compound and not a pure metal) has been reported due to its low refractive index and large band gap[38]. The other alkaline metals like Na/K are too reactive to be deposited in nm level.

Soft metals/non-metals: Among the elements present in the groups 13-16, only ALD of Al[39], Si[40] and Ge[41] have been reported.

ALD of Al is a technique for introducing metallic aluminum in nanoporous materials. For instance, an enhancement of the acidity and acid catalytic activity of US-Y zeolite and Zeotile-4 hierarchical material has been demonstrated with this process. However, the literature lacks a proper description of the reaction pathway and of the chemicals used for the deposition.

ALD of Si films on SiO_2 has been reported by Nakajima *et al.*[40] The prospective use is not only in the semiconductor industry but also for quantum devices. This might also be applicable for fabricating silicon-on-insulator substrates having an extremely flat thin Si layer. Like Si, Ge has extensive possible applications in the electronics and optics industry. However, Ge has more efficiency than Si in terms of electron and hole mobility[42]. There is room for material change from Ge to Si and possibly even the incorporation of Ge based transistors. ALD of elemental Ge has only been reported by Stickney *et al.*[41]. There is not much literature available for either of these elements and this field has huge prospect for further exploration. ALD of Te has been reported in conjugation with ALD of Ge[41]. Here the

ALD of Te has been used as bait for Ge ALD. There has been no reported use of Te metal/element ALD.

Transition metals/noble metals: Transition metals have a wide application in the semiconductor industry. The 3rd row metals and the noble metals have been widely studied through ALD and also CVD. The vast study might be due to the high reduction potential to the elements as seen in Table 1. Table 2 gives an overview of the practical uses of these metals.

The most promising metal precursor, co-reagent and the temperature used for the deposition of each transition metal by ALD is reported in Table 3. For further understanding of the transition metal ligands, the author recommends the PhD thesis by Thomas J. Knisley from Wayne State University[43].

Table 1: Reduction potential of selected metal cations.

$M^{x+} + xe \rightarrow M^0$	E^0 (V)[44]
Ti^{2+}	-1.63
Cr^{2+}	-0.74
Mn^{2+}	-1.18
Fe^{2+}	-0.44
Co^{2+}	-0.28
Ni^{2+}	-0.25
Cu^{2+}	0.34
Pd^{2+}	0.92
Pt^{2+}	1.19

Table 2: The practical use of transition metals and noble metals. The uses reported here are the applications after a thin film deposition of the elements.

Elements	Use as thin film
Ti	Diffusion barrier layer in interconnects.
Cr	Magnetic, catalytic, optical, and electrical applications.
Mn	memory and logic devices, sensors, flat panel displays, and battery technologies.
Fe	magnetic, catalytic, optical, and electrical applications.
Co	magnetoresistive devices, integrated circuits, lithium battery technologies and spintronics.
Ni	contact materials in metal oxide semiconductor field effect transistor (MOSFET) devices.
Cu	interconnecting material in the semiconductor chips.
Ru	Diffusion barrier layer in interconnects.
Ir	in DRAM electrodes, X-ray mirrors
Pd	responsive sensors and catalysts.
Pt	catalysis.
Os	suggested as adhesion layers and diffusion barriers for damascene metallization.

Table 3: Metal precursors, co-reagents and typical temperature for elemental deposition of the metals by ALD. The most promising technique has been reported here. Cu is not included in the list as it is discussed in the section 1.4.

Metal	Reference	Precursor	Co-reagent	Temperature (°C)
Ti	Ludviksson *et al.*[45]	$TiCl_4$	$AlH_3(NH_3)$	65-127
Cr	Sousa *et al.*[46]	$Cr(CO)_6$	O_2	Standard room temperature
Mn	Au *et al.*[47]	$Mn(tmhd)_3$	H plasma	Not mentioned
Co	Lee *et al.*[48]	$Co(amd^{iPr})_2$	NH_3	350
Ni	Kim *et al.*[49]	$Ni(dmamb)_2$	NH_3	300
Ru	Li *et al.*[50]	$(amd^{tBu})Ru(CO)_2$	NH_3	300
Ir	Aaltonen *et al.*[51]	$Ir(acac)_3$	O_2	225
Pd	Elam *et al.*[52]	$Pd(hfac)_2$	Formalin	200
Pt	Aaltonen *et al.*[53]	$CpPtMe_3$	O_2	200
Os	Hämälainen *et al.*[54]	$OsCp_2$	O_2	325

Most of the reactions as reported in Table 3 work at high temperature. This is harmful because it might lead to agglomeration. There is no unique ideal ALD process of deposition for all the transition metals.

For further knowledge about metal ALD, the reader is directed to a review article by Zaera *et al.*[35] where they discuss the current flaws in the technique and the potential of surface chemistry to overcome them.

1.4 ALD of Cu metal.

Among all the transition metals, there is an urgent need for Cu to be deposited by ALD technique. The reason has been discussed in section 1.1. Here we are going to discuss the Cu ALD work that has already been mentioned in the literature. We will discuss Cu ALD in the following order: precursors, co-reagents and surface interactions.

1.4.1. <u>Precursors</u>: The precursors that are used in ALD can be broadly categorized as either metal organic compounds or metal halides. This is irrespective of the target material to be deposited. Puurunen has given an overview of the metal ligands that are used in ALD[11]. The ligands can be halides, alkyls, cyclopentadienyls, alkoxides, ß-diketimates, alkylamides, silyamides and amidinates. Some of the ligands are seen in Table 3 for metals other than Cu and Table 4 and Table 5 for Cu. The requirements of an ideal precursor are depicted in Figure 10.

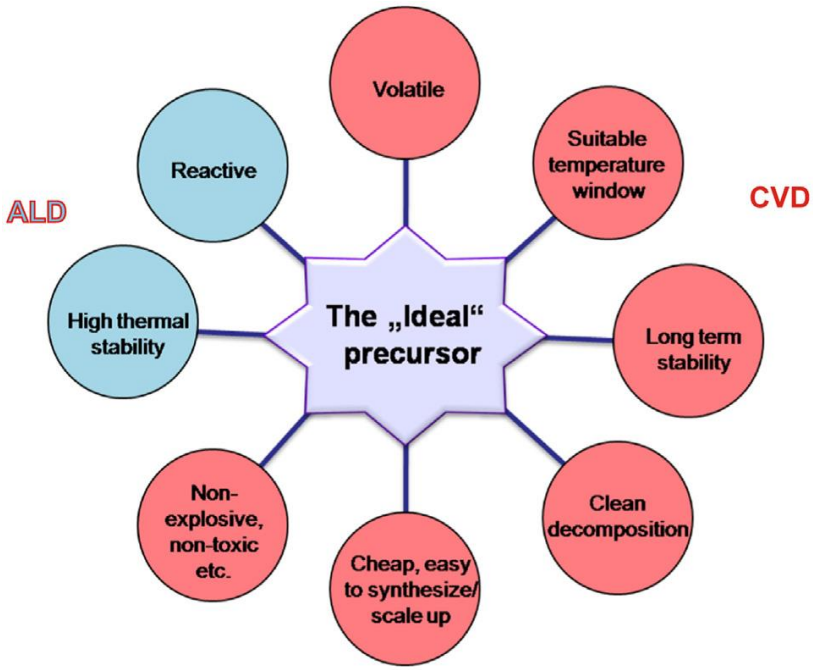


Figure 10: Summary of the most important characteristics for an ideal CVD (red) and ALD (red + blue) precursor. Reproduced from Anjana Devi review article[55].

The first reported ALD precursor is CuCl in a study by Mårtensson *et al.*[56]. This was followed by two sister papers by the same author. The papers were based on theoretical study. In the next decade studies on different Cu(II) precursors were reported. Some of the

important precursors are shown in Figure 11. The studied precursors vary in the electronegativity of the ligating atom like O in acac, hfac etc., N in $PyrIm^{iPr}$ and a mix of O and N in dmap. There are not many reports of a neutral ligand attached to the Cu center (Figure 11 (5)).

High reaction temperature is a problem for all the precursors as reported in Table 5. A big breakthrough in Cu ALD came with a report by Lee *et al.*[29]. They reported ALD at a reaction temperature of 120 °C. This was made possible by using an organometallic reagent $ZnEt_2$ as the reducing agent. The low reaction temperature, production of volatile by-products and fewer impurities in this reaction indicate good Cu ALD conditions. Hence this reaction has been studied in detail in this PhD. The merits and demerits of this reaction give a base for other novel methods as well.

Table 4: The table shows different Cu(I) compounds with the structure, corresponding name and the reference.

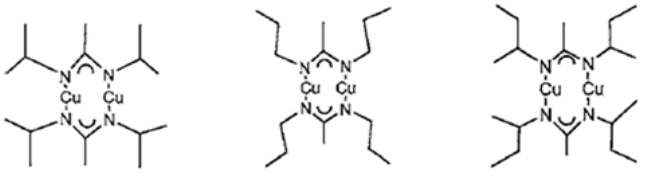
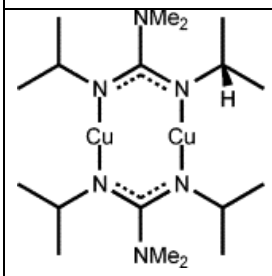
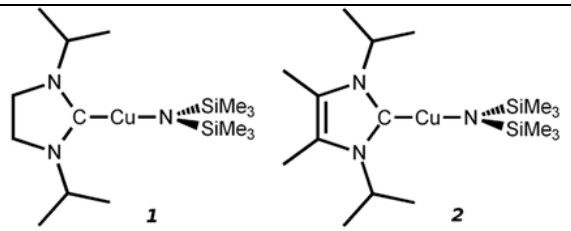
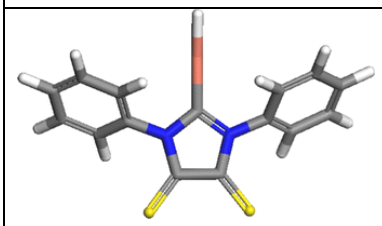
Structure of Cu(I) complexes	Nomenclature	Reference
 i ii iii	i- $[Cu(^{i}Pr\text{-}amd)]_2$ ii- $[Cu(^{n}Pr\text{-}amd)]_2$ iii- $[Cu(sec\text{-}Bu\text{-}amd)]_2$	Gordon *et al.*[57,58]
	copper(I) N,N-di-isopropylacetamidinate	Barry [59]
 1 2	1- 1,3-diisopropyl-imidazolin-2-2- ylidene copper(I)hexamethyldisil - azide. 2- 4,5-dimethyl-1,3-diisopropyl-imidazol-2-ylidene copper(I) hexamethyldisilazide	Coyle *et al.*[60,61]
	Sulfur substituted N-heterocyclic carbene (S-NHC)	Dey *et al.*[62]

Table 5: Different combinations of reducing agent and precursor for the purpose of Cu ALD, divided according to the co-reagents used in the deposition.

Co-reagent	Reference	Precursor	Temperature (°C)
H_2	Mårtensson *et al.*[63]	CuCl	360
	Mårtensson *et al.*[64]	$Cu(thd)_2$	190
	Utriainen *et al.*[65]	$Cu(acac)_2$	250
	Lim *et al.*[30]	$Cu_2(amd^{iPr})_2$	280
	Li *et al.*[57]	$Cu_2(amdsBu)_2$	190
	Kang *et al.*[66]	$Cu(hfac)_2$	25-100
H_2SiEt	Grushin *et al.*[67]	$Cu(PyrIm^{Ph})_2$	160-170
	Park *et al.*[68]	$Cu(nacnac^{cycle\text{-}Me,Me})_2$	100
	Park *et al.*[68]	$(nacnac^{cycle\text{-}H,Me})Cu(VTMS)$	120
	Thompson *et al.*[69]	$(nacnac^{H})Cu(VTMS)$	45
NH_3+H_2	Grushin *et al.*[67]	$Cu(PyrIm^{R})_2$ (R = Me, Et)	180
	Li *et al.*[57]	$Cu_2(amds^{Bu})_2$	160
NH_3	Törndahl *et al.*[70]	$Cu(hfac)_2$	283
	Li *et al.*[71]	$Cu_2(amds^{Bu})_2$	280
HCOOH, then N_2H_4	Knisley *et al.*[72]	$Cu(OCHMeCH_2NMe_2)_2$	180
Formic acid	Norman *et al.*[73]	$Cu(hfac)(tmvs)_2$	125
Zn	Juppo *et al.*[74]	CuCl	440-550
$ZnEt_2$	Lee *et al.*[29]	$Cu(dmap)_2$	100
	Vidjayacoumar *et al.*[75]	$Cu(PyrIm^{Et})_2$	130

Although Cu(II) precursors dominate the list of Cu ALD process, recently Cu(I) compounds have also become of importance. Initial work was done in Roy Gordon's group in Harvard University. Other Cu(I) compounds are still being explored. The aim is to bring

down the reaction temperature and prepare volatile but thermally stable copper compounds. A list of Cu(I) compounds, with the structures and the functional groups are presented in Table 4. The dominant ligands for Cu(I) compounds are amidinates, guanidinates and iminopyrrolidinates. Of late neutral carbene ligands in combination with other ligands have also been reported[60]. However, in some cases ALD of reported Cu(I) compounds resemble a thermal CVD type of reaction rather than ALD as showed by Ma *et al.*[76].

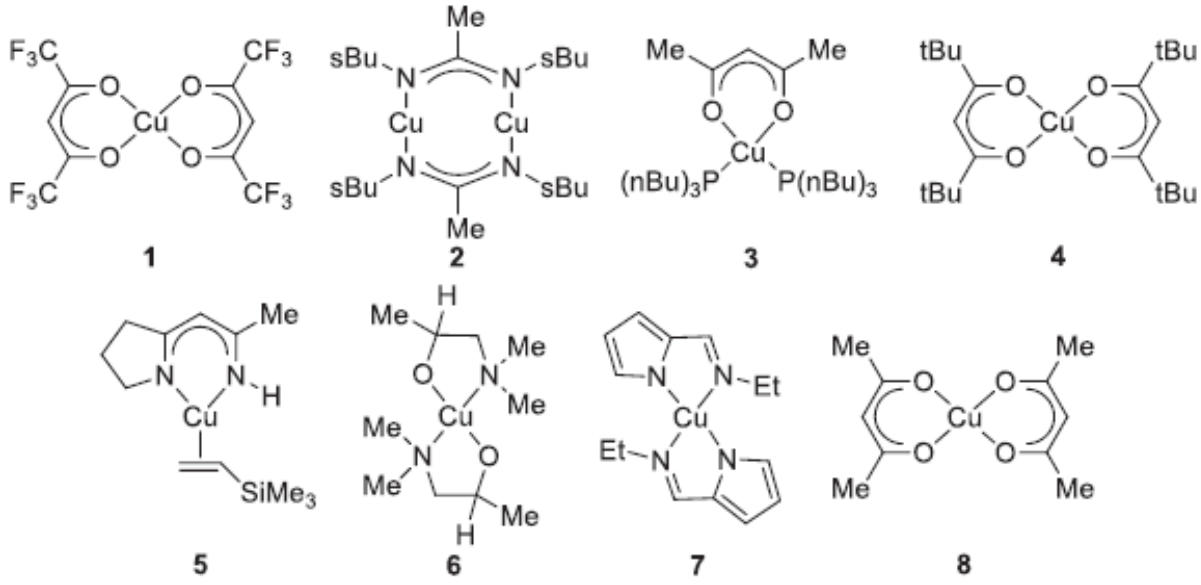


Figure 11: Common Cu ALD precursors. 1: $Cu(hfac)_2$ hfac = 1,1,1,5,5,5-hexafluoro-2,4-pentadionate. 2: $[Cu(sBu\text{-}Me\text{-}amd)]_2$ copper(I) N,N′-di-sec-butylacetamidinate . 3: bis(tri-butylphosphane)copper(I)acetylacetonate. 4: $Cu(tmhd)_2$ tmhd = = 2,2,6,6-tetramethyl-3,5-heptanedionat 5: Cu(I)-diketiminate diethylsilane. 6: $Cu(dmap)_2$, dmap = 3-dimethylamino-2-butoxide 7: Cu(II) pyrrolylaldiminate. 8: $Cu(acac)_2$ copper(II)acetylacetonate

1.4.2 Co-reagents:

In metal ALD chemistry, the co-reagents play a key role. The precursors have the metal cation in a high oxidation state that has to be reduced to zero for the elemental metal. The co-reagent often supplies electrons to achieve this. Another role of the co-reagent is to combine with the ligands from the metal precursor and form stable compounds that desorb from the surface. This holds true for all the metals discussed in section 1.3.

The most common co-reagent for Cu ALD is the hydrogen molecule. It can donate electrons to the metal center being reduced and also combine with anionic ligands to form protonated molecules. However, the use of molecular hydrogen has the disadvantage that in order to break the H-H bond, energy > 400 kJ/mol is needed[77]. The atomic hydrogen produced also has a high probability for recombination rather than taking part in the ALD process[62]. H-plasma might be a better choice due to lower temperature but H radicals are also subject to recombination[78].

Other non-metallic reducing agents are NH_3, NH_2-NH_2, HCOOH, H_2SiEt etc. (Table 5). NH_3 is a relatively stable molecule, but it has been found to work for Cu ALD with amide precursors[70]. The detailed mechanism for NH_2-NH_2 and HCOOH[72] will be discussed in this thesis in chapter 9. Although H_2SiEt has been tried for Cu ALD[67], it is not a common reagent as the possibility for Si impurities is high. Metal organic systems have also been used for the reduction of Cu metal (Table 5). A detailed mechanistic study for such transmetallation reaction is a part of this thesis and will be studied in chapters 3-5.

An alternative approach for Cu^0 formation would be the deposition of CuO film and subsequent reduction with H_2. However, a complete reduction of a CuO film might not always be possible. A similar approach can also be taken via reduction of Cu_3N. CVD deposition of Cu from Cu_3N has been tried[71].

1.4.3. <u>Surface interaction</u>: There are very few studies of the interaction of copper precursors with a surface. In one of these, Dai *et al.*[79] studies a Cu(I) compound on an OH terminated SiO_2 surface experimentally. As seen in Figure 12 the initial reaction is with the H from the –OH. Subsequently one of the ligands is protonated and is purged out of the system, thus leaving Si-O-Cu bonds with one ligand still bound to the adsorbate. Incoming H_2 strips away the ligands from Cu(I), donating an electron for deposition of metallic Cu(0). There is

agglomeration of copper at the end of cycle. The agglomeration might be facilitated by the high temperatures.

Dai *et al.*[80] in another work have reported the same $[Cu(sBu\text{-}amd)]_2$ precursor interacting with an Si-H surface. A loss in the IR bands for Si-H is seen after some time. This confirms the chemical interaction of the precursor with the surface. However, a detailed description of the course of the reaction has not been given.

Chabal *et al.*[81] have studied copper deposition on a Self-Assembled Monolayer (SAM). The Cu precursor used here is again copper di-sec-butylacetamidinate $[Cu(sBu\text{-}amd)]_2$ and the SAM is a carboxyl-terminated alkyl SAM. This study shows that Cu deposited with ALD forms a bidentate complex with the COOH groups during the first half cycle of ALD and the Si/SAM interface remains chemically intact after metal deposition. The non-damaging thin Cu film deposited by ALD protects the SAM, making it possible to deposit a thicker metal top contact leading ultimately to a controlled preparation of molecular electronic devices.

For further knowledge on ALD or Cu ALD, the author recommends the following review articles and book chapter – Ritala *et al.*[25,82], George[82,83], Roy[84], Elliott[85], Puurunen[86].

.

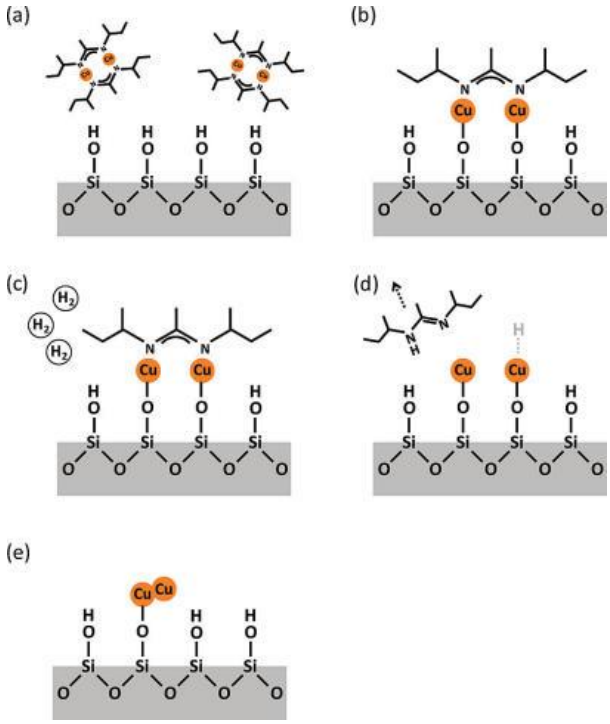


Figure 12: Schematic of reactions of $[Cu(sBu\text{-}amd)]_2$ (a,b) and H_2 (c,d) on the OH-terminated SiO_2 surface. (Reprinted with permission from American Chemical Society. Adapted from Dai *et al.*[79])

1.5 Objective of the thesis:

Understanding ALD reactions using Density Functional Theory calculations is not a common practice. There are comparatively fewer studies done to date relating the two techniques than pure experimental study. However, a proper understanding of the reactions through computational study will not only benefit general science but also help the existing ALD techniques.

In this work, our main goal is to find a suitable reaction for metal ALD in general and Cu ALD in particular. Initially a transmetallation reaction as proposed by Lee *et al.*[29] has been taken for the study. Models based on both gas phase and surface reactions are computed to find a pathway for copper deposition and avoid commonly known impurities. This study comprises Chapters 3, 4 and 5. It was found that the reaction has some intrinsic deficiencies when using $ZnEt_2$ as the co-reagent. An alternative reagent (metallocene) was further

proposed and tested in the laboratory and this comprises Chapter 6. Copper carbene compounds are reported as new source of copper precursor in the following two chapters (7 and 8). Winter and his group[72] reported a three step process for the deposition of transition metals. However, the mechanism for the reaction was not known. It is the only known technique to date where after each cycle; no ligand is attached to the Cu metal. Chapter 9 reports the atom by atom mechanistic details for Cu formation for this 3 step process. Chapter 10 reports a technique that can be used for the computational study of phase change in organometallic systems. However, no calculations have been done for this study. Chapter 11 concludes the thesis.

Each of the results chapters is either a published article in a peer review journal or else under preparation for publication. They have their special introduction, method section, results, discussion and conclusion. The last chapter weaves a complete story including the main points from all the chapters. The work reported here describes the Cu ALD but it is expected that most of the reactions and mechanistic concepts hold true for other transition metals.

2. Computational Techniques used

$$H\varphi = E\varphi$$

Running virtual experiments in the computer is a powerful technique to understand the chemistry of molecules. Also known as simulations, it is the connecting link between theory and experiments. It is of course crucially dependent on the computational power available. With the growth in computer power, new horizons are being exposed. A decade years back, molecules containing only 10-100 atoms could be explored with force field techniques but today a few 1000 atoms can also be simulated *ab initio*. This is possible through high parallelization of computer resources.

The aim of this section is to describe the quantum mechanical techniques used for the study. A clever use of the method helps to describe the structures, reactivity, thermodynamic and molecular dynamics of the reactions that are studied in this thesis.

2.1 The Schrödinger Equation:

One of the most important equations of 20st century is the Schrödinger Equation. The main idea behind many quantum chemical approaches is to determine the energy and properties of a molecule by determining an approximate solution to the time-independent, non-relativistic Schrödinger equation[87].

$$\hat{H}\Psi = E\Psi \quad \ldots (1)$$

where $\hat{H}$ is the Hamiltonian differential operator representing the total energy, E is the numerical value of the energy and ψ is the wave function of the system with electrons and nuclei. The square of the wave function ψ^2 is the probability distribution of the electrons and nuclei within the system. The Hamiltonian operator can be expressed as

$$\hat{H} = \hat{T}_n + \hat{T}_e + \hat{V}_n + \hat{V}_e + \hat{V}_{en} \quad \ldots (2)$$

$\hat{T}_n$ and $\hat{T}_e$ describe the kinetic energy (KE) of the nuclei and the electrons respectively. The other terms in the Hamiltonian constitute the potential energy part of the operator. $\hat{V}_n$ and $\hat{V}_e$ describes the Columbic potential of nucleus – nucleus and electron – electron repulsion respectively. The final term $\widehat{V_{en}}$ describes the Columbic attraction between the electrons and nuclei.

The Schrödinger equation for any molecule will have different solutions, corresponding to different stationary states and the state with the lowest energy is the ground state of the system. Unfortunately, the Schrödinger equation cannot be solved exactly for most many-body systems and therefore a few important approximations are made to simplify the computation of the Schrödinger equation.

According to Born-Oppenheimer approximation, due to the much heavier nuclei compared to the electron, the 1st and the 3rd terms are constant and the equation (2) modifies into equation (3) for the electrons alone.

$$\hat{H} = \hat{T}_e + \hat{V}_e + \widehat{V_{en}} \quad \ldots(3)$$

In general the Schrödinger Equation involving the electronic Hamiltonian is equation (4).

$$\hat{H}_{elec}\phi = E_{elec}\phi \quad \ldots(4)$$

An important theorem for quantum chemistry is the Variational Principle. The variation theorem states that for a given system with a Hamiltonian $\widehat{H}$, if Φ is any normalised, well-behaved function that satisfies the boundary conditions of the Hamiltonian, then

$$<\Phi|\hat{H}|\Phi> \geq E_0 \quad \ldots(5)$$

where E_0 is the true value of the lowest energy eigenvalue of $\hat{H}$. This principle allows us to calculate an upper bound for the ground state energy by finding the trial wave function Φ for which the integral is minimised (hence the name; trial wave functions are "varied" until the optimum solution is found).

These basic equations are described in detail in any of the quantum chemistry books. However, for our study we have followed the book of Szabo and Ostlund[87].

2.2 First Principle methods - Density Functional Theory:

There are two categories of first principle techniques. Firstly wave function based Hartree Fock (HF) theory and related post-HF methods like Møller–Plesset perturbation theory (MP), coupled cluster (CC) and configuration interaction (CI), and secondly Density Functional Theory (DFT), which is based on the electron density $\rho(r)$ of the molecule[88]. DFT is in principle an exact many body theory. An important advantage of using the electron density over the wave function is the much reduced dimensionality. Regardless of how many electrons one has in the system, the density is always a function of just the 3 spatial dimensions. DFT has become the most widely used electronic structure approach today.

Here the electron density of the atoms is computed as it is easy to deal with both computationally and conceptually. Named after the scientists who proposed the idea, density functional theory can be written as Kohn Sham (KS) equation[88] and is written as equation 6:

$$\left[-\frac{\hbar}{2m\nabla^2} - \sum_A \frac{Z_A e^2}{|r-R_A} + e^2 \int \frac{\rho(r')}{r-r'}\, dr + U(r)\right]\varphi = \varepsilon\varphi$$

…(6)

Here the first term denotes the kinetic energy, the second term denotes the nuclear attraction potential (where Z_A is the charge in the nucleus, r-R_A is the distance of the electron from the nucleus), the third term the Columbic repulsion potential of one electron with other electrons and the last term is the exchange correlation potential.

There is a double evaluation of the interaction of an electron to itself in the potential energy term. There are two ways to tackle the problem. The first is known as the LDA (local density approximation). Here the exchange and correlation energy is determined as an integral of a function of the total electron density (equation 8).

$$E_{XC}[\rho(r)] = \int \rho(r)\varepsilon_{XC}[\rho(r)]\, dr \quad \ldots. (8)$$

The term $\varepsilon_{XC}[\rho(r)]$ is the exchange-correlation energy per electron in a homogeneous electron gas of constant density. It can be derived from a uniform electron gas cloud, neutralized at the background of a positive charge. There are various improvements in the technique so that it can be error free of any pseudo energy term.

The second technique is known as generalized gradient approximation (GGA) where there is an added level of complexity. Here, in addition to the local density, there is an added term relating to the gradient of the density. Depending on the properties to be evaluated, LDA or else GGA is used. In this work, we use a GGA functional PBE (Perdew-Burke-Ernzerhof) for our calculation[89].

In addition to approximating $E_{XC,}$ the kinetic energy term $T[\rho(r)]$ must be formulated in terms of the electron density. As proposed by Kohn and Sham, the electron density can be written in terms of orthonormal orbitals φ_i, which relates DFT to the independent particle approximation form of HF theory.

$$\rho(r) = \sum_{i=1}^{N} | \phi_i |^2 \quad \ldots (8)$$

The Kohn-Sham orbitals are determined from the Kohn-Sham equations.

$$\hat{T}\psi_i + \widehat{V_{KS}}\psi_i = \varepsilon_i\psi_i \ldots (9)$$

$$\widehat{V_{KS}} = \widehat{V_H} + \widehat{V_{ext}} + \widehat{V_{XC}} \ldots (10)$$

$$V_{XC}[\rho] = \frac{\partial E_{XC}[\rho]}{\partial \rho} \ldots (11)$$

The terms ε_i, $\widehat{V_H}$, $\widehat{V_{ext}}$ are the Kohn-Sham orbital energies, the classical inter-electron Coulomb interaction and the external potential due to the nuclei respectively. The exchange correlation potential $\widehat{V_{XC}}$ is the functional derivative of the exchange-correlation energy equation 11).

The Kohn-Sham equations are solved in a self-consistent field fashion. Initially electron density is needed so that E_{XC} can be computed (equation 11). To obtain the electron density, an initial "guess" to the Kohn-Sham orbitals is needed. The Kohn-Sham equations (equation 9) are then solved to obtain an improved set of Kohn-Sham orbitals. The improved set of Kohn-Sham orbitals is then used to calculate a better density (equation 9) and E_{xc} (equation 11). This iterative process is repeated until the exchange-correlation energy and the density are self-consistent within a defined tolerance.

This section gives only a brief overview of DFT. There is no mention about the deficiency of the theorem or about latest developments in the field. For this the author requests the readers to follow the latest review articles or the book chapters related to the field[90-93].

2.3 Basis Sets:

The basis set is a set of mathematical functions from which the wave function or electron density of any arbitrary system can be constructed[94,95]. Essentially, almost all electronic structure methods today rely on an expansion of the unknown wave function in terms of a set of basis functions. Any type of basis function may in principle be used like exponential, Gaussian, polynomial, plane-wave, spline, Slater type orbitals, and numeric atomic orbitals. When selecting the basis function, it should be kept in mind that the electron density should describe the physical traits of the structure with reasonable accuracy.

In the present work we have used Gaussian type orbital (GTO) basis set as implemented in TURBOMOLE code[96]. This is because Slater type orbitals (STO) are difficult to compute. In contrast, GTO's are much faster to work with in the evaluation of the two-electron integrals than STO functions. For this reason GTO's are most popular and have been used in most of the cluster codes. The GTO functions can be written as a fixed sum over contraction coefficients and primitive Gaussian functions. Each primitive Gaussian function is specified by a fixed orbital exponent[97].

The "minimal" basis set consists of the minimum number of basis functions needed to describe the ground states of the component atoms in a molecule. For example, the minimal basis set for H_2O would be a 1s orbital for each hydrogen atom plus a 1s, 2s, 2px, 2py, and 2pz orbital for the oxygen atom. Because the contraction coefficients and orbital exponents are fixed, the size of a basis function on an atom cannot vary as the nature of the surrounding atoms changes. This problem is solved by replacing each orbital in the minimal basis set with two basis functions that differ in size. During the self-consistent-field process the coefficients for each basis function on the atom are optimized and hence the size of the orbital.

The other types of basis set like Gaussian type Pople basis set, or plane wave basis set are described in any standard text book[98,99].

2.4 Molecular Dynamics

Molecular Dynamics (MD) is a computational method that calculates the time dependent behavior of a molecular system. MD simulations provide detailed information on the fluctuations and conformational changes of any structure. They are also used in the determination of structures from x-ray crystallography and from NMR experiments. MD is based on Newton's second law of the equation of motion. From knowledge of the force on each atom, it is possible to determine the acceleration of each atom in the system. Integration of the equations of motion then yields a trajectory that describes the positions, velocities and accelerations of the particles as they vary with time. From this trajectory, the average values of properties can be determined. The method is deterministic; once the positions and velocities of each atom are known, the state of the system can be predicted at any time in the future or the past, subject to finite precision of computation.

In a molecular dynamics simulation, one often wishes to explore the macroscopic properties of a system through microscopic simulations, for example, to calculate changes in the binding free energy, or to examine the energetics and mechanisms of conformational change. The connection between microscopic simulations and macroscopic properties is made via statistical mechanics. Molecular dynamics simulations provide the means to solve the equation of motion of the particles and evaluate these mathematical formulas. With molecular dynamics simulations, one can study both thermodynamic properties and/or time dependent (kinetic) phenomena. Molecular dynamics simulations can be time consuming and computationally expensive. However, computers are getting faster and cheaper.

An ensemble is a collection of all possible systems that have different microscopic states but have an identical macroscopic or thermodynamic state. There exist different ensembles with different characteristics. A few of the main ensembles are enlisted below.

- Microcanonical ensemble (NVE) : The thermodynamic state characterized by a fixed number of atoms, *N*, a fixed volume, *V*, and a fixed energy, *E*. This corresponds to an isolated system.
- Canonical Ensemble (NVT): This is a collection of all systems whose thermodynamic state is characterized by a fixed number of atoms, *N*, a fixed volume, *V*, and a fixed temperature, *T*.
- Isobaric-Isothermal Ensemble (NPT): This ensemble is characterized by a fixed number of atoms, *N*, a fixed pressure, *P*, and a fixed temperature, *T*.
- Grand canonical Ensemble (μVT): The thermodynamic state for this ensemble is characterized by a fixed chemical potential, μ, a fixed volume, *V*, and a fixed temperature, *T*.

In principle there are two types of MD:

- Classical MD: The characteristics are shown below.

  degrees of freedom: atomic

  equations of motion: classical dynamics

  governing theory: statistical mechanics

- Quantum MD: The characteristics are shown below.

  degrees of freedom: electronic, nuclear

  equations of motion: classical dynamics

  governing theory: quantum statistical mechanics

Details of both the techniques can be followed in various books and research articles. Hence, the author directs the readers to the following references[100-103].

2.5 Population Analysis:

A frequent object of quantum chemical studies is the determination of the electronic configuration and net charge associated with each atom in a polyatomic molecule.

Information concerning atomic charge distribution is important in rendering a chemical interpretation of the wave function, leading to a meaningful interpretation and an ability to draw analogies between different chemical phenomena. From *ab initio* computations, a set of delocalized orbitals is obtained. Many properties can be explained in this way (for example partial bonds, bond order) that might not be calculated in other ways.

In this study we have chosen Natural Population Analysis (NPA). This is an alternative to the popular Mulliken Population Analysis (MPA). NPA is based on methods for optimally transforming a given wave function into localized form, corresponding to the one-center ("lone pair") and two center ("bonds") elements of the chemist's Lewis structure picture. In natural bond orbital (NBO) analysis, the input atomic orbital basis set is transformed via natural atomic orbital and hybrids into natural bond orbital. It gives a better picture of structures containing metals than MPA[104].

2.6 DFT methods in ALD:

In this work we have used DFT to study the electronic and atomic structure of model systems for ALD reactions (Figure 13). Transition metals have been widely studied by Density Functional Theory[93,105]. GGA functional have been proved to perform better than LDA for transition metal elements, including copper[105].

ALD reactions computed with DFT are not an alien concept. There have been many reports on applying DFT to ALD reactions. The main obstacle is the size of the ALD system. ALD is a macroscopic surface phenomenon. A small size simulation of 10 molecules might give an insight to the basic science of the atoms or molecules but it fails to answer the question of growth rate, kinetics, conformity and uniformity of the system for long times. These problems can only be overcome by studying large systems. However, at present this is not possible at the DFT level due to the lack of computational power. One alternative to this is

using non *ab initio* calculations like force fields methods. However, the use of force fields ALD calculations is not much known as the potentials for the systems are not developed. This could open prospects for future study. ALD reactions have been studied with DFT for many binary compound depositions. For example oxides[106], especially Al_2O_3[107], nitrides[108], and sulfides[109] and also for metal deposition[56,110,111] has been studied. DFT can successfully answer a wide range of questions that are not accessible with experimental study. The areas broadly studied are mechanism for the reactions taking place[33,112-114], adsorption of the precursors[115], interaction with the substrate especially Si/SiO_2[11] system, DFT-assigned spectra in order to detect the by-products[116], densification over the surface[117](hydroxyl coverage[118], ligand coverage[119,120]), computing side reactions[121], and kinetics of the reaction[122].

In this thesis we use TURBOMOLE program for our calculations because it is one of the fastest and most stable codes available for standard quantum chemical applications. It also has reasonable time and memory requirements. The DFT method in TURBOMOLE is combined with ultra-efficient and numerically stable algorithms for faster, cheaper and efficient computation. We have used resolution-of-the-identity (RI) algorithm for our study. We have tested our systems with GGA (PBE, BP86) and Hybrid (B3LYP) functional and SV(P) and TZVPP basis sets. We find that that computed energy differences change with various functional and basis sets combinations. However, the overall conclusion does not change. Chapter 6, Table 24 and Chapter 7, Section 7.3.3 shows the difference in energy using different basis sets and functional. We find that using PBE functional and SV(P) basis set gives a good description of the structural properties of copper precursors. Detailed comparisons between the experimental and theoretical structures of the copper precursors are shown in Chapter 3, Table 6. In addition, using PBE functional and SV(P) basis set is also computationally cost effective as we perform an all electron calculation for all systems (gas phase ~ 25 atoms and surface ~ 80 atoms).

Broadly we have used thermodynamics to study our systems and compare the exothermic vs endothermic reaction energies. Although in our study there are no explicit calculations of kinetics, there are several cases of implicit evaluation of the activation barrier. For example we have performed MD calculations at 120 °C in some cases and we find significant reaction pathways within 2 ps. This might indicate little or no reaction barrier for the process (Chapter 4 – Figure 29, Chapter 9 - Figure 55). Also in some cases (Chapter 4 – Figure 26, 27, 30, Chapter 5- Figure 33,34) we see various reaction intermediates for any particular reaction, where only one intermediate or product is more stable compared to the others. The rest of the reacting intermediates that are higher in energy can be regarded as an activation barrier for the process.

The reactions studied here are under the umbrella of ALD. However, they are valid for many branches of science like alternative thin film deposition, electrochemistry and thus have a wider application.

Future challenges for modeling ALD reactions are:

- computing volatility of the precursors[85]. At the end of the thesis, in Chapter 10 we report a prospective pathway by which the volatility can be computed.
- Simulation of surface reactions and inter material interfaces.
- Precursor chemistry directing nanomorphology[85].
- Exploring properties of the material after ALD[31].

For future knowledge about ALD simulations with DFT, the author recommends a book chapter[85] and a review article[31] by Simon D. Elliott.

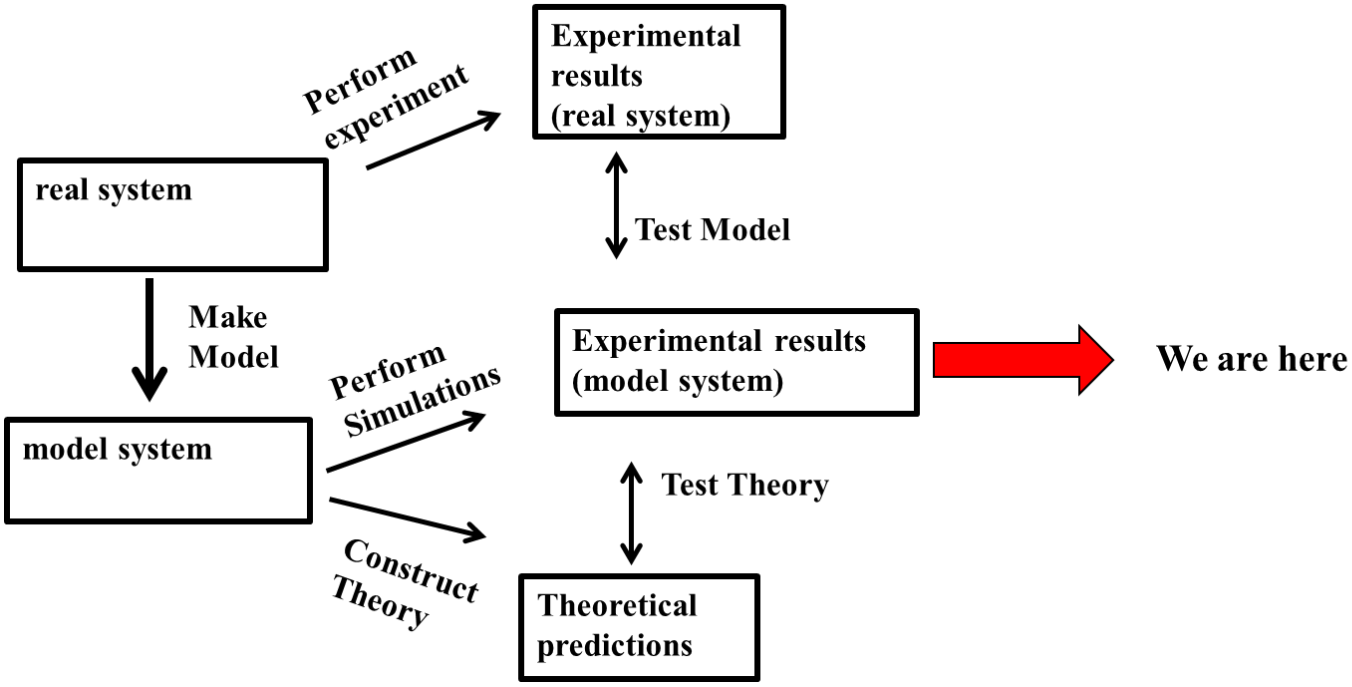


Figure 13: This scheme gives an overview of the parallelism of the real system and how we model and validate the computational techniques.

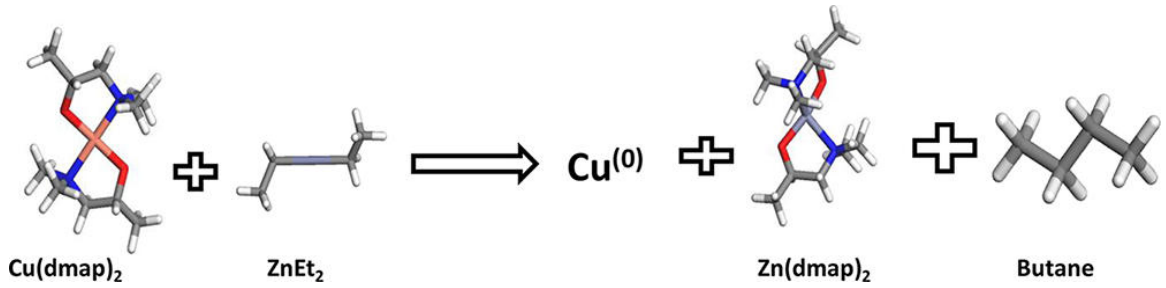
Organometallic Reducing Agents for Cu ALD

(Chapter 3 - 6)

Chapter 3: Mechanism for the atomic layer deposition of copper using diethylzinc as the reducing agent – a Density Functional Theory study using gas phase molecules as a model

This chapter was published in "Journal Of Physical Chemistry A" : It is available in *J. Phys. Chem. A*, 2012, *116* (35), pp 8893–8901 Authors: Gangotri Dey and Simon D. Elliott Copyright 2012. American Chemical Society.

The article can be found at: DOI 10.1021/jp304460z



Note: The paper has been modified for the thesis. The reference, table and figure numbers are in a sequence with the previous chapters. However, the equation numbers are only valid for this chapter.

Abstract: We present theoretical studies based on first principles density functional theory calculations for the possible mechanism of the atomic layer deposition (ALD) of copper by transmetallation from common precursors like $Cu(acac)_2$, $Cu(hfac)_2$, $Cu(PyrIm^R)_2$ R=^{i}Pr, R=Et, $Cu(dmap)_2$ and $CuCl_2$ where diethylzinc acts as the reducing agent. The effect on geometry and reactivity of the precursors due to the differences in electronegativity, steric hindrance and conjugation present in the ligands was observed. Three reaction types – disproportionation, ligand exchange and reductive elimination - have been considered that together comprise the mechanism for the formation of copper in its metallic state starting from the precursors. A parallel pathway for the formation of zinc in its metallic form has also been considered. The model Cu(I) molecule Cu_2L_2 has been studied, as Cu(I) intermediates at the surface play an important role in copper deposition. Through our study we see that accumulation of an LZnEt intermediate will result in zinc contamination either by the formation of Zn_2L_2 or metallic zinc. Ligand exchange between Cu(II) and Zn(II) should go via a Cu(I) intermediate, as otherwise it will lead to a stable copper molecule rather than copper metal. Volatile ZnL_2 will favor the ALD reaction as it will carry the reaction forward.

3.1. Introduction

A good replacement of the traditional reducing agents by an organometallic compound is reported by Lee *et al.*[29], who achieved copper deposition by the alternate and separate pulsing of copper dimethyl-2-propoxide $Cu(dmap)_2$ and diethylzinc at 120 °C. They have suggested that the precursor adsorbs on the surface through dipole-dipole interaction and have proposed the following transmetallation reaction:

$$Cu(dmap)_{2(g)} + ZnEt_{2(g)} \rightarrow Cu_{(s)} + Zn(dmap)_{2(g)} + butane_{(g)} \quad .....(1)$$

The by-products have been reported by them to desorb from the surface without decomposition at the low temperature. The use of a liquid co-reagent makes it possible to perform solution phase screening and so Vidjayacoumar *et al.*[75] have examined the

possibility of these kinds of ligand exchange reactions for deposition of copper from solution with organometallic reagents like trimethyaluminium and triethylborane as well as diethylzinc. They have also checked a wide range of ligands:

- copper(II) acetylacetonate $Cu(acac)_2$
- copper(II)hexafluoroacetylacetonate $Cu(hfac)_2$
- copper(II)N-isopropyl-2-pyrrolyl-aldiminate $Cu(PyrIm^{iPr})_2$ and
- copper(II)N-ethyl-2-pyrrolyl-aldiminate $Cu(Pyrlm^{Et})_2$.

Intermediates like LMEt (M= Cu, Zn, L= ligand), Cu_2L_2 and LEt have been detected in solution when diethylzinc was the reducing agent. Corresponding intermediates using trimethylaluminium and triethylborane were also detected in the solution phase study. They have come to the conclusion that diethylzinc is the best of the reducing agents due to its high reactivity compared to the other organometallic reagents that they have studied.

Understanding the mechanism of Cu ALD by transmetallation is the motivation for this work. The intermediates found during the course of analogous reactions in solution[75,123] give a first picture for the reaction pathway. However, an improved understanding of the mechanism at the atomic level will help us to find a better precursor and identify the problems related to existing organometallic reagents as the reducing agent. For this we have taken into consideration the same precursors used by Vidjayacoumar *et al.* along with the copper(II)dialkylamino-2-propoxide $Cu(dmap)_2$ that has been studied by Lee *et al.*. $CuCl_2$ data have also been calculated so as to find out about the simplest form of ligand. As co-reagent we consider diethylzinc. An assumption has been made here that all the ligands in the copper precursors are “innocent”, meaning that they themselves are neither oxidizing nor reducing[124].

In chemistry the reaction pathway is the step by step sequence of the elementary reactions by which overall chemical change occurs. Only the net chemical change is directly

observable for most chemical reactions and it is sometimes not possible to detect the individual steps. Atomic-scale calculations can be used to propose reactions pathways and assess their likelihood. In this paper, we use quantum chemical calculations of model molecules to analyze the various reaction pathways across a range of copper precursors. Exothermic (downhill) reactions are represented as negative reaction energies and are assumed to be more probable than endothermic reactions. In fact, the probability of a reaction occurring depends on how frequently the reacting species can meet each other during the pathway and also the free energy of activation of the reaction steps, which includes changes in geometry needed for activation. We have chosen model molecules to represent metal-ligand bonding at various reaction steps, but we are aware that the geometries do not resemble those of surface-bound species during ALD growth. Hence, we do not attempt to compute activation energies. Instead, our arguments are based on the impossibility of highly endothermic steps and the expected abundance of reactants and intermediates.

The transmetallation mechanism can be divided into three types of reactions as illustrated with the following:

- Disproportionation: $Cu(I)_2L_2 \rightarrow Cu(II)L_2 + Cu(0)$
- Ligand exchange: $CuL_2 + ZnEt_2 \rightarrow CuLEt + ZnLEt \rightarrow CuEt_2 + ZnL_2$
- Reductive elimination: $Et^- \rightarrow Et^+ + 2e^-$

One of the main aims in this work is to understand how these reactions combine in the overall ALD reaction (Eq.1) to form elemental copper. We also seek to find out whether alternative overall reactions are possible, such as:

$$CuL_{2(g)} + ZnEt_{2(g)} \rightarrow Cu_{(s)} + LZnEt_{(g)} + LEt_{(g)} \quad .....(2)$$

The formation of LEt and LZnEt as by-products is observed by Vidjayacoumar *et al.*[75,123] in solution phase, but these by-products have not been reported by Lee *et al.*[125] in the gas-surface ALD scenario. Through our study we see that Cu(I)L species (modelled by gas-phase

Cu_2L_2) are important intermediates and thus have been studied extensively. Another way for Cu to form is by disproportionation of the Cu(I) intermediate Cu_2L_2 but disproportionation involves no net transfer of electrons and hence cannot be a growth reaction.

3.2. Methods

3.2.1 Choice of Model Molecules:

Our focus in this study is on the differences in geometry and bonding strength of the various copper precursors. The precursor molecules CuL_2, $ZnEt_2$ and their ALD reaction products were modeled as isolated molecules in vacuum. We also used the gas-phase model to investigate molecules such as CuLEt and Cu_2L_2 that crudely resemble the oxidation state and bonding in likely reaction intermediates occurring on the growing surface during ALD. We have mainly considered the intermediates as proposed by Vidjayacoumar *et al.* in their work[123] along with other probable intermediate structures that can be formed but not detected experimentally. For example, one Cu(I) intermediate has been reported, *i.e.* Cu_2L_2, but as an alternative Cu_2LEt could also be formed during the reaction. We check the probability of formation of the intermediates through our calculation. A later study will develop a more realistic surface model (Chapter 4 - 5).

3.2.2 Computational Details:

The ground state electronic wave function of each molecule was calculated self-consistently within Kohn-Sham density functional theory (DFT) using the TURBOMOLE suite of quantum chemical programs[126,127]. We have described all atoms with all-electron basis sets, without the use of any effective core potential. The Perdew-Burke-Ernzerhof (PBE) functional[128] with the resolution-of-the-identity approximation (RI)[129,130] and valence double-zeta with polarization def-SV(P) basis set[131] was considered the most suitable level of calculation. No BSSE (Basis set superposition error) correction was required for a basis of this size. An even larger def-TZV(P)[129] basis set gives reaction energies that agree to less

than 10%, but are an order of magnitude more costly in computational time. For consistency, we will use the same SV(P) basis in our surface calculations, where computational requirements will be much higher. We validate our choice of basis set and functional by comparing with experimental data. For instance, in the case of $Cu(dmap)_2$, the calculations showed an expected level of agreement of the bond distances for Cu-O (1.91 Å theory, 1.86 Å exp) and Cu-N (2.09 Å theory, 2.06 Å exp)[132]. The coordination environment around copper is computed to be planar in this molecule, as observed by experiment.

All the neutral Cu(II) precursor molecules are open shell compounds (doublet spin, contamination <0.002) and the neutral $Cu(I)_2$ compounds are closed shell. The neutral Zn(II) and $Zn(I)_2$ compounds are closed shell compounds. The open shell compounds were computed using unrestricted DFT.

The entropy of selected precursors and the corresponding by-products has been calculated at 120 °C using vibrational analysis in TURBOMOLE[133]. This calculation helps us to determine the influence of temperature on the free energy of adsorption or desorption.

The most serious error in this gas-phase approach probably comes from using the isolated Cu(0) atom as a model for metallic Cu. Therefore to correct this, we have calculated both bulk Cu and the atom using a periodic code with the same density functional theory and we correct the gas-phase values by adding this energy difference $\Delta E(Cu_{(g)} \rightarrow Cu_{(s)})$ = -320 kJ/mol. The additional energy has been added to the reaction steps, which have metallic copper formation. To compute this energy, we have done a plane wave calculation using the VASP code[134] in which the valence electron states are expanded in a plane-wave basis set with an energy cutoff of 300 eV[135]. The electron exchange and correlation were treated within the same PBE functional. For the bulk $Cu_{(s)}$, k-point sampling is performed with 8×8×8 Monkhorst-Pack sampling grid. The bulk lattice constant is determined using the Murnaghan equation of state and agrees with the experimental value[136] within 6%, as is

typical of DFT. The same strategy has been employed for the reaction steps where metallic zinc is formed, although our interest is not in zinc formation *per se*.

3.3. Results

3.3.1.a Structure of Cu(II) and Zn(II) compounds

Selected parameters for the optimized structures of the Cu(II) precursors and the corresponding Zn(II) compounds are presented in Table 6. The computed bond lengths between metal and O are practically the same for the $M(acac)_2$ and $M(hfac)_2$ compounds (1.95-1.97 Å). As shown in Figure 14, the Cu complexes are planar (dihedral angle of 0-6° between four O atoms), consistent with the Cu(II):d^9 electronic structure, whereas the Zn analogues are distorted tetrahedral (dihedral angle ~75°), due to Zn(II):d^{10}. The computed structures of $M(dmap)_2$ are similar, although the M-O distance is shorter (1.89-1.91 Å), consistent with more anionic O. The computed frequency for the vibration of the Cu(II) atom out of the plane is 43 cm^{-1} for $Cu(dmap)_2$ and 34 cm^{-1} for $Cu(acac)_2$ precursors.

Bonding in the pyrrolylaldiminates is quite different. For $Cu(PyrIm^R)_2$ precursors, the bond length from Cu to the pyrrole nitrogen (1.98 Å) is smaller than that to the imine nitrogen (2.04-2.06 Å), but it is the reverse in the corresponding zinc compound (2.06 Å and 2.00-2.01 Å respectively). This indicates different resonance forms of the ligand when bound to Cu versus Zn, although there is probably substantial delocalization of negative charge in both cases within the plane of the ligand backbone. The $Cu(PyrIm^R)_2$ complexes are distorted substantially out of planarity around the Cu center (dihedral angles 45 ° and 33 ° for R=^{i}Pr and R=Et respectively), which is likely to cause strain in the electronic structure. Finally the monodentate complexes are computed to be bent ($CuEt_2$) or linear ($CuCl_2$, $ZnEt_2$, $ZnCl_2$).

3.3.1.b Structure of Cu(I) and Zn(I) compounds

One of the proposed intermediates for the reaction is Cu_2L_2[123]. We find that these are Cu(I) compounds, most stable when computed as closed shell singlet. As reported in other works

on copper precursors,[123,137] Cu_2L_2 are an interesting set of compounds, occurring in a variety of structures in terms of dihedral angle and intra-molecular Cu-Cu distance. The common feature is linear coordination about the Cu(I):d^{10} center. Our structural results for dimeric Cu(I) complexes using the same ligands and their Zn(I) analogues are shown in Table 7 and depicted in Figure 15. The intra-molecular Cu-Cu distance is short (2.4-2.5 Å, L=dmap, PyrIm), suggesting a bonding interaction, or longer in the case of a Cu-O-Cu bridge (3.0-3.1 Å, L=acac, hfac). In the cases of L=acac and L=hfac, one side of each bidentate ligand forms the Cu-O-Cu bridge and the complex is planar. By contrast, each ligating atom in L=dmap and L=PyrIm is coordinated to just one metal center and the resulting structures are distorted out of planarity (e.g. 24 ° Cu-N-N-Cu dihedral angle for L=$PyrIm^{iPr}$), probably due to steric interaction in the ligand sphere (Figure 14). The out of plane vibration of Cu atom in $Cu_2(dmap)_2$ is computed to have a frequency of 44 cm^{-1}. It is interesting to note the near-identical Cu-N distances in the pyrrolylaldiminates (1.88-1.90 Å) that indicate equal charge on the N atoms in the Cu(I) dimer. Overall we see that similar kinds of precursors have similar structures: $Cu_2(acac)_2$ and $Cu_2(hfac)_2$ can be grouped together and $Cu(PyrIm^R)_2$ R=^{i}Pr and R=Et can form another group.

Another set of Cu(I) and Zn(I) compounds that can be formed are Cu_2LEt and Zn_2LEt. These compounds have not been reported by the experimental group. However, the probability of the occurrence of corresponding surface species cannot be ignored. Here we discuss their probable structures and later their thermodynamic stability during the ALD reaction. Two Cu atoms in Cu_2LEt are bonded to the ligand and one of them to the Et group. The two Cu atoms are themselves joined by a bond of length 2.28-2.30 Å. The structures for L=dmap and L=$PyrIm^{iPr}$ are shown in Figure 15. The structure is similar to the above Cu(I) structure of Cu_2L_2 except that here one ligand has been replaced by the Et group on one Cu atom. The corresponding structure for Zn_2LEt is very different from copper, which may

illustrate that zinc prefers to be in +2 or 0 oxidation state. The optimized structure shows that the ligand and Et are bonded to the same Zn atom (probably +2 oxidation state), whereas the other Zn atom has no ligands (oxidation state zero) and is bonded only to Zn (Figure 17).

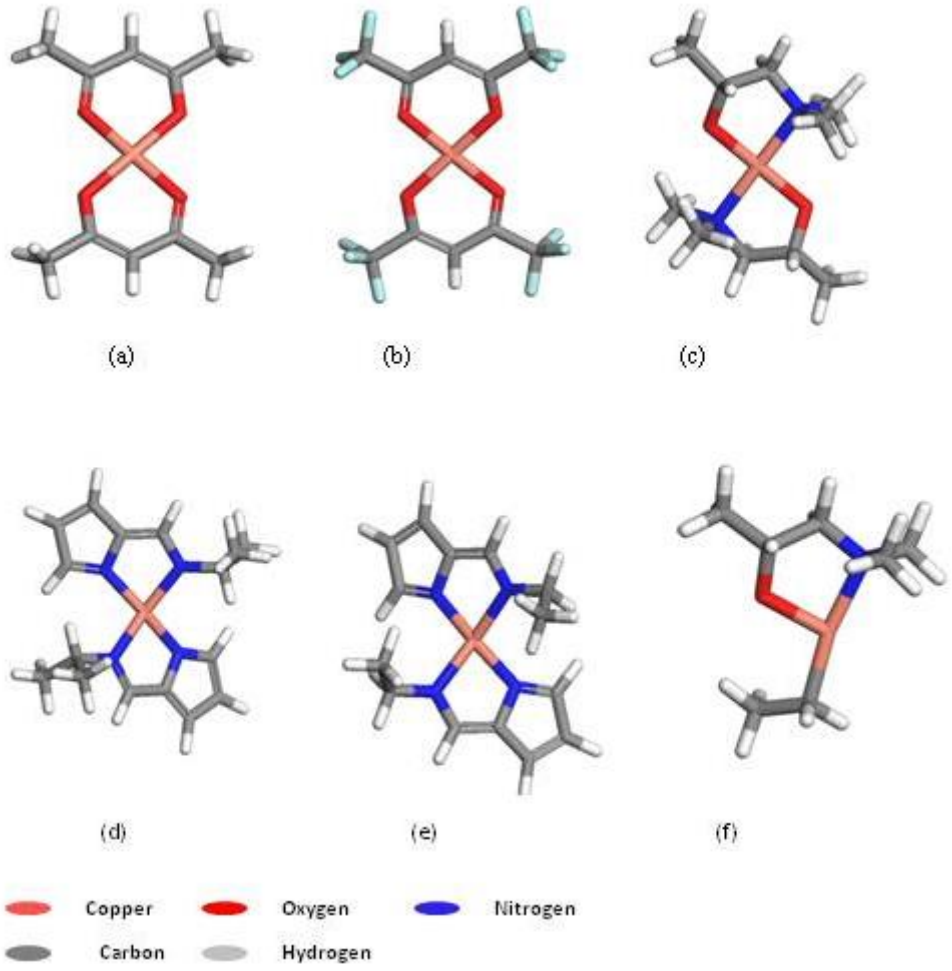


Figure 14: Stick representation of computed structures of precursors and intermediates. (a) $Cu(acac)_2$, (b) $Cu(hfac)_2$, (c) $Cu(dmap)_2$, (d) $Cu(PyrIm^{iPr})_2$, (e) $Cu(PyrIm^{Et})_2$ are the precursors used to understand the mechanism. (f) Cu(dmap)Et is a sample intermediate during the course of the reaction. The Zn by-products are similar to these structures, where the Cu atom is replaced with Zn. Quantitative differences in structure between the copper precursor and the zinc by-product are given in Table 6.

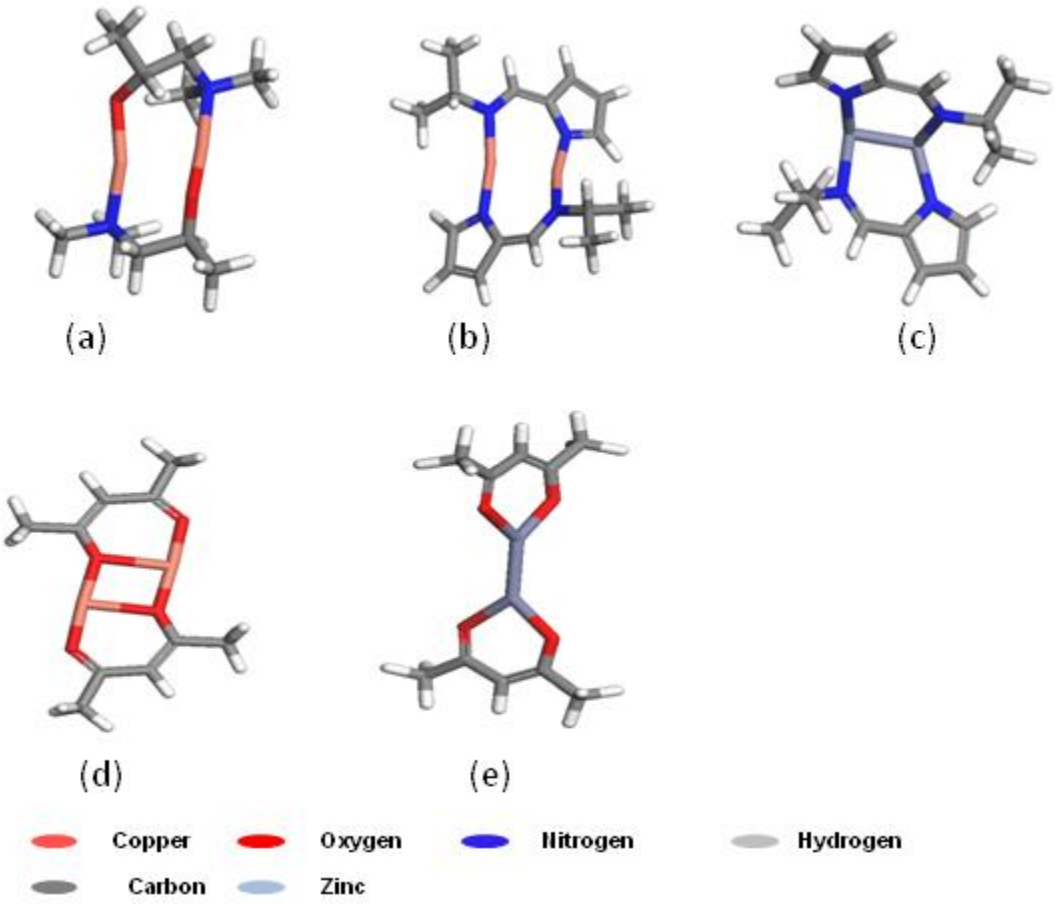


Figure 15: Stick representation of computed structures of intermediates of the type Cu_2L_2. (a) $Cu_2(dmap)_2$ (b) $Cu_2(PyrIm^{iPr})_2$ and (c) $Zn_2(PyrIm^{iPr})_2$ are nonplanar structures and (d) $Cu_2(acac)_2$ (e) $Zn_2(acac)_2$ are planar.

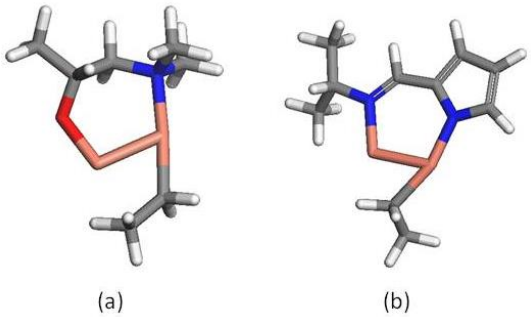


Figure 16: Cu_2LEt compounds where (a) L=dmap and (b) $L=PyrIm^{iPr}$

3.3.1.c Entropy

The computed entropy of the precursor and the by-products is reported in Table 8. The data show approximately equal entropy for zinc and copper molecules, indicating similar trends in adsorption or desorption with temperature. This is undesirable from the ALD viewpoint, as the zinc compounds might co-deposit along with the copper compounds. The butane molecule has less entropy than LEt and so is less sensitive to thermal effects during desorption. Breaking down the entropy calculation, we see that there is a contribution of ~33% from translational motion, ~27% from rotational motion and ~40% from vibrational motion in most of the cases.

3.3.2 Reaction Mechanism

Copper compounds: The computed energetics of the proposed reaction steps are listed in Table 9. Our starting point is the interconversion of Cu(0), Cu(I) and Cu(II) when complexed to the various ligands. Considering step I, we see that disproportionation of $Cu(I)_2L_2$ into $Cu(0)_{(s)}$ and $Cu(II)L_2$ is thermodynamically favored when L=acac, hfac, dmap and Et. For both L=PyrIm complexes on the other hand, the data show a driving force for $Cu(II)L_2$ to be reduced to $Cu(I)_2L_2$ in the presence of Cu(0), as might occur on adsorption onto a Cu surface during ALD.

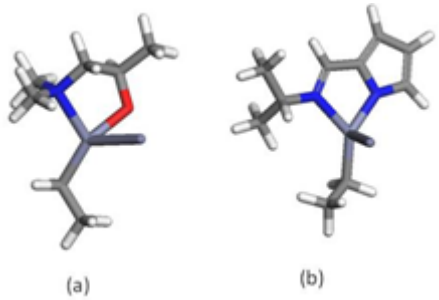


Figure 17: Zn_2LEt compounds with (a) L=dmap and (b) L=$PyrIm^{iPr}$.

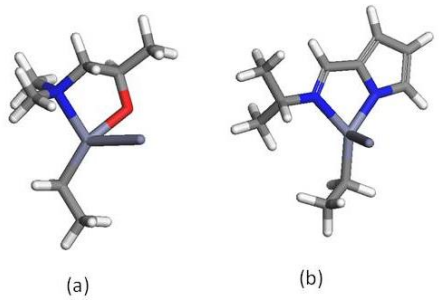


Figure 18 : Zn_2LEt compounds with (a) L=dmap and (b) L=$PyrIm^{iPr}$.

We assume that none of the ligands are reducing agents except Et^- and the simulations support this assumption. Reduction of copper is therefore only possible after exchanging a non-reducible ligand L for Et from Zn. Steps II and III in Table 4 are stepwise ligand exchange reactions for Cu(II) and Zn(II). The reactions are energetically neutral (within ±10 kJ/mol) for L=acac and $PyrIm^{iPr}$ and show moderate exothermicity and endothermicity (<20 kJ/mol) in both steps for L=hfac and $PyrIm^{Et}$ respectively, implying that the changes in bonding in Cu(II) and Zn(II) are quite evenly matched. $Cu(dmap)_2$ is seen to resist exchange of its first ligand by 50 kJ/mol, but not its second. The opposite is the case for L=Cl, where exchange of the first ligand is favored, but not the second. By contrast, exchanging L and Et between Cu(I) and Zn(II) (both d^{10}) is found to cost energy for all ligands, ranging from +9 kJ/mol for L=acac to +97 kJ/mol for L=$PyrIm^{iPr}$ (steps IV and V, Table 9).

Steps VII-X are possible redox reactions by which the Et^- ligand is oxidized to cationic Et^+, combines with an anion and is eliminated, while the Cu(II) or Cu(I) center is reduced to Cu(I) or Cu(0). The computed energetics for $CuEt_2$ form a baseline: reduction from Cu(II) to Cu(I) yields -226.4 kJ/mol per Cu (step VII or IX) and further reduction from Cu(I) to solid Cu(0) yields -388 kJ/mol (step X), with butane ("Et-Et") as the by-product.

Table 6: Optimized structural parameters of the copper precursors CuL_2 and their corresponding zinc compounds ZnL_2. The dihedral angle is between the four coordinating atoms of the ligand, for example in $Cu(acac)_2$ the angle is between the four oxygen atoms ∟O-O-O-O.

	Bond Length (Å) CuL_2			Dihedral Angle (°) CuL_2		Bond Length (Å) ZnL_2			Dihedral Angle (°) ZnL_2	
		Theory	Exp	Theory	Exp		Theory	Exp	Theory	Exp
$M(acac)_2$	Cu-O	1.95	1.92[75]	0.1	Sq. Planar[75]	Zn-O	1.96	1.99-2.03[138]	76.0	88.5[138]
$M(hfac)_2$	Cu-O	1.95	-	6.0	Sq. Planar[75]	Zn-O	1.97	-	74.7	-
$M(dmap)_2$	Cu-O Cu-N	1.91 2.09	1.86 2.06[132]	0.6	Sq. Planar[132]	Zn-O Zn-N	1.89 2.19	-	51.0	-
$M(PyrIm^R)_2$ R=iPr	Cu-N_{pyr} Cu-N_{im}	1.98 2.04	1.93-1.94 (R=nPr) 1.97-2.00[67]	45.0	45-55[75]	Zn-N_{pyr} Zn-N_{im}	2.06 2.01	-	78.9	-
$M(PyrIm^R)_2$ R=Et	Cu-N_{pyr} Cu-N_{im}	1.98 2.06	1.93-1.94 (R=Me) 2.00-2.01[67]	33.0	32-33[67]	Zn-N_{pyr} Zn-N_{im}	2.06 2.00	-	88.0	-

Table 7: Computed structural parameters for intermediate species Cu_2X_2 and Zn_2X_2. The dihedral angle is between the two coordinating atoms of one ligand and the copper atoms, for example in $Cu_2(acac)_2$ the angle is between two oxygen atoms of one acac and the copper atoms ∟Cu-O-O-Cu.

	Cu-N/Cu-O (Å)	Cu-Cu (Å)	Dihedral Angle (°)	Zn-N/Zn-O (Å)	Zn-Zn (Å)	Dihedral Angle (°)
$M_2(acac)_2$	Cu-O : 1.88	3.04	0.6	Zn-O : 1.98	2.33	0.6
$M_2(hfac)_2$	Cu-O : 1.89	3.11	0.4	Zn-O : 2.00	2.33	0.35
$M_2(dmap)_2$	Cu-O :1.83/1.86 Cu-N:1.96/1.99	2.48	18.1	Zn-N : 1.90 Zn-O : 2.21/3.10	2.35	9.59
$M_2(PyrIm^R)_2$ R=^{i}Pr	Cu-N_{pyr}: 1.88 Cu-N_{im} :1.90	2.44	24.2	Zn-N_{pyr} : 2.00 Zn-N_{im} : 2.10	2.28	6.68
$M_2(PyrIm^R)_2$ R=Et	Cu-N_{pyr}: 1.88 Cu-N_{im} :1.90	2.45	22.9	Zn-N_{pyr}: 2.03 Zn-N_{im} : 2.07	2.28	7.78

Table 8: Computed entropy (kJ/mol/K) of the precursors and the corresponding by-products calculated at 120 °C.

Ligand (L)	CuL_2	ZnL_2	LEt
acac	0.61	0.69	0.50
dmap	0.69	0.70	0.48
$PyrIm^R$ R=^{i}Pr	0.78	0.79	0.55
$PyrIm^R$ R=Et	0.71	0.72	0.50
Et	0.44	0.40	0.34

Table 9: Mechanism for the copper ALD is divided into three classes of reaction: ligand exchange, reductive elimination and disproportionation. The various reaction energies computed for different precursors are presented here.

Reaction		Step	ΔE (kJ/mol)						
			L=acac	L=hfac	L=dmap	L=PyrIm^{R} R=^{i}Pr	L=PyrIm^{R} R=Et	L=Cl	L=Et
Disproportionation	Cu_2L_2 → Cu+ CuL_2	I	-31.4	-12.6	-34.6	71.3	61.1	21.4	-75.0
Ligand exchange for Cu(II)-Zn(II)	CuL_2 +$ZnEt_2$ → LZnEt +LCuEt	II	4.7	-6.0	49.5	0.3	18.9	-34.9	
	LZnEt +LCuEt → $CuEt_2$ + ZnL_2	III	-3.9	-14.9	2.6	-2.9	19.1	21.2	
Ligand exchange for Cu(I)-Zn(II)	Cu_2L_2 + $ZnEt_2$→LZnEt + Cu_2LEt	IV	43.0	44.0	47.6	51.9	51.1	33.2	
	Cu_2LEt + LZnEt → Cu_2Et_2 + ZnL_2	V	9.2	27.3	39.7	96.9	84.1	49.4	
Ligand Exchange for Cu(II)-Cu(II)	2CuLEt → CuL_2 + $CuEt_2$	VI	1.6	16.8	-48.2	5.0	-11.3	20.3	
Reductive elimination	2LCuEt → Cu_2L_2 +Et-Et	VII	-268.3	-272.0	-315.0	-367.1	-373.1	-302.4	-226.4
	LCuEt → Cu + LEt	VIII	-73.5	-74.3	-164.9	-109.1	-160.7	-164.3	-331.1
	2LCuEt → Cu_2LEt + LEt	IX	26.2	18.3	-102.3	-98.2	-159.0	-87.7	-226.4
	Cu_2LEt → 2Cu + LEt	X	-143.2	-136.8	-197.5	-90.0	-132.4	-211.2	-388.3
Decomposition reaction	LEt → LH + C_2H_4	XI	38.5	59.7	149.3	152.6	113.9	125.7	147.9

Table 10: Mechanism for the copper ALD is divided into three parts: ligand exchange, reductive elimination and disproportionation. The various reaction energies are presented here for Zn compounds

Reaction		Step	ΔE (kJ/mol)						
			L=acac	L=hfac	L=dmap	L=PyrIm^R R=iPr	L=PyrIm^R R=Et	L=Cl	L=Et
Disproportionation	Zn_2L_2 → Zn + ZnL_2	I	65.2	73.6	2.4	-83.3	-100.1	86.8	32.7
Ligand exchange for Zn(II)-Cu(II)	ZnL_2 + $CuEt_2$ → LZnEt +LCuEt	II	-3.9	-14.9	2.6	-2.9	19.1	-21.2	
	LZnEt + LCuEt → CuL_2 + $ZnEt_2$	III	4.7	-6.0	49.5	-0.3	18.9	34.9	
Ligand exchange for Zn(I)-Cu(II)	Zn_2L_2 + $CuEt_2$ → LCuEt + Zn2LEt	IV	140.7	119.7	-29.1	-110.0	-109.2	16.5	
	Zn_2LEt + LCuEt→Zn_2Et_2 + CuL_2	V	-116.8	-87.8	-9.2	-23.3	-48.2	51.2	
Ligand exchange for Zn(II)-Zn(II)	2ZnLEt → ZnL2 + $ZnEt_2$	VI	-2.4	4.2	-3.9	-2.4	-26.7	35.8	
Reductive elimination	2LZnEt → Zn_2L_2 + Et-Et	VII	-94.6	-96.4	-33.3	54.0	46.4	-78.0	-59.7
	LZnEt → Zn + LEt	VIII	224.5	219.3	138.1	189.9	136.0	154.0	154.5
	2LZnEt → Zn_2LEt + LEt	IX	303.9	280.3	104.0	166.1	107.7	105.4	-59.7
	Zn_2LEt → 2Zn + LEt	X	145.1	158.2	172.1	213.8	164.3	203.6	203.6

Considering the other ligands in a mixed complex of the type Cu(II)LEt, step VII is the redox reaction Cu(II)→Cu(I)+butane. The computed energies are very negative for all L (-134 to -186 kJ/mol of Cu), meaning that the reaction is highly thermodynamically favored, even more so than $CuEt_2$. This can be traced back to the tendency for disproportionation of the various Cu_2L_2 complexes. The most exothermic reactions are for the pyrrolylaldiminates. Alternatively, LEt can be produced from such mixed complexes by the complete reduction Cu(II)→$Cu(0)_{(s)}$ (step VIII) and this is somewhat less thermodynamically favorable (-73 to -165 kJ/mol-Cu). It is to be noted that in PyrIm cases, it is favored for the Et^+ to be attached to the N_{pyr} and not N_{im}. Butane (step VII) is therefore the thermodynamically favored by-product of reductive elimination from two neighboring Cu(II)LEt. Step VIII can be broken down into step IX producing Cu(I) followed by step X. So, by construction, step VIII is half the reaction energy of the sum of step IX and step X. Loss of LEt from Cu(II) complexes (step IX) is favored only for L=dmap, PyrIm, and with a lower ΔE than loss of butane (step VII). Loss of LEt from Cu(I) complexes (step X) is favored for all L. Of course, there is an unknown kinetic barrier associated with the structural and electronic changes needed to bring Et^+ to bond with O or N of the ligand L so as to form LEt.

Zinc compounds: Even though they may not be desirable in ALD, the same reactions are in principle possible for Zn as for Cu, and the computed data for Zn complexes are shown in Table 10. To the best of our knowledge, Zn(I) complexes have not yet been isolated and they are therefore only regarded as potential intermediates in this reaction mechanism.

Disproportionation (step I) of Zn_2L_2 is thermodynamically favored for both PyrIm ligands (ΔE=-83 and -100 kJ/mol of Zn_2L_2), is energetically neutral for L=dmap and is not favored for L=acac, hfac, Cl and Et. The ligands thus behave in roughly the opposite way compared

with disproportionation of Cu. In particular, ΔE=+33 kJ/mol for Zn_2Et_2 means that the reverse reaction – ligand transfer from $ZnEt_2$ to Zn(0) – will be favored.

Clearly, the energetics for ligand exchange from Zn(II) to Cu(II) (steps II and III, Table 9) must by definition mirror those for Cu(II) to Zn(II) (Table 10). However there are some differences for Zn(I)/Cu(II) ligand exchange (steps IV and V), which can be exothermic in both steps (L=PyrIm), near neutral (L=dmap) or endothermic in the first step and exothermic in the second (L=acac, hfac). We find both Zn(I) and Cu(II) to have unpaired electrons on the metal center.

Reductive elimination of ligands from Zn complexes is also substantially different to that from Cu. The baseline values for decomposition of $ZnEt_2$ to $Zn(0)_{(s)}$ (+155 kJ/mol per Zn, step VIII) and Zn_2Et_2 to $Zn(0)_{(s)}$ (+102 kJ/mol-Zn, step X) show that reduction to Zn metal and butane is not favorable, unlike Cu. In line with this, the calculations show that reductive elimination from most Zn-L complexes is endothermic. The reduction reaction forming butane is moderately favored in some cases (step VII: -95, -97 and -33 kJ/mol for L=acac, hfac, dmap respectively) but not for L=PyrIm, in contradiction of the trend for Cu-L. As in the case of Cu, the formation of butane is favored over formation of LEt as the by-product of reduction of Zn.

3.4. Discussion

3.4.1 Geometry of the compounds:

Cu(II) complexes favor a planar geometry because of the Cu(II): d^9 electronic configuration, but in molecules like $Cu(PyrIm^R)_2$, high steric hindrance between the two rigid ligands means that the molecules distort out of planarity. These effects are explained by Raithby *et al.*[139]. In the Cu_2L_2 compounds the Cu-O/N bonds are shorter (and hence probably stronger) than those of the CuL_2 counterparts, despite lower cationic charge on Cu. This seems to reflect less steric hindrance between ligands that are arranged around a

larger core of two Cu atoms. In addition, each Cu(I):d^{10} adopts linear coordination that is more flexible than the planar Cu(II) case. In this way, we see that L=PyrIm favors Cu(I) over Cu(II), explaining the driving force towards partial reduction in the presence of bulk Cu(0) (reaction steps VII and IX) and against disproportionation (step I, Table 9). L=acac, hfac also have a rigid backbone, but in contrast with L=PyrIm, the CH_3 and CF_3 groups are arranged away from the Cu(II) centre and cause less steric hindrance. L=dmap is also relatively flexible within the Cu(II) coordination sphere. This means that there is little distortion out of planarity, and hence less driving force towards reduction of Cu(II) for L=acac, hfac and dmap. It is therefore favorable for Cu_2L_2 to disproportionate into CuL_2 and Cu(0) in these cases and this may be a route by which Cu(0) is formed. We speculate that the planar precursors with rigid ligands $Cu(acac)_2$ and $Cu(hfac)_2$ may resist the distortion that would be necessary for the Cu center to approach a planar substrate and adsorb. Instead of adsorbing via the copper atom, an alternative adsorption mode for all CuL_2 would be via the ligand, which because it is bidentate could bridge surface-Cu and adsorbate-Cu. Explicit calculations of molecule surface adsorption will be needed to clarify these points.

The Cu(I) intermediates Cu_2L_2 have various bonding characteristics. In case of PyrIm and dmap precursors, the ligand binds to two copper atoms. The bonding in case of acac type precursors is different: the ligand not only binds to the two copper atoms but one of the ligand O atoms bridges two copper atoms at the same time. The metal-ligand bond lengths are different in each of the cases, as stated in Table 6. The molecule that appears to be least rigid is $Cu_2(dmap)_2$. This may mean that the dmap precursor can be adsorbed onto a surface via a Cu(I) intermediate more easily than the others. This is due to the absence of conjugation in the ligand as well as less steric hindrance between ligands.

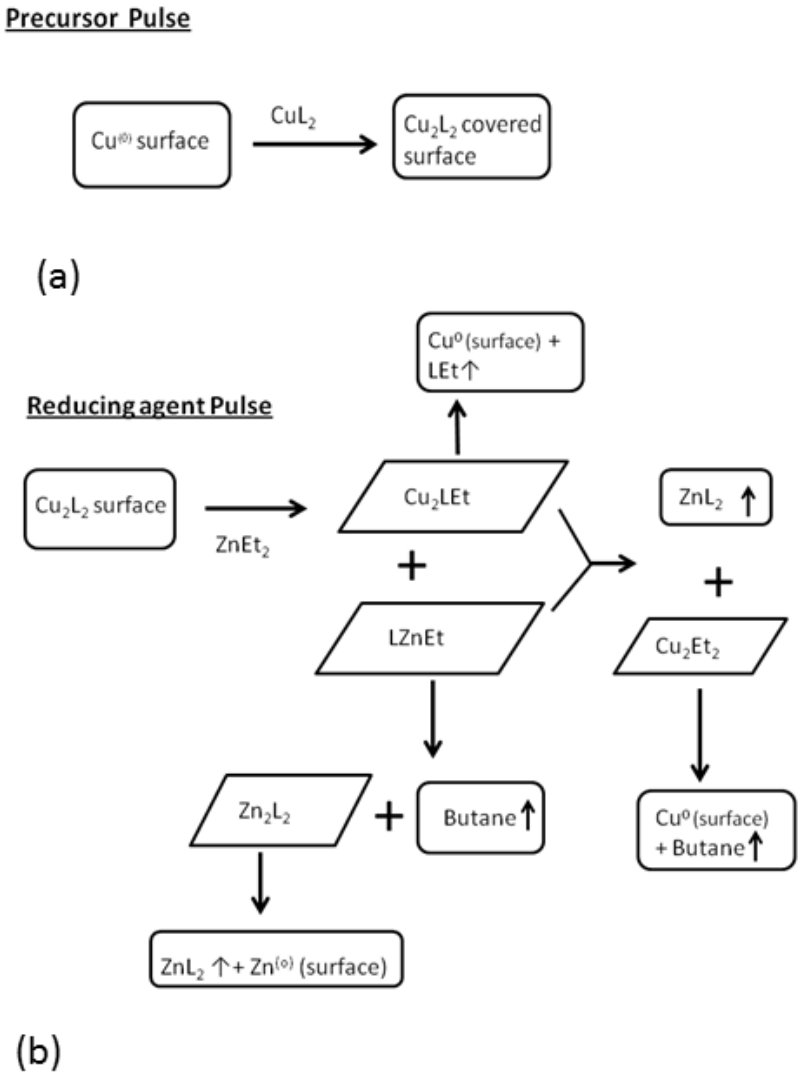


Figure 19: (a) and (b) shows the flow chart to depict the possible ALD mechanism for both the precursor pulse and the reducing agent pulse respectively. Rectangular shapes denote the starting reagents and the end products and slanted boxes denote the intermediates. The upward arrow designates desorption of volatile species.

3.4.2 Reactions

The most thermodynamically favorable gas phase reactions in both the pulses are depicted in Figure 19. It shows a general overview of the reactions that might take place irrespective of the precursors used.

Precursor Pulse - In an ALD reaction, during the first pulse of the precursor over the surface, the copper might comproportionate from Cu(II) in the precursor and from Cu(0) of the surface to form a Cu(I) dimer, as seen in the reverse case of step I in Table 9. The possibility for this reaction to occur is high for the PyrIm precursors as shown by its exothermicity and low for acac, hfac and dmap precursors (small endothermicity). Therefore, after the precursor pulse, a saturated Cu(I) surface is expected, especially for PyrIm. These data reveal nothing about kinetics; there might be differences in the rates of reaction and in the time needed to saturate Cu(I) over the surface. The reverse reaction, disproportionation, might take place during the purge step as the excess CuL_2 is purged out of the system. Here acac, hfac and dmap are the most likely precursors to undergo this reaction and revert to Cu(0).

Reducing agent pulse - During the reducing agent pulse, diethylzinc approaches a surface saturated with Cu(I). It can follow the slightly endothermic reaction (step IV) to yield Cu_2LEt and LZnEt. The following reaction (step V) can only take place if the product ZnL_2 is very volatile and can be easily purged out of the system. Judging by the thermodynamics of the reactions, we can say that step V is probably less favorable for PyrIm precursors than for the rest of the precursors. However, we see from Table 9 that the ligand exchange for Cu(II) (steps II and III) is more favorable than for Cu(I) (steps IV and V) in most of the cases of the different precursors that have been studied here. Thus, if unreacted Cu(II) precursor is left in the system, it will undergo half ligand exchange to produce LCuEt and LZnEt. Further, a competition between reductive elimination and ligand exchange will arise (step III and step VII). If reductive elimination is kinetically faster than ligand exchange, it will produce a Cu(I) saturated surface, which we denote Cu_2L_2. On the other hand, if reductive elimination is slower than ligand exchange, there is the possibility of complete exchange to give $CuEt_2$ and ZnL_2 (step III).The probability of ligand exchange can be increased by increasing the

concentration of diethylzinc in this case. If the produced ZnL_2 is volatile, it will drive step III forwards following Le Chatelier's principle. The $CuEt_2$ product is stable against reduction and hence step III reduces the probability of formation of copper metal. Hence, we can say that a complete ligand exchange between Cu(II) and Zn(II) without the intermediate formation of Cu(I) is to be avoided due to the formation of stable $CuEt_2$ at the end of the reaction.

The simultaneous formation of Cu_2Et_2 along with ZnL_2 in step V helps in the formation of metallic copper, since Cu_2Et_2 can then undergo reductive elimination (as seen in step X when L=Et) to yield butane and metallic copper. In case the products of step IV, Cu_2LEt and LZnEt, are allowed to accumulate at the surface, Cu_2LEt will probably dissociate to give metallic copper and LEt, as all these reactions for the different ligands are exothermic in nature. However, LZnEt might form the dimer Zn_2L_2 and butane gas as seen in step VII. The dimer Zn_2L_2 might accumulate in the system for acac and hfac type precursors but it will disproportionate into Zn and ZnL_2 for the rest of the precursors. Thus there is more probability of Zn contamination in the case of PyrIm type precursors.

In all the reactions quoted in Table 9 and Table 10, we find that the most thermodynamically-preferred by-product is butane rather than LEt for similar types of reaction (step VII and step VIII). However, the probability of formation of LEt cannot be ignored as the computed reaction energy is exothermic. Of course, kinetics and surface concentrations will dictate which product actually occurs; *i.e.* whether LEt eliminates from a single LCuEt unit (step VIII) or whether butane can form from adjacent 2LCuEt (step VII). Entropy data show us that once the LEt is formed then it has more probability of being desorbed from the surface at elevated temperatures, as it has higher entropy. Thus, if LCuEt is not allowed to accumulate in the system, LEt formation is favorable. The LEt has some probability of decomposing into LH and C_2H_4 (step IX) but in all the cases for different

precursors we see that this reaction is less favored, with the reaction energy increasing from acac type precursors to the PyrIm type.

We conclude that the surface after the reducing agent pulse in ALD is saturated with either Cu_2Et_2 or Zn_2L_2 type species. Cu_2Et_2 is unstable and gives metallic copper and diethylcopper. Reduction of Cu(II) to Cu(0) is generally energetically favored over reduction of Zn(II) to Zn(0) as observed in step I and VIII in Table 9 and Table 10.

As the concentration of ligands and metals changes on the surface during an ALD experiment, we expect different reaction steps to predominate. For instance, we expect complete copper ligand exchange to be favored when diethylzinc is in excess during the reducing agent pulse as seen in steps III and V. The likely by-products are butane (after the decomposition of Cu_2Et_2 as seen in step X), ZnL_2 and some $CuEt_2$. On the other hand, the high concentration of CuL_2 in the Cu precursor pulse will cause reductive elimination of Et fragments resulting in Cu(I) species like Cu_2L_2 or Cu_2LEt as in steps VII and IX. The probable by-products are LEt and butane. Thus we see the pathway that was proposed by Lee *et al.*[29] for the formation of copper in its metallic form, equation (1), is only favored when there is an excess of the reducing agent $ZnEt_2$.

Choice of ligands: During exposure to PyrIm precursors, the formation of a Cu(I) intermediate on the surface is favorable, but in the subsequent reducing steps, the co-deposition of zinc metal along with copper is likely to take place. Thus, although PyrIm precursors enjoy the benefit of not having any oxygen in the ligand, which reduces the probability of formation of copper oxide in any of the steps, the probability of zinc formation is high. We suggest that this can be avoided if the LZnEt intermediate is not allowed to accumulate in the system. For instance, a volatile ZnL_2 by-product might carry reaction step V in the forward direction and thus prevent the accumulation of LZnEt.

For acac and hfac precursors, the initial step of formation of Cu_2L_2 might be slow as the computed model reaction is endothermic. During the reducing agent pulse, the formation of copper in its metallic form is probably favorable as the important reaction steps in our model are exothermic in nature. However, a saturated surface of Zn_2L_2 is expected along with copper metal.

The dmap precursor follows the same trend as the acac and the hfac precursors. Here a simultaneous co-deposition of copper and zinc is likely, although the copper deposition is favored in terms of reaction energy.

Based on this study of the transmetallation reaction with diethylzinc, we suggest that one of the best methods of improving the transmetallation reaction at low temperatures is to choose a ligand that makes the ZnL_2 species very volatile. If this molecule can be continuously purged out of the system it will drive the reaction forward and simultaneously produce Cu(0). Accumulation of LZnEt might prove harmful as it might dimerize to give Zn_2L_2, which dissociates to give zinc metal in cases like PyrIm and also forms a saturated surface of Zn_2L_2 in other cases.

Transmetallation can also be improved by choosing a metal in the reducing agent which is less likely to be co-deposited along with copper, i.e. the metals far away from copper in the electrochemical series. Reducing agents containing transition metals like vanadium, chromium or manganese might be helpful.

A complete ligand exchange with diethylzinc is to be avoided as it will lead to the formation of $Cu(II)Et_2$, which is stable and hence does not give metallic copper. Therefore the formation of copper via a Cu(I) intermediate should be targeted and this can be achieved by reductive elimination of Cu(II) intermediates to give either butane or LEt gaseous by-products.

None of the precursors studied here is ideal as they all have advantages and disadvantages. We find that the dmap precursor is preferred over the others due to the flexibility of the ligand, less probability of co-deposition of the zinc metal and exothermic reaction energies in the important reaction steps.

3.5. Conclusion

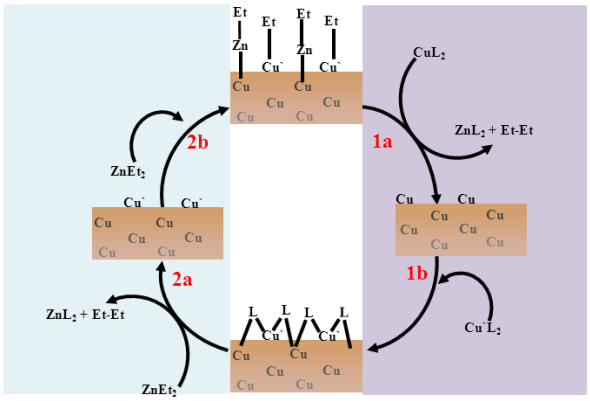
We have used DFT to study the geometry and energetics of precursors and model intermediates during the reaction steps involved in the transmetallation ALD of Cu using diethylzinc. The reaction steps are disproportionation, ligand exchange and reductive elimination. We have investigated the effect of various ligands or the ethyl group on the stability of intermediates and by-products, including those of Cu(II), Cu(I) and Cu(0) via model molecules. Through our study we have seen that the choice of precursor ligand (L) strongly affects the structure of the $Cu(I)_2L_2$ intermediate, which plays a decisive role in determining the mechanism of copper deposition. However similar kinds of ligands can be grouped together and have similar features.

After the Cu(II) precursor pulse we predict that the surface is probably covered with a Cu(I)L-like intermediate. During the reducing agent pulse, a complete ligand exchange between Cu(II) and Zn(II) is to be avoided as it will result in a stable $CuEt_2$ compound, i.e. without the formation of a Cu(I) intermediate. The formation of butane gas (Et-Et) is more likely than LEt as a by-product. When ZnL_2 is volatile it will carry the reaction forward. Contamination of the film can occur in the form of adsorbed Zn(L)-like intermediates or Zn in its metallic state. Thus, although the proposal to use an organometallic reagent as the reducing agent for copper ALD was an innovative idea by Lee *et al.*[29], the specific use of diethylzinc may result in zinc contamination as zinc is close to copper in the electrochemical series. Other reducing reagents which have metals far away from copper in the series should be considered as alternatives. The above reaction pathway shows the difference between the

commonly used precursors. The electronegativity, steric hindrance and the aromaticity present in the ligands all play important roles in deciding the direction of flow of the reactions. Of the set studied here, $Cu(dmap)_2$ is probably the best and $Cu(PyrIm^R)_2$ the worst to be used as a precursor in this process.

Chapter 4: Quantum chemical study of effect of precursor stereochemistry on dissociative chemisorption and surface redox reactions during the atomic layer deposition of the transition metal copper

This chapter has been submitted to Journal of Physical Chemistry C



Note: The paper has been modified for the thesis. The reference, table and figure numbers are in a sequence with the previous chapters. However, the equation numbers are only valid for this chapter.

Abstract: Using quantum chemical calculations, we investigate surface reactions of copper precursors and diethylzinc as the reducing agent for effective Atomic Layer Deposition (ALD) of Cu. The adsorption of various commonly used $Cu^{(II)}$ precursors is explored. The precursors vary in the electronegativity and conjugation of the ligands, and flexibility of the whole molecule. Our study shows that the overall stereochemistry of the precursor governs the adsorption onto its surface. Formation of different $Cu^{(II)}/Cu^{(I)}/Cu^{(0)}$ intermediate complexes from the respective $Cu^{(II)}$ compounds on the surface is also explored. The surface model is a (111) facet of a Cu_{55} cluster. $Cu^{(I)}$ compounds are found to cover the surface after the precursor pulse, irrespective of the precursor chosen. A pair of CuEt intermediates or the dimer Cu_2Et_2 reacts in order to deposit a new Cu atom and release gaseous butane. In this reaction, two electrons from the Et anions are donated to copper for reduction to metallic form. This indicates that a ligand exchange between the Cu and Zn is important for the success of this transmetallation reaction. The effect of the ligands in the precursor on the electron density before and after adsorption onto the surface has also been computed through population analysis. In the $Cu^{(I)}$ intermediate, charge is delocalized between the Cu precursor and the bare copper surface, indicating metallic bonding as the precursor densifies to the surface.

4.1. Introduction

In the previous Chapter 3, we propose probable reactions that might take place during transmetallation ALD. Here $ZnEt_2$ was considered as the reducing agent. Broadly the overall transmetallation reactions were broken down into disproportionation, ligand exchange and reductive elimination. It was found that copper and zinc reaction energies were comparable and hence, it is inevitable that there is co-deposition of zinc along with copper. The pathway by which $Cu^{(0)}$ can be deposited was found to be the disproportionation reaction of the $Cu^{(I)}{}_2Et_2$ compound. This indicates that ligand exchange between the two metals (Cu and Zn)

is very important as a way to bring Cu and Et together. The paper mentioned that similar type of ligands have similar features and can be grouped together. $Cu^{(I)}{}_2L_2$ (L = ligand) compounds play a crucial role in understanding the mechanism. This is because after the precursor pulse, the copper compounds always tend to form these $Cu^{(I)}$ compounds. The paper also mentioned other side reactions that might take place.

However, ALD is predominantly a surface phenomenon and the gas phase model could only give a view of probable reactions that might take place at the surface. Finding a stable intermediate species on the surface indicates a pathway for the ALD reactions. Computed adsorption energies of the different species are a measure of their relative stability, thus revealing the dominant surface compounds that can be found after different ALD pulses. In some cases, the gas phase reactions show exothermic reaction energies, indicating a probable pathway for the reaction mechanism, but the same reactions might not take place on the surface due to slow kinetics, lack of interaction between the intermediates or a strong substrate effect.

The mechanism of a reaction is the atomically-resolved pathway that is followed by the reactants in order to form the products via the intermediates. It is important to understand the mechanism in order to determine the kinetics, possible side reactions and also impurities. ALD reaction mechanisms have been studied in many cases. For example, Mui[140] *et al.* studied silicon nitride formation using a cluster model, Elam[28] *et al.* studied ALD of ZrO_2 using *in situ* mass spectrometry and first principle calculations, Heyman[141] studied different cycles in ALD of Al_2O_3 using $AlCl_3$ and H_2O, Leskela[142] and co-workers studied ALD of Ru and Pt using an *in situ* quadrupole mass spectrometer (QMS) and a quartz crystal microbalance (QCM) and Widjaja[143] *et al.* studied ALD of HfO_2 from $HfCl_4$ and H_2O using first principle calculations.

Ab initio calculations can give valuable insights into the mechanism of ALD reactions[144]. Short-lived intermediates can also be studied using these calculations, which might not be possible through experiments[145]. In most of the cases, Density Functional Theory (DFT) has been the preferred level of computation, because it provides a reliable description of chemical reactions at reasonable computational cost. It is computationally cheaper than other first principle techniques like Møller–Plesset second order perturbation theory or Coupled Cluster[87,146] and so allows larger systems to be computed. Computational study builds a bridge between the theoretical understanding and experimental data for various chemical reactions in ALD.

The ligand in the precursor plays a crucial role in ALD mechanism. It dictates the volatility of the precursor, surface adsorption and densification on the surface. Computing surface adsorption shows the structures of the precursors on the surface. Densification is defined as the increase in density due to improved metal (M) and ligand (L) M-L packing, associated with an increase in coordination numbers of metal and ligand[147]. Although densification has been shown to be important in ALD of oxides[120], it has hardly been discussed before for metals[144]. The computed adsorption structures for Cu compounds show the densification that can take place for this metal.

In our current work, we use a surface model to study the cycles in Cu ALD during the transmetallation reaction as proposed in equation 1 (see Figure 20). We compare various copper(II) precursors and consider $ZnEt_2$ as the reducing agent. Each ALD cycle comprises a precursor pulse and a co-reagent pulse[14]. Different surface reactions take place during each pulse. During a precursor pulse (denoted as pulse 1), the copper complexes CuL_2 come onto a surface covered with Et ligands from the previous co-reagent pulse. During the reducing agent pulse (denoted as pulse 2), $ZnEt_2$ comes onto a surface already covered with ligands (L) from the copper precursor. Thereafter, during either or both pulses, reactions may take place

at the surface between ligands and Et groups and volatile by-products may be produced. After saturation has been reached, a particular type of ligand always dominates the surface.

In order to study these reactions, we have divided them into parts as shown in Figure 20. Each ALD pulse is conceptually broken into parts ‘a’ and ‘b’. Based on our prior study of this system[33], we expect that the following reactions take place in part 1a where co-reagent is present at the surface.

- Ligand exchange between the two metals (Cu/Zn).
- Formation of half and fully ligand exchanged Cu and Zn surface intermediates like LZnEt and LCuEt and volatile products like ZnL_2 and butane.
- Further reactions and decomposition of these intermediates.
- Formation of new Cu surface layer.

In part 1b, we study the system when an excess of the copper precursor is admitted to the bare copper surface without any co-reagent left. The following reactions are expected to take place.

- Adsorption of unreacted Cu precursors onto a bare surface.
- Dissociation of the copper precursor on the surface.

Part 2 deals with the reactions during the reducing agent pulse. All the reactions that take place in 1a are also expected to take place in 2a. However, in this case the surface is initially covered with precursor ligand (L).

In part 2b, the following reactions are expected to take place.

- Adsorption of $ZnEt_2$ onto a bare copper surface.
- Reaction of Et ligands with surface Cu atoms.

The transition from part ‘a to b’ in both pulses ‘1 and 2’ is marked by the formation of a new copper layer. In pulse 1, copper deposits from the copper precursor and in pulse 2,

copper deposits from the $Cu^{(I)}$ intermediates. This course of the reaction is cyclic as seen in the following:

1a → $Cu_{new\text{-}layer}$ → 1b →2a →$Cu_{new\text{-}layer}$ →2b →1a …….

In this study we will study the reactions in parts 1b and 2b that take place on a bare copper surface. This can be assumed to be the situation in the latter half of every pulse after complete exhaustion of the other ligand. For this reason we start from a bare Cu surface and study the adsorption of each precursor and the stability of $Cu^{(I)}$ intermediates[25] at the surface stable adsorbates as they are an important prerequisite for growth as otherwise the unreacted precursor complex will be expelled out of the reactor. Just as importantly, Cu-containing surface intermediates should not desorb and other by-products should desorb cleanly so as to avoid impurities in the film. We therefore compute the adsorption/desorption energies of the copper precursors CuL_2, intermediate compounds Cu_2L_2 and by-products ZnL_2, Et-Et and L-Et . The potential energy change for the transformation from $Cu^{(II)}$ to $Cu^{(I)}$ for three different ligands is also studied. These are all the possible reaction steps that may be followed in part 1b of the pathway for $Cu^{(0)}$ deposition.

For part 2b of the ALD cycle, we study the interaction of $ZnEt_2$, the reducing agent, with a bare copper surface. This takes place when all the surface bound ligands from the precursors have interacted with the incoming $ZnEt_2$ compounds and have been eliminated. The excess $ZnEt_2$ that is present may then interact with the newly formed bare copper surface.

Our aim is to screen many reactions and precursors and map out the likely pathway from the thermodynamic reaction energies. Given the large number of possible species, we do not consider the kinetics of competing reaction steps and so no transition states have been computed in this study.

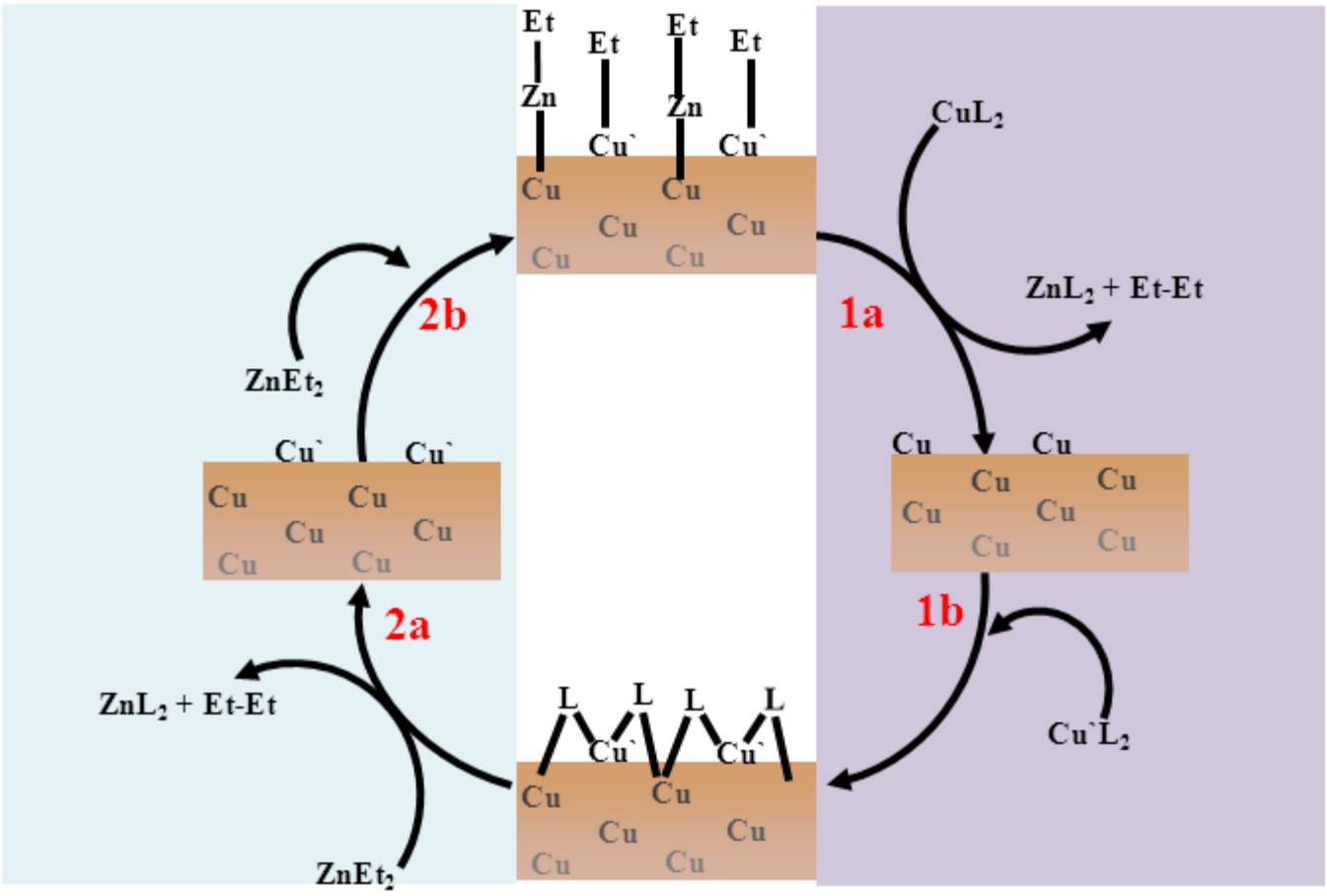


Figure 20: This figure shows various ALD cycle for proposed transmetallation reaction between copper precursor CuL_2 and reducing agent $ZnEt_2$. Each ALD pulse has been divided conceptually into two halves (a, b). The Cu precursor pulse on the right side with light pink shade is denoted as 1 and the reducing agent pulse on the left side with light blue shade is denoted as 2. Section 1a describes the reaction in a mixed surface between the incoming copper precursor and previously adsorbed Et ligands. Section 1b describes the reaction when the Et ligand has been exhausted and fresh copper precursor adsorbs onto a bare copper surface. Section 2a involves the same reactions as 1a but this is during the reducing agent pulse when incoming $ZnEt_2$ interacts with previously adsorbed ligands from the Cu precursor. Section 2b shows the reaction when an excess of reducing agent adsorbs onto a bare copper surface.

4.2. Methods

We have used first principles Density Functional Theory as implemented in the TURBOMOLE 5.8 program[96,127]. The Perdew-Burke-Ernzerhof (PBE)[128] functional was used with the resolution of identity (RI) approximation[129,130]. A valence double zeta with

polarization basis set denoted by def-SV(P)[129] was used for all electrons. We used the larger triple zeta basis set TZVPP[148,149] and dispersion functional D3[150] to check the accuracy of the level of calculation in a previous study[62]. It was seen that energy difference changed by 4-8%, especially when using the dispersion functional D3. However, the computational cost of these calculations was much higher and the qualitative results in terms of reaction mechanism were not affected. Therefore, due to its adequate accuracy, we have used the PBE/def-SV(P) method in this study.

An fcc Cu_{55} cluster, which is in the shape of a coin with (111) faces, was taken as a surface model. The bare cluster has C_{3v} symmetry (Figure 21). The copper coin is an open shell doublet system with a HOMO - LUMO energy difference of 1.8 kJ/mol. The $Cu^{(II)}$ precursors are open shell doublets. Therefore, all the calculations with adsorbate on the cluster were open shell triplet calculations computed within the unrestricted DFT formalism with negligible spin contamination. This is the same model as used by Larsson *et al.*[151] and in our previous studies[60,62]. Some of the adsorbates cover the entire copper surface and overlap the edges of the cluster. However, a bigger cluster is computationally very expensive. The edge effect that arises is already discussed in another study[62]. Correcting for this gives an energy difference of ~8% and the qualitative adsorption energies do not change. Hence, the adsorption energies quoted in this work have an error limit in this range.

A comparative study of the reactive adsorption of the more commonly used $Cu^{(II)}$precursors onto the surface has been carried out. The precursors are copper$^{(II)}$acetylacetonate $Cu(acac)_2$, copper$^{(II)}$pyrrolylaldehyde $Cu(PyrAld)_2$, copper$^{(II)}$N-isopropyl-2-pyrrolylaldiminate $Cu(PyrIm^{iPr})_2$, copper$^{(II)}$dimethylamino-2-propoxide $Cu(dmap)_2$ and copper$^{(II)}$-bis(4N-(ethylamino)pent-3-en-2-onate commonly known as AbaCus$^{(TM)}$. The precursors vary in the electronegativity of the ligating atom, π conjugation present in the ligands and also steric hindrance in the coordination shell (Figure 22).

The energy of adsorption of the precursors to the bare surface has been calculated by this equation:

$$\Delta E_{ad} = E(\text{Pre+Coin}) - E(\text{Coin}) - E(\text{Pre}) \quad \ldots(4)$$

where E(Pre+Coin) denotes the total energy of the optimized geometry of the copper precursor adsorbed onto the bare copper surface, E(Coin) denotes the total energy of the optimized bare copper surface model, and E(Pre) denotes the total energy of the relaxed copper precursor in the gas phase.

The entropy of the precursor molecules S(Pre) has also been calculated in the gas phase from vibrational analysis using TURBOMOLE[133]. The entropy has been calculated at T = 393 K as this is a typical target temperature for Cu ALD. After the precursor is adsorbed onto the surface, it loses its translational and rotational degrees of freedom and this is probably the major contribution to the entropy change. It is therefore assumed that $S(\text{Pre+Coin}) \approx S(\text{Coin}) + S_{vibr}(\text{Pre})$ and so the entropy change is $\Delta S_{ad} \approx -S_{trans+rot}(\text{Pre})$. $\Delta G_{ad} = \Delta E_{ad} - T\Delta S_{ad}$ denotes the free energy needed by the precursors to be adsorbed onto the surface. A lower more negative ΔG_{ad} value for the precursors indicates that the adsorption is favored. Likewise a higher more positive value for the by-products means that desorption is favored. The change in molecular structures from the free to the adsorbed state is also noted. *Ab initio* Molecular Dynamics (aiMD) using the same PBE functional and def-SV(P) basis set has been conducted on the $ZnEt_2$ molecule from an initial temperature of 393 K within the isothermal and isobaric ensemble. The total duration of the aiMD simulation was 2.17 ps.

All the precursors feature copper in formal oxidation state II and some of the surface intermediates studied here like Cu_2L_2 have copper in the oxidation state I. However, population analysis has been carried out in order to understand the actual charge distribution in different structures. Natural Population Analysis (NPA)[152] has been chosen as it exhibits

better numerical stability for compounds containing metal atoms than other methods like Mulliken population analysis[104]. Nevertheless we note that these results are subject to the systematic problem of approximate DFT in localizing electrons in partially occupied metal d states (e.g. $Cu^{(I)}$ vs $Cu^{(II)}$).

4.3. Results

This section is divided into four parts. In section 4.3.a we study the copper precursor adsorption onto a bare copper surface for various precursors. In section 4.3.b we study the stability of Cu_2L_2 compounds on the surface. In section 4.3.c, we study the change in charge distribution of the copper compound, from the gas phase, to the adsorbed CuL_2 and Cu_2L_2 compounds. Section 4.3.d considers the interaction of the $ZnEt_2$ with the bare copper surface. The initial three sections are relevant to part 1b of the ALD cycle and the latter section to part 2b.

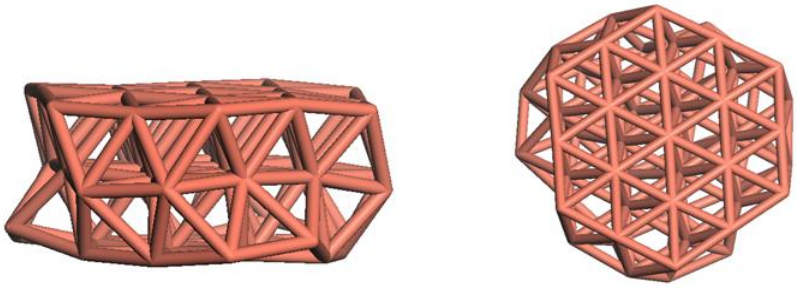


Figure 21: Side view and top view of the 3-layer deep Cu_{55} cluster, which is used as a model for the Cu(111) surface to investigate the adsorption of the copper precursors, intermediates and by-products.

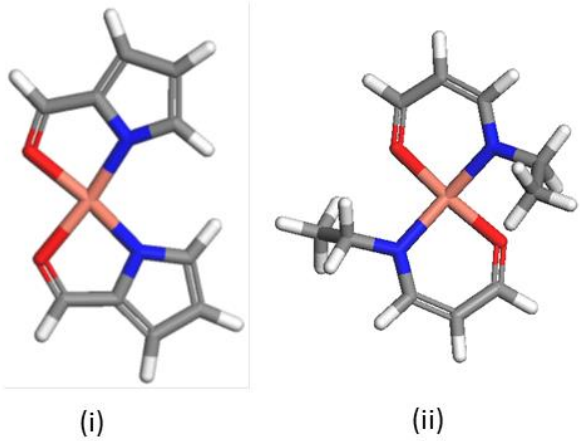


Figure 22: Lowest energy isomer computed in gas phase for potential Cu ALD precursors. (i) $Cu(PyrAld)_2$ (ii) $AbaCus^{(TM)}$. Structural parameters are quoted in Table 11. Color code: Red = oxygen, Blue = nitrogen, Grey = carbon, White = hydrogen, Light brown = copper.

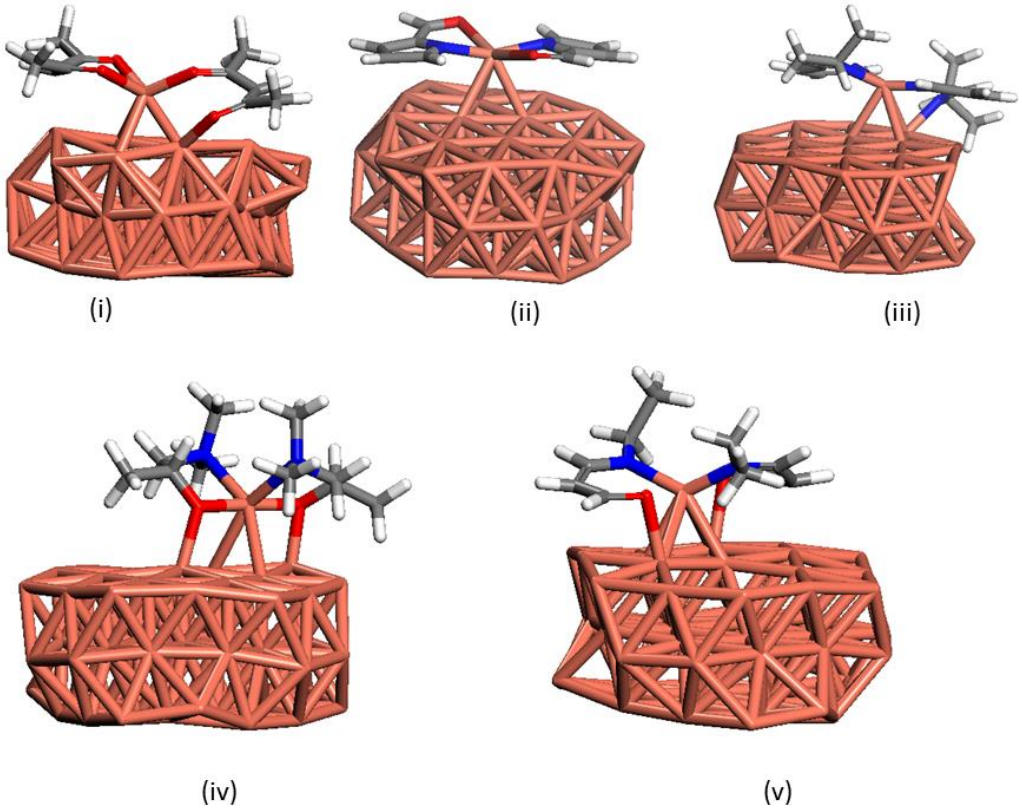


Figure 23: Optimized structures of precursors adsorbed onto the bare copper (111) surface. (i) $Cu(acac)_2$, (ii) $Cu(PyrAld)_2$, (iii) $Cu(PyrIm^{iPr})_2$, (iv) $Cu(dmap)_2$, (v) $AbaCus^{(TM)}$. The energetic of the adsorption energy is in Table 12 and the structural changes in the precursor

before and after adsorption in Table 11. Color code: Red = oxygen, Grey = carbon, White = hydrogen, Light brown = copper, Blue = nitrogen.

4.3.a. Adsorption of copper precursors onto bare copper surface:

Five different precursors that differ in electronegativity of the ligating atom, π conjugative stability in the ligands and steric hindrance have been considered here. The comparison allows us to understand their adsorption onto a bare copper surface (Figure 23). A precursor that has strong adsorption is beneficial, as it will not be purged out of the reactor without first saturating the surface. Stronger adsorption energies of intermediates give an idea of the dominant species that can be present at any time during the ALD reaction.

- $Cu(acac)_2$ (Figure 14 (a)) has O atoms in the ligand attached to the copper center. The ligand has conjugated O-C-C-C-O π system in which the negative charge is delocalized.

- $Cu(PyrAld)_2$ (Figure 22(i)) has both N and O as ligating atoms and has a conjugated bonds present in O-C-C-N fused to a pyrrole ring. It has a distorted tetrahedral structure about the Cu center. It has a mirror symmetry across a horizontal plane through the copper center.

- $Cu(PyrIm^{iPr})_2$ (Figure 14 (d)) is similar to $Cu(PyrAld)_2$ except that (a) it has higher steric hindrance due to the presence of an isopropyl group attached to the imine nitrogen and (b) the electronegative atoms attached to the copper are N and N, not N and O as in the case of PyrAld.

- $Cu(dmap)_2$ (Figure 14 (c)) is different from the above precursors as the ligand does not have any conjugation present. Otherwise, it is comparable to $Cu(PyrAld)_2$ as it has 4-atom O-C-C-N ligating unit, but no fused ring. It does not have a mirror plane and ligating atoms are arranged anti about Cu.

- Copper-bis(4N-(ethylamino)pent-3-en-2-onate AbaCus$^{(TM)}$ (Figure 22(ii)) is a precursor, which is similar to $Cu(dmap)_2$ but has conjugation present in its ligand. It does not have a mirror image and the N and the O lie opposite to each other across a horizontal plane through the copper center.

The difference between gaseous and adsorbed structures is shown in Table 11 for copper precursors. The bond length between the metal Cu and the O/N atom in ligand, as well as the distance from the nearest surface copper atom is noted. When some of the precursors are adsorbed onto the coin, there is considerable change in metal-ligand bonding and the dihedral angle between the four ligating atoms. For example, the ∟O-N-O-N angle in $Cu(dmap)_2$ changes from 0.6° to 104°.

We see that the structure of the precursor affects the adsorption onto the surface. A planar complex like $Cu(acac)_2$ that is free of any bulky substituent, has better access to the surface copper atoms. There is partial transfer of the ligand from the complex to the surface, where the ligands form extra bonds with the surface copper atoms (Figure 23 (i)). The bond length between the Cu_{pre} (in the precursor) and ligand O lengthens from 1.95 Å to > 2.10 Å.

The $Cu(PyrAld)_2$ precursor is also free of steric hindrance from bulky substituents but it has an almost tetrahedral structure around Cu_{pre}. In order for the precursor to adsorb, the Cu_{pre}-O bond dissociates to a length of 2.61/2.72 Å, much longer than the normal Cu-O bond found in an organometallic compound[153] (1.92 Å) (Figure 23 (ii)). The O remains unbounded to both Cu_{pre} and $Cu_{surf.}$

When the lowest energy isomer of $Cu(PyrIm^{iPr})_2$ is put onto a bare copper surface, it is seen in the calculations that it does not chemisorb. This is because of the bulky ^{i}Pr groups, which are on the opposite sides of the plane of the precursor compound (Figure 24). The steric hindrance is lower with an alternative isomer where the ^{i}Pr groups are on the same side of the

plane (Figure 23(iii)). The difference in energy between the two gas phase isomers is 5 kJ/mol. We see molecular adsorption of the precursor only after the transformation.

$Cu(dmap)_2$ also shows molecular adsorption onto the surface. The ligand O atoms form extra bonds with the surface atoms (Figure 23(iv)). However, the Cu-ligand bonds of the precursor complex do not dissociate.

In AbaCus, (Figure 23(v)), the steric hindrance that arises from the Et group on imino N in the ligand does not hinder the adsorption. The Et groups occupy the space above the plane of the molecule while the Cu_{pre} atom adsorbs to the surface below. The O atoms in the precursor break from the Cu_{pre} and bond to the Cu_{surf}. The Cu_{surf}-O distances are 2.55 Å and 2.17 Å.

The computed energies for the adsorption of Cu precursors and desorption of the by-products are reported in Table 12. The data can be interpreted as in the following example. It is computed that $Cu(acac)_2$ has an adsorption energy of ΔE_{ad} = -258 kJ/mol at 0 K. However, it faces an energy of ΔG^{393}_{ad} = -79 kJ/mol at 393 K because of the entropy factor ΔS_{ad} = -0.5 kJ/mol.K and $T\Delta S_{ad}$ = -179 kJ/mol. A similar interpretation with different results can be made for all the complexes in Table 12. From these data we see that the less sterically hindered acac precursor has the highest ΔE_{ad}. This is followed closely by $PyrIm^{iPr}$, dmap and AbaCus precursors. The least negative ΔE_{ad} is for PyrAld. It is seen that, except for $Cu(PyrAld)_2$, all other precursor complexes show favorable adsorption at ALD temperatures, $\Delta G^{393}_{ad} < 0$.

Adsorption of $CuEt_2$ has also been explored as this compound might be formed after a ligand exchange with $ZnEt_2$. It is seen that ΔE_{ad} is strongest in this case as against any of the above precursors.

After adsorption, the Cu_{pre} atom is in most cases computed to sit at a capping site on Cu(111), binding to three Cu_{surf} atoms (Figure 23 (i), (ii), (iii), (v)). This is seen for all precursors except dmap (Figure 23 (iv)) where the Cu_{pre} bridges between two Cu_{surf}. The ligand O atoms of acac, dmap and AbaCus also bind directly to Cu_{surf}. It is seen from Table 1

that this is associated with a lengthening of the Cu_{pre}-O bond. In the cases of dmap and PyrAld, N does not bond to Cu_{surf}, and so the Cu_{pre}-N bond is not lengthened as much.

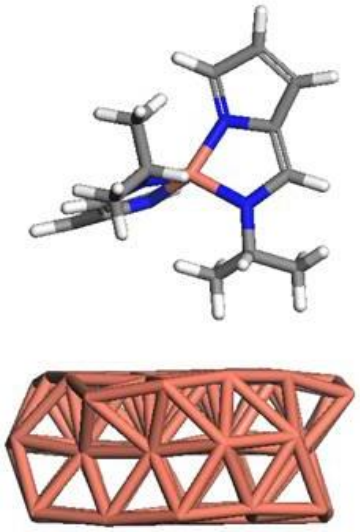
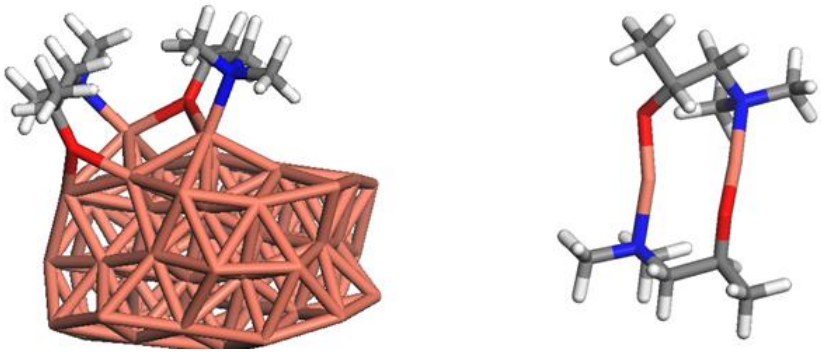


Figure 24: Lowest energy isomer of $PyrIm^{iPr}$ precursor, which does not chemisorb in any orientation onto the copper surface due to steric hindrance (Figure 23 (iii)). Color code: Red = oxygen, Blue = nitrogen, Grey = carbon, White = hydrogen, Light brown = copper.

(i)



(ii)

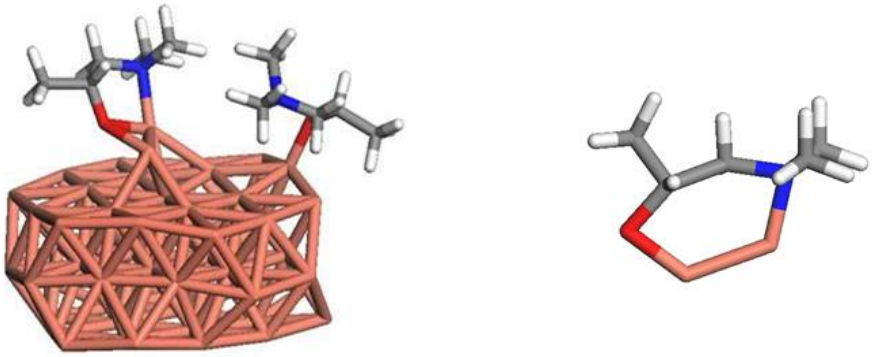


Figure 25: (i) The Cu_2L_2 (L=dmap) intermediate where there are two ligands, each attached to two adsorbed copper atoms. The corresponding gas phase structure is shown to the right. In the gas phase the distance between the two Cu atoms is $|Cu^{(I)}\text{-}Cu^{(I)}|_{(g)}$ 2.48 Å and after adsorption onto the surface the distance is $|Cu\text{-}Cu|_{surf}$ 3.55 Å. (ii) Cu_2L + L where the first ligand is attached to two adsorbed copper atoms. The corresponding gas phase structure is also shown. In this case $|Cu\text{-}Cu|_{(g)}$ = 2.51 Å and $|Cu\text{-}Cu|_{surf}$ = 2.67 Å.

Table 11: Comparison of the structural properties of copper precursors when in the gas phase and after molecular adsorption onto the surface. Comparison has also been made with possible copper$^{(I)}$ intermediate. The dihedral angle is between the four coordinating atoms to the copper in the precursor, for example in $Cu(acac)_2$ the angle is between four oxygen atoms ∟O-O-O-O. The distance from the copper in the precursor to the nearest copper atom on the surface has also been noted and is represented as Cu-Cu. Here L = ligand in the precursor.

Precursors		CuL_2 in the gas phase	CuL_2 adsorbed onto the surface	$Cu^{(I)}L$ adsorbed onto the surface
$Cu(acac)_2$	Cu-O (Å)	1.95	2.10/2.13/4.08	2.05
	∟O-O-O-O (°)	0.1	9.73	6.57
	Cu-Cu (Å)	-	2.49	2.50
$Cu(PyrAld)_2$	Cu-N (Å)	1.97	1.95/1.96	2.03
	Cu-O (Å)	2.03	2.72/2.61	2.05
	∟O-N-O-N (°)	158.81	167.98	15.09
	Cu-Cu (Å)	-		2.48
$Cu(PyrIm)_2^R$ R=^{i}Pr	Cu-N_{Ar}(Å)	1.98	1.94	2.06/2.00
	Cu-N_{Ali}(Å)	2.04	1.96	2.00
	∟N-N-N-N (°)	38.73	71.41	19.78
	Cu-Cu (Å)	-	2.72	2.44
$Cu(dmap)_2$	Cu-O (Å)	1.91	1.95	2.13
	Cu-N(Å)	2.09	2.09	2.16
	∟O-N-O-N (°)	0.6	104.25	114.54
	Cu-Cu (Å)	-	2.62	2.46
AbaCuS	Cu-O (Å)	1.99	2.55	2.04
	Cu-N(Å)	1.99	2.03	2.02
	∟O-N-O-N (°)	131.39	141.15	0.03
	Cu-Cu (Å)	-	2.53	2.44

$CuEt_2$	Cu-C(Å)	1.97/1.96	2.00/1.99	-
	∟C-Cu-C (°)	137.95	152.12	-
	Cu-Cu (Å)	-	2.37	-

Table 12: Computed molecular adsorption energy (ΔE_{ad}) of copper precursors onto the copper surface along with the computed entropy contribution ($T\Delta S_{ad}$) of the molecules at T = 393 K. ΔG_{ad}^{393} denotes the free energy. All the values are in kJ/mol. Table 13 shows the gas phase structure of precursor compounds and Figure 23 the adsorbed counterparts.

Ligand	ΔE_{ad}	$T\Delta S_{ad}$	ΔG_{ad}^{393}
acac	-258	-179	-79
PyrAld	-127	-171	44
$PyrIm^{iPr}$	-251	-200	-51
dmap	-249	-184	-64
AbaCus	-207	-175	-32
Et	-279	129	-150

Table 13: Computed adsorption energy (ΔE_{ad}), entropy contribution at 393 K ($T\Delta S_{ad}$) and free energy (ΔG^{393}_{ad}) of possible intermediates ($Cu_2^{(I)}L_2$) on the Cu surface during transmetallation reaction. All the values are in kJ/mol.

Ligand	Molecule	ΔE_{ad}	$T\Delta S_{ad}$	ΔG^{393}_{ad}
dmap	$Cu^{(I)}_2(dmap)_2$	-504	193	-311
$PyrIm^{iPr}$	$Cu^{(I)}_2(PyrIm^{iPr})_2$	-316	207	-109
acac	$Cu^{(I)}_2(acac)_2$	-309	186	-123
AbaCus	$Cu^{(I)}_2(Aba)_2$	-307	186	-121

4.3.b. Adsorbed Intermediates

It seems that $Cu^{(I)}_2L_2$ is an important intermediate that can be formed during the transmetallation reaction[33,75,123]. This stems from our previous study of the gas phase transmetallation reaction, where it was seen that after the precursor pulse, the surface is likely to be covered with these $Cu^{(I)}$ intermediates. Comproportionation of $Cu^{(II)}$ and $Cu^{(0)}$ to $Cu^{(I)}$ was found to be exothermic. However, the previous study did not explicitly consider surface reactions.

In the current study, we find that all Cu_2L_2 intermediates exist as molecules adsorbed on the surface. The theoretical adsorptions energies of these intermediates are reported in Table 13 in order to assess their stability against desorption. The $Cu^{(I)}$ intermediates seem to release the strain present in the corresponding $Cu^{(II)}$ precursors (Table 11). The open structure of Cu_2L_2 allows better access for the $Cu^{(I)}$ centers to the surface Cu atoms for bonding. This allows stronger adsorption to the surface (Table 13).

We have previously identified three types of $Cu^{(I)}$ compounds[33]: in Cu_2L_2 each ligand is attached to two copper atoms; in CuL there is no Cu-Cu bond and each ligand is attached to

only one Cu atom and in Cu_2L there is only one ligand attached to two copper atoms (Figure 25(ii)). In Cu_2L one of the Cu is formally in oxidation state zero and the other is in +1 oxidation state. In the current study, we find similar possibilities for $Cu^{(I)}$ adsorbates, validating the previous study (Figure 25).

Various reactions are possible for the $Cu^{(I)}$ intermediate. It can desorb from the surface or transform into another type of $Cu^{(I)}$ intermediate or else disproportionate into $Cu^{(II)}$ compounds and $Cu^{(0)}$. The computed energetics for these possibilities are shown in Figure 26 for L = dmap and Figure 27 for L = $PyrIm^{iPr}$. The desorption energies (ΔE_{des}) and free energies (ΔG_{des}) that include ΔS are also shown in the graphs. It is known that entropy always favors desorption. Hence, ΔG_{des} is always less than ΔE_{des} irrespective of the system studied. We see that amongst all the surface species, the $Cu^{(I)}$ intermediates are the most stable for all the ligands studied.

As seen in Figure 26 and Figure 27, the reaction energies for $Cu^{(II)}$ and surface $Cu^{(0)}$ atoms to comproportionate into $Cu^{(I)}$ are < -100 kJ/mol. Therefore, subject to overcoming the unknown kinetic barriers, the reaction is expected to take place. For the dmap ligand the most stable surface intermediates are $Cu^{(I)}{}_2L_2$ and Cu_2L (Figure 26) and for L = $PyrIm^{iPr}$, Cu_2L is the most stable (Figure 27). The desorption of the $Cu^{(I)}$ intermediates is not likely for the dmap ligand as the energies required are $\Delta G_{des}{}^{393}$ > 300 kJ/mol. However, $PyrIm^{iPr}$ compounds have more probability for desorption of the $Cu^{(I)}$ compounds ($\Delta G_{des}{}^{393}$ = -111 kJ/mol). This is because they show more tendency than dmap to retain the $Cu^{(I)}$ structure rather than $Cu^{(II)}$. This was seen in the gas phase studies as well[33]. However, $Cu^{(II)}L_2$ is energetically more likely to desorb than $Cu^{(I)}L_x$ in all the cases. Thus during step 1b of the copper precursor pulse, when all the pre-existing ligands from the reducing agent have been expelled from the system, the surface becomes covered with $Cu^{(I)}$ complexes.

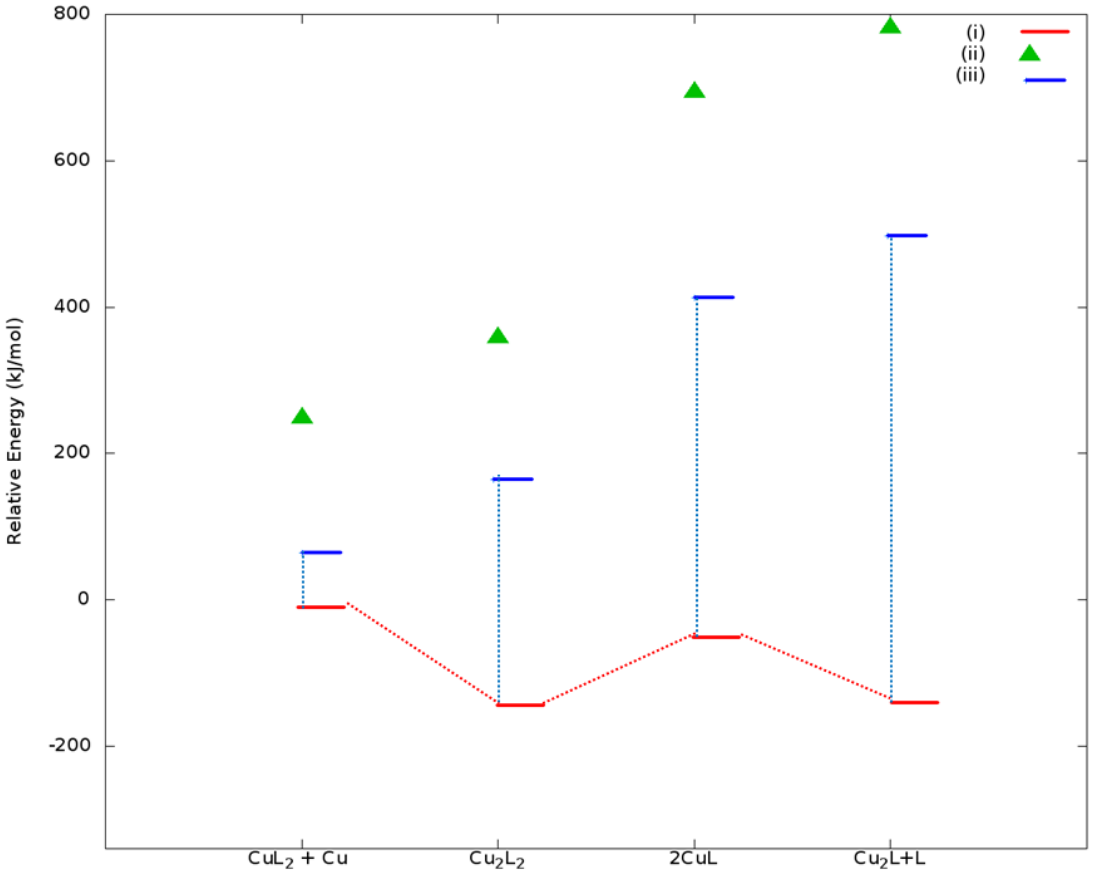


Figure 26: Energetics of surface intermediates during transmetallation when L = dmap is the ligand. The lower the energy in the graph, the more stable the system. (i) Red lines: The energy ΔE needed to transform the intermediate species into another on a bare copper surface. (ii) Green triangles: The desorption energy (ΔE_{des}) of the respective species into the gas phase relative to the red line. In the first structure the desorbed molecule is CuL_2, second Cu_2L_2, third CuL, and the last Cu_2L. (iii) Horizontal Blue lines: The free energy (ΔG^{393}) including the entropy factor at 393 K needed for the species in order to desorb into the gas phase relative to the red line. Any particular intermediate has the probability of either desorption from the surface (red → blue) or else can form another surface intermediate (red → red). The data are presented in the supplementary information. No barriers have been computed.

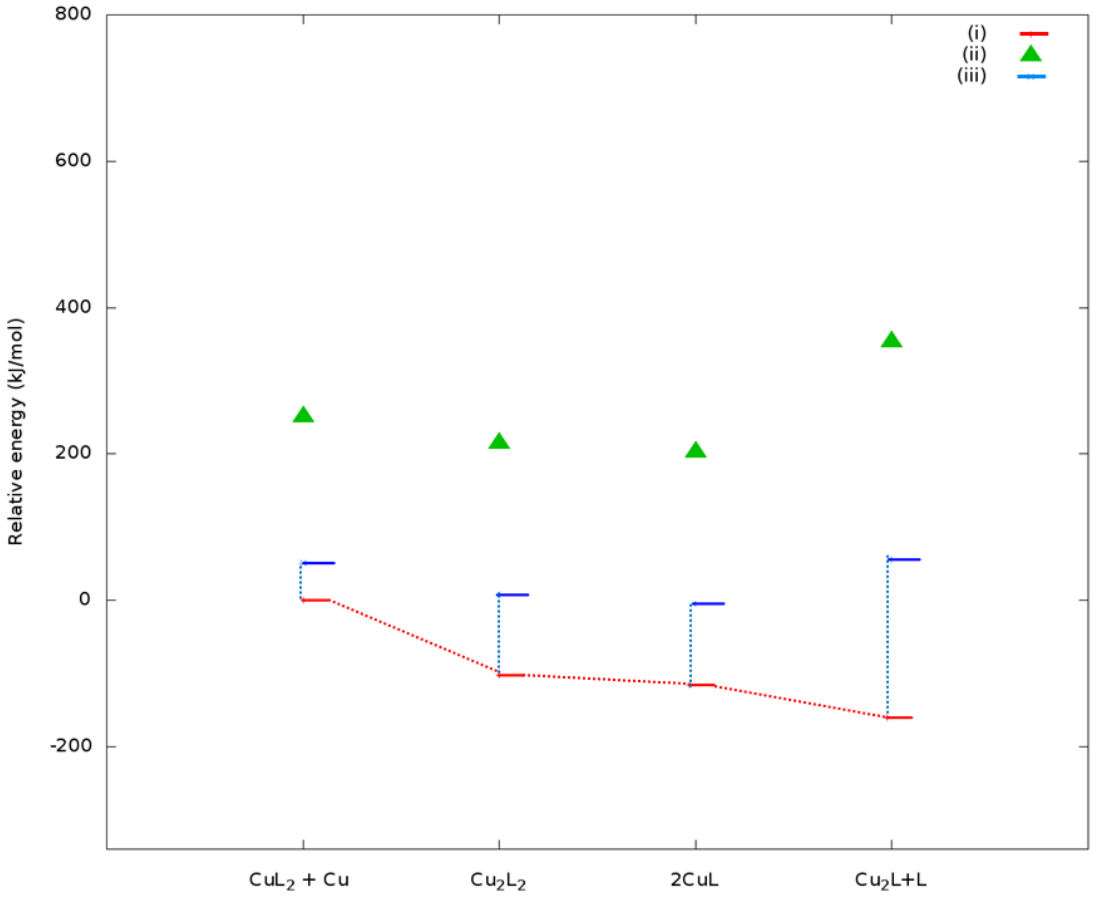


Figure 27: The graph shows similar results to that of Figure 26 but using L = PyrIm^{iPr} as the ligand.

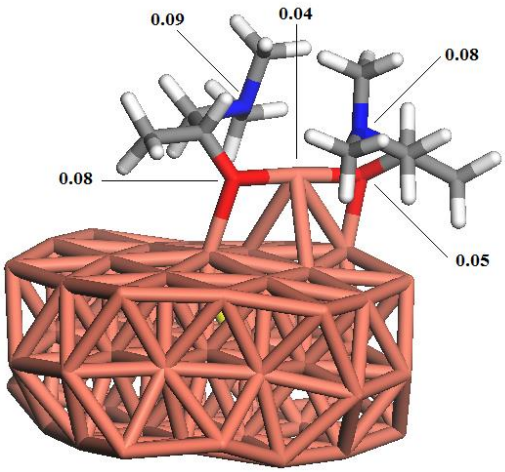


Figure 28: Optimized structure of Cu(dmap)$_2$ adsorbed on the (111) face of the copper coin. The differences in NPA charges on the Cu, O and N atoms between the gas phase precursor and the adsorbed precursor have been shown. The charges are more delocalized in the adsorbed structure compared to the gas phase and so the change is always positive. There are

also changes in the surface with a total change of charge ~0.40. Color code: Red = Oxygen, Blue = Nitrogen, Grey = Carbon, White = Hydrogen, Light brown = Copper.

Table 14: Population analysis with NPA of the net charge in units of electronic charge on groups of atoms in the CuL_2 precursor, both in the gas phases (Figure 22) and then adsorbed onto the surface (Figure 23). Negative sign indicates negative charge. The same study has been done for the corresponding $Cu^{(I)}{}_2L_2$ surface intermediate. Cluster surface refers to the (111) copper surface atoms of the whole coin.

Ligand	Gas Phase CuL_2			CuL_2 on the surface			
	Ligand 1	Ligand 2	Cu	Ligand 1	Ligand 2	Cu	Cluster surface
$PyrIm^{iPr}$	-0.82	-0.82	1.64	-1.14	-0.75*	0.98	0.96
dmap	-0.56	-0.56	1.13	-0.88	-0.87	1.09	0.62
AbaCus	-0.59	-0.59	1.18	-0.94	-0.90	0.91	0.93

	Gas Phase Cu_2L_2				Cu_2L_2 intermediate on surface				
	Ligand 1	Ligand 2	Cu^1	Cu^2	Ligand 1	Ligand 2	Cu^1	Cu^2	Cluster surface
$PyrIm^{iPr}$	-0.66	-0.66	0.66	0.66	-0.92	-0.96	0.69	0.69	0.44
dmap	-0.64	-0.63	0.64	0.63	-0.69	-0.70	0.62	0.52	0.25
AbaCus	-0.68	-0.67	0.68	0.68	-0.86	-0.76	0.69	0.71	0.22

4.3.c. Population Analysis of $PyrIm^{iPr}$, dmap and AbaCus precursors:

Table 14 shows the population analysis using NPA of three CuL_2 compounds before and after adsorption onto the surface. They are chosen such that the ligand varies in electronegativity (N, O as in dmap and AbaCus but N,N in $PyrIm^{iPr}$), flexibility in the precursor (conjugation in the ligands AbaCus, $PyrIm^{iPr}$ but no conjugation in dmap) and size of the ring including copper (five membered ring in dmap and $PyrIm^{iPr}$ but six membered

ring AbaCus). For CuL_2 adsorption in all three cases, each ligand gains -0.3 negative charge on adsorption to the Cu (111) surface and the surface donates this amount of charge. The exception is for the second ligand in the $PyrIm^{iPr}$ precursor, which is an artifact of the calculation because the ligand is bound towards the edge of the copper cluster. The positive charge initially on the Cu atom in the precursor becomes shared between the surface and adsorbed Cu (Table 14). This delocalization may contribute to stabilization of the adsorbed copper complexes and can be interpreted as metallic bonding. The redistribution of charge over the copper surface is less for the Cu_2L_2 compound compared to CuL_2. The charge left on the two adsorbed Cu_2L_2 centers and the ligands are roughly the same, regardless of precursor.

4.3.d. Interaction of $ZnEt_2$ with a bare copper surface:

In this section, we explore the $ZnEt_2$ interaction with a bare copper surface. This takes place in an ALD chamber when there is an excess of the reducing agent and the previously-adsorbed ligands from the precursors are exhausted. This can be assumed to take place at the latter half of the reducing agent pulse (Figure 20, step 2b).

After finding the minimum energy structure of $ZnEt_2$ adsorbed on the copper surface, we have conducted an aiMD study of this adsorbate at typical ALD temperature. Within the very short simulation time of 2.17 ps, we see that the adsorbate $ZnEt_2$ dissociates into ZnEt and Et fragments and that these two fragments attach themselves to the copper cluster. The bond distance between the Zn and the detached Et is 2.37 Å as opposed to 2.08 Å in $ZnEt_2$. Figure 29 shows the steps that take place in the above reactions. The adsorption of ZnEt to the copper surface (ΔE_{ad} = -264 kJ/mol) is computed to be stronger than that of $ZnEt_2$ (ΔE_{ad} = -115 kJ/mol) and so desorption of the ZnEt fragment is unlikely. The adsorption of ZnEt is even stronger than all the copper precursors studied here. Therefore, at the end of the reducing agent pulse we predict that there are fragments of Cu_{surf}-Et and ZnEt on the copper surface.

We suggest that Cu_{surf}-Et can undergo similar surface reactions as outlined for Cu-dmap and Cu-$PyrIm^{iPr}$ in the previous section (4.3.b). Therefore, we explore the stability of the Et ligand attached to $Cu^{(I)}$ or $Cu^{(II)}$ at the surface and desorption of the respective complexes. Figure 30 shows the graph for this study. Once again, various $Cu^{(I)}$ surface compounds are found to be more stable intermediates than those of $Cu^{(II)}$. Formation of $CuEt_2$ and its desorption is not favored. However, it is striking that in this case the deposition of $Cu^{(0)}$ and the desorption of butane from the surface is energetically favored (ΔE = -156 kJ/mol relative to two neighboring CuEt intermediates).

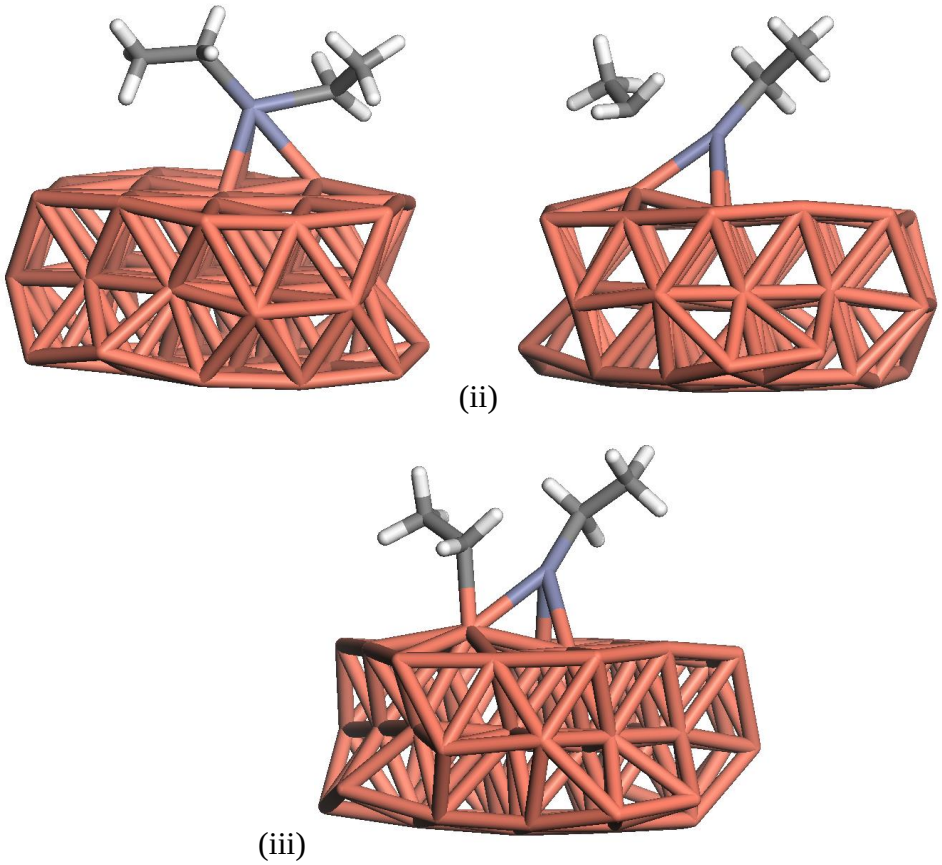


Figure 29: *Ab initio* Molecular Dynamics study for $ZnEt_2$ on Cu(111) surface. (i) Time t=0 shows $ZnEt_2$ attached to the surface. (ii) At time t=1.17 ps breaking of the C-Zn bond is apparent. Distance between C-Zn is 2.38 Å (C from the ethyl group). (iii) At time t=2.17ps, ZnEt and Et are separately attached to the copper surface. The above structures are not

optimized geometries. Color code: brown=copper, blue-grey=zinc, grey=carbon and white=hydrogen.

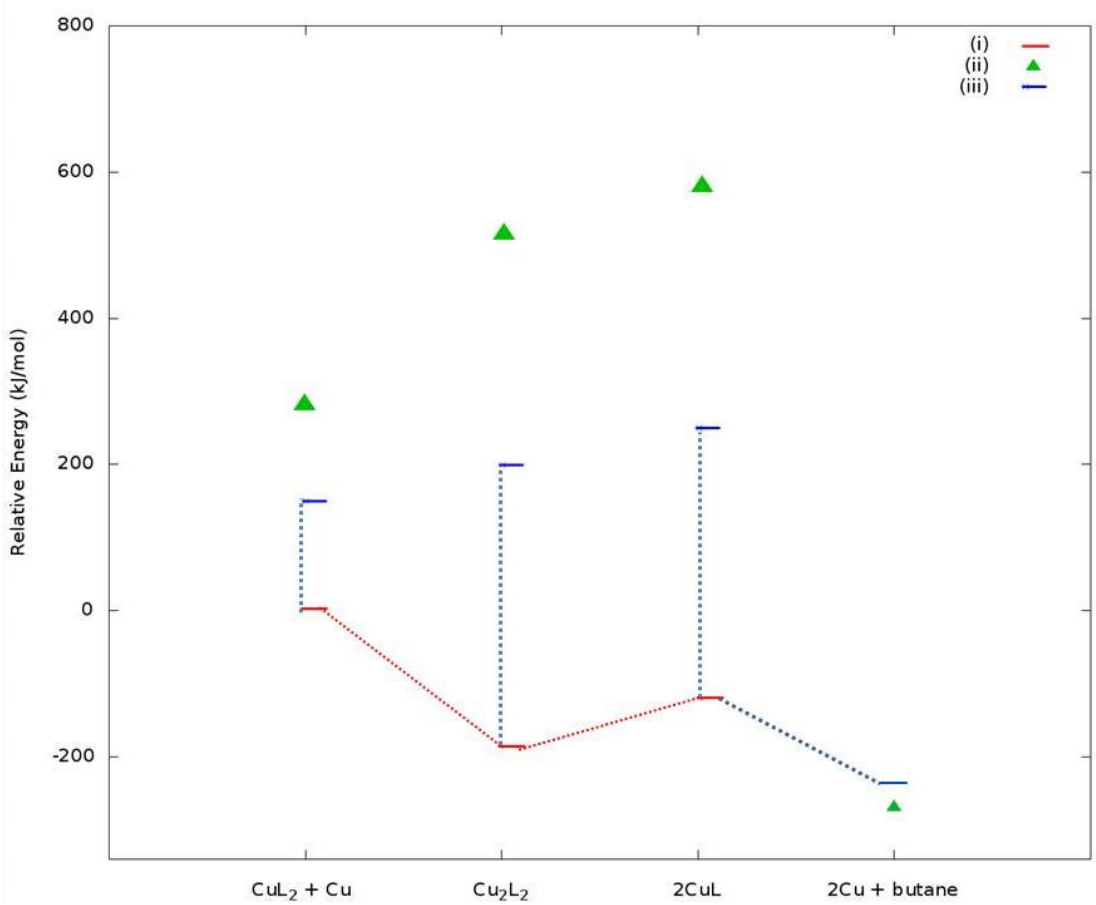


Figure 30: The graph shows similar results to that of Figure 26 but using L = Et as the ligand. The most important reaction shown in the graph is the interaction between two CuEt and formation of butane with deposition of $Cu^{(0)}$. The same reaction can also be formed when Cu_2Et_2 dimer dissociates. The last intermediate has two new Cu atom adsorbed to the surface and butane in gaseous form.

4.4 Discussion:

Through the above adsorption energies, we can assess whether adsorption of the precursors onto the surface plays an over-riding role in the overall process of Cu ALD. A weak adsorption of the compounds (e.g. $Cu(PyrAld)_2$) might indicate poor surface coverage. The energetics also shows that auxiliary reactions that lead to the formation of Cu_2L_2 type surface compounds are inevitable in the precursor pulse. These are discussed below in

sections 4.4.a and 4.4.b. The interaction of the $ZnEt_2$ with the bare copper surface during the co-reagent pulse is discussed in the last section 4.4.c.

4.4.a. Adsorption of CuL_2 onto the surface:

The strength of adsorption (ΔE_{ad} in Table 12) for different copper precursors CuL_2 (L= ligand) onto the bare Cu (111) surface is computed to be in the following order:

L = Et>acac >dmap > $PyrIm^{iPr}$ > AbaCus>>PyrAld

We see that the entropy factor is of similar range for most of the precursor compounds (Table 12). Therefore, the difference between the adsorption energies ΔE_{ad} is primarily responsible for the difference between the free energies (ΔG^{393}_{ad}).

The factors determining ΔE_{ad} are discussed in the following paragraphs. The bond distance between the copper atom in the adsorbed precursor (Cu_{pre}) and the nearest copper atom in the surface (Cu_{surf}) follows the order (Table 11):

$PyrIm^{iPr}$>PyrAld>dmap >AbaCus> acac>Et.

The distances are in the range 2.37 Å – 2.72 Å. It might be expected that the adsorption is strongest for the precursor that has the shortest distance to the Cu_{surf}. However, comparing the two trends presented above, we see that this holds for the strongest bound two compounds (Et and acac), but not for the rest. An alternative explanation might be the steric hindrance and the overall strain present in the precursor complex that hinders adsorption. The extra bonds formed between the precursor ligands Cu_{surf} atoms after adsorption also might be important.

To examine this, we first consider the $Cu(acac)_2$ precursor. The complex is planar as expected for a $Cu^{(II)}$ compound[154]. The complex does not have any bulky substituents above or below the plane. In addition no inter-ligand interaction distorts the complex (Table 13(i)). This planar complex can thus easily approach the Cu(111) surface, allowing Cu_{pre} to access the surface Cu atoms. The favorable adsorption geometry is reflected in a short Cu_{pre} - Cu_{surf}

distance and high ΔE_{ad} for $Cu(acac)_2$. Indeed, $Cu(acac)_2$ adsorbs dissociatively, forming strong bonds between the O (in the ligand) and Cu_{surf}. This might also contribute to its stronger adsorption than the other precursors. However, formation of these extra bonds with the Cu_{surf} may be a disadvantage for the overall process, as it may be difficult for the ligand to be eliminated from the system. Hence, ΔG_{ad} of the precursor solely is not enough to determine the quality of the precursor and a detailed mechanistic study for the ligand exchange reactions is also important.

The lowest energy isomer of $Cu(PyrIm^{iPr})_2$ features bulky ligands (^{i}Pr) that point perpendicular to the plane of the precursor complex (Figure 14 (iii)). This brings in a high steric hindrance between the precursor molecule and the surface. This also distorts the $Cu^{(II)}$ complex out of the planar geometry (Table 11). The bulky substituents prevent the approach of the Cu_{pre} center to the surface and no adsorption geometry could be found. However, in the modified precursor, one side of the complex is free of bulky substituents, which allows the Cu_{pre} to approach the surface and adsorb (Figure 23 (iii)). This example shows that steric hindrance between the precursor complex and the flat (111) surface is important for determining adsorption to the surface. It is likely that adsorption onto a rough or defective surface would be easier.

Adsorption energies for the $PyrIm^{iPr}$ and dmap precursors are comparable (Table 12). From its geometry the modified $PyrIm^{iPr}$ isomer (Figure 23 (iii)) seems to experience comparable steric hindrance to the dmap complex (Figure 23(iv)) during adsorption. This is because both these precursor molecules have flexible alkyl group's perpendicular to the plane of the complex that can be oriented away from the surface. The dmap ligand has two methyl groups attached to the amino nitrogen while $PyrIm^{iPr}$ has ^{i}Pr substitution on the imine nitrogen. Both the precursors show molecular adsorption onto the surface. However, the $PyrIm^{iPr}$ ligand is based on a conjugated π system, while dmap is not. This makes the dmap

ligand more flexible than $PyrIm^{iPr}$. The dmap ligand thus forms extra bonds between O and the surface Cu atoms, without breaking that of Cu_{pre}-O which contributes to stronger adsorption. The Cu_{surf} - Cu_{pre} distance is 2.72 Å for $PyrIm^{iPr}$ and 2.62 Å for dmap. The electronegativity of ligating atoms (N,N vs O,N) and the charge distribution of the two precursors is different (Table 14) but this does not seem to be the primary factor dictating the adsorption of the precursor. $Cu(dmap)_2$ precursors have been reported to undergo decomposition by β-hydride elimination[132], which is a pathway to uncontrolled CVD and not ALD. Hence, $Cu(dmap)_2$ type precursors should be used with caution when tested for ALD reactions.

AbaCus is a six membered complex with an ethyl group on the amino nitrogen. The substituents and the π conjugation affect the orientation of the ligands around the copper center, giving a torsional angle of 131° between the four ligating atoms in the gas phase. The ethyl substituents both point towards one side of the distorted plane of the complex, which makes the other side of the plane free for adsorption. The results are a short bond distance between the Cu_{surf} and Cu_{pre} atoms and new Cu-O bonds (Figure 23(v)). However, there is evidently substantial strain in the adsorbed complex, possibly because of distortion of the π system, as indicated by the lengthening of the Cu-O/N bonds by 0.5 Å, and the overall adsorption energy is low.

The PyrAld precursor has a torsional angle ~ 30° between the two ligands attached to the copper center. This is due to inter-ligand repulsion between H's of the two fused pyrrole rings in the two ligands (Figure 22 (ii)). This non-planarity makes it hard for the Cu_{pre} to approach the surface copper atoms. The O in the precursor does not bond to the surface copper atoms as it is a part of the fused ring. The five membered Cu-containing ring of the PyrAld complex increases the strain compared to the six membered AbaCus, although the torsional angle of AbaCus is greater than that of PyrAld. The Cu_{surf} – Cu_{pre} distance is 2.67 Å.

The PyrAld complex remains poorly chemisorbed onto the surface (ΔE = -127 kJ/mol, Figure 23(ii)). When combined with entropy at typical temperatures, these computed energetics indicates that adsorption is not thermodynamically favored. The pyrrole ring does seem to affect the adsorption structure of PyrAld and $PyrIm^{iPr}$ as in both cases there is a longer Cu_{pre} - Cu_{surf} bond with new ligand to surface bonds.

In a review paper Puurunen[11] has described the intrinsic advantage of less hindered precursor molecules for adsorption onto the surface. The author mentions that chemisorbed sterically crowded precursors can shield reactive sites at the surface from being accessible to other unreacted precursor molecules and that this may result in irregular growth of film. Thus, among the studied precursors, acac and dmap are expected to have the intrinsic quality of higher surface coverage compared to the other precursor compounds, leading to higher growth rate and better film quality in ALD.

The above discussion shows that access of the Cu_{pre} atom to the surface is the most important factor in chemisorption of these complexes. The tendency for $Cu^{(II)}$ complexes to be planar is therefore advantageous. However, when there are bulky ligands present, especially on the ligating electronegative atoms adjacent to the Cu atom, the gas-phase complex twists itself to form a tetrahedral structure. The metal center is then well encapsulated within the ligand shell, which makes it difficult for Cu_{pre} to access the surface[155] (e.g. $PyrIm^{iPr}$). In these cases the adsorption energy is low. In the other planar precursors, Cu_{pre} bonds to Cu_{surf} and we find that the ligating atoms can also bond to the surface metal atoms, contributing extra adsorption energy. The exception is when a fused pyrrole ring makes the ligand too rigid (PyrAld and $PyrIm^{iPr}$). This might be valid for precursor molecules of other metals too, particularly planar d^9 cations. Figure 31 summarizes how possible substitution sites in the precursor complex can affect the adsorption to the copper surface. The same can be concluded for precursors of other metals.

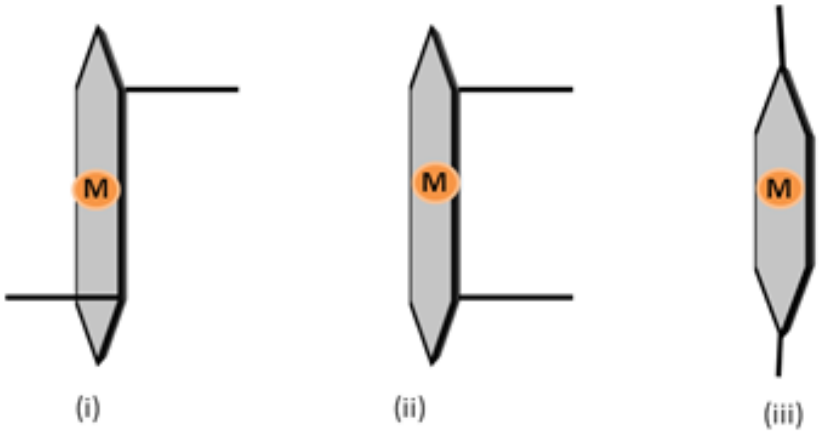


Figure 31: This picture shows the probable places where substitution favors the adsorption of the copper precursors. It has been assumed the precursor is a hexagonal complex. In (i) the substitution is in two opposite direction of the plane. There is no adsorption site as the Cu_{pre} cannot access the surface. In (ii) the substitution is in one direction of the plane, which makes the other plane available for adsorption site. In (iii) the substuation is in the same plane as the copper complex. This does not hinder adsorption.

The adsorption free energies (Table 11, ΔE_{ad}) for the copper precursors to the bare copper surface indicate strong bonding between most complexes and the surface. Strong bonding may in principle be due to ionic, covalent or metallic bonding and it seems that all three contribute to this case, giving rich behavior that varies with precursor stereochemistry. The additional effect of dispersion interaction certainly merits future study. Focusing on the metallic Cu_{pre}-Cu_{surf} interaction, this may be interpreted as a move towards higher coordination for Cu_{pre} as it chemisorbs. This is therefore another example of densification as a key driving force during ALD reactions. Zydor *et al.*[156] have simulated the effect of a bulky ligand in the $Ti(CpMe_5)(OMe)_3$ and H_2O ALD process that explains the experimentally observed lack of ALD of the oxide as due to the inability of the hindered Ti center to chemisorb on the substrate. Here we observe similar results but for Cu precursors and ALD of metals. Thus, our study shows that the most sterically hindered precursors do not chemisorb to the surface and so may not participate in all subsequent reactions that lead to metal ALD.

4.4.b. Non-ALD reactions of Cu_2L_2:

Regardless of the ligand, $Cu^{(I)}$ compounds are computed to have stronger adsorption (Table 13) to the surface than $Cu^{(II)}L_2$ (Table 12). This means that desorption of the $Cu^{(I)}$ intermediates is less likely. The potential energy diagrams illustrate this point (Figure 26, Figure 27 and Figure 30). This is probably because of less steric crowding around the Cu_2 core compared to the corresponding $Cu^{(II)}$ precursor compound (Figure 25). The $Cu^{(I)}$ has better access to the surface copper atoms and the bond distance to Cu_{surf} is always lower than for the corresponding copper precursors. This is seen for all the ligands we have studied here. The ligand atoms also form extra bonds with the under-coordinated surface copper atoms, thus increasing the adsorption energy. There is no difference in charge distribution over the Cu atoms between ligands with and without conjugated π systems (Table 14).

The potential energy diagram is different for the two precursors (L = dmap in Figure 26 and L=$PyrIm^{iPr}$ in Figure 27). We see that the desorption energy for the various $Cu^{(I)}$ species is higher with the dmap ligand than with $PyrIm^{iPr}$. This is probably due to the flexibility present in the dmap ligand, which allows the ligand to break from Cu_{pre} and bind to the surface copper atoms more strongly than its $PyrIm^{iPr}$ counterpart. The conjugation present in the $PyrIm^{iPr}$ ligand does not allow the ligand to form additional bonds with the surface atoms and so desorption of the complexes is easier, which would be determined for ALD.

The $Cu^{(I)}$ compounds are formed from the incoming $Cu^{(II)}$ precursors and $Cu^{(0)}{}_{surf}$ atoms, which means that surface $Cu^{(0)}{}_{surf}$ atoms are temporarily consumed in step 1b. However, in the subsequent $ZnEt_2$ pulse (step 2a), there is formation of intermediate CuEt or Cu_2Et_2, which decompose to form $Cu^{(0)}$ and butane (Figure 30). Likewise, $ZnEt_2$ consumes some surface $Cu^{(0)}$ during dissociative chemisorption in step 2b, but this is restored along with new $Cu^{(0)}$ in the subsequent step 1a of the Cu pulse. The transmetallation ALD cycle

thus involves redox cycling of the entire Cu surface, with comproportionation to $Cu^{(I)}$ in steps 1b and 2b followed by reductive elimination of butane in steps 2a and 1a. Only the latter steps contribute to net growth of $Cu^{(0)}$ at the surface, which is likely to be a fraction of the overall Cu undergoing redox cycling. A similar picture has been described and quantified for redox ALD of noble metals[157].

The higher adsorption energies for the $Cu^{(I)}$ compounds of dmap ligands studied here suggest that a $Cu^{(I)}$ precursor should be preferred over a $Cu^{(II)}$ precursor. This holds true provided other requisite precursor properties are also fulfilled (e.g. volatility). There have been reports of $Cu^{(I)}$ compounds used as ALD precursors[29,76,78] . In a recent study we have seen that $Cu^{(I)}$carbene compounds are promising precursors[60,61]. However, $Cu^{(I)}$ compounds can disproportionate and deposit metal through a CVD pathway rather than through self-limiting ALD, so that stability may limit the use of $Cu^{(I)}$ compounds in ALD.

4.4.c. Interaction of co-reagent $ZnEt_2$ with the surface:

The advantages of $ZnEt_2$ as a reducing agent are that it is volatile and cheaply available. But the co-deposition of Zn with Cu makes it a poor choice. As seen from the adsorption energy, $Zn^{(I)}$ has stronger adsorption than $Zn^{(II)}$. Thus, Zn may persist in (I) oxidation state instead of desorbing as ZnL_2, unless a ligand exchange reaction between the Cu and Zn takes place. The interaction of the $ZnEt_2$ fragments with a mixed surface of ligands from the precursor will be examined in another study later. The current study has clearly shown how CuEt fragments, formed either by ligand exchange or decomposition of $ZnEt_2$, are ultimately unstable against butane and $Cu^{(0)}$ formation.

4.5. Conclusion:

We have computationally explored a part of the surface reactions during the transmetallation process for Cu ALD using DFT. Interactions of Cu(II) precursor molecules and the $ZnEt_2$ molecule with a bare copper surface have been studied (parts 1b and 2b, Figure

20). In this paper, we did not consider the interaction of the compounds in a mixed surface during the early part of the ALD pulse (as depicted in parts 1a and 2a).

The general tendency of gas-phase $Cu^{(II)}$ complexes is to be planar. However, distortions occur due to bulky ligand groups interacting with each other. We see that precursors with less steric hindrance and planar geometry have strong adsorption to the surface, which is a positive indication for ALD. This is because the precursor can access the surface atoms relatively easily and form strong metallic bonds with the under coordinated surface Cu atoms. Ligands may also bond to surface Cu and/or dissociate from the adsorbate complex. At the end of the Cu precursor pulse, we predict that the surface will be covered in ligands attached to $Cu^{(I)}$ atoms. In all the cases studied here, we see that the adsorption does not depend so much on the electronegativity of the ligands as on the flexibility of the precursor complex and the orientation of alkyl substituents. Examining five precursors, we see that the $Cu(dmap)_2$ precursor adsorbs more strongly onto the surface due to the flexibility present in the ligand. Hence, we conclude that dmap-type ligands are best for the ALD of Cu and other transition metals. $Cu(dmap)_2$ has also been previously used in experiments due to its high decomposition temperatures, low non-volatile residue and high sublimation rate[158]

$ZnEt_2$ is found to dissociate into a ZnEt fragment and Et on a bare copper surface. The ZnEt adsorbs to the copper surface more strongly than $ZnEt_2$ and then many Cu precursors. Therefore, impurities from residual ZnEt are inevitable during the ALD reaction unless there is complete exchange of Et with the ligands from the copper precursor. Hence, there is a need to find other reducing co-reagents that have less probability of producing impurities.

Achieving a surface covered with Cu_{surf}-Et is the key step for the deposition and growth of $Cu^{(0)}$, since a pair of these type of surface intermediates self-decomposes forming butane and liberating two electrons in order to deposit an atom of Cu metal. Overall in this

transmetallation reaction it is the Et ligand that donates the electron to copper for its reduction to copper metal.

Supplementary Information:

Table A: The desorption energy (ΔE_{des}), free energy (ΔG^{393}_{des}) and reaction energy for transformation into one another, for various $Cu^{(I)}$ intermediates and $Cu^{(II)}$ species onto the surface where L = dmap. The energy of $CuL_{2(ads)}$ and $Cu_{(s)}$ has been arbitrarily chosen as 0. The desorption energies are with respect to the most stable geometry of the respective particular intermediate. The energies are in kJ/mol.

	ΔE_{des}	ΔG^{393}_{des}	Reaction Energy
CuL_2^* + Cu	249	64	0
$Cu_2L_2^*$	358	165	-146
$2CuL^*$	694	414	-42
Cu_2L^* + L	782	500	-141

**Desorption is with respect to these molecules.*

Table B: The desorption energy (ΔE_{des}), free energy (ΔG^{393}_{des}) and reaction energy for transformation into one another, for various $Cu^{(I)}$ intermediates and $Cu^{(II)}$ species onto the surface for L = $PyrIm^{iPr}$. The energy of $CuL_{2(ads)}$ and $Cu_{(s)}$ has been arbitrarily chosen as 0. The desorption energies are with respect to the most stable geometry of the particular intermediate. The energies are in kJ/mol.

	ΔE_{des}	ΔG^{393}_{des}	Reaction Energy
CuL_2^* + Cu	251	51	0
$Cu_2L_2^*$	215	8	-111
$2CuL^*$	203	-3	-112
Cu_2L^* + L	354	54	-160

**Desorption is with respect to these molecules.*

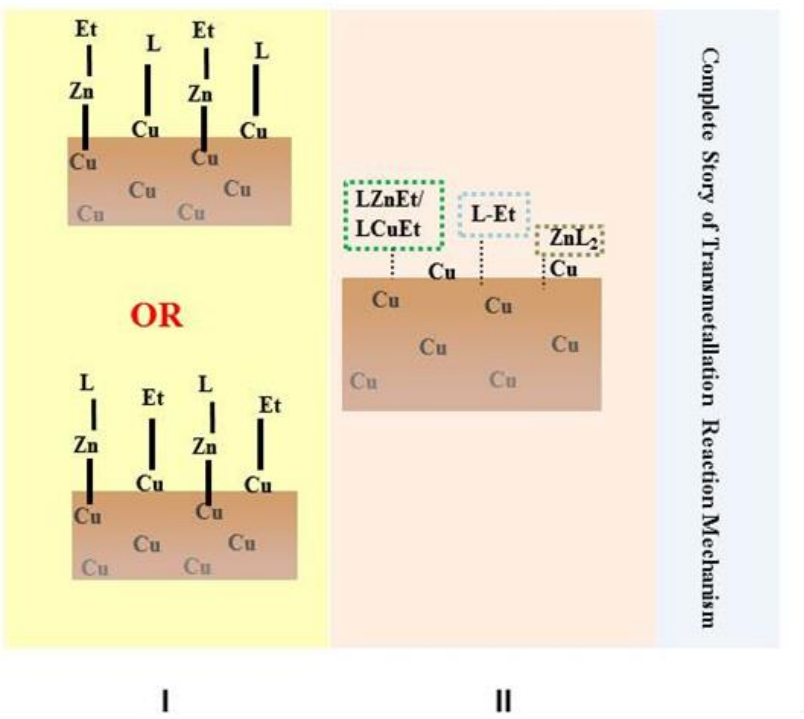
Table C: The desorption energy (ΔE_{des}), free energy ($\Delta G^{393}{}_{des}$) and reaction energy for transformation into one another, for various $Cu^{(I)}$ intermediates and $Cu^{(II)}$ species onto the surface for L = Et. The energy of $CuL_{2(ads)}$ and $Cu_{(s)}$ has been arbitrarily chosen as 0. The desorption energies are with respect to the most stable geometry of the respective particular intermediate. The last energy shows the geometry where the butane remains desorbed over the surface. The energies are in kJ/mol.

	ΔE_{des}	$\Delta G^{393}{}_{des}$	Reaction Energy
CuL_2^* + Cu	259	150	0
$Cu_2L_2^*$	516	200	-178
$2CuL^*$	576	250	-113
2Cu + butane	-	-	-269

**Desorption is with respect to these molecules.*

Chapter 5: Transmetallation reaction mechanism for Atomic Layer Deposition of Copper Using Diethylzinc as the Reducing Agent

Note: The paper has been modified for the thesis. The reference, table and figure numbers are in a sequence with the previous chapters. However, the equation numbers are only valid for this chapter.



Abstract: In this chapter we investigate the reaction mechanism pathway of surface transmetallation for copper precursors and $ZnEt_2$ as the reducing agent for Atomic Layer Deposition (ALD) of copper. Two different copper precursors $Cu(PyrIm^{iPr})_2$ (conjugated ligand, N in the ligand, five membered fused ring structure) and $Cu(dmap)_2$ (non-conjugated ligand, N and O in the ligand, five membered ring) have been mainly considered for this study. It is seen that complete ligand transfer between the metals (Cu/Zn) is selective and is favorable for precursors only without any conjugation in the ligands like dmap. The desorption energies of different half ligand exchanged copper and zinc compounds LMEt (M=Cu/Zn) have also been evaluated in order to account for probable pathways for copper formation and account for any impurity. The study is based on thermodynamic stability of reactants, probable intermediates and by-products. Natural Population Analysis (NPA) has been conducted to understand the charge transfer between various models.

5.1. Introduction

In a typical ALD reaction there are two pulses: Precursor pulse and Co-reagent pulse. For the transmetallation reaction process in this study, the co-reagent pulse is of $ZnEt_2$. The transmetallation reaction process has been reported for solution phase[75,123] as well as surface study[29]. The different cycles for the transmetallation reaction process have been described in Figure 19 in Chapter 4. The reactions after a precursor pulse are denoted by '1' and the reactions for co-reagent pulse are denoted by '2'. This is further subdivided in part a and b showing the reactions at the beginning of the pulse and at the end of the pulse respectively. Part 1b and 2b have already been discussed in the previous Chapter 4. In this part, we study the reactions in part 1a and 2a. In part 1a, the precursor interacts with Et covered surface from the previous reducing agent pulse. In part 2a, $ZnEt_2$ interacts with the surface covered with remnant ligands from the precursor. These two reactions are in principle similar and hence they have been studied together.

In Chapter 4, we have explored the adsorption energies of different copper precursors and $ZnEt_2$ as the co-reagent. We have studied different Cu(I) and Zn(I) intermediates that can be formed onto the surface after precursor and co-reagent pulse respectively. However, no step wise transmetallation reaction mechanism was studied. No pathway has been shown for the Cu-Zn alloy formation that has been mentioned in experiments. Hence, in this section we will study the atom by atom transmetallation reaction for the deposition of Cu. This has been done by collating the results from the previous chapter and exploring pathways for copper deposition in mixed surface that has been studied in this chapter.

We have taken two commonly used precursors for our study:

- copper(II)dimethylamino-2-propoxide $Cu(dmap)_2$
- copper(II)N-isopropyl-2-pyrrolyl-aldiminate $Cu(PyrIm^{iPr})_2$

The differences in their gas phase and surface adsorbed structures can be found in the previous Chapter 4, section 4.3.a. The previous chapter showed that $Cu(dmap)_2$ has very strong adsorption to the bare copper surface due to its intrinsic flexible structure. $Cu(PyrIm^{iPr})_2$ is structurally contrasting to $Cu(dmap)_2$ due to the presence of high steric hindrance, conjugation in the ligands and change in electronegativity. A modified $Cu(PyrIm^{iPr})_2$ has been taken where the two ^{i}Pr face the same direction in order to avoid high steric hindrance present in the original precursor (Chapter 4, section 4.3.a). Hence, these two precursors have been taken for studying the transmetallation reaction process. Other precursors like $Cu(acac)_2$ and AbaCus have also been computed so as to understand the stability of the Cu/Zn intermediates and Zn by-products on the surface.

Two competitive reactions for the copper deposition have been proposed in Chapter 3 (equations 1-2). In equation 1 there is full ligand exchange reaction taking place to form ZnL_2 and in equation 2 there is half ligand exchange reaction.

$$CuL_2 + ZnEt_2 \rightarrow Cu + ZnL_2 + Et\text{-}Et\uparrow \quad ..(1)$$

$$CuL_2 + ZnEt_2 \rightarrow Cu + LZnEt + LEt\uparrow \quad ..(2)$$

Our study is based on computing the thermodynamic stability of the different modelled intermediates. Reactions 1 and 2 are based on ligand exchange reactions between the two metals. In our study, we will evaluate the energetics of ligand exchange for dmap and $PyrIm^{iPr}$ precursors. Formation of half ligand exchanged compounds like LZnEt and LCuEt have been proposed by Vidjayacoumar *et al.*[75] and in Chapter 3 we have discussed the probability of their formation using a gas phase model. In this study, we evaluate the surface energetics for their formation onto the surface and their subsequent desorption from the surface. In an ideal ALD reaction, the by-products should not persist at the surface and form impurity. The desorption energy of the Zn compounds and other organic by-products have been computed.

The probable reaction pathway for an ideal transmetallation reaction has been studied in the last section. We show how only certain precursors can undergo the transmetallation reaction process.

5.2. Methods:

The same method as in Chapter 4, section 4.2 has been used here.

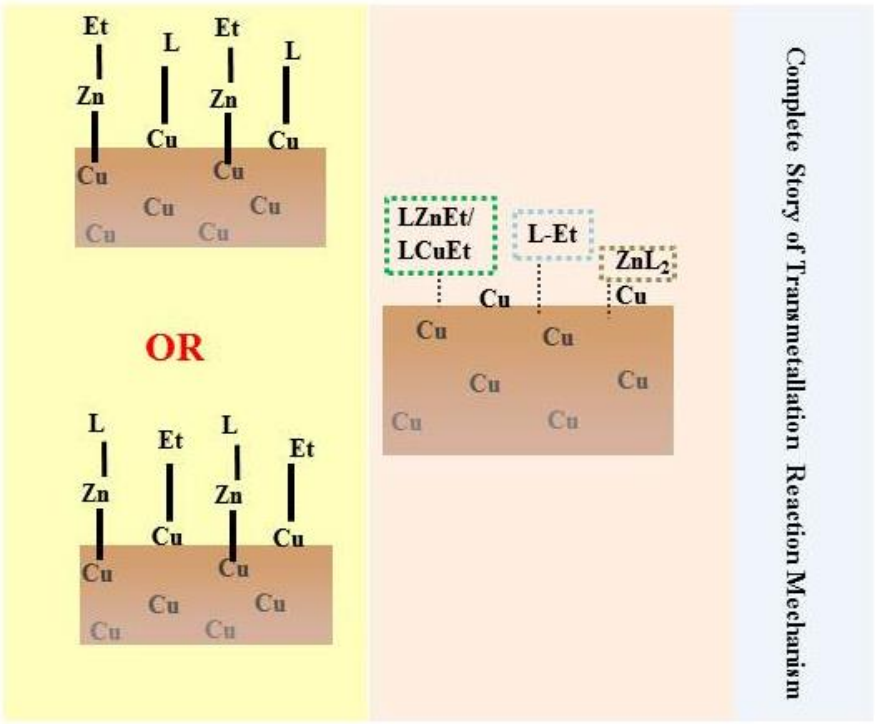


Figure 32: The picture shows the division of parts for this chapter. Here, we are studying the chemistry of a mixed surface that is seen in an ALD chamber after the precursor and $ZnEt_2$ pulse. The most stable structure of Cu and Zn atoms attached to precursor ligand L or Et is explored in part 5.3. The desorption energies of the Cu and Zn by-products are seen in part 5.4. The complete story of transmetallation reaction is seen at the end 5.5.

Results and Discussion (5.3 – 5.5):

This section is divided into three parts:

- 5.3 – In this part, (i) we initially discuss the most stable Cu and Zn fragments on the copper surface in absence of the alternative metal in the adsorbate. (ii) Further, we discuss the probability of ligand exchange between the two metals. (iii) In this section, we discuss the electron flow between the intermediates. (iv) Auxiliary side reactions that are possible on the surface have been discussed at the end.
- 5.4 - (v) In this section, we discuss the desorption energies of the half ligand exchanged compounds (LCuEt and LZnEt) and (vi) also the by-products (ZnL_2, L-Et and butane).
- 5.5 In this part we discuss the ideal transmetallation reaction mechanism.

Part - 5.3

(i) Stable Cu/Zn intermediate onto the copper surface in absence of the alternative metal in the adsorbate:

In this section we will explore the potential energies of different Zn/Cu intermediates in absence of the other metal in the adsorbate. Different ligands (L = dmap, $PyrIm^{iPr}$) have been considered in combination with Et as it is the common ligand from the co-reagent $ZnEt_2$. Figure 33 and Figure 34 shows the reaction when Cu and Zn metal adsorbates are in excess respectively and the other ligand is attached to the surface copper atoms. These models show the probable pathway for the reaction during any part of the ALD cycle when either of the metal compounds is in excess.

Cu: When M = Cu and L = dmap the formation of CuEt or CuL with the other ligand attached to the surface is energetically comparable (difference ~10 kJ/mol) (Figure 33). However, the pathway for the transformation via the intermediate formation of LCuEt costs energy (> +50 kJ/mol), which may be interpreted as the activation barrier for the ligand exchange between the surface copper atom and the rough surface. The formation of $LEt_{(g)}$ and deposition of $Cu_{(s)}$ costs much more energy (> 200 kJ/mol).

When L = $PyrIm^{iPr}$, the most stable intermediate is CuEt and L attached to the surface copper atom. There is an energy gain of 60 kJ/mol for ligand exchange from the reactant (CuL + Et-Cu_{surf}) and product (CuEt+ L-Cu_{surf}). The probability is to proceed via the formation of LCuEt is high as it costs only 10 kJ/mol. Thus, we see that CuEt is formed in this case through ligand exchange between the surface copper and the adsorbate copper. The formation of $LEt_{(g)}$ along with the deposition of copper is thermodynamically not favorable.

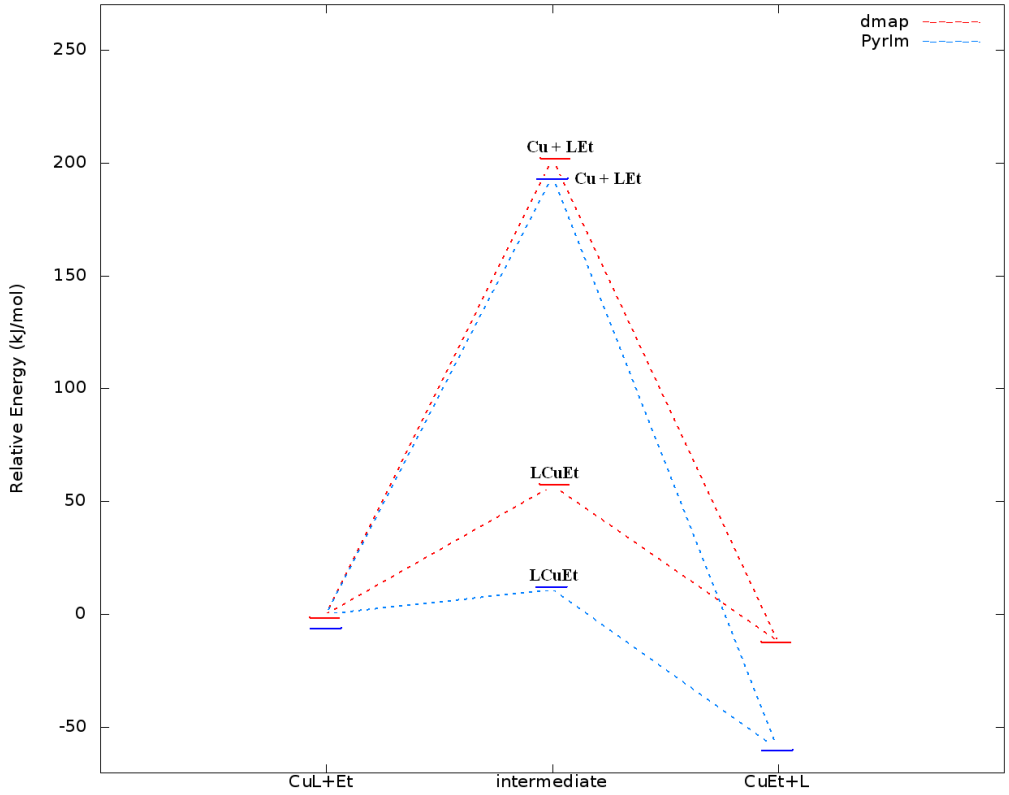


Figure 33: The graph shows the ligand exchange between the copper in the precursor and copper from the surface for two ligands L = dmap and PyrIm^{iPr}. The pathway might follow two different intermediates for each L. It might either form an intermediate redox compound of LCuEt or else there might be formation of gaseous LEt with the deposition of Cu. The two ligand exchanged intermediates have similar energy when L = dmap. But for L = PyrIm^{iPr} the intermediate with the ligand attached to the copper surface is more stable due to downhill in energy.

Zn: When M = Zn and L =PyrIm^{iPr}, the most stable intermediate is ZnEt and L attached to the copper surface (Figure 34). The formation of LZnEt is thermodynamically uphill from both the fragments. Hence, ligand exchange between the Zn and Cu_{surf} via LZnEt pathway has less possibility. This is in accordance with Figure 35 as seen in the section (ii) where a ligand exchange is not favorable between Zn and Cu metals. There is less possibility of any formation of $LEt_{(g)}$ as the reaction costs 88 kJ/mol as computed in 0K.

When L = dmap and M = Zn, the most stable intermediate is ZnL with Et bound to the surface copper atoms. The formation of intermediate like LZnEt, $LEt_{(g)}$ and deposition of

$Zn^{(0)}$, is uphill in energy. This is in accordance with Figure 36, where ZnL fragment is also the most stable. This might be due to the less steric hindrance present in the adsorbate Zn compound.

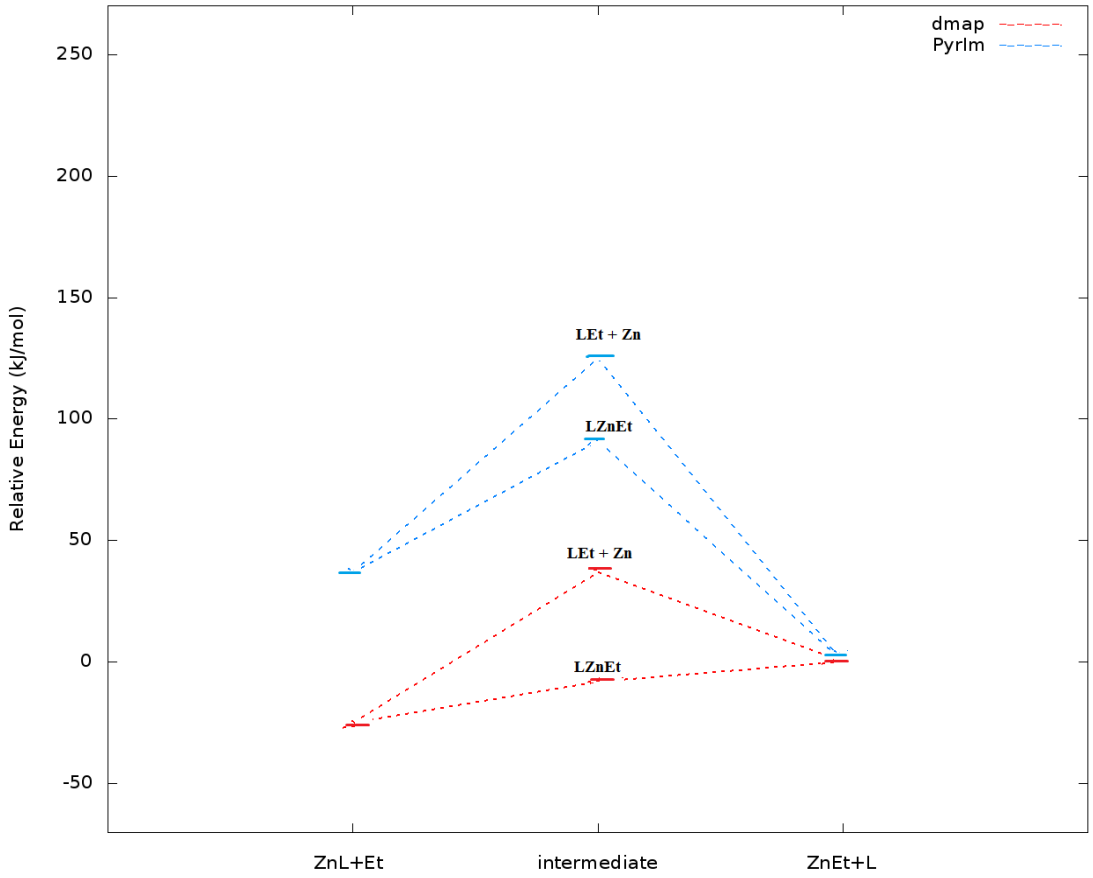


Figure 34: The graph shows the ligand exchange between the Zn in the reducing agent and copper from the surface for two ligands L = dmap and $PyrIm^{iPr}$. The pathway might follow two different intermediates. Zn(dmap) is more stable than ZnEt and ZnEt is more stable than $Zn(PyrIm^{iPr})$ in terms of ligand exchange with the copper surface.

(ii) Is ligand exchange possible between the two adsorbate metals?

The transmetallation reaction mechanism for the deposition of copper is based on the concept of ligand exchange between the Cu and Zn metals as seen in Equation 1. However, no direct evidence of this ligand exchange onto the surface has ever been proved either in experimental study or in surface calculations.

In this part we explore the energetics of ligand exchange reactions between the two metals (equations 3-5). The ligands chosen are dmap and $PyrIm^{iPr}$ (from the precursor) and Et (from the reducing agent). The energetic graphs (Figure 35 and Figure 36) show the ligand exchange for $PyrIm^{iPr}$ and dmap respectively.

ZnEt + CuL → ZnL + CuEt …(3)

ZnEt + CuL → Cu + LZnEt …(4)

ZnEt + CuL → Zn + LCuEt …(5)

PyrIm^{iPr}: In Figure 35, we explore the ligand exchange reaction between the two metals Cu and Zn taking L = $PyrIm^{iPr}$ as an example. The energy of ZnEt and CuL adsorbed onto the surface has been chosen as the base line value. All the other reaction energies are calculated with respect to this base line. A higher value in energy (positive energy compared to the baseline) indicates that the reaction is thermodynamically less feasible as the energy is uphill. Lower value in energy (negative energy compared to the baseline) indicates that the reaction is likely to take place.

Ligand exchange between the two metals (Cu/Zn) is seen to be less likely in this case as the energy of the exchanged intermediate (ZnL + CuEt) is more positive than (ZnEt + CuL) by 26 kJ/mol (Figure 35). In addition, the intermediate formation of LCuEt or LZnEt with the deposition of the other metal is also higher in energy (51 kJ/mol and 17 kJ/mol respectively). However, the later reaction as in equation 4 might be possible as the energy is only 17 kJ/mol. Formation of gaseous product LEt and deposition of the two metals is much higher in energy (> 200 kJ/mol). Hence, ZnEt and CuL is the most stable form during the transmetallation reaction for $PyrIm^{iPr}$ precursor. This indicates that transmetallation is thermodynamically not favorable for $PyrIm^{iPr}$ type ligand.

The above reason can be attributed to the short bond between Cu and N atom in the $PyrIm^{iPr}$ ligand due to the conjugation in its ligand as seen in Table 6, Chapter 3. This makes

the ligand exchange difficult between the two metals. Thus ligands with conjugation seem not to be a good choice for the transmetallation process. Even when there is a mixture of Zn and surface Cu metals, the $PyrIm^{iPr}$ ligand always prefers to remain attached to surface Cu atoms rather than Zn. This can be due to the stronger Cu-N rather than Zn-N (Table 6, Chapter 1). The reluctance of the ligand exchange might also hold true for other ligands with conjugation like acac, hfac etc as reflected in the bond between the metals (Cu/Zn) and the ligating atom in the precursor. Lower probability for the formation of $LEt_{(g)}$ (Figure 33 - Figure 35) and higher energy of CuL intermediates compared to the Cu_2L_2 as seen in Chapter 4 can be attributed to the same reason.

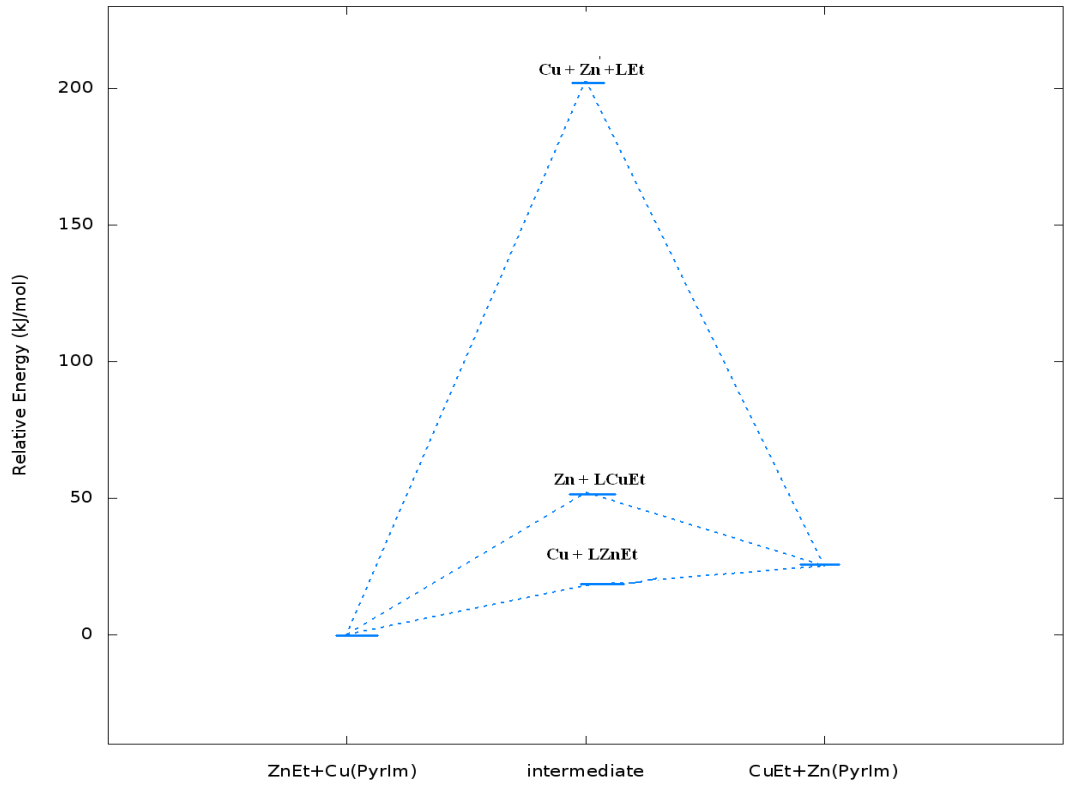


Figure 35: Graph shows the energetics of ligand (L = $PyrIm^{iPr}$) exchange between the two metals Cu and Zn following three possible intermediate pathways. All the intermediates are higher in energy compared to the reactants and products. It shows that ligand exchange is unfavourable for $PyrIm^{iPr}$ ligand. The energy values are presented in the supplementary data.

Dmap: Figure 36 shows the ligand exchange reactions using L = dmap. The same thermodynamic principles as followed in the case of $PyrIm^{iPr}$, has also been used here. A ligand exchange between the two metals is computed to be favorable in this case. This is indicated by the negative reaction energy of products ZnL + CuEt compared to the reactants CuL + ZnEt (-38 kJ/mol). The intermediate energy to form LZnEt and co-deposition of Cu is also thermodynamically favorable as it has negative energy compared to the reactant. This half ligand exchanged compound can also itself lead to the formation of $Cu^{(0)}$. The formation of LCuEt and co-deposition of $Zn^{(0)}$ is also possible as the energy for this reaction is only 17 kJ/mol higher than that of the reactants ZnEt + CuL. Like $PyrIm^{iPr}$, the formation of gaseous product LEt and deposition of Cu and Zn metal is also highly unfavoured (160 kJ/mol).

Compared to $PyrIm^{iPr}$, dmap is a flexible ligand as there is no conjugation in the ligand framework. Hence, ligand exchanged intermediates CuEt and Zn(dmap) can be formed onto the surface (Figure 36). Formation of Cu and LZnEt is lower in energy than Zn and LCuEt. This is an additional pathway for the formation of $Cu^{(0)}$ to that of disproportionation of Cu_2Et_2 intermediates and interaction of two CuEt surface adsorbed intermediates as seen in the previous Chapter 4. However, the Zn compound formed in this case (LZnEt) has strong adsorption to the copper surface as seen in the Part II, which might lead to Zn impurities that is not desirable (Figure 20). By comparison, a third pathway involving the formation of LEt and co-deposition of the metals is high in energy and unlikely to be important.

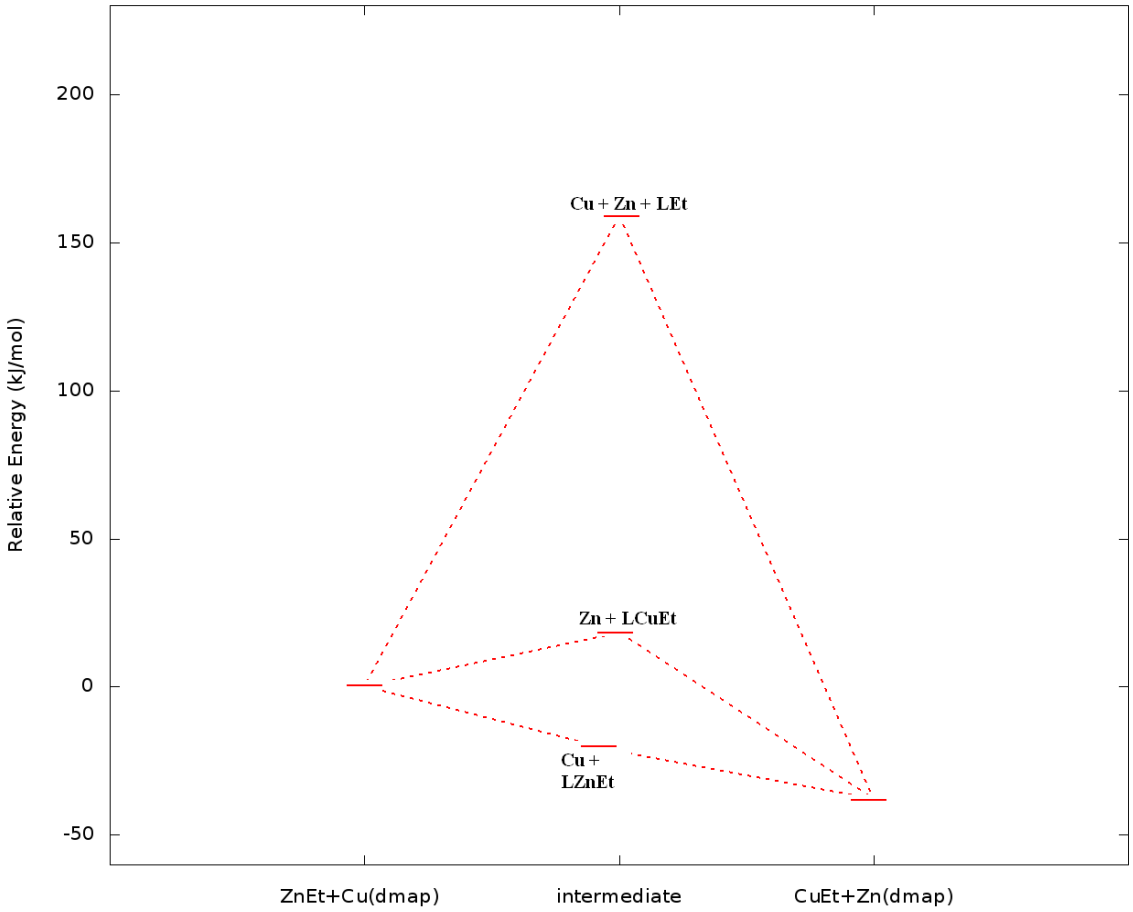


Figure 36: Graph showing the energetics of ligand (L = dmap) exchange between the two metals Cu and Zn following three possible intermediate pathways. It shows that ligand exchange is favourable for dmap ligand as the reaction is downhill. The energy values are presented in the supplementary data present at the end of the chapter.

(iii) Electron flow during ligand exchange reaction

Population analysis of four important models (where L = PyrIm^{iPr}, dmap) has been carried out to understand the transfer of charge between surface bound species. These models are representative of those used for Figure 35 and Figure 36, as follows:

- model I containing ZnEt and CuL adsorbed to the surface (reactants)
- model II containing the Zn$^{(0)}$ and LCuEt adsorbed to the surface (intermediate)
- model III containing the Cu$^{(0)}$ and LZnEt adsorbed to the surface (intermediate)
- model IV containing CuEt and ZnL adsorbed to the surface (products)

Here, we have used Natural Population Analysis for our study. Nevertheless we note that these results are subject to the systematic problem of approximate DFT in localizing electrons in partially occupied metal d states (e.g. Cu(I) vs Cu(II)). Table 15 shows the population analysis data for L = $PyrIm^{iPr}$ and dmap.

$PyrIm^{iPr}$: Table 15 shows that model I exhibits neutral charge on the copper surface and charges of 0.9 and 0.7 on Zn and Cu respectively. Model II shows the bare neutral copper surface donating negative charge to the adsorbate Zn. The surface in turn becomes positively charged. The high reaction energy (51 kJ/mol, Figure 35) representing model II shows that the charge transfer is improbable as the reaction energy is endothermic. Model III shows that relative to model I, the copper atom gains 0.7 units of negative charge to form $Cu^{(0)}$. It gets 0.5 and 0.2 from the zinc and the copper surface respectively. The low reaction energy ~ 17 kJ/mol as seen in Figure 35 indicates the feasibility of the reaction and possible charge transfer to copper. In model IV, the charge of Zn, L and Et is same as in model I. However, the charge between the surface Cu and CuEt is shared. The surface is positively charged and donates the charge to CuEt.

Dmap: Table 15 shows that the copper surface donates negative charge to the Zn adsorbate in model II compared to model I. In Model II zinc gains 0.5 units of negative charge (0.2 units from the copper surface, 0.1 from the CuL and 0.1 from the departing Et group). The lower energetics as seen in Figure 36 indicates the possibility of the charge transfer from model I to model II for the formation of Zn. In model III, copper has gained 0.2 units of negative charge mainly from zinc relative to model I. Model IV shows mostly equivalent charge to model I. However, the charge in Cu from CuEt is 0.2 and that in Et is -0.2, which is 0.3 units less and more respectively than model I. This shows that in this case, the Cu and Et both approach neutrality, unlike similar model in $PyrIm^{iPr}$.

In both the cases, except for model IV in dmap, the charge on Et and the ligands (L) always remains constant.

Table 15: Population analysis for L = $PyrIm^{iPr}$ and dmap precursor using four different models. Model I denotes ZnEt and CuL adsorbed onto a bare copper surface. Model II denotes LCuEt and metallic zinc over the surface. Model III denotes LZnEt and metallic copper onto the surface. Model IV shows adsorbed CuEt and ZnL

Ligand	Fragment	Model I - ZnEt and CuL	Model II - LCuEt and Zn	Model III - LZnEt and Cu	Model IV - CuEt and ZnL
$PyrIm^{iPr}$	copper cluster Cu_{55}	0.0	0.4	0.2	0.3
	adsorbed Zn atom	0.9	0.3	1.3	1.0
	adsorbed Cu atom	0.7	0.8	0.0	0.4
	ethyl ligand	-0.6	-0.6	-0.7	-0.7
	precursor ligand L	-1.0	-1.0	-0.9	-1.0
dmap	copper cluster	0.0	0.2	0.0	0.0
	adsorbed Zn atom	0.9	0.4	1.1	0.8
	adsorbed Cu atom	0.5	0.6	0.3	0.2
	ethyl ligand	-0.6	-0.5	-0.7	-0.2
	precursor ligand L	-0.7	-0.6	-0.7	-0.7

(iv). Auxiliary side reactions:

During the step 2a as in Figure 19, there might be interaction between CuL and ZnL. The possibility of such a reaction is high for flexible ligands like dmap. The computed energetics for this is quoted in Table 16. From the energetics as seen in the table, we can conclude that the possibility for such a reaction is high as the reaction is exothermic. This leads to the formation of $Cu^{(0)}$ and ZnL_2 as by-product. This can be accounted as another

pathway for the formation of $Cu^{(0)}$. Desorption energies of the ZnL_2 will be presented in section vi in Part II.

Contamination of Zn in transmetallation reaction has been reported before[75]. One pathway for this contamination is from $Zn^{(I)}$ as discussed in Chapter 4. Another probable pathway is from $Zn^{(0)}$. From Table 16, we see that when two ZnEt fragments from the reducing agent come close enough to interact but do not undergo the reaction. Hence, the probability of Zn contamination is less.

Table 16: Computed energetics of auxiliary side reactions during the transmetallation reaction process. The energies are quoted in kJ/mol.

Reaction No.	Reaction	L= $PyrIm^{iPr}$	L= dmap
6	$CuL_{(ads)} + ZnL_{(ads)} \rightarrow ZnL_{2(ads)} + Cu_{(s)}$	-200.56	-20.47
7	$2ZnEt_{(ads)} \rightarrow Zn_{(s)} + Butane_{(g)}$	20.50	

Part - 5.4

(v). Desorbed half ligand exchanged product (LMEt)

As seen in Figure 33, Figure 34, Figure 35 and Figure 36 LCuEt and LZnEt compounds may be formed during the ligand exchange reactions for few ligand complexes. This has also been seen through the NMR study by Vidjayacoumar *et al.*[75,123] and through the DFT study in Chapter 3. In this section we will explore the geometry of these desorbed half ligand exchanged compounds (Table 17 and Table 18) and compare them with corresponding gas phase and surface adsorbed precursors. The gas phase structures of these compounds are

present in Figure 37 and the adsorbed structures are in Figure 38 for M = Cu. The desorption energies of these compounds are present in Table 19. In addition to dmap and $PyrIm^{iPr}$, acac and AbaCus compounds have also been studied for better understanding the difference in the desorption energy with respect to change in electronegativity, conjugation in the ligands and five to six membered ring complexes.

The order of desorption energies for the LMEt (M=Cu/Zn) is as follows:

dmap < $PyrIm^{iPr}$ < acac < AbaCus

LCuEt: The dmap compound has the least desorption to the surface (ΔE_{des} = 281 kJ/mol, ΔG_{des}[393] = 123 kJ/mol) as it is a flexible ligand that also forms additional bonds with the Cu_{surf}. $PyrIm^{iPr}$ and acac are nearly as weakly desorbed. The bond distance between the Cu_{LCuEt}-Cu_{surf} is shortest for $PyrIm^{iPr}$ ligand (Table 17) and hence it has weak desorption to the surface. But the ΔE_{des} do not exceed that of dmap due to non-formation of extra bond with the Cu_{surf}. The LCuEt compound from acac form additional bonds with the Cu_{surf}, but the ligating atoms (N/O) breaks from the conjugation with the adjacent atoms in gas phase structure. This bond breaking costs energy and it is not entirely compensated by the formation of additional bonds with the surface atoms. Hence, acac is less strongly bound than the non-conjugated dmap ligand and $PyrIm^{iPr}$ ligand. The AbaCus compound does not form an extra bond with the surface copper atoms. Hence, it is the least stable adsorbate and strongly desorbed from the surface.

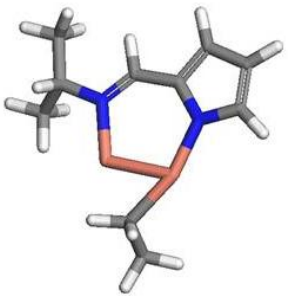
The computed bond distance Cu_{surf} - Cu_{LCuEt} is in the range 2.42 - 2.57 Å. This bond is shorter than that of CuL_2 adsorbed to the surface (2.49 – 2.72 Å) for the main precursor and longer than that of adsorbed $Cu^{(I)}$ compounds (~2.46 Å) (see Chapter 4, Table 11). LCuEt compounds have better access to the Cu_{surf} atoms compared to the corresponding precursors (CuL_2). For example in the case of L = dmap, the ΔE_{des} of CuL_2 is 249 kJ/mol and LCuEt is

281 kJ/mol (Table 18). However, the ΔE_{des} for Cu_2L_2 is 504 kJ/mol. This shows that the strength of desorption of the half ligand exchanged copper compounds lies between those of the precursor compound and $Cu^{(I)}$ compound. This is due to release of the steric hindrance from the adjoining ligand groups in CuL_2. Thus, LCuEt stays weakly desorbed onto the surface regardless of the ligand (Table 19).

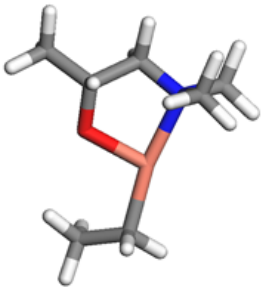
The above data shows that flexible ligands have the weakest desorption energy to the surface due to the formation of additional bonds. Five membered ring compounds have weaker desorption than six membered ring intermediates. This might be due to the tendency of the five membered ring compounds to release the strain that is present in the gas phase structure and form additional bonds. The effect of change in the electronegativity of the ligands is not a predominant factor. This is in accordance with the desorption energy of the copper precursors as seen in Chapter 4.

LZnEt: The order of the desorption energies are in accordance with LCuEt. Thus, the reason for stronger or weaker desorption can be co-related to that of LCuEt counterpart. However, the bond between Zn and the respective ligating atom is weaker compared to the corresponding LCuEt compound (Table 17). The distance from Cu_{surf} to Zn_{LZnEt} is within the range of 2.09 - 2.60 Å. In some cases the distance from Cu_{surf} to Zn_{LZnEt} is longer (acac) while in some others it is shorter (AbaZns) than the corresponding Cu intermediates. However, in all the cases ΔE_{des} of LZnEt is more favourable than that of LCuEt by an average of 100 kJ/mol. This may be due to poor Cu_{surf} – $Zn^{(II)}$ bonding. Even so, desorption of the Zn compounds is not thermodynamically favored at 393 K ($\Delta G_{des} > 0$). In case LZnEt is formed during transmetallation reaction process, persistence of Zn compounds like dmap might lead to Zn impurities. This has often been suggested in experimental papers. However, the formation of LZnEt compounds is possible only for dmap type ligands as seen in Part I

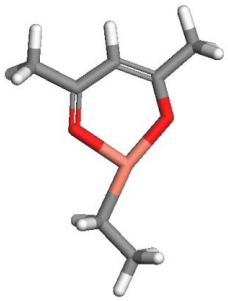
Compared to the respective ZnL_2 compound (as seen in section vi), the bond strength between the Zn and the ligating atom is also lower for LZnEt (Table 18). This is indicated by the longer bond length between the Zn_{LZnEt} and the ligating atom. Steric hindrance is released in LZnEt relative to the corresponding ZnL_2 complexes. This in turn decreases the bond length between Zn_{LZnEt} and Cu_{surf} and tends to decrease the desorption energy to the surface. However, the ΔE_{des} for LZnEt is not always more favourable than that of the respective ZnL_2 complexes. For less sterically hindered flexible compounds like dmap, the surface desorption energy for the two complexes (dmap)ZnEt and $Zn(dmap)_2$ is similar. This is because the methyl group on the amino N of dmap point's perpendicular to the plane of the complex in both the molecules is unhindered. Likewise, we compute a similar desorption energy for both (acac)ZnEt and $Zn(acac)_2$. However, for bulky ligands like $PyrIm^{iPr}$, compounds like $(PyrIm^{iPr})ZnEt$ have favourable ΔE_{des} than $Zn(PyrIm^{iPr})_2$. This is because there is less crowding around Zn in the former case. The situation is similar for AbaZns complexes..



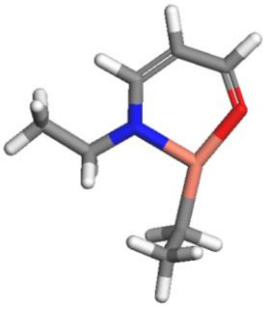
(i)



(ii)



(iii)



(iv)

Figure 37: Lowest energy isomer computed in gas phase for potential LCuEt compounds. (i) L = $PyrIm^{iPr}$ (ii) L = dmap (iii) L = acac (iv) L = $AbaCus^{(TM)}$. The corresponding Zn compounds can be obtained by a change in the central copper atom to zinc. Structural parameters are quoted in Table 17 for copper and Table 18 for zinc compounds. Color code: Red = oxygen, Blue = nitrogen, Grey = carbon, White = hydrogen, Light brown = copper.

Table 17: Comparison of the computed bond distances of copper precursors when in the gas phase and after molecular adsorption onto the surface. The structures of half ligand exchanged LCuEt are also given. The distance from the copper in the precursor to the nearest copper atom on the surface has also been noted and is represented as Cu-Cu. Here L = ligand in the precursor.

Precursors		CuL_2 in the gas phase	CuL_2 adsorbed onto the surface	$LCu^{(II)}Et$ adsorbed onto the surface
$Cu(acac)_2$	Cu-O (Å)	1.95	2.10/2.13/4.08	2.09
	Cu-Cu (Å)	-	2.49	2.50
$Cu(PyrIm)_2^R$ R=^{i}Pr	Cu-N_{Ar}(Å)	1.98	1.94	1.97
	Cu-N_{Ali}(Å)	2.04	1.96	2.29
	Cu-Cu (Å)	-	2.72	2.43
$Cu(dmap)_2$	Cu-O (Å)	1.91	1.95	1.97
	Cu-N(Å)	2.09	2.09	2.33
	Cu-Cu (Å)	-	2.62	2.57
AbaCuS	Cu-O (Å)	1.99	2.55	2.20
	Cu-N (Å)	1.99	2.03	1.98
	Cu-Cu (Å)	-	2.53	2.48

Table 18: The computed bond distances and the dihedral angle of the zinc compounds when in the gas phase and after adsorption onto the surface. The dihedral angle is between the four coordinating atoms to the zinc atom in the precursor, for example in $Zn(acac)_2$ the angle is between four oxygen atoms ∟O-O-O-O. The distance from the zinc atom in the precursor to the nearest copper atom in the surface has also been measured and is denoted by Zn-Cu.

Precursors		By-product ZnL_2	By-product ZnL_2 adsorbed onto the surface	$LZn^{(II)}Et$ adsorbed onto the surface
$Zn(acac)_2$	Zn-O (Å)	1.96	2.03/1.66/2.21	2.20
	∟O-O-O-O (°)	76.05	160.09	-
	Zn-Cu (Å)	-	2.59	2.55
$Zn(PyrIm)_2^R$ R=^{i}Pr	$Zn-N_{Ar}$(Å)	2.06	2.03	2.10
	Zn-N (Å)	2.01	2.08	2.15
	∟N-N-N-N (°)	78.97	47.58	-
	Zn-Cu (Å)	-	4.12	2.49
$Zn(dmap)_2$	Zn-O (Å)	2.19	2.38	2.26
	Zn-N (Å)	1.89	2.03	2.05
	∟O-N-O-N (°)	51.0	124.70	-
	Zn-Cu (Å)	-	2.74	2.60
AbaZnS	Zn-O (Å)	1.99	2.28/2.27	2.54
	Zn-N Å)	2.00	2.09	2.07
	∟O-N-O-N (°)	83.46	137.47	-
	Zn-Cu (Å)	-	2.52	2.09

Table 19: Computed molecular desorption energy (ΔE_{des}), entropy contribution at 393 K ($T\Delta S_{des}$) and free energy (ΔG^{393}_{des}) of possible half ligand exchanged (LMEt) on the Cu surface during transmetallation reaction. Here L = dmap, acac, AbaCus and PyrIm^{iPr} and M = Cu/Zn. The structure of the compounds has been shown in Figure 33. All the values are in kJ/mol.

Ligand	Molecule	ΔE_{des}	$T\Delta S_{des}$	ΔG^{373}_{des}
dmap	(dmap)CuEt	281	158	123
	(dmap)ZnEt	250	158	92
PyrIm^{iPr}	(PyrIm^{iPr})CuEt	263	167	96
	(PyrIm^{iPr})ZnEt	189	166	23
acac	(acac)CuEt	249	155	94
	(acac)ZnEt	164	152	8
AbaCus	(Aba)CuEt	218	153	65
	(Aba)ZnEt	152	153	-1

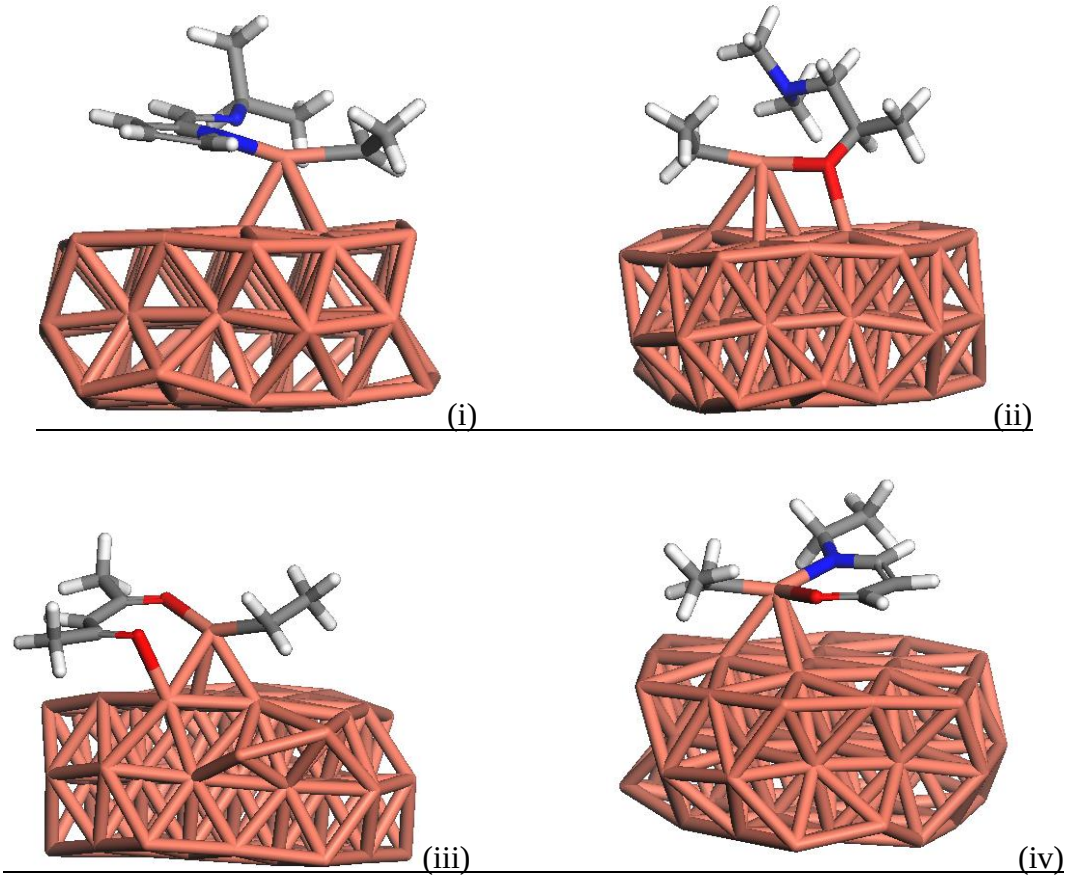


Figure 38: Optimized structures of LCuEt precursors adsorbed onto the bare copper (111) surface. (i) L = $PyrIm^{iPr}$ (ii) L = dmap (iii) L = acac (iv) L = $AbaCus^{(TM)}$. Structural changes between the gas phase structure and the adsorbed structure are shown in Table 17. Color code: Red = oxygen, Grey = carbon, White = hydrogen, Light brown = copper, Blue = nitrogen.

(vi). Desorption of the by-products:

In this section we will study the desorption energies of ZnL_2 and gaseous compounds like butane and LEt. Repeated ligand exchange may lead to formation of the ZnL_2 adsorbate and it is crucial to find out whether this by-product can lead to any impurity.

ZnL_2: For an ideal transmetallation reaction Zn compounds should not remain physisorbed. It should desorb from the surface as shown below.

$$ZnL_{2(ads)} \rightarrow ZnL_{2(g)}\uparrow \ldots(8)$$

The desorption energies of the ZnL_2 are listed in Table 19. $Zn^{(II)}$ compounds are known to have d^{10} electrons. Some $Zn^{(II)}$ by-product complexes like $Zn(acac)_2$, are subject to less steric hindrance in the gas phase compared to the adsorbed structures. Hence, they can chemisorb to form a Zn-Cu bond. The Zn-O bond breaks or else lengthens after adsorption like the copper counterpart as seen in previous chapter. This indicates weak desorption to the copper surface for these type of Zn compounds. We expect a mixture of Cu and Zn acac compounds to remain adsorbed on the surface resulting in formation of the Cu-Zn alloy brass. The flexibility present in the $Zn(dmap)_2$ by-product also makes it susceptible to adsorption rather than desorption. In this case, the O in the ligand forms extra bonds with Cu_{surf} (Figure 39 (iii)). This changes the O hybridization in the compound. There is dissociative adsorption for $Zn(dmap)_2$ and $Zn(acac)_2$ complexes. The desorption of these complexes onto the surface is endothermic and at 393 K, desorption is computed to be thermodynamically not feasible (Table 20). Thus using acac and dmap type precursors will result in Zn impurities.

$Zn(PyrIm^{iPr})_2$ by-products and other tetrahedral complexes like AbaZns retain their almost tetrahedral gas phase structures when adsorbed (Figure 39). The Zn centers therefore do not have access to the surface copper atoms. Hence, they remain physisorbed over the surface. In the case of AbaZnS and $ZnEt_2$, the desorption is favoured, with a computed $\Delta G^{393}_{des} < 0$ K. Thus, the compounds desorb from the surface and not account for Zn impurity.

Thus, we can say that ligand exchanged product in the case of dmap as seen in Figure 34 and Figure 36 might result in Zn impurity from the ZnL_2 and LZnEt compounds as they have poor desorption energies. However, the ligand exchanged product from other

compounds like $PyrIm^{iPr}$ have strong desorption energies. However, there is also less probability of their formation onto the surface (Figure 35 and Figure 37).

Table 20: Computed molecular desorption energy (ΔE_{des}) of zinc compounds onto the copper surface along with the entropy contribution ($T\Delta S_{des}$) of the molecules at T = 393 K. ΔG_{des}^{393} denotes the free energy. All the values are in kJ/mol.

Ligand	ΔE_{des}	$T\Delta S_{des}$	ΔG_{des}^{393}
acac	219	186	32
$PyrIm^{iPr}$	147	209	-61
dmap	212	185	27
AbaZnS	127	175	-48
Et	115	124	-8

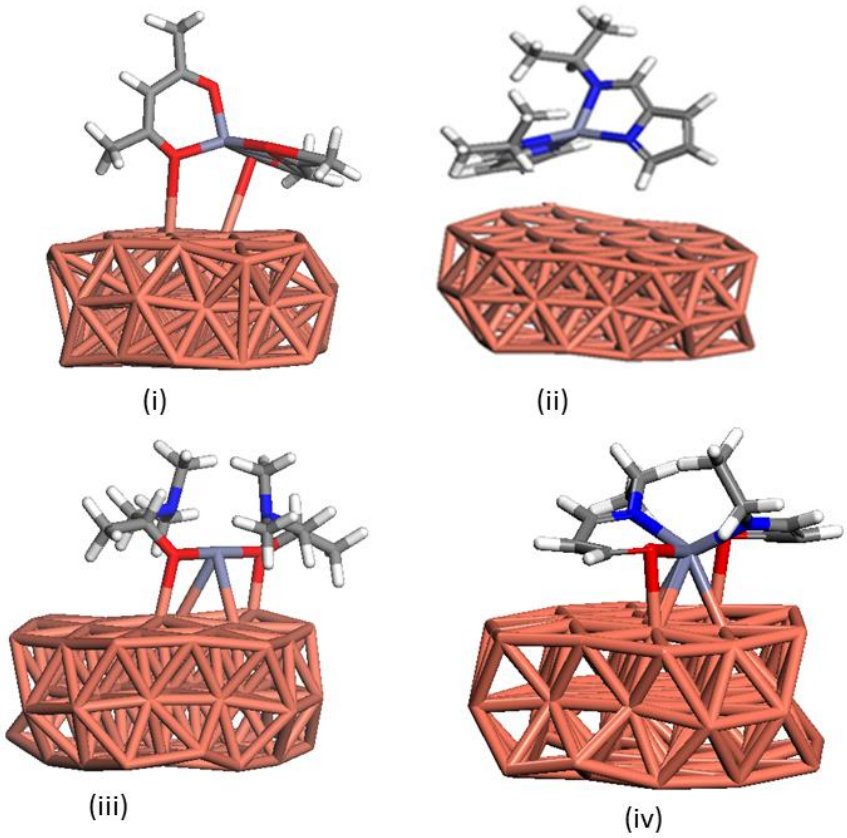


Figure 39: Potential Zn by-products adsorbed on the copper (111) surface. (i) $Zn(acac)_2$, (ii) $Zn(PyrIm^{iPr})_2$, (iii) $Zn(dmap)_2$, (iv) AbaZns. Color code: Red = oxygen, Grey = carbon, White = hydrogen, shaded grey = zinc, Blue = nitrogen.

Organic by-products: There is competition between the formation of two gaseous organic products (LEt and butane) following equations (1) and (2). It was suggested in Chapter 3, that both the products were likely to be formed as the gaseous by-products as the reactions are exothermic in nature. The computed data for desorption of these products from a Cu surface are given in Table 21. It is seen that desorption energy of LEt is less likely (ΔE_{des} = 70 kJ/mol for L = dmap and ΔE_{des} = 151 kJ/mol for L = PyrIm) at T = 0 K than that of butane (ΔE_{des} = 30 kJ/mol). At T = 393 K the situation remains the same, as ΔG_{des} is higher for butane than LEt. Hence, butane is the preferred by-product when the interaction with the surface is

considered. However, Figure 33 - Figure 36 show that the probability for the formation of LEt is negative.

Table 21: Computed molecular desorption energy (ΔE_{des}), entropy at 393 K ($T\Delta S_{des}$) and free energy (ΔG^{393}_{des}) of possible organic gaseous by-products on the Cu surface during transmetallation reaction. Here L = dmap and PyrIm^{iPr}. All the values are in kJ/mol.

Molecule (L-Et)	ΔE_{des}	$T\Delta S_{des}$	ΔG_{des}^{393}
butane	30.2	110.8	-80.6
dmap-Et	70.1	143.9	-73.8
PyrIm^{iPr}-Et	150.9	155.4	-4.4

Transmetallation Reaction

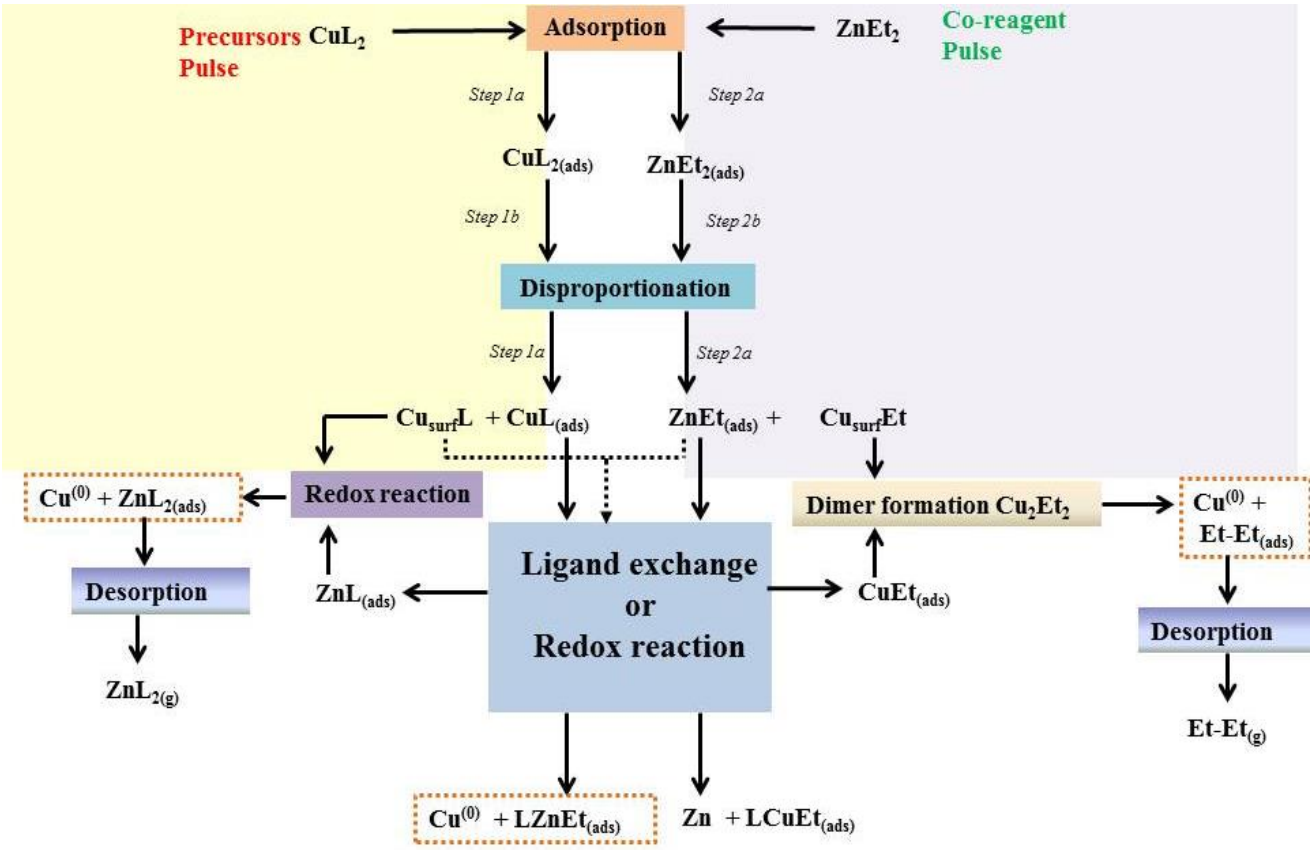


Figure 40: The flowchart shows the possible transmetallation reaction process for any copper precursor and $ZnEt_2$ as the co-reagent. The reactions progresses following the steps shown in the diagram. In case the energy computed for any step is endothermic, the reaction stops at that step indicating a dead end. The top left side indicates the reaction that happens in copper precursor pulse as in Step 1a and Step 1b in Figure 20, Chapter 4. The top right side indicates reaction after $ZnEt_2$ pulse as in Step 2a and 2b in the same diagram. The different processes are indicated in the boxes.

(vi). Complete story of the transmetallation reaction

The possible transmetallation reaction process is present in Figure 40, which shows the step wise conversion of $Cu^{(II)}$ in the precursor to $Cu^{(0)}$ via different intermediates. There are three possible pathways for copper deposition.

- 2CuEt → Cu + Et-Et - Interactions between two CuEt intermediates to form $Cu^{(0)}$ and butane. The CuEt can either be from the ligand exchanged product between CuL and

ZnEt or from the Et adsorbed to the surface copper atoms. The energetics of the reaction has been discussed in the previous chapter. It is a part of the reaction process at the end of step 2b as seen in Figure 20.

- CuL + ZnL → Cu + ZnL_2 - Complete transfer of ligands from Cu to Zn forming ZnL_2. The probability is high for dmap type ligands. However, the Zn by-products can cause impurities due to low ΔE_{des}. This is a part of step 2a as in Figure 19.
- ZnEt + CuL → Cu + LZnEt - $Cu^{(0)}$ can also be formed after the redox reaction between the $Zn^{(I)}$ intermediate and the $Cu^{(I)}$ intermediate to form the half ligand exchanged LZnEt compound along with the co-deposition of copper.

All the above mentioned reactions are marked in Figure 40 in a dotted lined box. From the above reactions we see that a ligand exchange or ligand transfer between the adsorbate copper and zinc metal is important for complete reduction of $Cu^{(II)}$ to $Cu^{(0)}$. Otherwise, there will be incomplete reduction of copper resulting in the surface covered with CuL. Our calculations show that the energetics of the ligand exchange reactions for effective Cu ALD is dependent on the type of precursor used. As seen in Figure 35 and Figure 36, it is only a flexible ligand like dmap that thermodynamically supports complete ligand exchange. Hence, the transmetallation process is selective with respect to ligands.

As seen in Figure 40, there are various pathways for possible Zn impurity during this transmetallation reaction.

- Impurity from ZnEt - In case the ZnEt intermediate does not undergo ligand exchange, as seen in the case of L = $PyIm^{iPr}$, it remains strongly adsorbed to the surface copper atoms (ΔE_{ads} = -264 kJ/mol) and is likely to be incorporated into the film as an impurity.

- Impurity from ZnL_2 - However, even if there is ligand exchange to form ZnL_2 compound, like in the case of dmap ligands, the desorption of ZnL_2 is endothermic . Thus, the zinc by-product will remain adsorbed to the surface giving impurity.
- Impurity from LZnEt – In case of redox reactions between the ZnEt and CuL, with the ligand transfer to Zn metal, the resulting LZnEt compound has strong bonding to the copper surface. Hence, it will result in Zn impurity.

Hence, when using $ZnEt_2$ as the reducing agent, we see that there are various pathways for incorporation of Zn into the system.

The overall transmetallation reaction process resembles a CVD type pathway for copper desorption rather than ALD. This is due to the possibility of several side reactions that take place in the reaction. One primary goal in an ideal ALD reaction is minimizing the possibility of any side reactions. However, the transmetallation process using $ZnEt_2$ as the reducing agent does not fulfill this criterion. Thus, we suggest other organometallic reducing agents for possible Cu ALD. We have proposed metallocene to be another choice of reducing agent as seen in the next chapter.

Part - 5.5

Conclusion:

The desorption energies of the by-products is dependent primarily on the stereochemistry of the compounds. This has also been seen for the copper precursors as in Chapter 4. The less sterically crowded half and full ligand exchanged products have similar desorption energies, like in the case of acac and dmap .

Cu and Zn intermediates compounds have low desorption energies and hence they are likely to cover the surface if formed. The Zn compounds have higher desorption energies than those of copper due to weaker Cu-Zn bonding than Cu-Cu bonding. However, the probability of their formation is dependent on the type of ligand used.

There are various pathways for copper deposition from the precursor. One of the primary sources of copper deposition is after the ligand exchange reaction with Zn and Cu resulting in the formation of Cu_2Et_2. This dimer disintegrates and forms metallic copper after the donation of an electron from Et. Other side reactions may also result in the deposition of copper.

During the transmetallation reaction process, along with pathways for copper formation, there are also pathways for Zn impurity incorporation. The strong adsorption of ZnEt, ZnL_2 and LZnEt in some cases indicates that Zn impurity is inevitable when using $ZnEt_2$ as a reducing agent. Hence, a change in the organometallic reducing agent is required.

The overall copper precursor and $ZnEt_2$ transmetallation reaction process has several side reactions. Also a transmetallation reaction process with $ZnEt_2$ is selective and not all the copper precursors undergo the ligand exchange process. Hence, other co-reagents should be explored. This will be seen in the next few chapters.

Supplementary Information

Table A: Reaction energies for Figure 33 and Figure 34. All the energies are in kJ/mol.

Reaction	L= PyrIm^{iPr}	L= dmap
CuL + Et → $Cu_{(s)}$ + $LEt_{(g)}$	194.78	202.3
CuEt + L → $Cu_{(s)}$ + $LEt_{(g)}$	254.27	190.50
CuL + Et → CuEt + L	-59.49	11.80
CuL +Et →LCuEt	10.89	57.38
CuEt + L →LCuEt	70.37	45.59
ZnEt + L → Zn +$LEt_{(g)}$	88.30	62.35
ZnEt + L →LZnEt	54.23	17.71
ZnL + Et →L + ZnEt	37.73	25.84

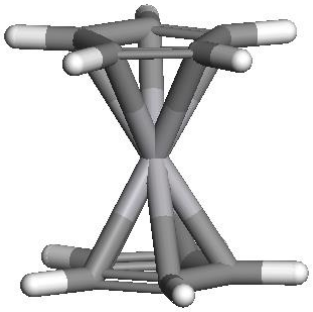
Table B: Reaction energies for Figure 35 and Figure 36. All the energies are in kJ/mol.

Reaction	L= PyrIm^{iPr}	L= dmap
CuL + ZnEt→CuEt + ZnL	25.84	-37.73
CuL + ZnEt → $Zn_{(s)}$ +LCuEt	51.98	17.97
CuL + ZnEt → $Cu_{(s)}$ +LZnEt	17.90	-21.00
CuL + ZnEt → $Zn_{(s)}$ + $Cu_{(s)}$ + $LEt_{(g)}$	203.00	159.53

Chapter 6: Metallocene as the reducing agent for atomic layer deposition of copper

This chapter has been prepared for submission. Here I have formulated the main idea, carried out the computational work and have driven the conclusion. This work has 80% computational work and 20% experimental carried out by AMSG group in Tyndall National Institute.

Note: The paper has been modified for the thesis. The reference, table and figure numbers are in a sequence with the previous chapters. However, the equation numbers are only valid for this chapter.



Abstract: In this chapter, we report the use of metallocene compounds as reducing agents for the deposition of the transition metal Cu from its common precursors. The initial study is performed using DFT calculations using gas phase models. The metallocene structures vary in the presence of the metal that is sandwiched between two cyclopentadiene rings and the copper precursors vary in the electronegativity of the ligand, steric hindrance as well as the conjugation in the ligands. The metal present in the metallocenes donates electrons to Cu(II) for its elemental deposition and itself undergoes oxidation from II to III/IV. The exothermic reaction energies and the availability of a monomer indicate that vanadocene is the most promising reducing agent. A solution phase study using the $Cu(acac)_2$ precursor and vanadocene as the reducing agent shows bulk copper deposition. This study thus demonstrates the use of metallocenes in the ALD of Cu or other transition metals such as Co or Ni.

6.1. Introduction:

As seen in Table 5 (Chapter 1), the most recent reducing agents for Cu ALD are metal-based compounds. Lee *et al.*[29] have proved that an organometallic reagent $ZnEt_2$ can act as the reducing agent for $Cu(dmap)_2$ precursor (dmap = $OCHMeCH_2$-NMe_2, dialkylamino-2-propoxide, Table 5 (Chapter 1)) and the mechanism has been discussed in details in Chapters 3-5.

These studies led us to explore other organometallic reagents that can be used for the reduction of Cu. From the literature, we found that vanadocene was used to form ultrafine magnetic iron from ferric chloride[159]. In a similar study, deposition of rhodium from [Rh(μ-Cl)$(C_2H_4)_2$] and vanadocene in presence of poly(vinylpyrrolidone) (PVP)[160] has been reported. These studies motivated us to explore the probable use of metallocenes as reducing agent for Cu ALD.

Metallocene is a compound typically consisting of two cyclopentadienyl anions (Cp, which is $C_5H_5^-$) bound to a metal centre (M) in the oxidation state II, with the general formula $(C_5H_5)_2M$. Metallocenes are used as homogenous catalysts in organic chemistry[161]. However, metallocenes are rarely used industrially.

Metallocene has been previously used in metal ALD for the deposition of the metal in the metallocene. For example, Os was deposited from osmocene and oxygen[54], Co from cobaltocene[162] and Pt from $CpPtMe_3$ and oxygen[53]. Certain metal oxides were also deposited from the respective metallocenes. For example ZrO_2 and HfO_2 were deposited from the corresponding *ansa*-metallocene precursor[26] and Fe_2O_3 was deposited using ferrocene and oxygen.

Solution phase chemistry has been widely applied for studying suitable combinations of precursor and co-reagent for effective ALD/CVD reactions[75,123,163]. This approach is rapid and straightforward, unlike time and resource intensive ALD/pulsed-CVD studies. Solution studies also allow for comparatively more facile analysis of the reaction pathways responsible for precipitation of the metal, thereby providing a starting point for consideration of the reaction pathways involved during ALD or pulsed-CVD. While the extent to which solution reaction pathways correlate with those in metal ALD has rarely been determined, solution thermolysis reactions employed in the study of CVD have in some cases provided strong evidence for mechanistic parallels between solution- and surface-based reactivity. In this study we will use a solution phase study to test our proposed combination of Cu precursor and metal organic co-reagent (metallocene).

In our study, we initially validate the proposed chemistry by gas phase reaction energies and then we further explore the surface adsorption energies of the by-products using DFT as a tool. Furthermore, a solution phase experimental study has been carried out using vanadocene the reducing agent and $Cu(acac)_2$ as the precursor.

6.2. Proposal for new Cu(0) pathway:

In this work, we initially propose that the metal cation in the metallocene can donate two electrons to Cu(II) for its reduction following equation (1)

$Cu^{+2}L_{2(g)} + M^{+2}Cp_{2(g)} \rightarrow Cu^{0}_{(s)} + M^{+4}Cp_2L_{2(g)}$ ….(1)

In the above reaction, there is complete transfer of the ligands (L) from copper precursor to metallocene. Here, both the ligands are transferred to the same metallocene molecule, which confers oxidation state IV on M from metallocene. An alternative to equation (1) can also be proposed as in equation (2).

$Cu^{+2}L_{2(g)} + 2M^{+2}Cp_{2(g)} \rightarrow Cu^{0}_{(s)} + 2M^{+3}Cp_2L_{(g)}$ …(2)

A third possibility is to use the metallocene to reduce an intermediate layer of CuO or CuS. Figure 41 describes pictorially how this reaction is expected to take place via the intermediate pathway of CuO/CuS. The direct and the intermediate steps are described in detail in section 6.4.

The reduction potential of some metallocenes are measured by Holloway *et al.*[164] using cyclic voltammetry. The trend in reduction potentials of the four metallocenes known to produce simple anions (V, Cr, Co, Ni) is that the more electron-rich metallocenes are easier it is to reduce. The experimental reduction potential of some of the metallocenes and copper are listed in Table 22. It shows that the Cu in I/II oxidation state always has a greater tendency to be reduced to Cu(0) compared to metallocene reduction from oxidation state III.

For the initial screening study five different commonly used copper precursors are used. They are as follows:

- copper$^{(II)}$acetylacetonate, $Cu(acac)_2$
- copper$^{(II)}$N-isopropyl-2-pyrrolyl-aldiminate, $Cu(PyrIm^{iPr})_2$
- copper$^{(II)}$dialkylamino-2-propoxide, $Cu(dmap)_2$

- copper$^{(II)}$pyrrolyl-aldiminate, $Cu(PyrIm)_2$
- copper$^{(II)}$pyrrolyaldehyde, $Cu(PyrAld)_2$.

Most of these precursors were studied earlier and the structural properties like bond angle, torsional angle, bond length have been reported by Dey *et al.*[33]. They are pictorially represented in Figure 14, Chapter 3. The copper precursors were tested with different metallocenes varying in the metal present in the compound. They can be represented as MCp_2 (M = Co, Ni, V, Cr and Fe, Figure 42). The energetics of other metallocene compounds like M = Hf, Mo, Ti, Ta, Zr are presented in the supplementary information. They do not exist in II oxidation state and can only be found in higher oxidation state of III/IV/V.

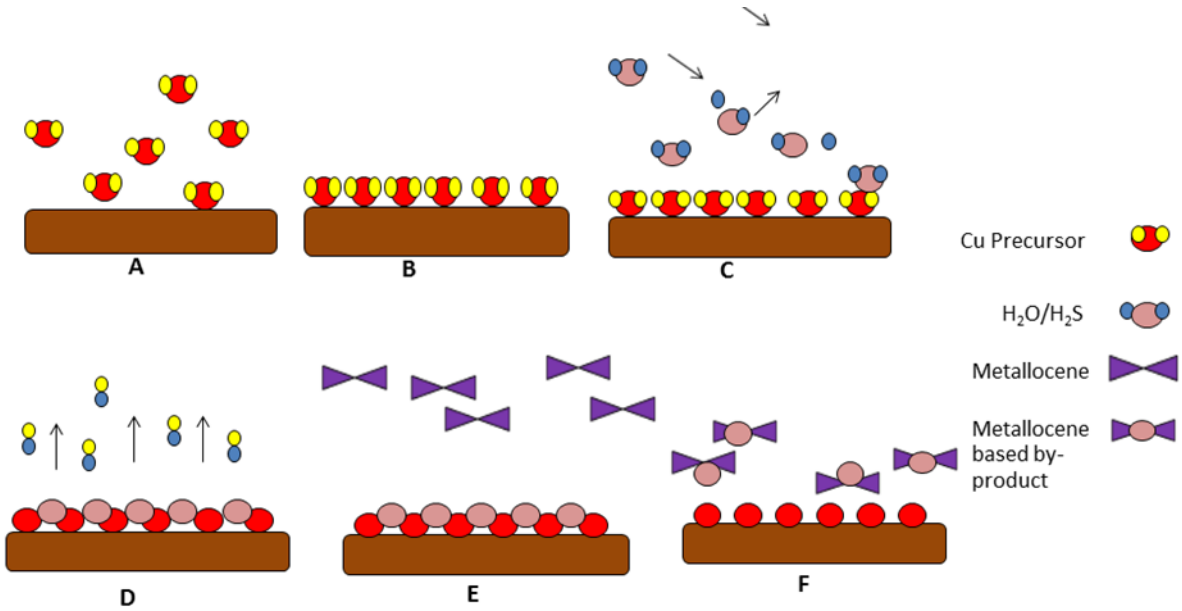


Figure 41: The picture shows the proposed deposition of copper from copper precursor with the intermediate formation of copper sulfide or copper oxide. 'A' shows the precursor pulse. 'B' shows the saturation of the precursors onto the surface. 'C' shows the H_2O or else H_2S pulse. 'D' shows the formation of oxide or else sulfide. 'E' shows the incoming metallocene and 'F' the deposition of copper with the formation of substituted metallocene products. Steps C and D can be omitted and there can be direct deposition of copper from the precursor as described in equations 1 and 2.

Table 22: Literature values for reduction potential of some of the metallocenes that are studied here and aqueous copper.

Molecule	Reduction Potential	Reference
$CoCp_2^+/CoCp_2$	-0.91 vs SCE	Koepp *et al.*[165]
$NiCp_2^+/NiCp_2$	-1.74 V vs. SCE	Denisovich *et al.*[166]
VCp_2^+/VCp_2	-0.70 V vs SCE	Choukroun *et al.*[159]
$CrCp_2^+/CrCp_2$	-1.04 V vs SCE	Ray *et al.* [167]
$FeCp_2^+/FeCp_2$	0.40V vs SCE	Gagne *et al.*[168]
Cu^+/Cu^0	0.52 V vs SCE	Samans[169]
Cu^{+2}/Cu^0	0.34 V vs SCE	Samans[169]
Cu^{+2}/Cu^{+1}	-0.16 V vs SCE	Samans[169]

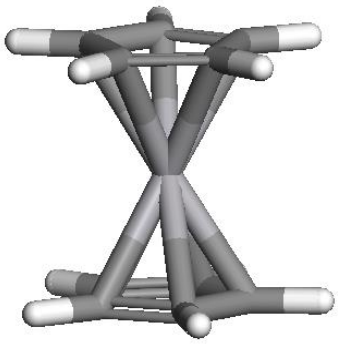


Figure 42: Stick model of (i) Vanadocene. Colour code: Grey – Carbon, White – Hydrogen, Light Grey – Vanadium, Dark Blue – Nitrogen.

6.3. Methods used:

6.3.i. Computational techniques:

In the gas phase model, all the Cu precursors are open shell as they are in II oxidation state. The metallocenes studied here are also in II oxidation state. The metallocene by-products are either in III or IV oxidation states. The metallocene and metallocene based by-products is susceptible to have multiple spin states. We have allowed the structures in different spin states to relax towards its own equilibrium geometry. Only the geometries with lowest energies have been considered. Open shell calculations are done using Unrestricted Kohn-Sham (UKS) and closed shell calculations are done through Restricted Kohn Sham (RKS).

The spin states of most stable metallocenes and metallocene based by-products are present in the supplementary information at the end of the chapter. The spin states using a higher basis set def-TZVPP[148] has also been checked. It was found that the most stable spin states are in correspondence with the one found using def-SV(P). All the spin states are also in accordance with the stable spin state as described by Swart[170]. Hence, the basis set and the functional chosen for this study is justified.

Spin contamination was negligible for most of the metallocene structures except for vanadocene. This problem with vanadocene is well known and has been reported by Swart[170] ($<S^2>$ = 1.75 here and the pure spin doublet is 0.75). A spin projection technique has been proposed by Wittbrodt *et al.*[171] in order to deal with this problem. The energy of pure spin doublet has been calculated using this proposal for structures showing spin contamination.

The range of spin contamination of the metallocene based by-products is in a negligible range as proposed by Grenhof *et al.*[172]. This is in exception to $V^{+4}Cp_2(acac)_2$ ($<S^2>$ = 0.91), $Cr^{+3}Cp_2(acac)$ ($<S^2>$= 1.69), $Cr^{+3}Cp_2(PyrIm^{iPr})$ ($<S^2>$ = 0.99), $Fe^{+3}Cp_2(acac)$ ($<S^2>$ = 1.33). In these cases, the previously used spin projection technique by Wittbrodt *et al.*[171] has been used to compute the energy of pure spin states.

Energetic in the reaction can either be exothermic or endothermic as indicated by ΔE. According to the rules of thermodynamics, exothermic reaction indicates the feasibility of the reaction. In this paper we will follow this thermodynamic principle.

6.3.ii. Experimental

All wet chemical tests were performed in a dry, oxygen free atmosphere of dinitrogen using Schlenk techniques and specialized glassware fitted with Young's taps. Vanadocene (95 % sublimed) was purchased from Strem Chemicals, Inc. Copper (II) acetylacetonate was purchased from Sigma Aldrich and purified via sublimation. All other solvents were bought anhydrous from Sigma Aldrich.

ALD experiments were carried out on a home - built reactor. Si(100) and Ru substrates were placed on a graphite block, whose temperature was controlled with two heating gaskets and a thermocouple in it connected through feed-troughs in a Klein flange in the front, and placed in the middle of a three-way steel tube with an inner diameter of 40 mm. The tube wall temperatures were heated to 135° C with a heating tape wrapped around it and the tube was evacuated with a mechanical pump to pressures below 0.1 Torr. The precursors $Cu(acac)_2$ and vanadocene were stored in Swagelok stainless-steel containers and were heated to 130° C and 85° C respectively. The precursors were exposed to the substrate with Swagelock ALD valves. The opening sequences were controlled with a LabView program. The scanning electron microscopy (SEM) micrographs were taken with a Quanta FEG 656 microscope using secondary electrons mode.

6.4. Results and Discussion (Computational study):

We propose three different possible pathways for the use of metallocenes (MCp_2) as the reducing agent in ALD, described respectively in sections 6.4.a.i, 6.4.a.ii and 6.4.a.iii.

6.4.i. Reduction by abstraction of ligands from the precursor:

Cu is transferred into the ALD chamber via a pulse of precursor $Cu(II)L_2$, leading to a surface covered in ligand L. The adsorption of these precursor compounds onto the surface has been described by Dey *et al*.[173] The unabsorbed precursor can be purged out of the system, as in standard ALD. We propose that a metallocene $M(II)Cp_2$ is introduced as the second pulse. It can abstract ligands from the precursor, desorbing as $M(III)Cp_2L$ or $M(IV)Cp_2L_2$ and also simultaneously donating one electron per ligand to the surface so as to yield Cu(0). This is followed with a purge, and the cycle is repeated.

First step: surf + $Cu(II)L_{2(g)}$ → surf-$Cu(II)L_2$…(3)

Second step: surf-$Cu(II)L_2$ + $M(II)Cp_{2(g)}$ → $Cu(0)_{(s)}$ + $M(IV)Cp_2L_{2(g)}$…….(1)*

surf-$Cu(II)L_2$ + $2M(II)Cp_{2(g)}$ → $Cu(0)_{(s)}$ + $2M(III)Cp_2L_{(g)}$ …….(2)*

We have used DFT calculations to test this proposal using five copper precursors with different metallocenes as mentioned in section 2. However, for this wide screening, we have only used gas phase molecules and corrected for bulk Cu(0), and not explicitly considered adsorption. This corresponds to modifying equations (1)* and (2)* to give the overall ALD equations (1) and (2) as seen below.

$Cu(II)L_{2(g)}$ + $M(II)Cp_{2(g)}$ → $Cu(0)_{(s)}$ + $M(IV)Cp_2L_{2(g)}$…….(1)

$Cu(II)L_{2(g)}$ + $2M(II)Cp_{2(g)}$ → $Cu(0)_{(s)}$ + $2M(III)Cp_2L_{(g)}$ …….(2)

The computed reaction energies for equations (1) and (2) are shown in Table 23. The adsorption energies of the different precursors onto the surface as in equation 3 have been computed in another study[174]. However, when comparing the overall ALD reactivity of different precursors with the same kind of metallocenes, we see that there is uniformity in the reaction energies and all the precursors behave the same. The precursors used here differ in the electronegativity of the ligands attached, conjugation present and steric hindrance. The reaction energies only vary with the metallocenes that are used.

Unsurprisingly the reaction energies for equations 1 and 2 follow the same trend. If reaction 1 has an exothermic reaction energy, then reaction 2 generally shows the same. However, only in the case of $CrCp_2$, the reaction of equation 1 is endothermic while reaction 2 is exothermic (Table 23), probably reflecting that the substituted metallocene compound has reached a stability in reaction 2.

When using vanadocene as a reducing agent, it is computed to show exothermic reaction energies for all the cases (Table 23). The same conclusion can be made for tantalocene (see supplementary information for energetics) but it is not available in II oxidation state. V has d^3 configuration in the unreacted metallocene. V donates one or two electrons to Cu in order to reach d^2 and d^1 configuration in the respective by-products. The donation of electrons is promoted by the higher (more positive) reduction potential of Cu metal as seen in Table 22. The difference between the reaction energies of equations 1 and 2 are > +150 kJ/mol for most of the cases. Vanadocene can be readily purchased. These factors show that vanadocene is a good option as the reducing agent.

Cr is in group 6 in the periodic table and it has d^4 configuration in chromocene. It can in principle donate one or two electrons to copper in order to form d^3 and d^2 configurations. When the $CrCp_2$ based by-products have reached the stability of d^3, they do not donate an extra electron in order to reach d^2 configuration. The probable reason is high ionization energy[175]. It has been reported that chromocene forms $CrCp^+$ easily by electron transfer[164]. Hence, this favors the electron donation to copper.

$FeCp_2$ has 18 electrons in its valence shell that is the nearest noble gas configuration[176] and thus enjoys extra stability. Consequently reactions that remove electrons from Fe are found to be endothermic in nature. Other metallocenes like $CoCp_2$ and $NiCp_2$ that have beyond 18 electrons also show endothermic reaction energies. Although $CoCp_2$ is a common one

electron reducing agent in the laboratory, it cannot follow the pathway described in equation 1 and 2.

Table 23: This table shows the energetics of five different copper precursors interacting with different metallocene compounds to form metallic Cu following equation 1 and 2. The energies are computed using DFT as the level of calculation and def-SV(P) as the basis set. In cases like vanadocene where the computed ground state has spin contamination, the energies are corrected using the spin projection formula described by Swart[170]. The energies are quoted in kJ/mol. The energy values in italics indicate endothermic reactions.

	$Cu(acac)_2$		$Cu(dmap)_2$		$Cu(PyrAld)_2$		$Cu(PyrIm)_2$		$Cu(PyrIm^{iPr})_2$	
	1	2	1	2	1	2	1	2	1	2
VCp_2	-7.8	-200.9	-81.8	-157.1	-68.0	-262.2	-11.0	-256.5	-7.6	-230.7
$CrCp_2$	*42.8*	-142.1	*20.0*	-172.2	-32.8	-242.8	*91.7*	-140.9	*100.4*	-257.0
$FeCp_2$	*229.9*	*459.2*	*187.0*	*347.4*	*273.0*	*217.8*	*324.2*	*200.4*	*354.8*	*212.3*
$CoCp_2$	*145.6*	*339.1*	*176.0*	*195.0*	*155.4*	*84.2*	*234.0*	*48.2*	*237.7*	*67.4*
$NiCp_2$	*95.6*	*127.6*	*173.9*	*63.9*	*189.3*	*128.5*	*180.7*	*13.9*	*187.2*	*20.8*

Although the ideal reaction would be the double transfer of the ligands to the metallocenes leading to the consumption of 1 mole of the metallocenes to 1 mole of the

precursor (equation 1), the reaction energies do not favor the proposal. In most of the cases described in Table 23, the reaction energies for equation 2 are more exothermic in nature than those of equation 1. The reason might be an increase in the steric hindrance when both the ligands from copper precursors are transferred to metallocene. The addition of the ligands to the metallocenes results in a considerable distortion of the compounds. In some cases, during addition of two ligands each new ligand is only monodentate despite being bidentate in the Cu precursor (supplementary information for the structure).

In all the above cases the Cp ligand attached to the metals is assumed to be inert. Any side reaction with Cp is doubtful as it is computed to cost > 250 kJ/mol to form Cp-H and VCp from VCp_2 and a gas-phase H atom (the H atom perhaps coming from oxidation of a ligand).

Other metallocenes like $TiCp_2$, $HfCp_2$, $MoCp_2$, $ZrCp_2$, $TaCp_2$ can also be suitable choices as reducing agent. The energetics for reaction of these metallocenes with the various copper precursors is mentioned in the supplementary information. Most of the reactions are exothermic, indicating the feasibility of this reaction. However, these metallocenes do not exist in oxidation state II and hence are not suitable.

The merits and the demerits of metallocenes that can be used as reducing agents are listed in supplementary information.

Sections 6.4.(ii) and 6.4.(iii) are alternative proposals to section 6.4.(i).

6.4.ii. Reduction by abstraction of oxygen:

In this section, we explore a pathway for the Cu(0) deposition via the intermediate formation of CuO in a 3-step ALD cycle. Previously Winter *et al.*[72] has described other 3 step process for Cu deposition. The reaction mechanism was studied by Dey *et al.*[173] in a following publication.

In this proposal, the first ALD pulse brings the precursor to the surface, forming a surface covered with ligands L (equation 3). In the second step, H_2O is pulsed into the reactor so as to eliminate HL and form a surface layer of copper oxide. Such ALD growth of

transition metal oxides is straightforward and has been tried for CVD reactions[177] as well as ALD reactions[65]. The metallocene $M(II)Cp_2$ is introduced as the third pulse and is expected to abstract oxygen from CuO. A complete reduction of the CuO layer needs a very strong reducing agent as indicated by Maimaiti *et al.*[178]. If the by-product desorbs from the surface as $O=M(IV)Cp_2$, it will simultaneously donate two electrons to the surface so as to yield Cu(0). A strong M=O bond should ensure that $O=M(IV)Cp_2$ desorbs from the surface without further reaction. This reaction proposal is shown in the equations below.

First step: surf + $Cu(II)L_{2(g)}$ → surf-$Cu(II)L_2$…(3)

Second step: surf-$Cu(II)L_2$ + $O_{(plasma)}$ → surf-Cu(II)O + $2HL_{(g)}$ ….(4)*

Third step: surf-Cu(II)O + $MCp_{2(g)}$ → $Cu(0)_{(s)}$ + $O=MCp_{2(g)}$ ….(5)*

Once again, for the purpose of screening, the above equations (4)* and (5)* can be modified to give the following equations (4) and (5):

$Cu(II)L_{2(g)}$ + $O_{(plasma)}$ → $Cu(II)O_{(s)}$ + $2HL_{(g)}$ ….(4)

$Cu(II)O_{(s)}$ + $MCp_{2(g)}$ → $Cu(0)_{(s)}$ + $O=MCp_{2(g)}$ ….(5)

The formation of CuO from oxygen plasma and common copper precursors are already known in the literature[177,179]. Hence, the reaction in equation 4 is feasible. The gas phase energetics of equation 5 is -361.2 kJ/mol. Thus it is also thermodynamically possible. Hence, this is an alternative method for copper deposition. Also the the metallocene by-product has high tendency to desorb (Table 25) and can be easily purged out of the system as described in section 6.4.iv.

6.4..iii. Reduction by abstraction of sulfur:

Like the deposition of Cu(0) via the intermediate pathway of CuO, Cu(0) can also be deposited from CuS. H_2S or any sulfide containing compound can be admitted into the ALD chamber, in order to obtain a sulfide covered surface (equation 6 below). ALD of CuS has been reported before[180]. The metallocene $M(II)Cp_2$ can be introduced in the third pulse. We

explore the energetics where the metallocene abstracts sulfur, forming $S=M(IV)Cp_2$ and simultaneously donates two electrons to the surface so as to yield Cu(0) as seen in equation 7.

The energetics is of equation (7) -196.49 kJ/mol. Hence, like the previous case of intermediate formation of CuO, the formation of CuS and subsequent reduction with metallocene is also a possible pathway. Our calculations show that the $S=M(IV)Cp_2$ desorbs from the surface (

Table 24). This decreases the possibility of incorporating S as an impurity during the reaction.

First step: surf + $Cu(II)L_{2(g)}$ → surf-$Cu(II)L_2$…(3)

Second step: surf-$Cu(II)L_2$ + $H_2S_{(g)}$ → surf-Cu(II)S + $2HL_{(g)}$ …(6)

Third step: surf-Cu(II)S + $MCp_{2(g)}$ → $Cu(0)_{(s)}$ + $S=MCp_{2(g)}$ …(7)

6.4.iv. Desorption of the by-products:

As discussed in previous studies, desorption of the by-products is an important aspect of ALD[174], as otherwise they will lead to impurities in the target material. In this section we will computationally explore the desorption energies of the possible by-products occurring at the surface. A negative energy ΔG_{des} indicates an endothermic adsorption reaction, which in turn shows that by-products have little chance of adsorption to the surface and are likely to desorb instead. A positive energy ΔG_{des} indicates the opposite situation.

The by-products produced in the above three sections are the substituted metallocenes in IV oxidation state (MCp_2L_2, MCp_2O, MCp_2S) and III oxidation state MCp_2L. For this study we have considered vanadocene as the metallocene compound and four ligands from the precursors.

Table 24 shows ΔG_{des} at 120 °C for the by-products with V^{+4} oxidation state and Table 25 for V^{+3} oxidation state. In both the tables we can see that desorption is favored as the desorption free energy is negative.

Table 24 also shows that more sterically hindered compounds have more likelihood of desorption (e.g. $VCp_2(acac)_2$). In some by-products such as $VCp_2(PyrIm^{iPr})_2$, the ligand opens and forms a linear chain with just one ligating atom attached to the metal center. This happens predominantly in the by-products from equation 5 where there is double addition of ligands to the metal center. The structure of some of the by-products is given in the supplementary information. However, they have not been explored further.

Table 24 also shows desorption energies for VCp_2O and VCp_2S. The ΔG_{des} at T = 393 K for both the VCp_2O and VCp_2S compounds are negative. For the VCp_2O and VCp_2S by-product, there is an alternative model that can be formed at the surface. It is VCp-O-Surf where the O binds to both VCp_2 and the surface and same model can be for VCp_2S. Through our calculations we see that the VCp_2-O-Surf has 57 kJ/mol more ΔE_{ad} compared to VCp_2O and 27 kJ/mol for VCp_2S-Surf compared to VCp_2S. Hence they can be easily purged out of the system. However, the entropy $T\Delta S$ factor favors desorption of both the products.

Table 24: Energies (ΔE_{des}) and Gibbs free energies of desorption (ΔG_{des}) including entropy contribution ($T\Delta S$) at T = 393 K of the vanadocene by-products as discussed in section 6.4.i, 6.4.ii and 6.4.iii. In all the cases the vanadium atom is in +4 oxidation state. Data are computed at PBE/SV(P) level and compared to PBE/TZVPP in selected cases (in parentheses).

Molecules	ΔE_{des}	$T\Delta S_{des}$	ΔG_{des}^{393}
VCp_2O	51.1 (129.8)	483.1 (483.4)	-432.0 (-353.6)
VCp_2S	54.4 (135.0)	481.4 (481.7)	-427.0 (-346.7)
$VCp_2(acac)_2$	211.6	1111.4	-899.8
$VCp_2(dmap)_2$	110.9	1422.2	-1311.3

$VCp_2(PyrAld)_2$	132.7	946.6	-813.9
$VCp_2(PyrIm^{iPr})_2$	79.6	1470.8	-1391.2

Table 25 : Energies (ΔE_{des}) and Gibbs free energies of desorption (ΔG_{des}) including entropy contribution ($T\Delta S$) at T = 393 K of the vanadocene by-products where the vanadium atom is in III oxidation state.

Molecules	ΔE_{des}	$T\Delta S_{des}$	ΔG_{des}^{393}
$VCp_2(acac)$	91.7	790.0	-698.3
$VCp_2(dmap)$	87.3	946.0	-858.7
$VCp_2(PyrAld)$	64.4	708.0	-643.6
$VCp_2(PyrIm^{iPr})$	102.1	941.0	-838.9

On the basis of the reaction energies we choose vanadocene as the best metallocene to be tested experimentally. The solution phase study and the surface reactions are described in the following two sections.

6.5. Solution phase reactions

In section 6.4.i. it is seen that vanadocene shows promise for use as the reducing agent in Cu ALD. Experimental testing has not yet been reported. Therefore, before undertaking deposition reactions from gas phase, a series of solution phase trials involving different ratios of $Cu(acac)_2$ to vanadocene, different solvents and reaction temperatures were performed to test the potential reduction of $Cu(acac)_2$ to Cu metal.

Tetrahydrofuran (THF) and methanol were investigated as solvents due to their difference in polarity with their dielectric constants being 7.5 and 33 respectively[181]. In both the cases, $Cu(acac)_2$ made a blue suspension in 4 ml of solvent (145 mg, 0.55 mmol). Vanadocene (100 mg 0.55 mmol) was seen to dissolve in both solvents (8 mL) giving dark

purple-black solutions. In all trials the vanadocene solution was added to the $Cu(acac)_2$ suspensions.

Using the more polar methanol as solvent, a green solution was produced on addition of the vanadocene solution to the $Cu(acac)_2$ suspension in a 2:1 molar ratio, in accordance with the literature precedent that vanadocene salts of this nature appear green[182]. After approximately 10 minutes of stirring, a Cu metal film began to form on the side of the reaction flask. This delay in Cu production could be due to an effect of the methanol, either via complexing with the vanadocene or coordinating with $Cu(acac)_2$ making the Cu centre and acac ligands more susceptible to interaction with the vanadocene. Kinetic barriers to the formation of such complexes might be the reason for the slow formation of the copper metal. Analysis of the supernatant using mass spectrometry showed a small peak at m/z = 280.3 that could correspond to the $[Cp_2V(acac)]^+$ or $[Cp_2V(OMe)]^+$ ion. Due to the fluxionality of the acac ligands, NMR spectroscopy proved unhelpful in determining the species present.

In order to see whether methanol makes a stable coordinative bond with $Cu(acac)_2$ and vanadocene, 100 mg of each compound was taken and stirred seperately in solution as was done at the start of the reaction. After stirring overnight at room temperature the solvent was removed from each mixture under vacuo and elemental analysis was carried out on the residue (Table 26). The probable structures of the coordinated vanadocene and $Cu(acac)_2$ are shown in Figure 44. DFT structural optimization shows that methanol can coordinate to both vanadocene and the copper precursor. The coordinated copper precursor complex can have one or more methanol compounds attached to it. However, it is seen, that only one methanol coordinates with the copper center in the precursor and distorts the planar structure. The computed bond length between the O in methanol and the Cu in the precursor is 2.6 Å compared to typical Cu-O bond length of ~1.9 Å[183]. The Cu-O bond length in acac precursor is 1.92 Å[33]. The second methanol forms a H-bonded compound with O in the precursor

(Figure 44 (ii) and (iii)). In the case of vanadocene coordination with methanol, DFT shows that there is only monocoordination of MeOH with the metal center and a second methanol molecule does not coordinate to any part of the vanadocene. The formation energies of the coordinated complexes are quoted in equations (8-11) Table 26. We see that the formation energies as explored through DFT calcuations are all negative and hence solvent coordination is feasible. Changes in entropy and solvation energies are neglected in these calculations. Nevertheless, they indicate that stable methanol adducts are formed for both the copper precursors and the vanadocene.

$Cu(acac)_2$ has been reported to undergo a photolysis reaction in isopropanol to yield metallic copper as a final product[184]. This effect was not seen after stirring the copper compound in methanol in natural light. The reduction to the metal must be an effect of the vanadocene, possibly via the coordination of a methanol ligand.

The reaction of vanadocene, $Cu(acac)_2$ and methanol is shown in equation 16 (Table 26) and is exothermic. The formation of $VCp_2(OMe)$ is favourable compared to $VCp_2(acac)$ due to less steric hindrance in the former compound. Hence, equation 16 is more favourable compared to equation 1.

In THF very little reaction was seen on addition of the vanadocene after stirring for several hours. After the application of heat up to 40° C the solution was seen to darken and decompose forming an insoluble material.

Through the DFT structural optimization of vanadocene attached to THF, it is seen that there is no coordination complex formed between these two compounds. This shows that THF behaves differently with vanadocene to methanol. However like methanol, THF coordinatively bonds to the $Cu(acac)_2$ precursor and coordination of two THF molecule to Cu is even possible (Figure 44 (v)). The planar structure of the acac complex is unaltered. The computed complexation energy is shown in equations 12-13, Table 26. Solvation of

vanadocene in THF is important for the reaction to take place. Hence, this inability of the THF to complex with VCp_2, might be the reason for THF soultion not to deposit Cu and follow reaction 16 as shown in Table 26.

Table 26: The table shows reaction and reaction energies for different solvents MeOH and THF coordination energies for $Cu(acac)_2$ and vanadocene. All the energies are in kJ/mol. '*' indicates that there is no optimized structure of the product.

Reaction No.	Reaction	Energy (ΔE)
8	$Cu(acac)_2 + MeOH \rightarrow [Cu(acac)_2(MeOH)]$	-43.6
9	$Cu(acac)_2 + 2MeOH \rightarrow [Cu(acac)_2(MeOH)].MeOH$	-97.7
10	$VCp_2 + MeOH \rightarrow [VCp_2(MeOH)]$	-35.7
11	$VCp_2 + 2MeOH \rightarrow [VCp_2(MeOH)].MeOH$	*
12	$Cu(acac)_2 + THF \rightarrow [Cu(acac)_2(THF)]$	-41.6
13	$Cu(acac)_2 + 2THF \rightarrow [Cu(acac)_2(THF)_2]$	-75.4
14	$VCp_2 + THF \rightarrow VCp_2(THF)$	*
15	$VCp_2 + 2THF \rightarrow VCp_2(THF)_2$	*
16	$2VCp_{2(g)} + Cu(acac)_{2(g)} + 2MeOH_{(g)} \rightarrow Cu^{(0)}_{(s)} + 2acac\text{-}H_{(g)} + 2VCp_2(OMe)_{(g)}$	-214.3

We see that the formation energies are all negative and hence feasible. Change in entropy and the solvation energies are neglected in these calculations. However, they indicate a stable methanol adduct for both the copper precursors and the vanadocene. In case of the copper precursor we see that the first methanol remains coordinatively bonded to the copper with the bond length between the O in methanol and the Cu in the precursor being 2.6 Å compared to typical Cu-O bond length of ~1.9 Å[183]. The Cu-O bond length in acac precursor

is 1.92 Å[33]. When there are more than two MeOH molecule, we see that the second molecule forms H-bonds with the O of two acac ligands. This extra stability gives a exothermic reaction energy to equation 9.

$Cu(acac)_2$ has been reported to undergo a photolysis reaction in isopropanol to yield metallic copper as a final product[184]. This effect was not seen after stirring the copper compound in methanol in natural light. The reduction to the metal must be an effect of the vanadocene possibly with the added coordination of a methanol ligand.

In THF very little reaction was seen on addition of the vanadocene after stirring for several hours. After the application of heat up to 40° C the solution was seen to darken and decompose forming an insoluble material.

Through the structural optimization of vanadocene attached to THF, it is seen that there is no coordination formed between these two compounds. This shows that bonding of THF with vanadocene behaves differently from solvent methanol. However, THF coordinatively bonds to acac precursor. Unlike methanol, there is double coordination between the THF and the copper precursor. The structure of the acac complex is unaltered. The initial solvation energy is shown in equations 12-13.

Table 27: Elemental Analysis of complexes with methanol adducts

Elemental Analysis	C %	H %
$(C_5H_5)_2V(CH_3OH)$ Theoretical	61.97	6.62
$(C_5H_5)_2V(CH_3OH)_2$ Theoretical	58.78	7.40
Actual Result	61.82	6.47
$(C_5H_7O_2)_2Cu(CH_3OH)$ Theoretical	44.97	6.18
$(C_5H_7O_2)_2Cu(CH_3OH)_2$ Theoretical	44.23	6.81
Actual Result	45.09	6.01

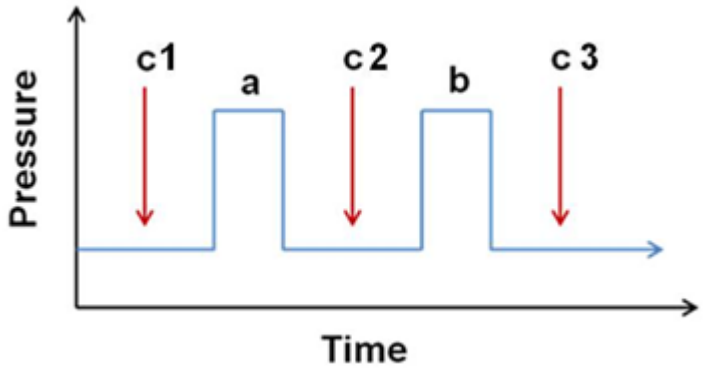


Figure 43: Schematic diagram showing the precursor pulsing sequence for [$Cu(acac)_2$] (a), Vanadocene (b) and the three different places for methanol (c) introduction.

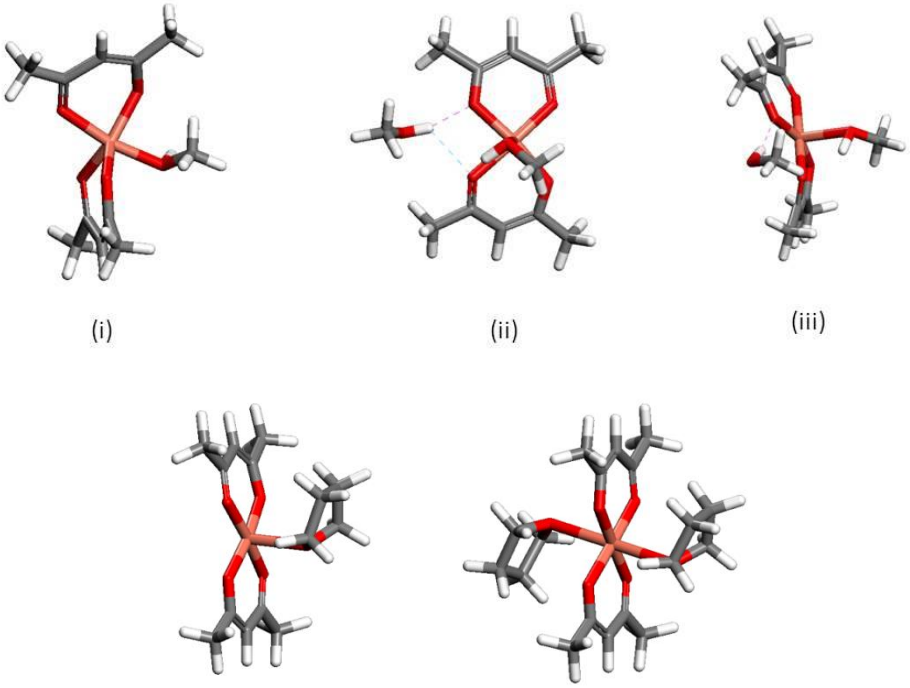
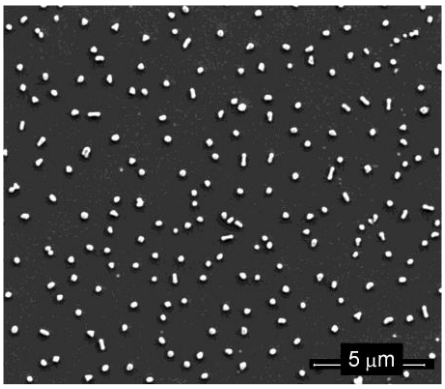


Figure 44: (i) Shows stick model of $Cu(acaca)_2(MeOH)$. Here the O from MeOH is coordinatively bonded to the copper in the copper precursor. (ii) shows two MeOH bonded to $Cu(acac)_2$. (iii) shows the side view of (ii). Here, one MeOH is coordinatively bonded to Cu and the other has H-bonding between the H from MeOH and O from the precursor. (iv) shows $Cu(acac)_2$ coordinatively bonded to THF. (v) shows $Cu(acac)_2$ co-ordinately bonded to two THF molecules.

a) 

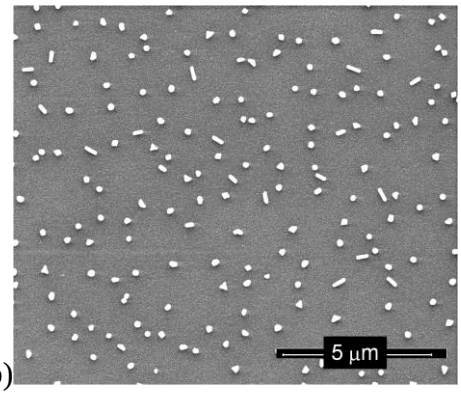
b) 

Figure 45: SEM images of experiments grown at 250 °C using ratios of $Cu(acac)_2$:vanadocene of a) 1:1 and b) 1:2 on Si(100) substrate.

6.6. Deposition onto Ru and Si surfaces from vapor

ALD reactions were attempted using a two-step process with $Cu(acac)_2$ and vanadocene and a three-step process incorporating a methanol step (Figure 43).

Initial experiments using only $Cu(acac)_2$ and vanadocene were carried out on Si(100) and Ru substrates at temperatures of 200 °C, 220 °C and 250 °C keeping the pulse length of $Cu(acac)_2$ at 0.2 s and vanadocene at 0.4 s. No growth was seen at 200 °C on either substrate. Some Cu growth was seen at 220 °C on Ru. More growth was observed at 250 °C on both substrates (Figure 45). Similar growth was seen when pulsing $Cu(acac)_2$ by itself at these temperature and is probably due to reaching the temperature for precursor decomposition (250 °C) and CVD[65].

Motivation by the solution phase study, methanol was introduced as a potential catalyst to either affect the surface before precursor addition or to react with a surface bound moiety after other precursors have been pulsed. Three-step ALD processes have previously proved successful for copper deposition[66,72]. Pulsing schemes are shown in Figure 44. The incorporation of a methanol step yielded no improvement from the two-step deposition process. The methanol seemed to hinder copper growth at all temperatures and gave no metal growth on either Si(100) or Ru substrates.

6.7. Conclusion:

In this study we see how an oxidisable metal center from a metallocene compound (MCp_2) can bring about the reduction of another metal center from a precursor (CuL_2). We tested the reductive property of various metallocenes along with different copper precursors at the DFT level. We find that there are many advantages of using a metallocene as a reducing agent for Cu ALD. They are:

- Less chance of side reactions and hence less impurities compared to transmetallation as described by earlier workers[33].
- Less substrate specific than the use of H_2, which is thought to work only in the presence of a catalyst such as Pd[65].
- Vanadocene and chromocene are commercially available.
- Reactions should be possible with a wide range of Cu precursors.

Among all the metallocenes, vanadocene is most favored due to its availability in the market and exothermic reaction energy for reduction of copper. The DFT analysis did not encompass the complete environment. Nevertheless, experimental results in methanol solution showed the predication to be true and copper metal was deposited. However, a change in the solvent with non-polar THF did not result in the same. Surface deposition on Ru and Si showed no growth below 220°C. Deposition was observed only above 250°C. Growth on Ru results in denser deposits of Cu nanoparticles as compared to the Si substrates.

The predicted reactions are tested in a Cu ALD process but similar reaction pathways can also be valid for Co, Ni and other transition metals

Supplementary Information:.

Table A: The merits and demerits of the different metallocenes that are studied.

	Positive points	Negative points
VCp_2	It is commonly available in monomer form. The reactions with different precursors are also computed to be exothermic in nature (Table 23).	-
$CrCp_2$	Commonly available and exists as monomer form. The reactions are exothermic in nature (Table 23)[167].	In few cases the reaction energies are endothermic.
$FeCp_2$	It is commonly available in monomer form.	Difficult for redox reactions to take place, as the metallocene compound has 18 e^- stability[185].
$CoCp_2$	It is commonly available in monomer form[167] that helps in the reaction as in equation 1 and 2.	Since it is a 19 electron compound, it is not stable. Even if it gives electrons to the system, it will tend to form an ionic compound like $[CoCp_2]^+X^-$[ref:185]. Reaction steps are also endothermic as indicated by positive reaction energy.
$NiCp_2$	It is commonly available in monomer form that helps in the reaction as in equation 1 and 2.	Like that of $CoCp_2$, it is a 20 e species and shows endothermic reaction energy. It might also form an ionic intermediate like Co.

Table B: This table shows the energetics of five different copper precursors interacting with metallocene compounds following equation 4 and 5. These metallocene compounds do not exists in II oxidation state. However, they may be an excellent candidate for the reducing agent, in case they are produced in II oxidation state. The energies are computed using a gas phase model choosing DFT as the level of calculation and def-SV(P) as the basis set. The energies are quoted in kJ/mol. Exothermicity (-ve reaction energy) indicates feasibility of the reaction.

	$Cu(acac)_2$		$Cu(dmap)_2$		$Cu(PyrAld)_2$		$Cu(PyrIm^{H})_2$		$Cu(PyrIm^{iPr})_2$	
	1	2	1	2	1	2	1	2	1	2
$TiCp_2$	-205.8	-532.2	-290.0	-437.1	-221.2	-534.1	-110.4	-511.9	-102.8	-495.9
$ZrCp_2$	-386.9	-658.0	-441.7	-539.8	-406.0	-653.4	-329.3	-634.2	-292.8	-616.9
$HfCp_2$	-452.0	-705.2	-471.1	-603.3	-428.3	-688.0	-362.0	-673.1	-324.6	-654.7
$TaCp_2$	-283.1	-545.6	-319.4	-441.0	-278.5	-586.1	-195.7	-599.1	-184.5	-575.8
$MoCp_2$	-107.1	-247.8	-170.7	-272.7	-156.6	-348.9	-81.1	-369.7	-72.3	-283.2

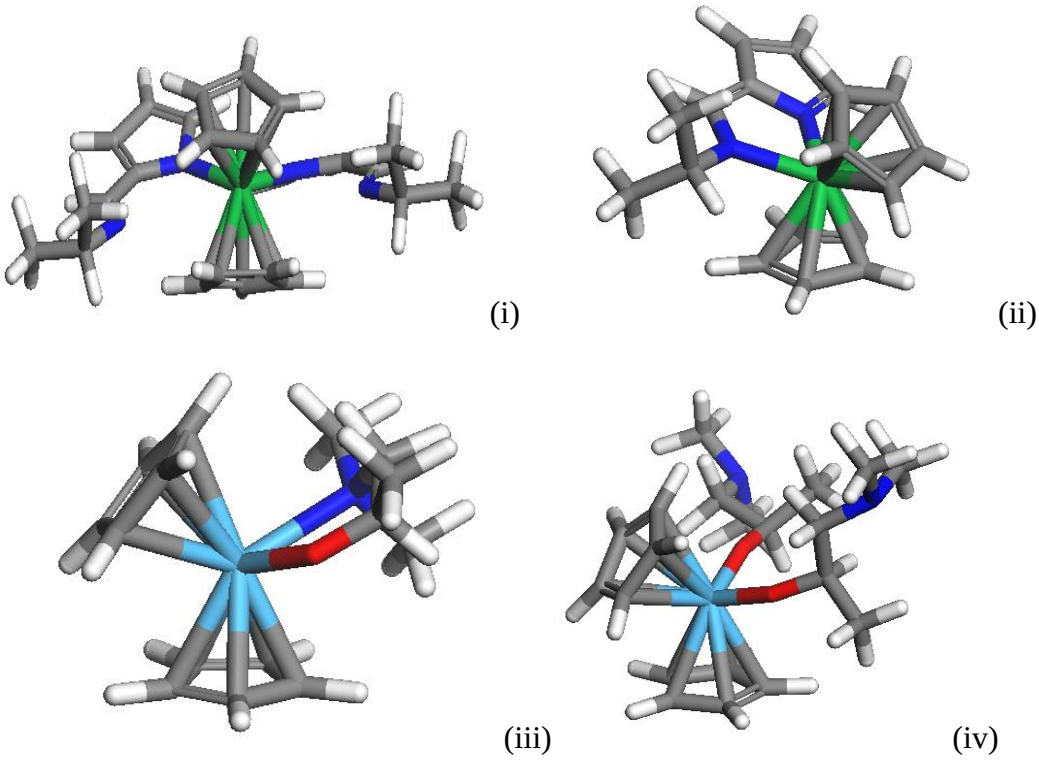


Figure: Stick model of (i) $TaCp_2(PyrIm^{iPr})_2$ (ii) $TaCp_2(PyrIm^{iPr})$. These are the by-products from equation 1 and 2 with tantalocene as the reducing agent and $Cu(PyrIm^{iPr})_2$ as the precursor. (iii) $HfCp_2(dmap)$ (iv) $HfCp_2(dmap)_2$. In (iv) it shows that the dmap ligand opens in the by-product with just the O atoms attached to the Hf. This happens in many by-products. Colour code: Grey – Carbon, White – Hydrogen, Light Grey – Vanadium, Dark Blue – Nitrogen, Green – Tantalum, Light blue – Hafnium, Red – Oxygen.

Table C: $<S^2>$ of the divalent metal cations in metallocene and the metal in the metallocene based by-products from the respective equations 1 and 2. The metal cations can have multiple spin states but only the lowest energies are presented here. The metallocene compounds are in the formal oxidation state of II and the substituted cations in III and IV. All the spin states for the metallocene are in accordance with the most stable spin state as described by Swart[170]. There are spin contamination in few cases. Spin projection technique has been used to compute the energy for the complexes with spin contamination.

Metallocene	No. of d electrons in the metal of the complex			metallocene	acac		dmap		PyrAld		PyrIm		$PyrIm^{iPr}$	
Equation	metallocene	1	2		1	2	1	2	1	2	1	2	1	2
VCp_2	3	1	2	Quartet (S^2=1.74)	Doublet (S^2 = 0.91)	Singlet	Doublet	Singlet	Doublet	Singlet	Doublet	Singlet	Doublet	Singlet
$CrCp_2$	4	2	3	Triplet	Singlet	Quartet (S^2 = 1.69)	Singlet	Quartet	Singlet	Doublet	Singlet	Doublet	Singlet	Quartet (S^2 = 3.80)
$FeCp_2$	6	4	5	Singlet	Quintet	Quartet (S^2 = 1.33)	Quintet (S^2= 6.09)	Doublet	Quintet (S^2 = 6.12)	Doublet	Singlet	Doublet	Singlet	Doublet
$CoCp_2$	7	5	6	Doublet	Doublet	Singlet	Doublet	Singlet	Doublet	Singlet	Doublet	Singlet	Doublet	Singlet
$NiCp_2$	8	6	7	Triplet	Singlet	Doublet	Quintet	Doublet	Quintet	Doublet	Singlet	Doublet	Singlet	Doublet

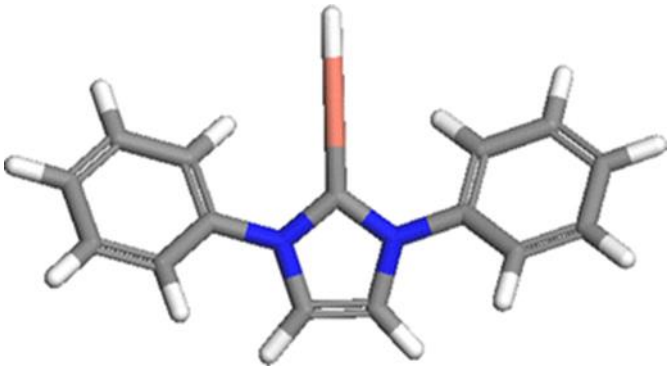
Copper Carbene Compounds

Chapter 7: Copper(I) carbene hydride complexes acting both as a reducing agent and precursor for Cu ALD - A study through Density Functional Theory

.

This chapter was published in “Theoretical Chemistry Accounts” : Authors - Gangotri Dey and Simon D. Elliott. Reprinted with permission.

The article can be found at: DOI 10.1007/s00214-013-1416-y



Note: The paper has been modified for the thesis. The reference, table and figure numbers are in a sequence with the previous chapters. However, the equation numbers are only valid for this chapter.

Abstract: We propose dual functional copper complexes that may act both as reducing agents and as Cu sources for prospective Cu atomic layer deposition. The example here is a CuH carbene complex, which can donate the H^- anion to another Cu precursor forming neutral by-products and metallic Cu(0). We compute that such a reaction is thermodynamically possible because the Cu–H bond is weaker than that of Cu–C (from the carbene). Most other neutral ligands such as PPh_3 and BEt_3 show opposite order of bond strengths. We also find that substitution in the carbene by electronegative groups reduces the Cu–H bond strength. This further facilitates the donation of H^- to the surface. The most promising copper carbene precursor is computed to be 1,3-diphenyl-4,5-imidazolidinedithione copper hydride (S-NHC)–CuH.

7.1. Introduction

Hydrogen (H_2) can be viewed formally as a proton donor and hydride donor and so can be used in various different ways for copper formation. First, it can be used to protonate the ligand (L) that is attached to the copper centre and simultaneously reduce copper to metallic form.

$$CuL_{2(g)}+H_{2(g)}\rightarrow Cu(s)+2HL(g) \quad \ldots.(1)$$

Alternatively, if there is a sulfide or nitride covered surface, it can combine to form H_2S or NH_3, respectively, leaving elemental Cu on the surface.

$$surf\text{-}CuS+H_{2(g)} \rightarrow surf\text{-}Cu+H_2S_{(g)}\uparrow \quad \ldots.(2)$$

There have been similar attempts to convert other copper binary compounds such as Cu_3N[71] into copper metal by using molecular hydrogen. However, in order to crack the H–H bond, energy in excess of 400 kJ/mol is required[77]. Providing this as thermal energy means a high deposition temperature, which has been considered responsible for copper agglomeration. As an alternative, H plasma has often been used for the reduction[186].

However, the narrow and deep interconnect features where the Cu is to be coated increase the probability of re-formation of a H_2 molecule rather than a reactive H radical. Thus, a thermal ALD technique is being targeted for deposition of Cu in these applications.

If a new hydride source can be found with the following criteria, then it can be regarded as a good alternative to molecular hydrogen.

- Weakly bound hydride: Hydride should be easily donated by the compound without needing high thermal energy to break the bond.
- Exothermic reaction: The overall ALD reaction between the reagents producing Cu(0) should be exothermic in nature.
- Precursors adsorb readily: The precursors that are used in the ALD reaction should have strong adsorption onto the growing copper surface.
- By-products desorb readily*:* By-products that remain adsorbed onto the surface may lead to impurities. Thus, by-products that can be easily desorbed should be favored.
- Free of foreign metals: Metals that are close to copper in the electrochemical series have a high chance of co-deposition along with copper. Thus, a non-copper organometallic reducing agent should be avoided even if it has other desirable properties.
- Commercially available chemical: Being easily available in the market and cheap would be an added advantage.
- Volatile and stable during delivery: The hydride source should be volatile at low temperature and stable during delivery into the reactor in the gas phase.

Ritala *et al*.[187] have proposed in 2004 a technique to deposit Al_2O_3 with two Al compounds AlR_3 and $Al(OR)_3$. The use of only Al in the two reagents helps to reduce the changes in

impurity and improve the quality of deposition. In this paper, our main target is to achieve a similar deposition technique for Cu metal from two Cu precursors.

Recently, Cu carbenes have been considered as a new family of precursor compounds[76,188]. A carbene is a neutral molecule containing carbon with two bonds and two unshared electrons, i.e., R_2C: Carbenes are thus strong Lewis bases and candidates as neutral ligands in metal complexes. The first persistent carbene was prepared by Wanzlick's group in 1970s. They formed imidazole-2-ylidene carbene by the deprotonation of an imidazolium salt. It was believed that these imidazole-based carbenes, with a $4n + 2$ π-electron ring system, should be more stable than the 4,5-dihydro analogues, due to Hückel-type aromaticity. The carbene molecule is not isolated, but obtained as a coordination compound with, e.g., mercury, copper and isothiocyanate[23,61,189]. Copper carbene complexes have a number of uses in organic chemistry. For instance, a copper carbene complex with Cl has been widely studied for possible use in alkylation, allylation and reduction in organic chemistry[190-192]. A copper(I) carbene OH complex has been used for C–H bond activation[193]. Copper(I) hydride complexes such as $CuH(PPh_3)$ are known to be mild reducing agents[194] and intermediates during catalysis reactions.

In this work, we are proposing a modified 1,3-diphenyl-imidazolin-2-ylidene copper hydride complex that has been synthesized by Mankad *et al.*[195], as a suitable hydride donor and as a source of Cu (as seen in Figure 46). Donation of hydride as a reducing agent broadens the chemistry of its use as the resulting proton can bond with various anionic ligands from other copper precursors and form neutral by-products that can be readily purged out of the system. Related *N*-heterocyclic copper hexamethyldisilazides $(NHC)Cu(Si(NMe)_2)_2$ have been studied by Coyle *et al.*[60]. In this work, we use DFT to examine the potential of the copper carbene hydride complex to be used for Cu ALD.

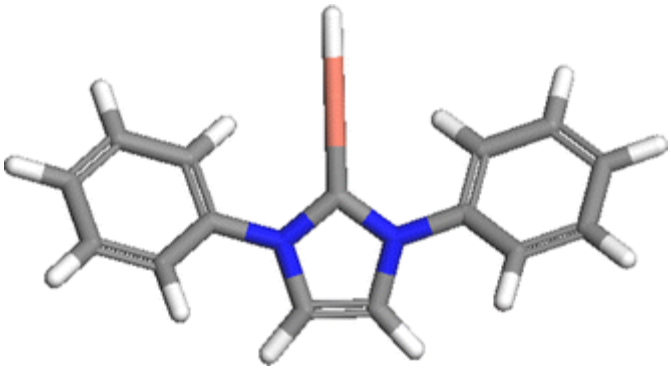


Figure 46: The N-heterocyclic-Cu hydride 1,3-diphenyl-imidazolin-2-ylidene (NHC) copper hydride. Color code: brown copper, white hydrogen, blue nitrogen, gray carbon

7.2. Methods

Selected geometries were re-optimized with triple zeta TZVPP basis set[148,149] and PBE+D3 dispersion corrected functional[150], first separately and then together to check the effect on reaction energies (Sect. 3.3, Chapter 3). The same copper surface is used here as in the previous chapters.

7.3. Results and discussion: evaluation of the copper carbene as a new precursor and reducing agent

We use the criteria in Sect 7.1 to evaluate the copper carbene complexes as new alternative sources of both hydride and copper.

7.3.1. Weakly bound hydride source

We seek a Cu–H bond that is sufficiently weak to break during ALD, but stable during delivery.

Therefore, using quantum chemical calculations, we have explored bond energies in the copper carbene complexes via Eqs. 3 and 4. Equation 3 shows the homolytic dissociation of the complex to form XCu and neutral H (X = ligand) while Eq. 4 refers to homolytic dissociation of the same into CuH and X. In reality of course, these bond dissociation energies may be modified by adsorption and by the presence of co-reagents. We have taken neutral ligands such as PPh_3 and BF_3 to understand the chemistry of bond breaking.

$$XCuH \rightarrow XCu + H \quad \ldots(3)$$

$XCuH \rightarrow CuH + X$ ….(4)

The computed ΔE values for these reactions at $T = 0$ K are presented in Table 28 along with the bond length of Cu to the ligating atom in the ligand. The Cu–H bond length remains almost constant (1.5 Å) in all the cases regardless of ΔE for Eq. 3.

Table 28: Homolytic bond dissociation energy for copper ligand complexes XCuH according to Eqs. 3 and 4 with the copper-ligating atom bond length shown as Cu–X

Ligand (X)	Cu–X (Å)	ΔE(kJ/mol)	
		Equation 3	Equation 4
PPh_3	2.21	216.3	169.8
$P(OEt)_3$	2.19	228.5	167.3
BEt_3	2.13	165.2	106.6
BF_3	2.20	139.6	57.9
N-heterocyclic carbene (NHC)	1.91	231.1	241.5
Sulfur substituted *N*-heterocyclic carbene (S-NHC)	1.90	200.1	247.0
Methyl substituted *N*-heterocyclic carbene (CH_3-NHC)	1.90	248.8	239.6
Oxosubstituted *N*-heterocyclic carbene (O-NHC)	1.89	269.1	281.0

Table 28: Homolytic bond dissociation energy for copper ligand complexes XCuH according to Eqs. 3 and 4 with the copper-ligating atom bond length shown as Cu–X

Ligand (X)	Cu–X (Å)	Δ*E*(kJ/mol)	
		Equation 3	Equation 4
Chlorosubstituted *N*-heterocyclic carbene (Cl-NHC)	1.90	231.3	236.2

From Table 28, we can see that the P- and B-based ligands give complexes with stronger Cu–H bonding (Eq. 3) than Cu–X (Eq. 4), assuming that there is no chemical effect at the surface that changes the energetics of Cu–H versus Cu–X dissociation. We find that the NHC complex (Figure 46) shows a difference between Δ*E* values of <12 kJ/mol. However, when we substitute two hydrogen atoms at 4,5 positions on the heterocycle with sulfur atoms as in Figure 47, the difference is around 47 kJ/mol. This substituted ligand in the compound is called 1,3-diphenyl-4,5-imidazolidinedithione copper hydride (S-NHC)CuH. This lower bond strength for Cu–H compared to Cu–X enables the Cu–H bond to break first and liberate a H radical (homolytic fission) or anion (heterolytic fission), which can act as the electron donor to the Cu centers. The difference in Δ*E* is very little if we substitute with other electron-withdrawing groups (–I inductive effect) such as Cl^-. If we substitute with positive inductive effect (electron donating) groups such as $–CH_3$, then the energy difference is reversed. We conclude that an electron-withdrawing group on the heterocycle is favorable for making the hydride accessible.

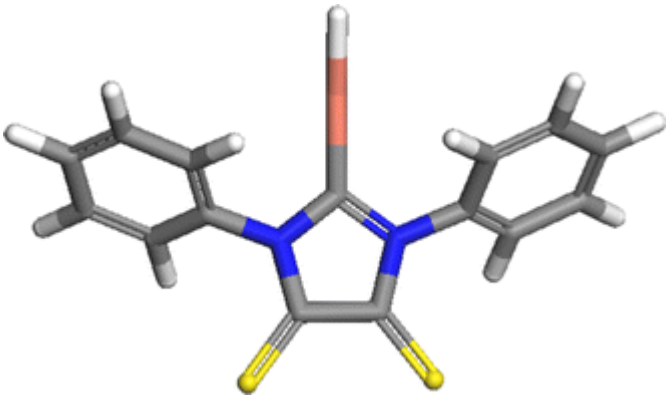


Figure 47: (S-NHC)CuH showing S substituted for H at 4 and 5 positions.

Color code: brown copper, white hydrogen, blue nitrogen, gray carbon, yellow sulfur

7.3.2. Exothermic reaction energy

The next metric that we computed to assess the suitability of the copper carbene, both as a precursor and also as a reducing agent, is the reaction energy of the proposed ALD reaction. Deposition of copper from the single source copper carbene might be possible via a CVD-type reaction at elevated temperatures rather than ALD. However, our interest is in ALD and so at least two reagents are necessary.

One ALD reaction in which we propose using the carbene as a reducing agent is as follows:

$$2(\text{S-NHC})\text{CuH}_{(g)}+\text{CuL}_{2(g)}\rightarrow 3\text{Cu}(0)_{(s)}+2\text{LH}_{(g)}+2(\text{S-NHC})_{(g)} \quad \ldots\ldots(5)$$

Here, L is the ligand from the second precursor. In (S-NHC)CuH, the S-NHC is a spectator ligand that does not have any specific role. The H has the dual role of delivering electrons to Cu(I)/Cu(II) and also bonding with the ligand L in order to form a neutral by-product. The second copper precursor $\text{CuL}_{2(g)}$ has the dual role of delivering the copper atom and also providing ligands to saturate the surface and later bond with the H from the copper carbene complex. The ligand (L) can be dmap (diphenylamine-2-propoxide), acac (acetylacetonate) or any other commonly used ligand [33].

The two ligands studied here differ in the π conjugation (present in the acac ligand) and also in the electronegativity of the ligating atom. Both the precursors have exothermic reaction energies of similar magnitude for Eq. 5. For the dmap precursor, the computed

reaction energy is −22 kJ/mol, and for the acac precursor, it is −28 kJ/mol at T = 0 K. This shows that the reaction is feasible for different copper precursors, with only a weak dependence on the precursor used. However, the exact magnitude of the exothermicity is probably dependent on the method used.

Cu can also be deposited by a three-step ALD process. A thin layer of CuS or else Cu_3N can be deposited in the first two ALD steps. The sulfide or the nitride layer can then be reduced by (S-NHC)CuH in the third step, resulting in the deposition of $Cu_{(s)}$. ALD of CuS[180] is known in the literature, and deposition of Cu with Cu_3N has also been tried before[71]. The different steps are shown in Figure 48.

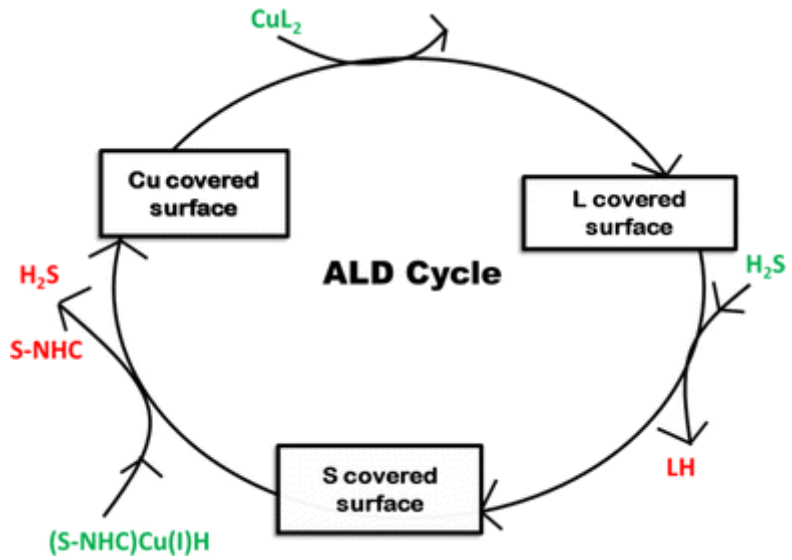


Figure 48: Flowchart showing the three-step ALD cycle for the deposition of Cu with the intermediate formation of CuS layer. *L* ligand and *S* sulfide

For the reduction in copper sulfide, the probable reactions are presented in Eq. 6 and those for copper nitride are presented in Eq. 7. If H_2S or NH_3 are used as the co-reagents to generate CuS or Cu_3N respectively from CuL_2, then the ALD reaction energies for these three-step processes are identical to those of the two-step ones (Eq. 5).

$$2(\text{S-NHC})\text{CuH}_{(g)}+\text{CuS}_{(s)}\rightarrow 3\text{Cu}(0)_{(s)}+\text{H}_2\text{S}+2(\text{S-NHC})_{(g)} \ldots (6)$$

$$3(\text{S-NHC})\text{CuH}_{(g)}+\text{Cu}_3\text{N}_{(s)}\rightarrow 6\text{Cu}(0)_{(s)}+\text{NH}_{3(g)}+3(\text{S-NHC})_{(g)} \ldots (7)$$

7.3.3. Precursors should adsorb and by-products should desorb readily

It is a criterion for successful ALD that the reactants adsorb but the by-products desorb from the surface, even at low temperatures. Therefore, another metric is the free energy of adsorption onto or desorption from the bare copper surface, modeled by a Cu(111) facet on a 55-atom Cu cluster. There is molecular adsorption for all the compounds listed in Table 29. NH_3,H_2S, acacH and dmapH show physisorption on the bare copper surface. However, there are significant differences in the ΔG values due to the entropy factor. As shown in Table 29, we find that $\Delta G>0$ at $T = 120$ °C for all reactants (except the CuL_2 precursors) and by-products, indicating that desorption is always favored. The (S-NHC)CuH precursor adsorbs strongly onto the copper surface through bonds between the under coordinated Cu surface and the S atoms.

We can see that the (S-NHC)CuH compound adsorbs more strongly than the corresponding compound without any sulfur substitution Figure 49 (c,d). Thus, the sulfur containing compound will be a better choice as a precursor. The by-products S-NHC and NHC are computed to desorb readily, as evidenced by the positive values of their adsorption free energy. The adsorption energies for the two carbene precursors were checked by optimization at the SV(P)/PBE+D3 level of calculation at first. This gives ΔE_{ad} of −573.7 kJ/mol for (S-NHC)CuH and −311.6 kJ/mol for (NHC)CuH, 4–10 % greater than the uncorrected PBE values in Table 29. At TZVPP/PBE+D3 level of calculation, we obtain ΔE_{ad} of −592.6 kJ/mol for (S-NHC)CuH and −320.6 kJ/mol for (NHC)CuH, 14–8 % greater than the SV(P)/PBE values in Table 29. The (S-NHC)CuH has larger change in ΔE_{ad} compared to the non-sulfated precursor. This indicates slight under-bonding with the smaller basis and without dispersion. The computational cost of the larger basis precludes us from applying it to all the other adsorption energies.

Table 29: Energy of adsorption of the molecules onto a Cu(111) model surface computed by SV(P)/PBE. Negative energy shows that adsorption of the molecule is favorable. The entropy contribution of the molecules has been calculated at T = 120 °C. The energies are in kJ/mol

Molecules	ΔE_{ad}	$T\Delta S_{ad}$	ΔG_{120ad}
(S-NHC)CuH	−518.4	638.2	119.8
(NHC)CuH	−296.6	677.6	381.0
$Cu(acac)_2$	−258.4	179.2	−79.2
$Cu(dmap)_2$	−249.0	184.0	−64.9
NH_3	−47.1	95.8	48.7
H_2S	−43.8	47.7	3.8
S-NHC	−253.0	608.4	355.4
NHC	−182.1	648.4	460.3
acacH	−91.5	339.8	248.3
dmapH	−102.1	497.4	395.3

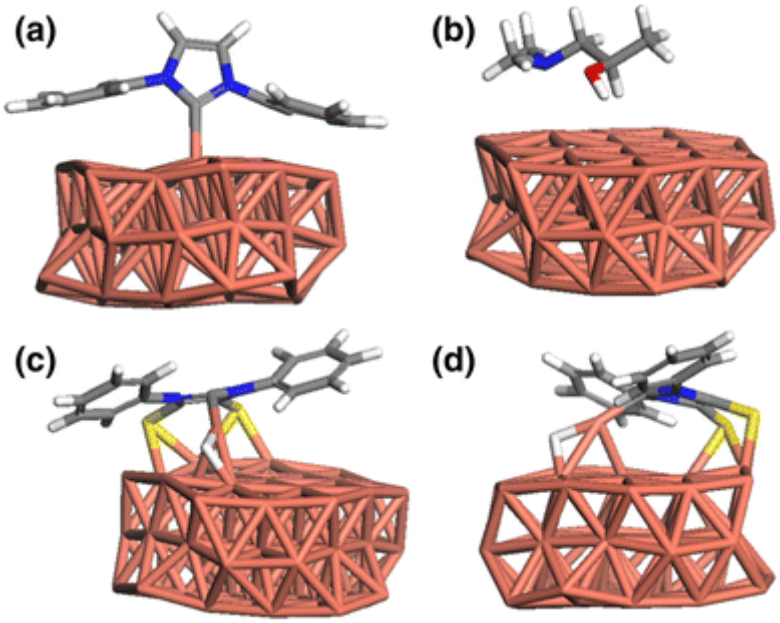


Figure 49: (a) NHC carbene chemisorbed onto the bare copper surface via C. (b) dmapH protonated ligand physisorbed onto the surface. (c) (S-NHC)CuH adsorbed onto the surface via Cu and S. (d) is the same as c from a different viewpoint. C*olor* code: *brown* copper, *white* hydrogen, *blue* nitrogen, *gray* carbon, *yellow* sulfur.

The by-product NH_3 has low adsorption energy and hence can be easily desorbed. However, H_2S has a free energy of adsorption approximately equal to zero and therefore is less likely to desorb. Free protonated ligands such as acacH and dmapH also have poor adsorption energies and hence can be readily desorbed. Testing the adsorption of the molecules near the edge of the cluster with the larger precursor molecules, we find that the adsorption energy increases by around 30 kJ/mol as the larger adsorbate wraps around the cluster edge.

There can be a competing reaction to Eq. 5 where the carbene does not desorb from the surface but stays attached to the copper atom. This is described in Eq.8. However, our calculations show that desorption of free carbenes is highly favoured (Table 29). We therefore suggest that the Eq. 8 is unlikely. Likewise, competing reactions for the 3-step ALD Eqs. (9, 10) in which (S-NHC)Cu adducts persist is possible.

$2(\text{S-NHC})CuH_{(g)} + CuL_{2(g)} \rightarrow Cu(0)_{(s)} + 2LH_{(g)} + 2(Cu(0)\text{S-NHC})_{(s)}$ …(8)

$2(\text{S-NHC})CuH_{(g)} + CuS_{(s)} \rightarrow Cu(0)_{(s)} + H_2S_{(g)} + 2(\text{S-NHC})Cu(0)_{(s)}$ ..(9)

$3(\text{S-NHC})CuH_{(g)} + Cu3N_{(s)} \rightarrow 3Cu(0)_{(s)} + NH_{3(g)} + 3(\text{S-NHC})Cu(0)_{(s)}$ …(10)

We can also use the data in Table 29 to assess the viability of the proposed two-step (Eq. 5) and three-step (Eqs. 6, 7) ALD process. A two-step process without intermediate formation of the binary compound might be a better choice because the protonated ligands (LH) desorb more readily from the surface than NH_3 and H_2S. A three-step process might therefore increase the chances of impurities.

To summarize this section, we see that the proposed new precursors (S-NHC)CuH adsorb strongly and the by-products desorb readily, thus fulfilling an important requirement for a good ALD reaction to take place.

7.3.4. Free of foreign metals

There is no foreign metal present in the proposed system, and hence, there is no chance of any impurity coming from the co-deposition of another metal as happens for the reaction with $ZnEt_2$[29]. C, N and O impurities are expected from the possible thermal decomposition of the ligands.

7.3.5. Synthesizable and commercially available

Although copper carbene compounds have not been functionalized yet with S in this way, a Pd carbene has been functionalized at 4, 5 carbons with ester groups by Hara *et al.* [196].

7.3.6. Volatile and stable during delivery

Since the –I electron-withdrawing (inductive effect) substituted copper compounds have not been synthesized yet, we cannot comment about stability during delivery. However, (NHC)CuH complexes have a tendency to be in dimer form as mentioned by Mankad *et al.*[195]. The probable dimer structure optimized with DFT is presented in Figure 49. The dimer is computed to be nearly isoenergetic with a pair of monomers (dimerization costs ΔE =

5kJ/mol).However, the monomer structure is favoured by entropy. Coyle *et al.*[61] mention in their work that the copper carbene compounds synthesized by them show low volatility in thermogravimetric analysis (TGA).

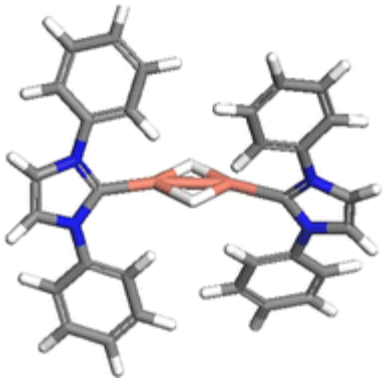


Figure 50: N-heterocyclic - Cu hydride dimer. Color code: brown copper, white hydrogen, blue nitrogen, gray carbon. The computed dihedral angle between C–Cu–Cu–C where the C is from the ligated carbene molecule is 16 °

7.4. Conclusion

As new precursors for Cu ALD, we propose *N*-heterocyclic copper carbene hydrides, substituted with –I (electron-withdrawing inductive) groups. An example is 4,5 imidazolidinedithione-*N*-heterocyclic copper carbene (S-NHC)CuH. Due to the weak bond between copper and hydrogen in (S-NHC)CuH, the hydride anion is readily available as a reducing agent. A second Cu precursor is needed as co-reagent to complete the ALD cycle. Thus, low-temperature ALD can perhaps be carried out, and the problem of islanding can perhaps be alleviated in this manner. As the computed ALD reaction energies are exothermic for our test cases, we can conclude that the proposed ALD reactions are feasible.

When using an organometallic reagent as a reducing agent, there is always the danger of reduction in the metal centre, which may lead to unwanted co-deposition of that metal. Here, we propose a Cu-based reducing agent, so that co-deposition is desirable. We find that such co-deposition of copper from the copper carbene complex is always favored. We can also see that the reactant adsorbs more readily to the surface than the corresponding by-products, such as the protonated acac ligand. This indicates that the by-products can be desorbed from the

surface in a clean ALD process. A current disadvantage of the process is that the proposed precursor is not commercially available.

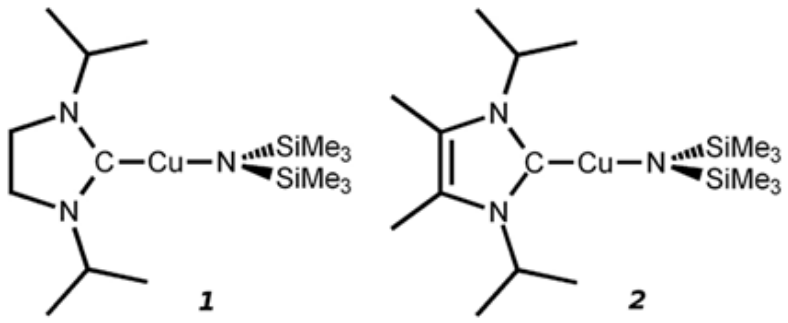
Thus, we propose a S substituted copper(I) carbene hydride functioning both as a reducing agent and as a copper source for the ALD of copper metal.

Chapter 8: Deposition of Copper by Plasma-Enhanced Atomic Layer Deposition Using a Novel N-Heterocyclic Carbene Precursor

This chapter was published in Chemistry Of Materials as Coyle *et al. Chem. Mater.*, 2013, 25 (7), page 1132–1138

The article can be found at: DOI 10.1021/cm400215q

For this chapter I have done the computational part and have drawn the conclusion for the mechanism. This work has 75% experimental work and 25% computational work.



Note: The paper has been modified for the thesis. The reference, table and figure numbers are in a sequence with the previous chapters. However, the equation numbers are only valid for this chapter.

Abstract: Two novel N-heterocyclic carbene (NHC)-containing copper(I) amides are reported as atomic layer deposition (ALD) precursors. 1,3-Diisopropyl-imidazolin-2-ylidene copper hexamethyldisilazide (1) and 4,5-dimethyl-1,3-diisopropyl-imidazol-2-ylidene copper hexamethyldisilazide (2) were synthesized and structurally characterized. The thermal behavior of both compounds was studied by thermogravimetric analysis (TGA), and they were both found to be reasonably volatile compounds. Copper metal with good resistivity was deposited using plasma-enhanced atomic layer deposition. The precursor demonstrated self-limiting behavior indicative of ALD, and gave a growth rate of 0.2 Å/cycle. Compound 2 was unsuccessful as an ALD precursor under similar conditions. Density functional theory calculations showed that both compounds adsorb dissociatively onto a growing copper film as long as there is some atomic roughness, via cleavage of the Cu-carbene bond.

This is a part of a published paper by Coyle *et al*[60]. Only the section relating to the computational study and experimental data relating to the computational results has been presented here. The details of the experimental section can be found in the paper.

8.1. Introduction:

Several potential copper(I) and copper(II) precursors have been reported for chemical vapour deposition (CVD) and atomic layer deposition (ALD), including β-diketonates[197], β-diketiminates[68], amidinates[57], guanidinates[198], aminoalkoxides[199] and pyrrolylaldiminates[67]. Of these precursors, the exclusively N-bonded ligands are interesting due to their lack of Cu-O bonds, making them less susceptible to oxygen inclusion in the deposited copper film as well as in the barrier and adhesion layers.

It is interesting that copper amides have not been a prevalent precursor for ALD. It is known that copper(I) amides typically produce a tetrameric structure[200], and copper(I) amides are more thermally stable than alkyl or alkoxo species[201]. Thus, it has been difficult to isolate

a thermally stable copper amide precursor that exhibits sufficient volatility to be considered for CVD or ALD. However, monomeric copper(I) species are well-studied in catalysis. Specifically, copper(I) NHCs are well-known to exhibit good thermal stability during C-H bond activation[202] and can drastically increase the thermal stability in sensitive Cu(I) species[203,204]. Thus, the synthesis and thermal characterization of copper(I) amides stabilized by NHCs was undertaken to examine their suitability as ALD precursors. This design strategy is common for group 11 precursors, and recent success has been shown for the plasma enhanced ALD of Ag films[205,206].

Herein is reported novel copper(I) NHCs: 1,3-diisopropyl-imidazolin-2-ylidene copper hexamethyldisilazide (1) and 4,5-dimethyl-1,3-diisopropyl-imidazol-2-ylidene copper hexamethyldisilazide (2) (Figure 51). The choice of ligands was paramount for the design of this new copper precursor[201]. Preliminary screening showed that hexamethyldisilazide ($N(SiMe_3)_2$) provided excellent thermal stability to Cu(I), where alkyl amides are known to allow plating of copper metal.[9] It was less clear from the outset whether an unsaturated NHC (imidazol-2-ylidene) or saturated NHC (imidazolin-2-ylidene) would allow for better precursor properties and for better metal deposition. Preliminary screening of unsaturated NHCs showed that an imidazol-2-ylidene with a methyl-substituted backbone provided a more thermally stable copper compound than an unsubstituted imidazol-2-ylidene. Preliminary screening showed backbone substitution of imidazolin-2-ylidenes proved to be unnecessary as such NHCs afforded copper compounds with sufficient thermal stability. Interestingly, our preliminary screening lead us to choose NHCs with different stabilities towards dimerization; the dimer from the carbene in 2 is unknown, whereas the dimer from the carbene in 1 is a volatile olefin[207].

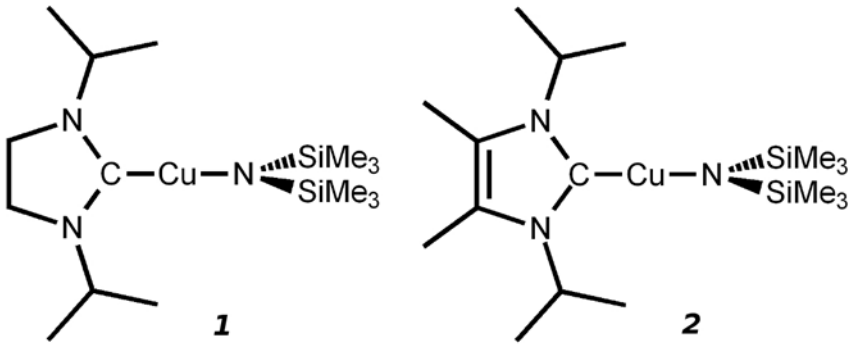


Figure 51: The structures of 1,3-diisopropyl-imidazolin-2-ylidene copper hexamethyldisilazide (1) and 4,5-dimethyl-1,3-diisopropyl-imidazol-2-ylidene copper hexamethyldisilazide (2).

Some Cu(I) precursors are well known to undergo disproportionation reactions to Cu(0) and Cu(II), which has been exploited in the CVD of copper metal films[208]. This process relies on the clean purging from the deposition zone of the Cu(II) product along with any stabilizing Lewis base employed in the Cu(I) precursor. Cu(II) hexamethyldisilazide compounds are unknown and Cu(II) amide compounds are exceptionally rare[209-211]. The attempted synthesis of $Cu[N(SiMe_3)_2]_2$ results in the isolation of $[CuN(SiMe_3)_2]_4$. CVD of copper metal films from $[CuN(SiMe_3)_2]_4$ have been reported at 200°C under a flow of H_2 without any indication of a disproportionation component to film growth[212]. Both of the NHCs used in 1 and 2 are volatile at room temperature when not coordinated; however their affinities for a copper surface are investigated herein. Additionally, explicit atomic-scale insight into ALD chemistry has been obtained through simulations using Density Functional Theory (DFT)[31]. Here we use DFT to compare the probable adsorption mechanism of the carbene-based Cu precursors 1 and 2.

8.2. Results and Discussion

In both cases, the copper is in a linear geometry with the ligands staggered and roughly orthogonal. The Cu-N bonds (1.84 Å for 1 and 1.87 Å for 2) are shorter than reported

for the copper(I) hexamethyldisilazide tetramer (1.92 – 1.93 Å)[212], but similar to copper alkyl amide compounds[200]. The longer amide contact in 2 might be due to the steric bulk of the backbone methyl groups forcing the carbene's isopropyl groups to orient toward the amide moiety, in turn forcing back the amide group. The copper-carbon bonds fall in the range of other monomeric, linear N-bonded Cu-NHC complexes[204,213,214], suggesting that the shortened Cu-N bond might be due to enhanced back bonding to the copper. This also suggests that the copper amide bond might be stabilized to cleavage upon adsorption of the compound at a growing copper surface, suggesting that the carbene will be lost upon chemisorption . Compound 1 was successful at depositing copper metal using PE-ALD while Compound 2 failed to do so. The details of the experiments can be found in the paper by Coyle *et al.*[60].

DFT calculations were carried out on these precursors in the gas phase and adsorbed to model copper surfaces. The computed structures were in good agreement with the X-ray structural analysis, with all bond lengths agreeing within 5 pm (Table 30). The dissociation energy of each ligand from the copper center was calculated to determine which bond was likely to break upon chemisorption at a copper surface. The two chemical equations considered were:

$$NHC\text{-}Cu(I)\text{-}N(SiMe_3)_2 \rightarrow [NHC\text{-}Cu(I)]^+ + [N(SiMe_3)_2]^- \quad \ldots(1)$$

$$NHC\text{-}Cu(I)\text{-}N(SiMe_3)_2 \rightarrow NHC + Cu(I)\text{-}N(SiMe_3)_2 \quad \ldots(2)$$

In both 1 and 2, it was found that the copper-nitrogen bond (Eq. 1) was about twice as strong as the copper-NHC bond (Eq. 2), (646 kJ/mol vs. 293 kJ/mol for 1; 636 kJ/mol vs. 298 kJ/mol for 2). Thus, the amide will remain bound to the Cu atom during adsorption, while the carbene may dissociate. Natural population analysis (NPA) was used to compute the charge distribution in the gas phase precursor. In both 1 and 2, the copper atom and silylamide moiety have approximately equal, but opposite, charge, while the NHC is neutral

(to within <0.1 of an electronic charge). This confirms that copper is in the oxidation state +1 and that the conjugation present in the NHC of 2 has negligible effect on the overall charge distribution.

Table 30: Selected bond lengths and bond angles for the structures of 1 and 2.

Compound 1			Compound 2		
Selected Bond Lengths (Å)					
	Experimental (data from the paper[60])	computational		Experimental (data from the paper[1])	computational
Cu-N3	1.836(4)	1.869	Cu-N3	1.870(2)	1.869
Cu-C1	1.870(5)	1.897	Cu-C1	1.881(2)	1.897
N1-C1	1.330(7)	1.356	N1-C1	1.360(3)	1.367
N1-C2	1.472(7)	1.470	N1-C5	1.404(3)	1.397
N2-C1	1.336(6)	1.356	N2-C1	1.365(3)	1.372
N2-C3	1.444(9)	1.471	N2-C7	1.394(3)	1.399
Si1-N3	1.680(6)	1.742	N3-Si2	1.692(2)	1.742
Si2-N3	1.701(5)	1.742	N3-Si1	1.697(2)	1.741
C2-C3	1.531(12)	1.538	C5-C7	1.338(4)	1.384
Selected Bond Angles (°)					
N3-Cu-C1	179.2(2)	178.3	N3-Cu-C1	178.60(9)	175.5
C1-N1-C2	114.2(5)	112.1	C1-N1-C5	111.0(2)	111.4
C1-N2-C3	114.7(6)	112.5	C1-N2-C7	111.6(2)	111.4
Si1-N3-Si2	128.2(3)	128.2	Si2-N3-Si1	131.26(13)	128.1
Si1-N3-Cu	116.5(3)	116.0	Si1-N3-Cu	113.19(11)	113.0
Si2-N3-Cu	115.3(3)	115.1	Si2-N3-Cu	111.21(11)	113.0
N1-C1-N2	106.6(5)	107.9	N1-C1-N2	103.9(2)	104.5
N1-C1-Cu	127.0(4)	128.0	N1-C1-Cu	127.26(19)	130.6
N2-C1-Cu	126.3(5)	128.0	N2-C1-Cu	128.88(19)	130.6

The precursors are brought to the model copper surface and relaxed in order to determine their adsorption energy (ΔE_{ad}). The precursor Cu atom optimises to a distance of 5.4 Å from the nearest surface Cu atom. The precursor contacts the surface via the alkyl substituent, at shortest Cu-H distances of 2.4 Å to the nearest Cu atom. These are non-bonded distances, indicative of molecular physisorption. The computed ΔE_{ad} is -174 kJ/mol

for both compound 1 and compound 2, although there is some uncertainty in this value because of the poor description of physisorption by DFT. Explicit inclusion of van der Waals interactions in the DFT functional may give a more accurate value[215,216], but the use of such functional for organometallic reagents adsorbed onto metal surfaces is not yet well established[217] and hence is beyond the scope of our study[217].

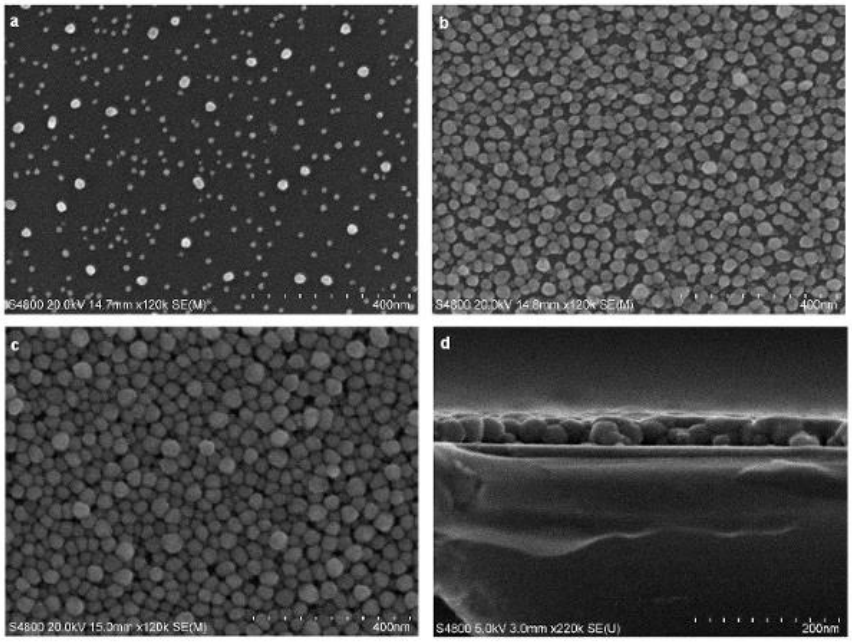


Figure 52: Scanning electron micrographs of deposited copper films. a) Plan view of copper nanoparticles deposited using a 1 s pulse length. b) Plan view of crystalline copper deposited using a 4 s pulse length. c) Plan view of crystalline copper deposited using a 6 s pulse length. d) a profile of crystalline copper deposited using a 6 s pulse length.

Table 31: Computed adsorption energy ΔEad (kJ/mol) of the precursors and their probable by-products on the models for a smooth Cu(111) surface and for a rough surface with one extra Cu+.

Adsorbate	Surface model	Compound 1	Compound 2
Precursor molecule	smooth	-174	-174
NHC	smooth	-61	-83
$Cu(NHC)^+$	rough	-364	-353
$[N(SiMe_3)_2]^-$	smooth	-378	
$CuN(SiMe_3)_2$	rough	-408	

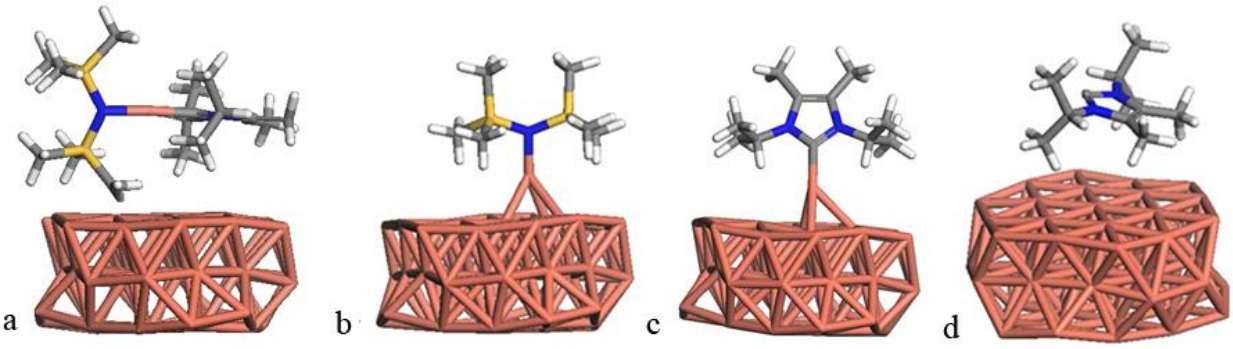


Figure 53: Optimized geometries of (a) 2 molecularly physisorbed on a smooth Cu (111) surface; (b) $CuN(SiMe_3)_2$ chemisorbed on the smooth surface; (c) NHC from 2 chemisorbed onto a rough surface; (d) NHC from 2 physisorbed on the smooth surface.

It appears that steric hindrance in $N(SiMe_3)_2$ prevents the coordinatively-unsaturated Cu, C and N atoms of the precursor from coming close to the surface (Figure 53). The only pathway to chemisorption is therefore after the precursor has dissociated. Table 31 shows ΔE_{ad} for the products after dissociation of the precursor. The non-aromatic carbene of compound 1 adsorbs slightly more weakly to the surface compared to the aromatic carbene of compound 2. However, both the adsorption energies are low and, consistent with this; the computed distances indicate that no chemical bonds are formed to the Cu surface. Hence we predict that

the carbenes are physisorbed and can be easily desorbed from the surface. Figure 53(a) shows the geometry of the NHC of compound 2 on the surface.

It appears that steric hindrance in the -$N(SiMe_3)_2$ moiety prevents the coordinatively unsaturated Cu, C and N atoms of the precursor from coming close to the surface (Figure 53). The only pathway to chemisorption is therefore through dissociation of the precursor at the Cu-NHC bond. The adsorption energies show that the carbene of 1 and 2 can adsorb to the smooth surface with comparable energies (Table 31). For a smooth copper surface, the adsorption energies are low and - consistent with this the computed distances indicate that no chemical bonds are formed to the Cu surface. However, when a rough surface (modeled by an additional copper(I) adatom) is considered, the NHC ligands bind to this surface site with adsorption energies that are comparable to those of the Cu-$N(SiMe_3)_2$ moiety. The DFT data do not show any significant difference between the saturated carbene (from 1) and unsaturated carbene (from 2) in terms of energetics of dissociation or adsorption during the Cu pulse. This indicates that differences between the ALD chemistry of these two precursors arise after the Cu pulse, probably during the plasma H_2 pulse. Further studies are under way to determine the differences in the surface chemistry of these two compounds.

8.3 Conclusion

Two novel NHC-containing compounds 1,3-diisopropyl-imidazolin-2-ylidene copper hexamethyldisilazide (1) and 4,5-dimethyl-1,3-diisopropyl-imidazol-2-ylidene copper hexamethyldisilazide (2) were synthesized and structurally characterized. Compound 1 was found to have excellent volatility and thermal stability over an extended period of time. It was successfully employed as an ALD precursor using hydrogen plasma as a reducing agent. The deposited films had a growth rate of 0.2 Å/cycle and were crystalline. The films showed good resistivity.

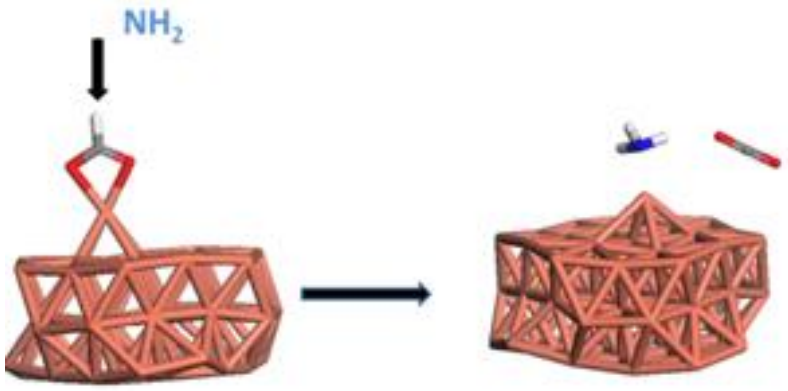
Compound 2 showed excellent volatility but poorer thermal stability than 1. Under similar conditions to the ALD of 1, it did not afford a copper metal film. DFT studies of both precursors showed good dissociative chemisorption to a copper surface, with cleavage of the precursor at the carbene-copper bond, indicating similar surface chemistry during the Cu precursor pulse in ALD.

3-Step Cu ALD process

Chapter 9: Copper reduction and atomic layer deposition by oxidative decomposition of formate by hydrazine.

This chapter was published in RSC Advances, 4, 34448. Authors: Gangotri Dey and Simon D. Elliott

The article can be found at: DOI 10.1039/C4RA07003H



Note: The paper has been modified for the thesis. The reference, table and figure numbers are in a sequence with the previous chapters. However, the equation numbers are only valid for this chapter.

Abstract: Mechanistic study of a three step method for the deposition of copper to be used in interconnects. It is a promising technique for Atomic Layer Deposition (ALD) of pure metal.

9.1 Introduction:

Knisley *et al.*[72] proposed a new technique for Cu ALD at low temperature. They have reported that the deposition starts from 80 °C and that the growth rate becomes constant at 120 °C, with no growth seen above 160 °C. Each ALD cycle consists of three pulses: $Cu(dmap)_2$, a protic acid (formic acid) and hydrazine. Knisley's proposal holds promise for deposition of other metals too. Initial deposition results were also reported from $Ni^{(+2)}$ complexes[72].

The proposed overall reaction independent of the surface can be written as follows:

$$Cu(dmap)_{2(g)} + 2HCOOH_{(g)} + N_2H_{4(g)} \rightarrow Cu^{(0)}_{(s)} + 2CO_{2(g)} + 2dmap\text{-}H_{(g)} + 2NH_{3(g)} \quad \ldots.(1)$$

There is no direct evidence for the formation of copper formate at the surface in Knisley's work. However, Ravindranathan *et al.*[218] have shown by chemical analysis and infrared spectroscopy that an aqueous solution of copper formate undergoes rapid reduction to copper metal at ambient temperature upon treatment with hydrazine hydrate. Hydrazine has been used previously as a catalytic reducing agent for aromatic nitro compounds in the presence of finely divided metals[219], but equation (1) implies that N is itself reduced along with Cu in this case. However, the mechanistic detail of this process is unknown and this forms the motivation for our work.

9.2. Method:

The same gas phase technique as used in Chapter 3 has been used here. The surface calculations are of the same principle as mentioned in Chapters 4 and 5.

9.3. Results and Discussion

In order to understand the mechanism we will pose a series of questions in the following sections. Reactions that are thermodynamically favoured have negative reaction energies. The set of reactions presented here are the most energetically feasible ones out of the wide range that we have investigated.

There are three steps in the reaction process at surface:

a) Interaction of the precursor with the surface

Surface + $Cu(dmap)_{2(g)}$ → $Cu(dmap)_{2(ads)}$ → $Cu(dmap)_{(ads)}$

b) Interaction of formic acid with the precursor fragments

$Cu(dmap)_{(ads)}$ + HCOOH → ?

c) Interaction of hydrazine with the precursor and formic acid fragments.

$Cu(dmap)_{(ads)}$ + HCOOH + NH_2-NH_2 → ?

Part (a) is described in previous studies and we take the conclusion from these papers to build our model. Part (b) is described in section (i). Part (c) is described in sections (ii) to (iii).

(i) How do precursor fragments interact with formic acid?

When $Cu(dmap)_2$ adsorbs to a Cu surface, its most stable state is found[9,23] to be $Cu^{(+1)}$(dmap). Therefore, in order to understand the further interaction with formic acid, we have taken a model system that has one dmap ligand adsorbed to a Cu (111) surface.

This shows an adsorption energy of ΔE_{ad} = -647 kJ/mol relative to the gas-phase dmap anion and cationic coin (Table 32, Figure 54). To the optimised geometry of this $Cu^{(+1)}$dmap adsorbate we brought in HCOOH (Figure 55). During a 300 step MD study of 2 ps duration, at 393 K from this geometry, we see that the oxygen of the dmap anion on the surface spontaneously abstracts the protonic H from formic acid (floating near it) to form a protonated ligand dmap-H. The remaining formate anion ($HCOO^-$) bonds with a copper atom on the surface. The adsorbed optimized structure of HCOOH shows a ΔE_{ad}= -33 kJ/mol onto

the bare copper surface (Table 32, Figure 54 (ii)). The adsorption energy of the formate anion alone is ΔE_{ad} = -565 kJ/mol relative to the gas-phase anion (Table 32). The overall reactions with desorption of the dmap-H ligand and adsorption of formate anion may thus be written:

$dmap^-_{(surf)} + HCOOH_{(g)} \rightarrow dmap\text{-}H_{(g)} + HCOO^-_{(surf)}$ ….(2)

This reaction is computed to be exothermic: ΔE = -56 kJ/mol at T=0 K.

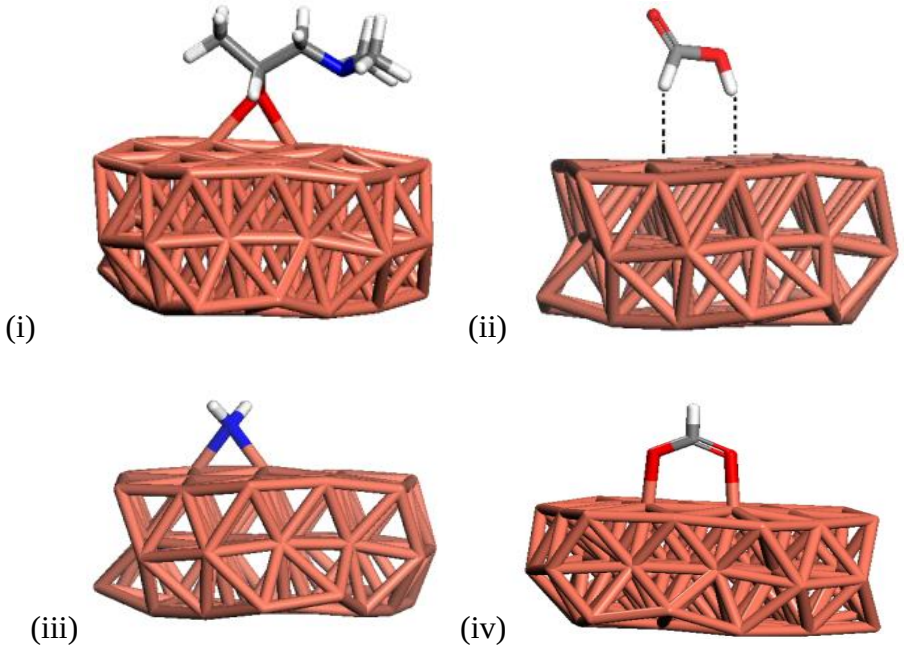


Figure 54: Optimized structure of (i) dmap ligand adsorbed on the smooth model copper surface, (ii) physisorbed formic acid (iii) adsorbed NH_2 radical, (iv) adsorbed formate anion. (Figure 57 for formate adsorption onto a rough surface). Colour code: brown=Cu, blue=N, red=O, grey=C, white=H.

Table 32: The adsorption energies (ΔE_{ad}) of the following adsorbate from their respective gas phase geometries adsorbed onto the copper surface. The energies are in kJ/mol.

Adsorbate	Adsorption Energy (ΔE_{ad})
$dmap^-$	-647
$HCOO^-$	-565
HCOOH	-33
NH_2	-240
N_2H_4	-109
NH_3	-42
CO_2	23

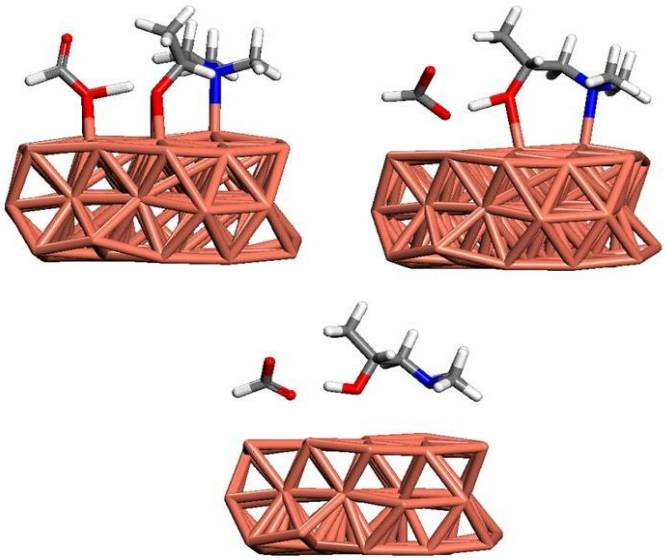


Figure 55: Some snapshots of MD simulation of dmap anion interacting with formic acid in order to form copper formate and dmap-H. The above structures are not optimized. Colour code: brown=Cu, blue=N, red=O, grey=C, white=H.

Table 33: Reaction energies showing the gas phase dissociation of NH2-NH¬2 and $(CH_3)_2N$-NH_2 molecule. All the energies are in kJ/mol.

Reaction No.	Reaction	Reaction Energy (ΔE)
3	NH_2-NH_2→ $2NH_2$	54.7
4	NH_2-NH_2 →NH + NH_3	44.9
5	NH_2-NH_2→N_2 + $2H_2$	209.8
6	$(CH_3)_2N$-NH_2→$(CH_3)_2N$ + NH_2	293.0
7	$(CH_3)_2N$-NH_2 → NH + $(CH_3)_2NH$	270.0
8	$(CH_3)_2N$-NH_2→ N_2 + $2CH_4$	400.0

(ii) In which form does the hydrazine react?

Hydrazine might disintegrate into active species when it comes in contact with the surface (surface catalysed reaction) or else thermal energy might split the molecule in the gas phase already. In order to find out what active species are likely to be present when hydrazine is admitted to the chamber, we have computed the possible dissociation reactions of hydrazine in the gas phase, as given in Table 33 (reaction no. 3-5). The $T\Delta S$ (T =393 K) is 32.6 kJ/mol, 24.0 kJ/mol, 63.2 kJ/mol for equations 3, 4 and 5 respectively. Thus the entropy contribution makes the total ΔG ~ 20 kJ/mol for equations (3) and (4). However, ΔG is > 140 kJ/mol for equation (5). Hence this suggests that the formation of gas phase radicals NH_2 or NH is most favourable if there is some additional thermal energy. The use of NH_2 radicals in the formation of pure metals like Co has been investigated before by Hideharu *et al.*[162]

We compute the energy of adsorption (Table 32) of a NH_2 radical onto the Cu surface to be ΔE_{ad}= -240 kJ/mol-NH_2 (Figure 54 (iii)). Molecular adsorption of N_2H_4 shows ΔE_{ad} = -109 kJ/mol (Table 32. By Hess's law we see that surface formation of $NH_{2(ads)}$ from $N_2H_{4(ads)}$ releases -316.3 kJ/mol of energy (Figure 56). These high adsorption energies might indicate that N persists at the surface as an impurity in the film. However, we know that Cu_3N is an

unstable compound[25] and so ultimately N incorporation is probably not favoured. The formation of NH from N_2H_4 is not explored as it is unreactive over a surface, which will be seen in the next section. Thus the disintegration of hydrazine takes place either in the gas phase into NH_2 and NH or over the surface into NH_2.

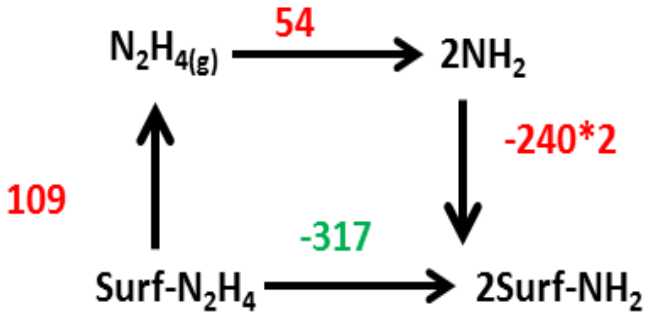


Figure 56: Hess cycle showing the formation of surface adsorbed NH_2 from surface adsorbed N_2H_4. All the energies are in kJ/mol of hydrazine.

The gas phase dissociation of 1,1-dimethyl hydrazine can be compared with that of NH_2-NH_2. The reaction energies (ΔE) are described in Table 33 (reaction no. 6-8). The $T\Delta S$ for reaction (6) is 28.6 kJ/mol, for (7) is 20.4 kJ/mol and for (8) is 36.0 kJ/mol. Thus the entropy factor cannot overcome the reaction energies. This suggests that hydrazine is a better source of NH_x radicals (x=1, 2) than substituted hydrazine.

(*iii) How do the NH_x radicals react with copper formate?*

To investigate the subsequent reactions, we have brought the NH and NH_2 radicals close to the atoms of the adsorbed copper formate moiety from the previous reaction steps. The possible sites for NH and NH_2 attack are Cu, O and H.

We see that when we bring the NH_2 towards Cu, perpendicular to the plane of the adsorbed copper formate, it forms a Cu-N adduct, without any further change. When the radical is brought towards formate H or towards O in same plane as the formate moiety (Figure 57), it abstracts the H and spontaneously forms NH_3 and CO_2 during the geometry optimization.

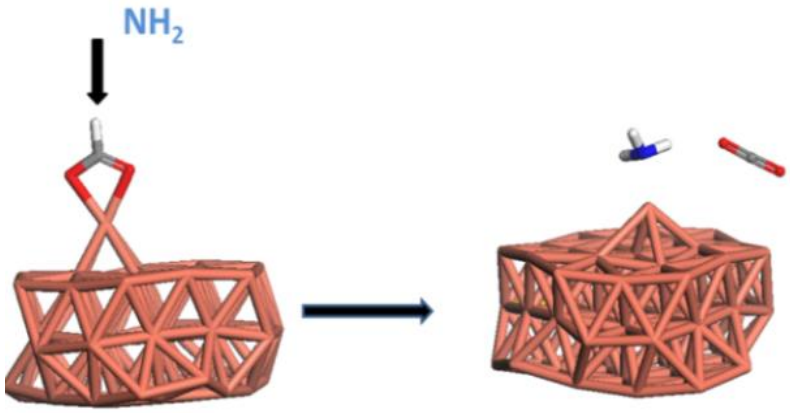


Figure 57: When the NH_2 radical attacks the H of Cu(HCOO), it forms CO_2 and NH_3 as by-products, leaving an atom of copper metal on the surface. Colour code: brown=Cu, blue=N, red=O, grey=C, white=H.

For this surface reaction we compute the following energy change

$Cu^{(+1)}OOCH_{(surf)} + NH_{2(g)} \rightarrow Cu^{(0)}_{(s)} + CO_{2(g)} + NH_{3(g)}$

ΔE = -467 kJ/mol …. (9)

In case we include desorption energy for the NH_2 from the surface (ΔE_{ad} = -240 kJ/mol, Table 32), we see that the above reaction energy can be corrected to -227 kJ/mol. The $T\Delta S$ for this reaction is 78.7 kJ/mol at T = 393 K. Thus ΔG is -305.7 kJ/mol for the overall surface reaction. Here we see that the C in $Cu^{(+1)}OOCH$ is in its +2 oxidation state and transforms to +4 oxidation state in CO_2 giving away one electron to $N^{(-2)}H_2$ to form $N^{(-3)}H_3$ and another electron to $Cu^{(+1)}$ to form $Cu^{(0)}$.

In a similar way, the NH radical was placed in a plane perpendicular to the copper formate at different positions, close to Cu, H and O. In all the cases we find that the NH moves close to the surface atoms and away from the adsorbed copper formate. The NH then attaches itself to the coordinatively unsaturated Cu atoms on the surface.

Finally, we compute the adsorption energy of the by-products: $\Delta E_{ad}(NH_3)$ = -42.0 kJ/mol and $\Delta E_{ad}(CO_2)$ = +23.0 kJ/mol at T=0 K (Table 32). At T=393 K the $T\Delta S$ is 95.8

kJ/mol for NH_3[62] and for CO_2 is 39.7 kJ/mol. Hence the adsorption of these by-products is thermodynamically not favoured.

Redistribution of the reaction energy from equation (9) would thus be sufficient to break even the N-N bond in hydrazine (~50 kJ/mol, equation 3) and desorb the by-products from the surface.

We have observed in the above reactions that surface intermediates like NH_2 radicals are formed after the dissociation of the hydrazine molecule. This radical reacts spontaneously with the formate to deposit copper and produce CO_2 and NH_3 by-products. This provides evidence that equation (1) takes place as proposed by Knisley *et al.* We calculate that ΔE= -172 kJ/mol-Cu at T=0 K for equation (1) by making use of the adhesion energy of bulk Cu of -320 kJ/mol-Cu calculated with VASP[33].

(iv) How does hydrazine react with higher acid copper compounds?

It is interesting to ask whether other protonic acids can function in the same way as formic acid in this process. The above reaction (1) was altered so as to consider acetic acid following the equation (10) and for propanoic acid according to equation (11) as in Table 34.

This assumes that the NH_2 radical abstracts an alkyl radical from adsorbed acetate or propanoate, breaking a C-C bond. The computations yielded ΔE= -58 kJ/mol for equation (10) and -98 kJ/mol for equation (11). These ALD reaction energies are less negative than that of equation (1), which may be attributed to the cost of breaking the strong C-C bond in these acids.

To investigate this reaction pathway, we bring the NH_2 radical near to the structure of adsorbed copper acetate, and observe during geometry optimization that the NH_2 radical coordinates with the coordinatively unsaturated surface copper atoms, rather than spontaneously abstracting the methyl radical. Thus, although the overall ALD reaction energy is moderately exothermic, energy barriers exist that make the surface-mediated reaction with

higher acids less likely to take place than the previous case of HCOOH. Nevertheless, the overall exothermicity indicates that the reaction might proceed via this mechanism in the solution phase, as mentioned by Knisley *et al.*[72].

Another pathway for the higher acids is shown in equations (Table 34, reaction no: 12 -13) that proposes reductive elimination of H from the alkyl groups (*i.e.* breaking C-H rather than C-C). We compute ΔE=+18 kJ/mol for reaction (12) and +90 kJ/mol for (13) indicating that these reactions are endothermic and less probable than reactions (10) and (11).

Table 34: Gas phase reaction energies showing the interaction of hydrazine with higher acids and dmap precursor.

Reaction No.	Reaction	Reaction Energy (ΔE) (kJ/mol)
10	$Cu(dmap)_{2(g)} + 2CH_3COOH_{(g)} + NH_2\text{-}NH_{2(g)} \rightarrow Cu^{(0)}_{(s)} + 2dmap\text{-}H_{(g)} + 2CO_{2(g)} + 2CH_3\text{-}NH_{2(g)}$	-58
11	$Cu(dmap)_{2(g)} + 2CH_3CH_2COOH_{(g)} + NH_2\text{-}NH_{2(g)} \rightarrow Cu^{(0)}_{(s)} + 2dmap\text{-}H_{(g)} + 2CO_{2(g)} + 2CH_3CH_2\text{-}NH_{2(g)}$	-98
12	$Cu(dmap)_{2(g)} + 2CH_3COOH_{(g)} + NH_2\text{-}NH_{2(g)} \rightarrow Cu^{(0)}_{(s)} + 2dmap\text{-}H_{(g)} + 2CO_{2(g)} + 2NH_{3(g)} + CH_2{=}CH_{2(g)}$	18
13	$Cu(dmap)_{2(g)} + 2CH_3CH_2COOH_{(g)} + NH_2\text{-}NH_{2(g)} \rightarrow Cu^{(0)}_{(s)} + 2dmap\text{-}H_{(g)} + 2CO_{2(g)} + 2NH_{3(g)} + 2CH_2{=}CH_{2(g)}$	90

9.4. Conclusions

DFT calculations have been used to investigate the surface reactions of a three step ALD process for the deposition of Cu as proposed by Knisley *et al.* Those authors proposed the formation of intermediate Cu formate at the surface and its reaction with hydrazine. Here, we confirm the stability of the formate intermediate and find the atom-by-atom mechanism

for the reaction with hydrazine and deposition of Cu metal. All the elemental reaction steps are computed to be exothermic. The reaction process has been summarized in Table 35.

In a parallel study, it has been computed that the $Cu(dmap)_2$ precursor adsorbs strongly to the surface, which is the first step of the ALD cycle. In the second step formic acid is pulsed into the chamber. It has been observed in our simulation that the dmap ligand abstracts the protonic H from formic acid and desorbs as dmap-H, leaving formate adsorbed to the surface. In the final step, hydrazine is pulsed into the chamber and probably dissociates at the surface to form the NH_2 radical. This radical abstracts $H^{(0)}$ from the formate anion. Spontaneous decomposition of the resulting anion to CO_2 causes reduction of a surface metal cation to $Cu^{(0)}$. The predicted by-products are NH_3 and CO_2. Hydrazine partially oxidises formate, which through its complete decomposition to CO_2 reduces $Cu^{(+1)}$ to $Cu^{(0)}$ (Figure 58). This suggests that the search for co-reagents in metal ALD should not be limited to traditional reducing agents like H_2, but can also include reagent combinations that release electrons during oxidative decomposition.

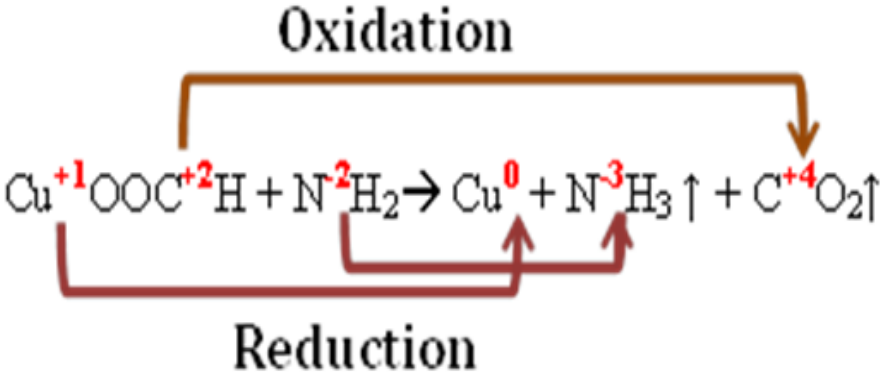


Figure 58: Redox reaction of equation 1

Table 35: Summary of the key reaction energies of the 3-step process

Reaction No.	Reaction	Reaction Energy (ΔE) (kJ/mol)
2	dmap-$_{(surf)}$ + $HCOOH_{(g)}$ → dmap-$H_{(g)}$ + $HCOO^-_{(surf)}$	-56
9	$Cu^{(+1)}OOCH_{(surf)}$+ $NH_{2(ad)}$ →$Cu^{(0)}_{(s)}$ + $CO_{2(g)}$ + $NH_{3(g)}$	-227
1	$Cu(dmap)_{2(g)}$+ $2HCOOH_{(g)}$ + $N_2H_{4(g)}$ → $Cu^{(0)}_{(s)}$ + $2CO_{2(g)}$ + 2dmap-$H_{(g)}$ + $2NH_{3(g)}$	-172 kJ/mol-Cu

Proposal for the Future

Chapter 10: Computing Phase Change in Organometallic Compounds

$$ln\left(\frac{P_1}{P_2}\right) = \frac{\Delta H}{R}\left(\frac{1}{T_1} - \frac{1}{T_2}\right) + C$$

Generally, the volatility of a new precursor is not known before synthesis. In practice the cost of synthesizing a new precursor through the addition of chemical compounds, laboratory equipment and human power sums up to few million euros[220]. If one could estimate the volatility of the new compound before its synthesis, then it could not only benefit science but also have an impact in the economy.

Computational analysis of the volatility of a novel precursor prior to its synthesis is a challenge. Low volatility helps to easily deliver the precursor into the ALD chamber. Lower reaction temperatures are therefore possible and thermal decomposition (CVD) is less likely. In the following section we propose a prospective technique by which we can compute the volatility of a precursor prior to its synthesis.

The main target of this project is to develop a computational tool where the range of phase change of a precursor can be estimated prior to its synthesis. In principle, one can compute the properties of a single molecule using *ab initio* techniques[87] like HF, MP2, CC2 etc. But it is computationally expensive to calculate macroscopic properties associated with an entire phase (e.g. boiling point, melting point) using the existing *ab initio* techniques. This is because in order to understand the phase change, > 1000 molecules need to be simulated[221]. On an average each copper precursor molecule has 25 atoms. Thus, it should be computationally possible to simulate 25,000 atoms together. Application of analytical potentials using the principles of statistical mechanics might be computationally cheaper and can act as a bridge between the macroscopic phenomenon and microscopic states. Figure 59 compares the existing sequence of events for the synthesis of new precursor with a new proposal for the future.

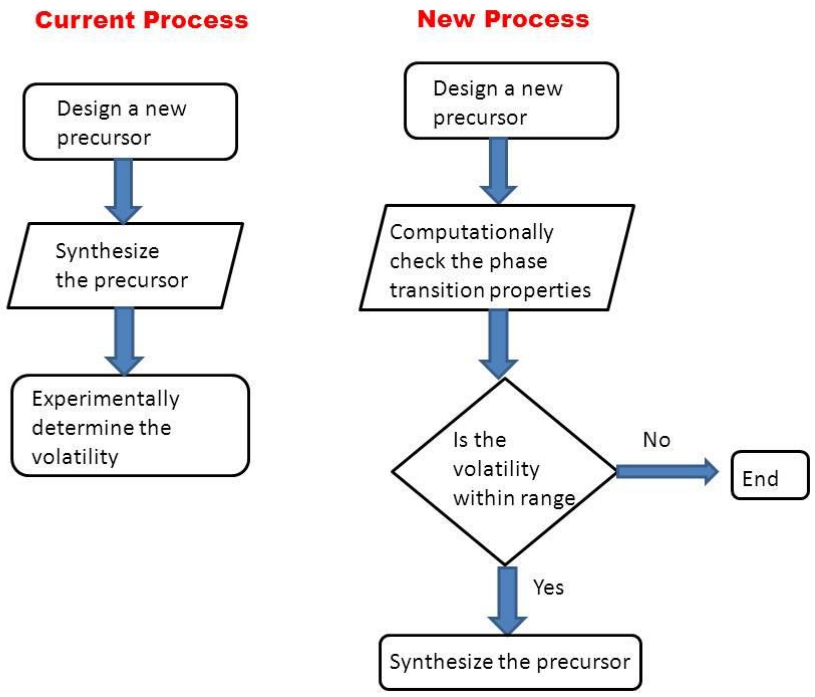
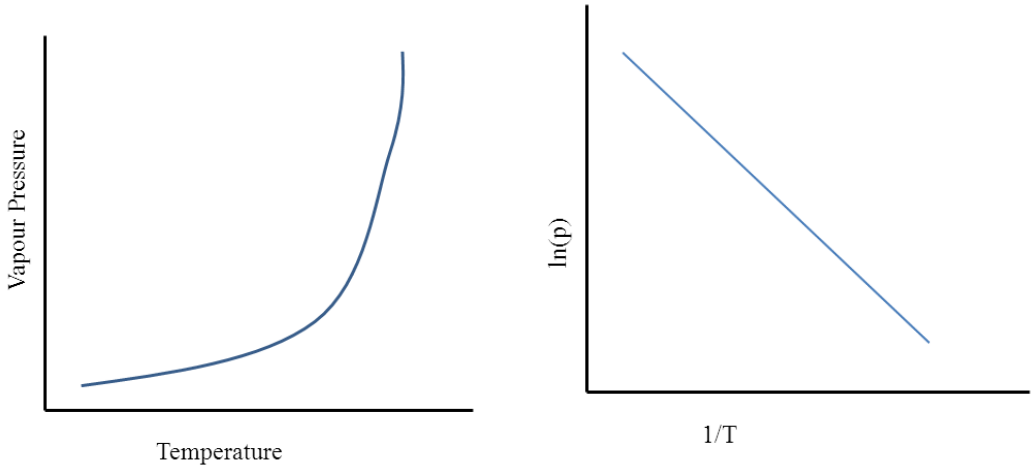


Figure 59: Comparison between the current procedure for precursor synthesis and evaluation and a proposal for the future.

10.2.a. Background



(i) (ii)

Figure 60: Plots of pressure vs temperature using the Clausius-Clapeyron equation.

The phase transition of any material from liquid to gas can be derived from the Clausius-Clapeyron equation (equation 1).

$$\ln\left(P_1/P_2\right) = \frac{\Delta H}{R}\left(\frac{1}{T_1} - \frac{1}{T_2}\right) + C \quad \text{……..(1)}$$

where P_1 and P_2 are two vapor pressures at two different temperatures T_1 and T_2. The enthalpy of vaporization (assuming that we are computing the liquid to vapor transformation) is given by ΔH in the above equation, R being the universal gas constant and C being the Antoine constant. This relationship between the vapor pressure of a liquid and the temperature is plotted in Figure 60 (i). The same formula can be expressed in a different way as a straight line as in Figure 60 (ii). The derivation of the equation from the second law of thermodynamics for a homogeneous system can be found in any standard text book[97].

Phase transitions are collective phenomena that occur over time and length scales that are not directly accessible by molecular dynamics or simple constant-volume Monte Carlo simulations. One of the key concepts in statistical mechanics is an ensemble. In general, an ensemble is a collection of microstates of system of molecules all having in common one or more extensive properties. There are various types of ensemble like Canonical ensemble (NVT), Grand-canonical ensemble (TVμ)[97] etc. where one physical property (in the bracket) can be evaluated keeping the other two constant. Here T = temperature, V = volume, N = number of particles and μ = chemical potential. Many different ensembles can be proposed by changing different parameters.

10.2.b. Research Approach

A fairly recently proposed type of ensemble is the Gibbs Ensemble (μPT)[222]. This ensemble helps to compute the phase transition of a material at different temperatures and pressures. This is done by equalizing the chemical potential between different phases using the methods mentioned below. The vapor pressure is then computed using the Clausius-Clapeyron equation.

This Gibbs ensemble approach requires that particles are computed in two different cells, each containing one of the phases. The thermodynamic requirement for phase co-existence states that the two cells should be in equilibrium. The temperature, pressure and chemical potential of all components should therefore be the same in the two cells. If for instance the system temperature is specified in advance, then the remaining two variables μ, P are satisfied by performing three types of Monte Carlo moves.

- Displacement of particles within each (to satisfy internal equilibrium).
- Fluctuations in the volume of the two regions (to satisfy equality of pressure).
- Transfer of particles between regions (to satisfy equality of chemical potentials of all components).

After achieving the equality in the chemical potential pressure and temperature, the graph can be computed for pressure and temperature as seen in Figure 61.

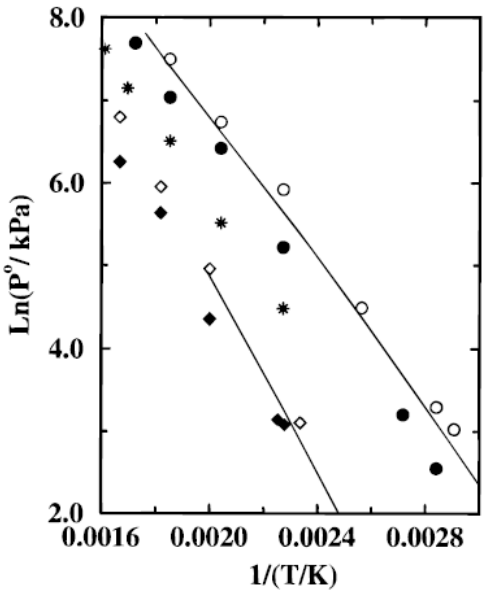


Figure 61: The figure shows the Clausius - Clapeyron equation plot for various alkanes as studied by Martin *et al.*[223] The solid lines depict the experimental data (upper curve, n-octane; lower curve, n-dodecane). Open circles, filled circles, and stars show the simulation results of the TraPPE, SKS, and OPLS force fields for n-octane, respectively. Open and filled diamonds represent the TraPPE and SKS results for n-dodecane.

Recently Errington *et al.* [224,225] have proposed new ensembles to compute the pressure vs temperature curve. They are reservoir grand canonical Monte Carlo, growth expanded ensemble, isothermal-isobaric ensemble and grand-canonical temperature-expanded ensemble. They have studied *n*-octane, cyclohexane, water, 1-propanol and a few other organic compounds and have obtained the pressure vs temperature curve to an accuracy of 20%. The new ensembles are all reported to be robust. However, the technique has not yet been validated with organometallic compounds, where there is a metal center and an organic framework. At the existing state of the art only force field techniques can be applied to such systems as *ab initio* calculation is very expensive.

In principle the pressure vs temperature curve can be studied using either Gibbs ensemble Monte Carlo (GEMC) or Errington's proposed ensembles. However, there are a few deficiencies in the technique. There are various force field methods like CHARMM, AMBER, TraPPE etc. But neither has force fields for organometallic copper compounds. It has been widely quoted that for GEMC calculations the TraPPE model works the best[223,226-228]. Towhee[229] simulation package, have been used in the previous studies[223,226,227] in order to calculate GEMC. Errington *et al.*[224,225] have an in house program which serves similar purpose but with their ensembles.

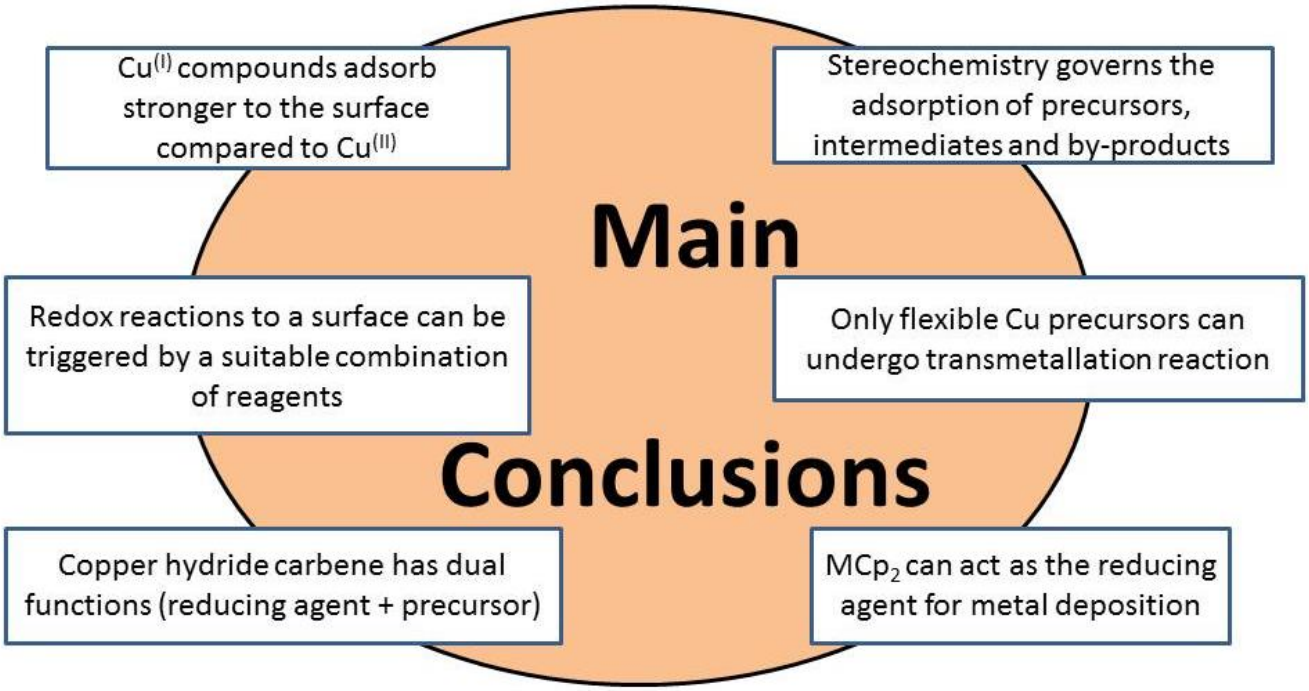
10.2.c. Benefit from the project

The computation of the phase change for organometallic systems would not only benefit the Chemical Vapor Deposition (CVD) community but also broaden the knowledge of other organometallic compounds. The investigation of the phase change can be started with copper compounds and then extend it to other metal compounds of importance. The experimental phase change (P vs T plot) for $Cu(acac)_2$ (acac = acetylacetonate) have been reported by

Colominas *et al*.[230] and Mao *et al*.[231]. This can lead to a good starting point for evaluating the computational results for new precursor compounds.

Computationally detecting the phase change (P vs T graph) of any organometallic compound at different temperatures and precursors has not been reported before and hence is a novel field of research. The existing techniques like GEMC might help in the development of the process. However, the existing codes of GEMC cannot compute the type of organometallic compounds proposed as no parameters for metal has been implemented. Development in the codes is important for this project.

Chapter 11: Conclusion



This study was aimed at understanding the precursor chemistry, transmetallation reaction mechanism and novel reaction pathways for Cu ALD. Our study leads to the proposal of new precursor compounds, improvement in the structures of existing copper precursors and suggestion for alternative co-reagents for an effective Cu ALD.

The choice of a precursor is vital for any ALD reaction. However, due to lack of available data in the literature on structural parameters and volatility of a given precursor and proper understanding of the reaction chemistry, it is difficult to decide on the most suitable precursor type. This is especially true when a new material is to be deposited. In order to solve these problems, taking an example of metal ALD we have studied the intrinsic chemistry of common Cu precursors and some co-reagents. The reaction chemistries of some existing Cu ALD processes are explained and new processes are proposed. Volatility calculations are not possible as they are too expensive at the existing state of the art. However, a proposal to compute the same for any organometallic compound at a reasonably cheaper cost has been stated.

The adsorption of precursors and desorption of by-products are important for an efficient ALD reaction. Our calculations show that the stereochemistry governs the adsorption and desorption of most of the compounds (Chapter 4 and Chapter 5). For copper precursors, the access to the surface copper atoms is important as the precursor adsorbs via Cu-Cu bonding as opposed to Cu-ligand bonding.

$ZnEt_2$ has been tested as the reducing agent for the transmetallation reaction following Lee *et al.*'s proposal[29]. Gas phase reaction pathways showed that the reaction mechanism can be grouped according to the precursor type. Reaction energies for producing Cu(0) and Zn(0) are comparable and hence, Zn impurity is inevitable (Chapter 3). Computation of the surface reaction mechanism showed that complete transmetallation is feasible only for flexible precursors like $Cu(dmap)_2$ (Chapter 5).

The above study leads us to explore other organometallic reagents as reducing agents. We explored the prospective use of oxidisable metallocene MCp_2 compounds as electron donors. This was tested both computationally and experimentally. It was found that although vanadocene causes deposition of copper from methanol solution it fails to do so when tested over a surface (Chapter 6).

Our study showed that Cu(I) intermediates play a crucial role in the mechanism of Cu ALD irrespective of the precursor chosen. After the precursor pulse, the surface is inevitably covered with Cu(I) compounds. This is because they have strong adsorption onto the surface. Thus, using a Cu(I) compound as a precursor might be a better choice than Cu(II) precursor. However, the known Cu(I) compounds have low volatility and decompose onto the surface giving CVD growth rather than ALD. This led us to explore other prospective Cu(I) compounds (Chapter 7 and Chapter 8) to be used as precursors. Both are copper carbene compounds. While N-heterocyclic-Cu hydride (CuH(NHC)) is a theoretical proposal from our work, $(NHC)CuN(SiMe_3)_2$ is synthesized in Carleton University and we showed the pathway for Cu deposition on the surface. CuH(NHC) has the potential of acting both as a reducing agent due to the formation of H^- and as a copper source. Hence, this compound can decrease the possibility of metal impurity as found in the case of $ZnEt_2$. $(NHC)CuN(SiMe_3)_2$ is a thermally stable compound < 130°C that could be successfully delivered to the ALD chamber. The thermal stability is more than the average copper compounds. Thus, these copper carbene precursors are important.

In Chapter 9, we explored the chemistry of a three step reaction pathway where two reagents that are otherwise oxidizing in nature can react to release electrons for copper reduction. This study indicates that redox reactions at a surface can be triggered by a suitable combination of reagents.

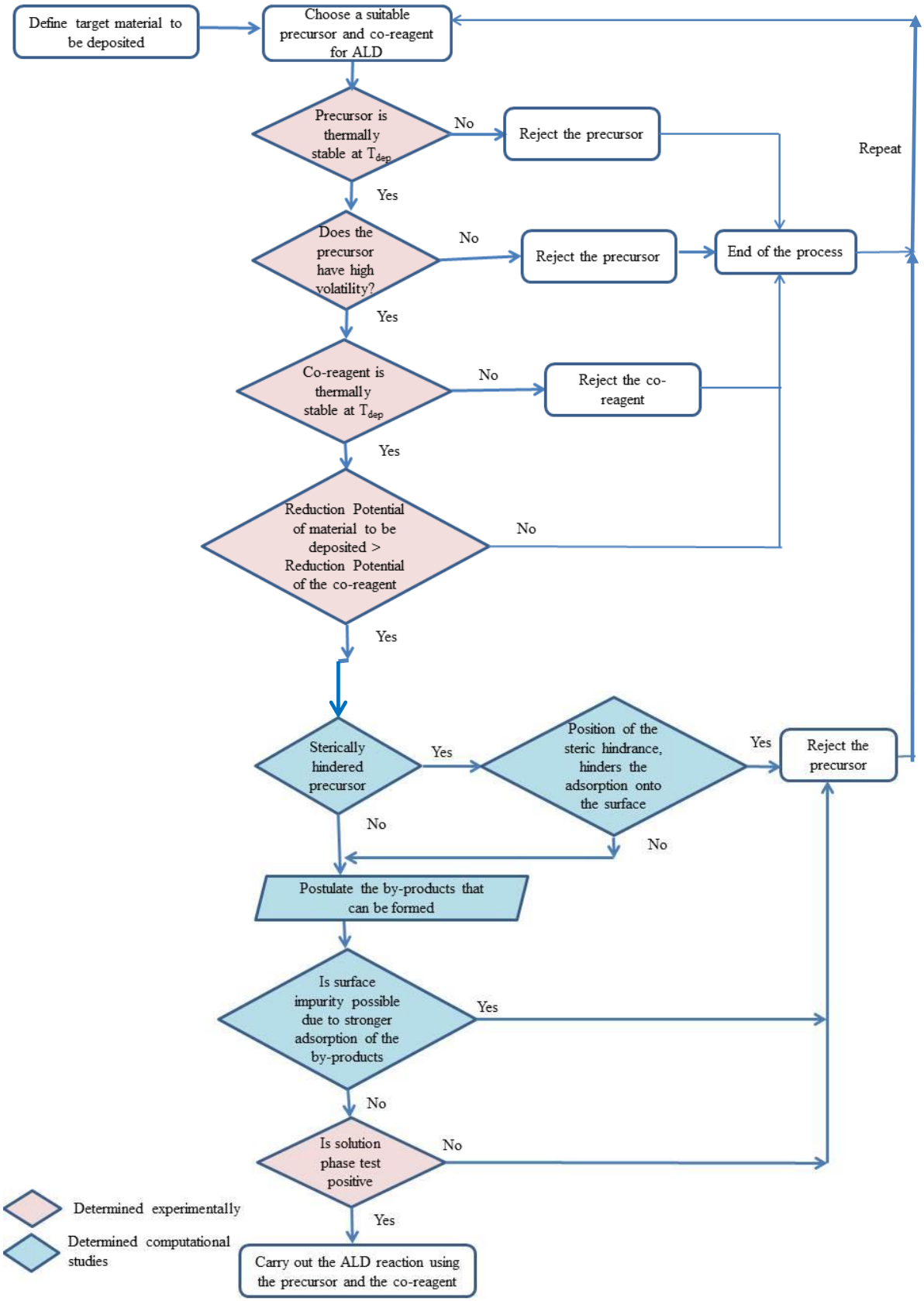


Figure 62: Metrics for screening suitable precursor and co-reagent prior to testing in an ALD reactor.

Through this study, we have been able to develop metrics for the suitability of a candidate metal ALD chemistry between precursor and co-reagents (Figure 62). A proper precursor and co-reagent combination can be chosen by step by step testing of each metric. The assessment requires both experimental data and theoretical calculations. Hence, more synergy between the two is important.

In this thesis we discussed reaction stoichiometry, surface reactions (metal over metal) and side reactions for different Cu ALD processes. These questions remain unanswered for most of the known ALD reaction processes as mentioned by Zaera[35]. Sometimes these questions can only be answered with the help of quantum chemical study. The benefit of the study comes from atomistic understanding of the chemical processes. This has shown the deficits in the known processes and allowed various pathways for future development to be proposed.

However, there is room for improvement. Firstly the exact reason for agglomeration of copper is not known. The surface chemistry between the substrate (Co/Ru/TaN for interconnect) and copper metal can be studied for further understanding. The island growth might be an intrinsic property of copper that is inevitable on all the substrates. Secondly, modelling surface reactions continues to be very expensive. Implementation of force field techniques to study ALD reactions might be a prospective cheaper pathway, but potentials for the copper precursors are not yet developed. Thirdly stronger co-reagents are needed for complete reduction of the metal center without leaving any impurities. The lack of Cu metal deposition processes in many cases has been mainly due to the absence of precursors and co-reactants that can deliver the appropriate properties for a successful ALD process. The finally study of the mechanisms by in situ characterization techniques should be promoted as crucial factor for the fundamental understanding of film growth.

Although this study was mainly focused on developing chemistry for Cu ALD, the same principles can also be applied to other transition metals like Co, Fe, Mn, W, Mo etc. There is a growing interest in the use of these metals in the electronic industry, as catalysts for fuel cells, and in gas sensors. Hence, the future can only be bright for these metals.

Workshop, Conferences and Schools Attended

- Irish National Stimulations Meeting (11th - 12th January 2011) Tyndall National Institute
- Winter School ENHANCE (25th - 26th January 2011) Ruhr University Bochum, Germany
- DFT and Beyond Workshop (12th - 22nd July 2011) - with a Poster FHI Berlin, Germany
- EuroCVD (4th- 9th September 2011) - with a Poster, Kinsale, Ireland
- Irish National Stimulations Meeting (12th - 13th January 2012) - with a Poster, Trinity College Dublin, Ireland
- Irish Chemistry Colloquim 2012 (14th - 15th June 2012) - with a poster (Best Poster Prize) University of Limerick, Ireland
- Baltic ALD conference 2012 (17th - 20th June 2012) - with a poster (Best Poster Prize from AVS) Dresden, Germany
- Irish Nanoweek Conference (17th - 18th September 2012) - with a poster Dublin, Ireland
- Tyndall Internal Postgraduate Poster Competition (July 2012) - (Best Poster Prize)
- Intel Conference (3rd - 4th October 2012) - Invited Talk Croke Park, Dublin, Ireland
- EMRS conference (26th May - 30th May 2013) - Poster Strasbourg, France
- Tyndall National Institute Industrial Day (17th - 19th September 2013) - Poster, Cork, Ireland
- Irish National Stimulations Meeting (26th - 27th May 2014) - Oral presentation, Queen's University, Belfast
- American Chemical Society Fall Meeting (10th – 14th August 2014) – 2 poster and 2 oral presentations, San Francisco, USA
- Tyndall Internal Postgraduate Poster Competition (July 2014)

List of Courses attended in PhD both in UCC and outside. UCC module codes are listed.

- Nanoelectronics – UE6005.
- Scientific Programming concepts – PH502.
- Stastical Data Analysis – ST6013.
- Theory and Application of Computational Work – CM7005.
- Information Literacy – PG6009
- Training courses in Presentation Skills, Scientific Writing Skills for a Public Audience, and Oral Communication of Science to a non-Scientific Audience.
- Workshop for Patent file and Trade Mark.

List of Publications:

- Copper(I) carbene hydride complexes acting both as a reducing agent and precursor for Cu ALD - A study through Density Functional Theory.
  Authors: *Gangotri Dey and Simon D. Elliott.*
  (Theoretical Chemistry Accounts, *2013, 133, 1*) (Link).

- Deposition of Copper By Plasma-Enhanced Atomic Layer Deposition Using a Novel N-Heterocyclic Carbene Precursor.
  Authors: *Jason P. Coyle, Gangotri Dey, Eric R. Sirianni, Marianna L. Kemell, Glenn PA Yap, Mikko Ritala, Markku Leskelä, Simon D. Elliott, and Sean T. Barry*
  (Chemistry of Materials, *2013, 25(7), 1132-1138*) (Link).

- The reaction mechanism for deposition of copper from various precursors with diethylzinc studied via a gas-phase model with first principles DFT.
  Authors: Gangotri Dey and Simon D. Elliott.
  (Journal of Phys. Chemistry A, *2012, 116, 8893-8901*) (Link).

- Copper reduction and atomic layer deposition by oxidative decomposition of formate by hydrazine.
  Authors: *Gangotri Dey and Simon D. Elliott.*
  (RSC Advances, 2014, *2014,4, 34448-34453*) (Link)

- Surface self-limiting reactions of various copper precursors and $ZnEt_2$ as the reducing agent in Atomic Layer Deposition of Cu – Study through DFT-I (*submitted to* Journal of Phys. Chemistry C).
  Authors: *Gangotri Dey and Simon D. Elliott.*

- Surface self-limiting reactions of various copper precursors and $ZnEt_2$ as the reducing agent in Atomic Layer Deposition of Cu – Study through DFT-II (*under preparation*).
  Authors: *Gangotri Dey and Simon D. Elliott.*

- Evaluation of metallocene as the reducing agent for the prospective atomic layer deposition of copper - Studied through DFT and solution phase chemistry (*under preparation*).
  Authors: Gangotri Dey, Jacquiline Wrench, Dirk Hagen, Lynnette Keeny, Ian Povey, Martin Pemble and Simon D. Elliott.

Reference

(1) Moore, G. E. *Proceedings of the IEEE* **1998**, *86*, 82.

(2) *International Technology Roadmap for Semiconductors* http://www.itrs.net/, 2011

(3) Lee, Soo G.; Kim, Yun J.; Lee, Seung P.; Oh, H.-S.; Lee, Seung J.; Kim, M.; Kim, I.-G.; Kim, J.-H.; Shin, H.-J.; Hong, J.-G.; Lee, H.-D.; Kang, H.-K. *Japanese Journal of Applied Physics* **2001**, *40*, 2663.

(4) Helmersson, U.; Lattemann, M.; Bohlmark, J.; Ehiasarian, A. P.; Gudmundsson, J. T. *Thin Solid Films* **2006**, *513*, 1.

(5) Doppelt, P. *Coordination Chemistry Reviews* **1998**, *178–180, Part 2*, 1785.

(6) Powell, R.; Ulman, A. *Ionized physical vapor deposition*; Academic Press, 1999; Vol. 27.

(7) Wasa, K.; Kitabatake, M.; Adachi, H. *Thin Film Materials Technology: Sputtering of Compound Materials*; Elsevier Science, 2004.

(8) George, S. M.; Ott, A. W.; Klaus, J. W. *The Journal of Physical Chemistry* **1996**, *100*, 13121.

(9) Suntola, T. *Materials Science Reports* **1989**, *4*, 261.

(10) Hitchman, M.; L.; Jenson, K. F. *Chemical Vapor Deposition: Principles and Applications* Hitchman & Jensen 1993.

(11) Puurunen, R. L. *Journal of Applied Physics* **2005**, *97*, 121301.

(12) Cho, H. J.; Kim, Y. D.; Park, D. S.; Lee, E.; Park, C. H.; Jang, J. S.; Lee, K. B.; Kim, H. W.; Ki, Y. J.; Han, I. K.; Song, Y. W. *Solid-State Electronics* **2007**, *51*, 1529.

(13) Kittl, J. A.; Opsomer, K.; Popovici, M.; Menou, N.; Kaczer, B.; Wang, X. P.; Adelmann, C.; Pawlak, M. A.; Tomida, K.; Rothschild, A.; Govoreanu, B.; Degraeve, R.; Schaekers, M.; Zahid, M.; Delabie, A.; Meersschaut, J.; Polspoel, W.; Clima, S.; Pourtois, G.; Knaepen, W.; Detavernier, C.; Afanas'ev, V. V.; Blomberg, T.; Pierreux, D.; Swerts, J.; Fischer, P.; Maes, J. W.; Manger, D.; Vandervorst, W.; Conard, T.; Franquet, A.; Favia, P.; Bender, H.; Brijs, B.; Van Elshocht, S.; Jurczak, M.; Van Houdt, J.; Wouters, D. J. *Microelectronic Engineering* **2009**, *86*, 1789.

(14) Mikko Ritala, M. L. *Academic Press ISBN 0-12-512909-2*, *1*, 103.

(15) Hall, R. N.; Racette, J. H. *Journal of Applied Physics* **1964**, *35*, 379.

(16) Delabie, A.; Caymax, M.; Brijs, B.; Brunco, D.; Conard, T.; Sleeckx, E.; Ragnarsson, L.-A.; Van Elshocht, S.; De Gendt, S.; Heyns, M. *ECS Transactions* **2006**, *1*, 433.

(17) George, S. M. *Chem Rev.* **2010**, *110*, 111.

(18) Profijt, H. B.; Potts, S. E.; van de Sanden, M. C. M.; Kessels, W. M. M. *J. Vac. Sci. Technol. A* **2011**, *29*.

(19) Potts, S. E.; Kessels, W. M. M. *Coordination Chemistry Reviews* **2013**, *257*, 3254.

(20) Potts, S.; Keuning, W.; Langereis, E.; Dingemans, G.; van de Sanden, M.; Kessels, W. *Journal of The Electrochemical Society* **2010**, *157*, P66.

(21) S. I. Kol'tsov, V. B. K., V. M. Smirnov, and V. B. Aleskovskii,; Khim, Z. P. *journal of Applied chemistry USSR* **1976**, *49*, 516.

(22) Kukli, K.; Ritala, M.; Leskelä, M. *Journal of the Electrochemical Society* **2001**, *148*, F35.

(23) Schönherr, H.-J.; Wanzlick, H.-W. *Justus Liebigs Annalen der Chemie* **1970**, *731*, 176.

(24) Matero, R.; Rahtu, A.; Ritala, M.; Leskelä, M.; Sajavaara, T. *Thin Solid Films* **2000**, *368*, 1.

(25) Leskelä, M.; Ritala, M. *Thin Solid Films* **2002**, *409*, 138.

(26) Black, K.; Aspinall, H. C.; Jones, A. C.; Przybylak, K.; Bacsa, J.; Chalker, P. R.; Taylor, S.; Zhao, C. Z.; Elliott, S. D.; Zydor, A.; Heys, P. N. *Journal of Materials Chemistry* **2008**, *18*, 4561.

(27) Elliott, S. D.; Scarel, G.; Wiemer, C.; Fanciulli, M.; Pavia, G. *Chemistry of Materials* **2006**, *18*, 3764.

(28) Elam, J. W.; Pellin, M. J.; Elliott, S. D.; Zydor, A.; Faia, M. C.; Hupp, J. T. *Applied Physics Letters* **2007**, *91*, 253123.
(29) Lee, B. H.; Hwang, J. K.; Nam, J. W.; Lee, S. U.; Kim, J. T.; Koo, S.-M.; Baunemann, A.; Fischer, R. A.; Sung, M. M. *Angewandte Chemie International Edition* **2009**, *48*, 4536.
(30) Lim, B. S.; Rahtu, A.; Gordon, R. G. *Nat Mater* **2003**, *2*, 749.
(31) Elliott, S. D. In *Semiconductor Science and Technology* 2012; Vol. 27.
(32) Emslie, D. J. H.; Chadha, P.; Price, J. S. *Coordination Chemistry Reviews* **2013**, *257*, 3282.
(33) Dey, G.; Elliott, S. D. *The Journal of Physical Chemistry A* **2012**, *116*, 8893.
(34) Bernal Ramos, K.; Saly, M. J.; Chabal, Y. J. *Coordination Chemistry Reviews* **2013**, *257*, 3271.
(35) Zaera, F. *Coordination Chemistry Reviews* **2013**, *257*, 3177.
(36) Putkonen, M.; Aaltonen, T.; Alnes, M.; Sajavaara, T.; Nilsen, O.; Fjellvåg, H. *Journal of Materials Chemistry* **2009**, *19*, 8767.
(37) Aaltonen, T.; Alnes, M.; Nilsen, O.; Costelle, L.; Fjellvåg, H. *Journal of Materials Chemistry* **2010**, *20*, 2877.
(38) Mäntymäki, M.; Hämäläinen, J.; Puukilainen, E.; Sajavaara, T.; Ritala, M.; Leskelä, M. *Chemistry of Materials* **2013**, *25*, 1656.
(39) Sree, S. P.; Dendooven, J.; Koranyi, T. I.; Vanbutsele, G.; Houthoofd, K.; Deduytsche, D.; Detavernier, C.; Martens, J. A. *Catalysis Science & Technology* **2011**, *1*, 218.
(40) Yokoyama, S.; Ohba, K.; Nakajima, A. *Applied Physics Letters* **2001**, *79*, 617.
(41) Liang, X.; Zhang, Q.; Lay, M. D.; Stickney, J. L. *Journal of the American Chemical Society* **2011**, *133*, 8199.
(42) Kamata, Y. *Materials Today* **2008**, *11*, 30.
(43) Knisley, T. J. *Wayne State University* **2012**, *Ph.D. thesis*.
(44) Knisley, T. J.; Kalutarage, L. C.; Winter, C. H. *Coordination Chemistry Reviews* **2013**, *257*, 3222.
(45) Ludviksson, A.; Nooney, M.; Bruno, R.; Bailey, A.; Kodas, T. T.; Hampden-Smith, M. J. *Chemical Vapor Deposition* **1998**, *4*, 129.
(46) Sousa, P. M.; Silvestre, A. J.; Conde, O. *Thin Solid Films* **2011**, *519*, 3653.
(47) Au, Y.; Lin, Y. B.; Gordon, R. G. *Journal of the Electrochemical Society* **2011**, *158*, D248.
(48) Lee, H. B. R.; Kim, W. H.; Lee, J. W.; Kim, J. M.; Heo, K.; Hwang, I. C.; Park, Y.; Hong, S.; Kim, H. *Journal of the Electrochemical Society* **2010**, *157*, D10.
(49) Kim, W. H.; Lee, H. B. R.; Heo, K.; Lee, Y. K.; Chung, T. M.; Kim, C. G.; Hong, S.; Heo, J.; Kim, H. *Journal of the Electrochemical Society* **2011**, *158*, D1.
(50) Li, H.; Farmer, D. B.; Gordon, R. G.; Lin, Y.; Vlassak, J. *Journal of the Electrochemical Society* **2007**, *154*, D642.
(51) Aaltonen, T.; Ritala, M.; Sammelselg, V.; Leskelä, M. *Journal of the Electrochemical Society* **2004**, *151*, G489.
(52) Elam, J. W.; Zinovev, A.; Han, C. Y.; Wang, H. H.; Welp, U.; Hryn, J. N.; Pellin, M. J. *Thin Solid Films* **2006**, *515*, 1664.
(53) Aaltonen, T.; Ritala, M.; Sajavaara, T.; Keinonen, J.; Leskelä, M. *Chemistry of Materials* **2003**, *15*, 1924.
(54) Hämäläinen, J.; Sajavaara, T.; Puukilainen, E.; Ritala, M.; Leskelä, M. *Chemistry of Materials* **2011**, *24*, 55.
(55) Devi, A. *Coordination Chemistry Reviews* **2013**, *257*, 3332.
(56) Mårtensson, P.; Larsson, K.; Carlsson, J.-O. *Applied Surface Science* **1998**, *136*, 137.
(57) Li, Z.; Rahtu, A.; Gordon, R. G. *Journal of the Electrochemical Society* **2006**, *153*, C787.
(58) Zhengwen Li, S. n. T. B., and Roy G. Gordon *Inorganic chemistry article* **2005**.
(59) Barry, S. T. *Coordination Chemistry Reviews* **2013**, *257*, 3192.
(60) Coyle, J. P.; Dey, G.; Sirianni, E. R.; Kemell, M. L.; Yap, G. P. A.; Ritala, M.; Leskelä, M.; Elliott, S. D.; Barry, S. T. *Chemistry of Materials* **2013**, *25*, 1132.

(61) Coyle, J. P.; Kurek, A.; Pallister, P. J.; Sirianni, E. R.; Yap, G. P. A.; Barry, S. T. *Chemical Communications* **2012**, *48*, 10440.
(62) Dey, G.; Elliott, S. *Theor Chem Acc* **2013**, *133*, 1.
(63) Mårtensson, P.; Larsson, K.; Carlsson, J.-O. *Applied Surface Science* **1999**, *148*, 9.
(64) Martensson, P.; Carlsson, J.-O. *Journal of the Electrochemical Society* **1998**, *145*, 2926.
(65) Utriainen, M.; Kröger-Laukkanen, M.; Johansson, L.-S.; Niinistö, L. *Applied Surface Science* **2000**, *157*, 151.
(66) Kang, S.-W.; Yun, J.-Y.; Chang, Y. H. *Chemistry of Materials* **2010**, *22*, 1607.
(67) Grushin, V. V.; Marshall, W. J. *Advanced Synthesis & Catalysis* **2004**, *346*, 1457.
(68) Park, K.-H.; Marshall, W. J. *Journal of the American Chemical Society* **2005**, *127*, 9330.
(69) Thompson, J. S.; Zhang, L.; Wyre, J. P.; Brill, D.; Li, Z. *Organometallics* **2012**, *31*, 7884.
(70) Törndahl, T.; Ottosson, M.; Carlsson, J.-O. *Journal of The Electrochemical Society* **2006**, *153*, C146.
(71) Li, Z.; Gordon, R. G. *Chemical Vapor Deposition* **2006**, *12*, 435.
(72) Knisley, T. J.; Ariyasena, T. C.; Sajavaara, T.; Saly, M. J.; Winter, C. H. *Chemistry of Materials* **2011**, *23*, 4417.
(73) Norman, J. A. T.; Perez, M.; Schulz, S. E.; Waechtler, T. *Microelectronic Engineering* **2008**, *85*, 2159.
(74) Juppo, M.; Ritala, M.; Leskelä, M. *J. Vac. Sci. Technol. A* **1997**, *15*, 2330.
(75) Vidjayacoumar, B.; Emslie, D. J. H.; Clendenning, S. B.; Blackwell, J. M.; Britten, J. F.; Rheingold, A. *Chemistry of Materials* **2010**, *22*, 4844.
(76) Ma, Q.; Guo, H.; Gordon, R. G.; Zaera, F. *Chemistry of Materials* **2011**, *23*, 3325.
(77) Cottrell, T. L. *The strengths of chemical bonds*; Butterworths, 1958.
(78) Hagen, D. J.; Connolly, J.; Nagle, R.; Povey, I. M.; Rushworth, S.; Carolan, P.; Ma, P.; Pemble, M. E. *Surface and Coatings Technology* **2013**, *230*, 3.
(79) Dai, M.; Kwon, J.; Halls, M. D.; Gordon, R. G.; Chabal, Y. J. *Langmuir* **2010**, *26*, 3911.
(80) Dai, M.; Kwon, J.; Langereis, E.; Wielunski, L. S.; Chabal, Y.; Li, Z.; Gordon, R. *ECS Transactions* **2007**, *11*, 91.
(81) Seitz, O.; Dai, M.; Aguirre-Tostado, F. S.; Wallace, R. M.; Chabal, Y. J. *Journal of the American Chemical Society* **2009**, *131*, 18159.
(82) Leskela, M.; Ritala, M. *Angewandte Chemie-International Edition* **2003**, *42*, 5548.
(83) George, S. M. *Chemical Reviews* **2009**, *110*, 111.
(84) Gordon, R. In *Atomic Layer Deposition for Semiconductors*; Seong Hwang, C., Ed.; Springer US: 2014, p 15.
(85) Elliott, S. In *Atomic Layer Deposition for Semiconductors*; Seong, H. C., Ed.; Springer US: 2014, p 47.
(86) Puurunen, R. L. *Chemical Vapor Deposition* **2005**, *11*, 79.
(87) Szabo, A.; Ostlund, N. S. *Modern Quantum Chemistry- Introduction to advanced electronic structure theory*; Dover Publications, INC.: Mineola, New York, 1982.
(88) Hohenberg, P.; Kohn, W. *Physical review* **1964**, *136*, B864.
(89) Ernzerhof, M.; Scuseria, G. E. *The Journal of Chemical Physics* **1999**, *110*, 5029.
(90) Kunte, G. V.; Shivashankar, S. A.; Umarji, A. M. *Measurement Science and Technology* **2008**, *19*, 025704.
(91) Chermette, H. *Journal of Computational Chemistry* **1999**, *20*, 129.
(92) Bickelhaupt, F. M.; Baerends, E. J. *Reviews in Computational Chemistry, Volume 15* **2000**, 1.
(93) Harvey, J. N. *Annual Reports Section "C" (Physical Chemistry)* **2006**, *102*, 203.
(94) Slater, J. C. *Physical Review* **1930**, *36*, 57.

(95) Boys, S. F. *Proceedings of the Royal Society of London. Series A, Mathematical and Physical Sciences* **1950**, *200*, 542.
(96) Ahlrichs, R.; Elliott, S. D.; Huniar, U. *Berichte Der Bunsen-Gesellschaft-Physical Chemistry Chemical Physics* **1998**, *102*, 795.
(97) Levine, I. N. *Quantum Chemistry*; Pearson Education, Limited, 2013.
(98) Simon, J. *An Introduction to Theoretical Chemistry*; Cambridge University Press: United Kingdon, 2003.
(99) Santra, B., Universitätsbibliothek, 2010.
(100) Marx, D.; Hutter, J. *Modern methods and algorithms of quantum chemistry* **2000**, *1*, 301.
(101) Hoover, W. G. In *Molecular Dynamics* 1986; Vol. 258.
(102) Car, R.; Parrinello, M. *Physical Review Letters* **1985**, *55*, 2471.
(103) Haile, J. M. *Molecular dynamics simulation: elementary methods*; John Wiley & Sons, Inc., 1992.
(104) Reed, A. E.; Weinstock, R. B.; Weinhold, F. *The Journal of Chemical Physics* **1985**, *83*, 735.
(105) Cramer, C. J.; Truhlar, D. G. *Physical Chemistry Chemical Physics* **2009**, *11*, 10757.
(106) Widjaja, Y.; Musgrave, C. B. *Applied Physics Letters* **2002**, *80*, 3304.
(107) Pinto, H. P.; Nieminen, R.; Elliott, S. D. *Physical Review B* **2004**, *70*, 125402.
(108) Tanaka, T.; Nakajima, T.; Yamashita, K. *Thin Solid Films* **2002**, *409*, 51.
(109) Lee, W.; Dasgupta, N. P.; Trejo, O.; Lee, J.-R.; Hwang, J.; Usui, T.; Prinz, F. B. *Langmuir* **2010**, *26*, 6845.
(110) Kwon, J.; Saly, M.; Halls, M. D.; Kanjolia, R. K.; Chabal, Y. J. *Chemistry of Materials* **2012**, *24*, 1025.
(111) Hukka, T. I.; Pakkanen, T. A.; D'Evelyn, M. P. *Surface Science* **1996**, *359*, 213.
(112) Elliott, S. D.; Greer, J. C. *Journal of Materials Chemistry* **2004**, *14*, 3246.
(113) Elliott, S. D. *Computational Materials Science* **2005**, *33*, 20.
(114) Siodmiak, M.; Frenking, G.; Korkin, A. *The Journal of Physical Chemistry A* **2000**, *104*, 1186.
(115) Tanskanen, J. T.; Bakke, J. R.; Bent, S. F.; Pakkanen, T. A. *The Journal of Physical Chemistry C* **2010**, *114*, 16618.
(116) Kwon, J.; Dai, M.; Halls, M. D.; Langereis, E.; Chabal, Y. J.; Gordon, R. G. *The Journal of Physical Chemistry C* **2008**, *113*, 654.
(117) Olivier, S.; Ducéré, J.-M.; Mastail, C.; Landa, G.; Estève, A.; Rouhani, M. D. *Chemistry of Materials* **2008**, *20*, 1555.
(118) Alam, M. A.; Green, M. L. *Journal of Applied Physics* **2003**, *94*, 3403.
(119) Ylilammi, M. *Thin Solid Films* **1996**, *279*, 124.
(120) Shirazi, M.; Elliott, S. D. *Chemistry of Materials* **2013**, *25*, 878.
(121) Mukhopadhyay, A.; Musgrave, C. B. *Chemical physics letters* **2006**, *421*, 215.
(122) Ren, J.; Zhang, Y.-T.; Zhang, D. W. *Journal of Molecular Structure: THEOCHEM* **2007**, *803*, 23.
(123) Vidjayacoumar, B.; Emslie, D. J. H.; Blackwell, J. M.; Clendenning, S. B.; Britten, J. F. *Chemistry of Materials* **2010**, *22*, 4854.
(124) Kaim, W. *European Journal of Inorganic Chemistry* **2012**, *2012*, 343.
(125) Kim, H.; Lee, H. B. R.; Maeng, W. J. *Thin Solid Films* **2009**, *517*, 2563.
(126) Ahlrichs, R.; Bär, M.; Häser, M.; Horn, H.; Kölmel, C. *Chemical Physics Letters* **1989**, *162*, 165.
(127) Schafer, A.; Huber, C.; Ahlrichs, R. *The Journal of Chemical Physics* **1994**, *100*, 5829.
(128) Perdew, J. P.; Burke, K.; Ernzerhof, M. *Physical Review Letters* **1996**, *77*, 3865.
(129) Eichkorn, K.; Weigend, F.; Treutler, O.; Ahlrichs, R. *Theoretical Chemistry Accounts: Theory, Computation, and Modeling (Theoretica Chimica Acta)* **1997**, *97*, 119.
(130) Sierka, M.; Hogekamp, A.; Ahlrichs, R. *The Journal of Chemical Physics* **2003**, *118*, 9136.

(131) Schafer, A.; Horn, H.; Ahlrichs, R. *The Journal of Chemical Physics* **1992**, *97*, 2571.
(132) Becker, R.; Devi, A.; Weiß, J.; Weckenmann, U.; Winter, M.; Kiener, C.; Becker, H. W.; Fischer, R. A. *Chemical Vapor Deposition* **2003**, *9*, 149.
(133) Deglmann, P.; May, K.; Furche, F.; Ahlrichs, R. *Chemical Physics Letters* **2004**, *384*, 103.
(134) Kresse, G.; Hafner, J. *Physical Review B* **1994**, *49*, 14251.
(135) Kresse, G.; Furthmüller, J. *Computational Materials Science* **1996**, *6*, 15.
(136) *American Institute Of Physics Handbook*; 3 ed.; Mc-Grawhill 1973.
(137) Coyle, J. P.; Johnson, P. A.; DiLabio, G. A.; Barry, S. T.; Müller, J. *Inorganic Chemistry* **2010**, *49*, 2844.
(138) Montgomery, H.; Lingafelter, E. C. *Acta Crystallographica* **1963**, *16*, 748.
(139) Paul R. Raithby, G. P.; Shields, F. H. A. a.; Motherwell, W. D. S. *Acta Crystallographica Section B* **1999**, *56*.
(140) Mui, C.; Widjaja, Y.; Kang, J. K.; Musgrave, C. B. *Surface Science* **2004**, *557*, 159.
(141) Heyman, A.; Musgrave, C. B. *The Journal of Physical Chemistry B* **2004**, *108*, 5718.
(142) Aaltonen, T.; Rahtu, A.; Ritala, M.; Leskelä, M. *Electrochemical and solid-state letters* **2003**, *6*, C130.
(143) Widjaja, Y.; Musgrave, C. B. *The Journal of Chemical Physics* **2002**, *117*, 1931.
(144) Elliott, S. D. *Semiconductor Science and Technology* **2012**, *27*, 074008.
(145) Pedersen, H.; Elliott, S. *Theor Chem Acc* **2014**, *133*, 1.
(146) Capelle, K. *Brazilian Journal of Physics* **2006**, *36*, 1318.
(147) Olivier, S.; Ducéré, J.-M.; Mastail, C.; Landa, G.; Estève, A.; Rouhani, M. D. *Chemistry of Materials* **2008**, *20*, 1555.
(148) Weigend, F.; Häser, M.; Patzelt, H.; Ahlrichs, R. *Chemical Physics Letters* **1998**, *294*, 143.
(149) Hattig, C. *Physical Chemistry Chemical Physics* **2005**, *7*, 59.
(150) Grimme, S. *Journal of computational chemistry* **2006**, *27*, 1787.
(151) Larsson, J. A.; Elliott, S. D.; Greer, J. C.; Repp, J.; Meyer, G.; Allenspach, R. *Physical Review B* **2008**, *77*, 115434.
(152) Cioslowski, J. *Journal of the American Chemical Society* **1989**, *111*, 8333.
(153) Liu, Y.-F.; Xia, H.-T.; Yang, S.-P.; Wang, D.-Q. *Acta Crystallographica Section C* **2008**, *64*, m91.
(154) Kanda, H.; Narumi, Y.; Hosokoshi, Y.; Suzuki, T.; Kawata, S.; Kindo, K.; Inoue, K.; Kaizaki, S. *Inorganica Chimica Acta* **2004**, *357*, 3125.
(155) Zydor, A.; Elliott, S. D. *Journal of Nanoscience and Nanotechnology* **2011**, *11*, 8089.
(156) Zydor, A.; Kessler, V. G.; Elliott, S. D. *Physical Chemistry Chemical Physics* **2012**, *14*, 7954.
(157) Elliott, S. D. *Langmuir* **2010**, *26*, 9179.
(158) Kalutarage, L. C.; Clendenning, S. B.; Winter, C. H. *Chemistry of Materials* **2014**, *26*, 3731.
(159) Choukroun, R.; de Caro, D.; Mateo, S.; Amiens, C.; Chaudret, B.; Snoeck, E.; Respaud, M. *New Journal of Chemistry* **1998**, *22*, 1295.
(160) Choukroun, R.; de Caro, D.; Chaudret, B.; Lecante, P.; Snoeck, E. *New Journal of Chemistry* **2001**, *25*, 525.
(161) Jany, G.; Gustafsson, M.; Repo, T.; Aitola, E.; Dobado, J. A.; Klinga, M.; Leskelä, M. *Journal of Organometallic Chemistry* **1998**, *553*, 173.
(162) Shimizu, H.; Sakoda, K.; Momose, T.; Koshi, M.; Shimogaki, Y. *J. Vac. Sci. Technol. A* **2012**, *30*, 01A144.
(163) Vidjayacoumar, B.; Ramalingam, V.; Emslie, D. J.; Blackwell, J.; Clendenning, S. *ECS Transactions* **2013**, *50*, 53.
(164) Holloway, J. D. L.; Bowden, W. L.; Geiger, W. E. *Journal of the American Chemical Society* **1977**, *99*, 7089.

(165) Koepp, H. M., Wendt, H., Strehlow, H. Z *Elektrochem* **1960**, *64*, 483.
(166) Gubin, S. P.; Smirnova, S. A.; Denisovich, L. I. *Journal of Organometallic Chemistry* **1971**, *30*, 257.
(167) Ryan, M. F.; Richardson, D. E.; Lichtenberger, D. L.; Gruhn, N. E. *Organometallics* **1994**, *13*, 1190.
(168) Gagne, R. R.; Koval, C. A.; Lisensky, G. C. *Inorganic Chemistry* **1980**, *19*, 2854.
(169) Samans, C. H. *Engineering metals and their alloys*; Macmillan: New York, 1949.
(170) Swart, M. *Inorganica chimica acta* **2007**, *360*, 179.
(171) Wittbrodt, J. M.; Schlegel, H. B. *The Journal of Chemical Physics* **1996**, *105*, 6574.
(172) Groenhof, A. R.; Swart, M.; Ehlers, A. W.; Lammertsma, K. *The Journal of Physical Chemistry A* **2005**, *109*, 3411.
(173) Dey, G.; Elliott, D. S. *RSC Advances* **2014**, *4*, 34448.
(174) Dey, G.; Elliott, s. D. *To be published*.
(175) Khan, F. A.; Clemmer, D. E.; Schultz, R. H.; Armentrout, P. B. *The Journal of Physical Chemistry* **1993**, *97*, 7978.
(176) Tolman, C. A. *Chemical Society Reviews* **1972**, *1*, 337.
(177) Holzschuh, H.; Suhr, H. *Appl. Phys. A* **1990**, *51*, 486.
(178) Maimaiti, Y.; Nolan, M.; Elliott, S. D. *Physical Chemistry Chemical Physics* **2014**, *16*, 3036.
(179) Waechtler, T.; Oswald, S.; Roth, N.; Jakob, A.; Lang, H.; Ecke, R.; Schulz, S. E.; Gessner, T.; Moskvinova, A.; Schulze, S. *Journal of The Electrochemical Society* **2009**, *156*, H453.
(180) Johansson, J.; Kostamo, J.; Karppinen, M.; Niinisto, L. *Journal of Materials Chemistry* **2002**, *12*, 1022.
(181) J. Clayden, N. G., S. Warren *Oxford University Press* **2001**.
(182) Doyle, G.; Tobias, R. S. *Inorganic Chemistry* **1968**, *7*, 2479.
(183) Goodenough, J. B. *Journal of Physics: Condensed Matter* **2003**, *15*, R257.
(184) Glebov, E. M.; Plyusnin, V. F.; Grivin, V. P.; Krupoder, S. A.; Liskovskaya, T. I.; Danilovich, V. S. *Journal of Photochemistry and Photobiology A: Chemistry* **2000**, *133*, 177.
(185) *Metallocenes an introduction to sandwich complexes*; illustrated ed.; Long, N. J., Ed.; Wiley,, 1998.
(186) Wu, L.; Eisenbraun, E. *Electrochemical and Solid State Letters* **2008**, *11*, H107.
(187) Ritala, M.; Kukli, K.; Rahtu, A.; Räisänen, P. I.; Leskelä, M.; Sajavaara, T.; Keinonen, J. *Science* **2000**, *288*, 319.
(188) Willcocks, A. M.; Pugh, T.; Hamilton, J. A.; Johnson, A. L.; Richards, S. P.; Kingsley, A. J. *Dalton Transactions* **2013**, *42*, 5554.
(189) Wanzlick, H. W. *Angewandte Chemie International Edition in English* **1962**, *1*, 75.
(190) Jurkauskas, V.; Sadighi, J. P.; Buchwald, S. L. *Organic Letters* **2003**, *5*, 2417.
(191) Pelss, A.; Kumpulainen, E. T.; Koskinen, A. M. *The Journal of organic chemistry* **2009**, *74*, 7598.
(192) Tominaga, S.; Oi, Y.; Kato, T.; An, D. K.; Okamoto, S. *Tetrahedron Letters* **2004**, *45*, 5585.
(193) Boogaerts, I. I. F.; Nolan, S. P. *Journal of the American Chemical Society* **2010**, *132*, 8858.
(194) Koenig, T. M.; Daeuble, J. F.; Brestensky, D. M.; Stryker, J. M. *Tetrahedron Letters* **1990**, *31*, 3237.
(195) Mankad, N. P.; Laitar, D. S.; Sadighi, J. P. *Organometallics* **2004**, *23*, 3369.
(196) K. Hara, Y. K., and M. Sawamura *Bulletin of the Chemical Society of Japan* **2006**, *79*.
(197) Chen, T. Y.; Omnès, L.; Vaisserman, J.; Doppelt, P. *Inorganica Chimica Acta* **2004**, *357*, 1299.
(198) Coyle, J. P.; Monillas, W. H.; Yap, G. P. A.; Barry, S. T. *Inorganic Chemistry* **2007**, *47*, 683.

(199) Park, J. W.; Jang, H. S.; Kim, M.; Sung, K.; Lee, S. S.; Chung, T.-M.; Koo, S.; Kim, C. G.; Kim, Y. *Inorganic Chemistry Communications* **2004**, *7*, 463.
(200) Gambarotta, S.; Bracci, M.; Floriani, C.; Chiesi-Villa, A.; Guastini, C. *Journal of the Chemical Society, Dalton Transactions* **1987**, 1883.
(201) Tsuda, T.; Watanabe, K.; Miyata, K.; Yamamoto, H.; Saegusa, T. *Inorganic Chemistry* **1981**, *20*, 2728.
(202) Gaillard, S.; Cazin, C. S. J.; Nolan, S. P. *Accounts of Chemical Research* **2011**, *45*, 778.
(203) Mankad, N. P.; Laitar, D. S.; Sadighi, J. P. *Organometallics* **2004**, *23*, 3369.
(204) Goj, L. A.; Blue, E. D.; Delp, S. A.; Gunnoe, T. B.; Cundari, T. R.; Pierpont, A. W.; Petersen, J. L.; Boyle, P. D. *Inorganic Chemistry* **2006**, *45*, 9032.
(205) Niskanen, A.; Hatanpää, T.; Arstila, K.; Leskelä, M.; Ritala, M. *Chemical Vapor Deposition* **2007**, *13*, 408.
(206) Kariniemi, M.; Niinistö, J.; Hatanpää, T.; Kemell, M.; Sajavaara, T.; Ritala, M.; Leskelä, M. *Chemistry of Materials* **2011**, *23*, 2901.
(207) Denk, M. K.; Thadani, A.; Hatano, K.; Lough, A. J. *Angewandte Chemie International Edition in English* **1997**, *36*, 2607.
(208) Jain, A.; Chi, K. M.; Kodas, T.; Hampden-Smith, M. *Journal of The Electrochemical Society* **1993**, *140*, 1434.
(209) Nyburg, S. C.; Parkins, A. W.; Sidi-Boumedine, M. *Polyhedron* **1993**, *12*, 1119.
(210) Harkins, S. B.; Mankad, N. P.; Miller, A. J. M.; Szilagyi, R. K.; Peters, J. C. *Journal of the American Chemical Society* **2008**, *130*, 3478.
(211) Melzer, M. M.; Mossin, S.; Dai, X.; Bartell, A. M.; Kapoor, P.; Meyer, K.; Warren, T. H. *Angewandte Chemie International Edition* **2010**, *49*, 904.
(212) James, A. M.; Laxman, R. K.; Fronczek, F. R.; Maverick, A. W. *Inorganic Chemistry* **1998**, *37*, 3785.
(213) Lin, J. C. Y.; Huang, R. T. W.; Lee, C. S.; Bhattacharyya, A.; Hwang, W. S.; Lin, I. J. B. *Chemical Reviews* **2009**, *109*, 3561.
(214) An, D.; Wang, J.; Dong, T.; Yang, Y.; Wen, T.; Zhu, H.; Lu, X.; Wang, Y. *European Journal of Inorganic Chemistry* **2010**, *2010*, 4506.
(215) Lundqvist, B. I.; Andersson, Y.; Shao, H.; Chan, S.; Langreth, D. C. *International Journal of Quantum Chemistry* **1995**, *56*, 247.
(216) Ruiz, V. G.; Liu, W.; Zojer, E.; Scheffler, M.; Tkatchenko, A. *Physical Review Letters* **2012**, *108*, 146103.
(217) Marom, N.; Tkatchenko, A.; Rossi, M.; Gobre, V. V.; Hod, O.; Scheffler, M.; Kronik, L. *J. Chem. Theory Comput.* **2011**, *7*, 3944.
(218) Ravindranathan, P.; Patil, K. C. *Thermochimica Acta* **1983**, *71*, 53.
(219) Furst, A.; Berlo, R. C.; Hooton, S. *Chemical Reviews* **1965**, *65*, 51.
(220) F. L. Paulauskas, C. D. W., C. C. Eberle, A. K. Naskar, and S. Ozcan. NOVEL PRECURSOR MATERIALS AND APPROACHES FOR PRODUCING LOWER COST CARBON FIBER FOR HIGH VOLUME INDUSTRIES. [Online Early Access].
(221) Eggimann, B. L.; Siepmann, J. I. *The Journal of Physical Chemistry C* **2007**, *112*, 210.
(222) Panagiotopoulos, A. Z. *Molecular Simulation* **1992**, *9*, 1.
(223) Martin, M. G.; Siepmann, J. I. *Journal of the American Chemical Society* **1997**, *119*, 8921.
(224) Rane, K. S.; Errington, J. R. *The Journal of Physical Chemistry B* **2013**.
(225) Rane, K. S.; Murali, S.; Errington, J. R. *J. Chem. Theory Comput.* **2013**.
(226) McGrath, M. J.; Kuo, I. F. W.; Ghogomu, J. N.; Mundy, C. J.; Siepmann, J. I. *The Journal of Physical Chemistry B* **2011**, *115*, 11688.
(227) Chen, B.; Siepmann, J. I.; Klein, M. L. *The Journal of Physical Chemistry B* **2001**, *105*, 9840.
(228) Ketko, M. H.; Rafferty, J.; Siepmann, J. I.; Potoff, J. J. *Fluid Phase Equilibria* **2008**, *274*, 44.
(229) Martin, M. G.

(230) Colominas, C.; Lau, K. H.; Hildenbrand, D. L.; Crouch-Baker, S.; Sanjurjo, A. *Journal of Chemical & Engineering Data* **2001**, *46*, 446.
(231) Mao, J.; Eisenbraun, E.; Omarjee, V.; Korolev, A.; Dussarrat, C. *ECS Transactions* **2011**, *35*, 125.